



**INVESTIGATION OF DIESEL-ETHANOL AND  
DIESEL-GASOLINE DUAL FUEL  
COMBUSTION IN A SINGLE CYLINDER  
OPTICAL DIESEL ENGINE**

**Dissertation submitted in partial fulfilment for the degree of  
Doctor of Philosophy**

**By**

**Mahmoudreza Mirmohammadsadeghi**

**Department of Mechanical and Aerospace Engineering  
Brunel University London**

**February 2018**



## **Abstract**

Ever growing population and increased energy consumption across all industries has resulted in higher atmospheric concentration of the greenhouse gases (GHG) and therefore an increase in the planet's average temperature, which has led to increasingly demanding and more strict legislations on pollutant sources, and more specifically, the automotive industry. As a consequence of all this, the demand for research into alternative energy sources has greatly increased.

In this study combustion characteristics, engine performance, and exhaust emission of diesel-ethanol and diesel-gasoline are investigated in an optical direct injection diesel engine. In particular, effects of different substitution ratios and diesel injection strategies are studied when the total fuel energy is kept constant. The three main substitution ratios used in this study include 45% (45% of fuel energy from port-injected ethanol/gasoline and 55% from direct injection diesel), 60%, and 75%.

The engine used for this investigation is a Ricardo Hydra single cylinder optical engine running at 1200 rpm. In-cylinder pressure measurement is used for calculating all engine parameters, heat release rate, and efficiency. In addition to the thermodynamic analysis of the combustion parameters, high speed camera was used alongside with a copper vapor laser or the high speed image intensifier in the high speed video imaging for the optical analysis of the effect of the above-mentioned parameters on autoignition and combustion processes, while Horiba particulate analyser and AVL smoke meter were utilized in monitoring and recording emissions for every tested condition. Depending on the testing conditions, such as injection strategy and intake conditions, both dual-fuel operations were able to deliver high efficiency and improved emissions compared to that of a pure diesel engine operation, with the diesel-gasoline operation offering more consistency in improved thermal efficiency, and the diesel-ethanol operation delivering lower emission output. The optical analysis of the combustion represents the main difference in the flame propagation, distribution and quality for each substitute fuel and its substitution percentage, as well as the condition under examination.

## **Acknowledgements**

Firstly, I would like to thank Mr. Akira Ito of Komatsu Ltd. (IPA) for all of his moral and technical support and sharing his knowledge and experience in the course of this research.

I would also like to thank Mr. Andrew Selway and Mr. Eamon Wyse for their continued technical support, advice and assistance during this study.

Also, I would like to thank my beloved family, my parents, brother and sister, my wife, and my two dearest boys, for all their patience, unconditional love and support at every step of the way.

And last but by no means the least, with great respect and gratitude, I would like to thank Professor Hua Zhao for his guidance and supervision, and his continuous support, from the beginning of my undergraduate course to the end of my PhD research at Brunel University.

## Abbreviations

AC	Alternating Current
AKI	Anti-Knock Index
ASC	Ammonia Slip Catalyst
ATDC	After Top Dead Centre
BDC	Bottom Dead Centre
BMEP	Brake Mean Effective Pressure
BSFC	Brake Specific Fuel Consumption
BTDC	Before Top Dead Centre
CA	Cam Angle
CAI	Controlled Auto-Ignition
CFD	Computational Fluid Dynamics
CFR	Cooperative Fuel Research
CI	Compression-Ignition
CIDI	Compression-Ignition Direct-Injection
CLA	Causal Layered Analysis
CNG	Compressed Natural Gas
CO	Carbon Monoxide
CO <sub>2</sub>	Carbon Dioxide
COV	Coefficient Of Variation
CVL	Copper Vapor Laser
DAQ	Data Acquisition
DC	Direct Current
DI	Direct Injection
DICI	Direct-Injection Compression-Ignition

DOC	Diesel Oxidation Catalyst
DPF	Diesel Particulate Filter
ECU	Electronic Control Unit
EGR	Exhaust Gas Recirculation
EPA	Environmental Protection Agency
EU	European Union
EV	Electronic Valve
F/A	Fuel To Air Ratio
FFV	Flex Fuel Vehicles
FID	Flame Ionization Detector
FPGA	Field-Programmable Gate Array
FSN	Filter Smoke Number
GHG	Greenhouse Gas
HC	Hydrocarbon
HCCI	Homogeneous Charge Compression Ignition
HRR	Heat Release Rate
HSDI	High-Speed Direct Injection
IC	Internal Combustion
IMEP	Indicated Mean Effective Pressure
ISFC	Indicated Specific Fuel Consumption
LED	Light-Emitting Diode
LHV <sub>f</sub>	Latent Heat Of Vaporization Of Fuel
LIP	Laser-Induced Phosphorescence
LPG	Liquefied Petroleum Gas
LTC	Low Temperature Combustion
LTH	Low Temperature Heat Release

MFB	Mass Fuel Burnt
MJ	Megajoule
MON	Motor Octane Number
MPa	Mega Pascal
NDIR	Non-Dispersive Infrared
NMHC	Non Methane Hydrocarbon
NO	Nitric Oxide
NO <sub>x</sub>	Nitrogen oxide
PCCI	Premixed Charge Compression Ignition
PFI	Port Fuel Injector
PHRR	Peak Heat Release Rate
PM	Particulate Matter
PN	Pression Nominal
PPC	Partially Premixed Combustion
PRF	Primary Reference Fuel
RCCI	Reactivity Controlled Compression Ignition
RED	Renewable Energy Directive
RON	Research Octane Number
SCCM	Standard Cubic Centimetres Per Minute
SCR	Selective Catalytic Reduction
SI	Spark Ignition
SOC	Start Of Combustion
SOI	Start Of Injection
TDC	Top Dead Centre
THC	Total Hydrocarbon
TSCi	Transonic Combustion

UHC	Unburnt Hydrocarbons
UK	United Kingdom
USA	United States Of America
VBA	Visual Basic For Applications
VCO	Valve Covered Orifice
VVA	Variable Valve Actuation

# Table of Contents

Abstract.....	iii
Acknowledgements.....	iv
Abbreviations.....	v
Table of Contents .....	ix
List of Figures .....	xv
List of Tables.....	xxiii
Chapter 1. Introduction.....	2
1.1 Background and Context.....	2
1.2 Scope and Objectives .....	4
1.3 Overview of Thesis .....	5
Chapter 2. Literature Review.....	7
2.1 History of Diesel CI Engine .....	7
2.2 Emissions .....	8
2.2.1 Nitrogen Oxides (NO <sub>x</sub> ).....	10
2.2.2 Particulate Matter (PM) .....	12
2.2.3 Hydrocarbons (HC).....	14
2.2.4 Exhaust Gas Recirculation.....	14
2.2.5 Exhaust Gas Aftertreatment .....	16
2.3 Modern Direct Injection CI Combustion .....	18
2.4 Alternative diesel engine combustion technologies .....	21
2.4.1 Homogeneous Charge Compression Ignition (HCCI).....	22
2.4.2 Premixed Charge Compression Ignition (PCCI) .....	26
2.4.3 Reactivity Controlled Compression Ignition (RCCI) .....	28
2.4.4 Low Temperature Combustion (LTC).....	29
2.4.5 Transonic Combustion (TSCi <sup>TM</sup> ).....	31
2.5 Dual Fuel Diesel Engine Technology.....	32

2.5.1	Diesel-Gas Dual Fuel.....	32
2.5.2	Diesel-Gasoline RCCI Combustion.....	37
2.5.3	Dual Fuel PPC.....	39
2.6	Ethanol For Dual-Fuel Engines.....	40
2.7	Optical Diagnostics, Engines and Analysis.....	49
2.7.1	In-cylinder studies of diesel dual fuel combustion .....	53
2.7.2	High Speed Imaging .....	55
2.8	Summary .....	56
Chapter 3.	Experimental Facilities, Methodology and Data Analysis.....	57
3.1	Introduction .....	57
3.2	Ricardo Single Cylinder Research Engine with Optical Access.....	57
3.2.1	General Description .....	57
3.2.2	Cylinder Head .....	59
3.2.3	Optical Configuration .....	59
3.2.3.1	Extended Piston and Cylinder Block.....	59
3.2.3.2	Optical windows.....	60
3.2.4	Crank Shaft Position System .....	62
3.2.5	Fuel Injection system .....	63
3.2.6	Intake System.....	68
3.2.6.1	Forced Induction.....	68
3.2.6.2	Intake Heating.....	69
3.2.6.3	EGR System .....	70
3.3	In-Cylinder Pressure Data Acquisition System.....	71
3.3.1	In-Cylinder Pressure Measurement.....	72
3.3.2	Data Acquisition System.....	72
3.3.3	Experimental Procedure.....	72
3.4	Optical Measurement .....	74

3.4.1	High Speed Camera .....	74
3.4.2	Copper Vapour Laser .....	74
3.4.3	High Speed Image Intensifier .....	75
3.5	Exhaust Emission Measurement .....	76
3.5.1	Horiba MEXA-7170 DEGR Motor Exhaust Gas Analyser .....	76
3.5.1.1	Horiba AIA-72X: CO and CO <sub>2</sub> Measurement .....	77
3.5.1.2	Horiba MPA -720: O <sub>2</sub> Measurement .....	78
3.5.1.3	Horiba FIA-720: unburned Hydrocarbon Measurement .....	79
3.5.1.4	Horiba CLA-720: NO <sub>x</sub> Measurement .....	80
3.5.2	AVL 415 Smoke Meter .....	81
3.6	Intake Air Flow Measurement .....	83
3.7	Data Analysis .....	84
3.7.1	Cylinder Volume Calculation .....	84
3.7.2	Engine Combustion and Heat Release Analysis .....	85
3.7.2.1	Indicated Mean Effective Pressure .....	85
3.7.2.2	Indicated Specific Fuel consumption .....	86
3.7.2.3	Fuel Mass Fraction Burned Analysis .....	86
3.7.2.4	Heat Release Rate .....	88
3.7.2.5	Cumulative Heat Release .....	89
3.7.2.6	Ignition Delay .....	90
3.7.2.7	Combustion Efficiency .....	90
3.7.3	Engine Efficiencies Calculation .....	90
3.8	Fuel Injection Calibration .....	91
3.8.1	Diesel Direct Injector Calibration .....	92
3.8.1.1	Setup .....	92
3.8.1.2	Results .....	92
3.8.2	Port Fuel Injector Calibration .....	96

3.8.2.1	Setup .....	96
3.8.2.2	Results .....	96
3.9	Lambda Calculation Based on Exhaust Gas Composition.....	97
3.10	Summary.....	99
Chapter 4. Thermodynamic and Emission Analysis of Diesel-Ethanol Dual Fuel Operation 100		
4.1	Introduction .....	100
4.2	Experiments.....	100
4.3	Test Conditions.....	101
4.4	Results and Discussion.....	102
4.4.1	Effect of Intake Air Temperature and EGR with 60% Substitution Ratio 102	
4.4.2	Comparison of Single and Split Diesel Injection with 60% Substitution Ratio and Intake Air Temperature of 150°C.....	110
4.4.3	Effect of Substitution Ratio with Single Diesel Injection, Intake Air Temperature of 150°C, and no EGR .....	113
4.5	Summary .....	118
Chapter 5. Thermodynamic and Emission Analysis of Diesel-Gasoline Dual Fuel Operation 120		
5.1	Introduction .....	120
5.2	Experiments.....	120
5.3	Test Conditions.....	121
5.4	Results and Discussion.....	122
5.4.1	Effect of Intake Air Temperature and EGR (Exhaust Gas Recycling) with 60% Substitution Ratio .....	122
5.4.2	Comparison of Single and Split Diesel Injection with 60% Substitution Ratio and Intake Air Temperature of 150°C.....	130
5.4.3	Effect of Substitution Ratio with Single Diesel Injection, Intake Air Temperature of 150°C, and no EGR .....	135

5.5	Summary .....	141
Chapter 6. Comparison of Diesel-Ethanol and Diesel-Gasoline Dual Fuel Operations 143		
6.1	Introduction .....	143
6.2	Thermodynamic and Emission Comparison at Various Intake Conditions with 60% Substitution Ratio and Single Diesel Injection.....	144
6.3	Thermodynamic and Emission Comparison with Varying Injection Timing and Ignition Delay with Constant Intake Conditions.....	151
6.4	Summary .....	156
Chapter 7. In-cylinder Optical Measurements and Analysis of Dual Fuel Combustion 159		
7.1	Introduction .....	159
7.2	Optical Measurement Setup .....	159
7.3	Test Conditions.....	162
7.4	Results and Discussion.....	163
7.4.1	Diesel only and Diesel-Ethanol dual fuel combustion.....	163
7.4.2	Diesel-Gasoline Operation.....	175
7.5	Summary .....	183
Chapter 8. Conclusions..... 185		
8.1	Summary .....	185
8.2	Evaluation.....	185
8.2.1	Dual Fuel Operation.....	186
8.2.2	Comparing the Thermodynamic Properties and Emission Testing of Different Fuel Mixtures .....	187
8.2.3	High-Speed Optical Analysis.....	189
8.3	Future Work.....	191
References.....		194
Appendix 1: Software Screenshots .....		219

Appendix 2: Hydra Airflow Rate Graph.....	220
Appendix 3: Diesel fuel specification.....	221
Appendix 4: Diesel fuel analysis .....	222
Appendix 5: Ethanol fuel specification.....	223

## List of Figures

Figure 1.1 The Change in Euro Emission regulations [6] .....	3
Figure 1.2 Global Ethanol Production [8].....	4
Figure 2.1 Pollutant concentrations in diesel engine exhaust gas with a varied air-fuel ratio [12] [13].....	9
Figure 2.2 Relative concentration of pollutant emissions in diesel exhaust gas before after-treatment [10] [11].....	9
Figure 2.3 Typical particulate composition with an standard oxidation catalyst [12] [20].....	13
Figure 2.4 influence of the exhaust gas recirculation rate on noise, specific fuel consumption and HC and PM emissions as a function of the NOX emissions for different injection pressures at 2,000 rpm and 50% load [12] (g/kg : grams of emission per kilo grams of fuel mixture combusted).....	16
Figure 2.5 Exhaust gas flow and chemical reactions in the aftertreatment system of a modern diesel engine. Adapted from [37] [36].....	17
Figure 2.6 Typical DI Engine Heat Release Rate Diagram Identifying Different Diesel Combustion Phases [2] .....	19
Figure 2.7 Conceptual Schematic of Conventional diesel Combustion [49] [50] .....	20
Figure 2.8 In-cylinder fuel-air equivalence ratio versus temperature range for Conventional Diesel Combustion as well as alternative Diesel Combustion strategies such as LTC, HCCI and PCCI. Adapted from [51].....	21
Figure 2.9 Engine combustion research concepts compared to conventional spark ignition (SI) and Direct Injection Compression Ignition (DICI). Blue indicates a reactive fuel like diesel while orange indicates a none-reactive fuel like gasoline [52] [53].....	22
Figure 2.10 Combustion systems of direct injection diesel engine and direct injection compression ignition gasoline engine (Left) and PCCI (Right) [100].....	28

Figure 2.11 Diagram showing the temperature ranges for soot and NOX formation and the regions for conventional diesel, SI, HCCI, and diesel LTC engines [106] [107] [108].....	29
Figure 2.12 Details of combustion processes in diesel engine [117].....	33
Figure 2.13 Dual fuel pilot injection pressure-crank angle diagram [117].....	34
Figure 2.14 Heat release diagram of diesel fuel operation (engine speed 3000 rpm, engine torque 9.65 N-m) [117] .....	34
Figure 2.15 Dual fuel pilot injection heat release diagram (engine speed 3600 rpm, engine torque 5.15 N-m) [117] .....	35
Figure 2.16 Measured Engine Emissions as a Function of Gasoline Percentage [125]. .....	39
Figure 2.17 EU Fuel Ethanol Production Main Producers (source: EU FAS Posts) [143].....	45
Figure 2.18 EU Fuel Ethanol Production Main Consumption (source: EU FAS Posts) [143].....	46
Figure 2.19 A. 3D schematic showing main components of the optical engine including the extended piston assembly and optical piston. – B. Optical-access Diesel piston bowl showing location of quartz windows. – C. Comparison of optical-access and all-metal engine combustion chamber geometries [155]. .....	50
Figure 2.20 Comparison of: <b>A.</b> Pressure traces obtained on optical and all-metal engine, SOI 340°CA, simulated EGR, 1500 rpm, 2 bar IMEP, $P_{inj}$ . 1000 bar, standard Diesel fuel. – <b>B.</b> Measured engine-out HC emissions obtained on optical and all-metal engines for a SOI timing sweep, EGR 45% (simulated EGR on optical engine), standard Diesel fuel. – <b>C.</b> Piston wall temperature measurements acquired in squish zone for the optical-access (quartz/titanium) and all-metal (aluminium) pistons, 1200 rpm, SOI 350°CA, 45% EGR without skip-firing. Ensemble-averaged LIP data over 100 engine cycles at each Crank Angle position. – <b>D.</b> Heat release rates obtained on optical engine with all-metal and optical pistons showing effect of adjusting engine coolant temperature [155]. .....	51

Figure 3.1 Front View of the Ricardo Hydra Engine .....	58
Figure 3.2 Side View of the Ricardo Hydra Engine .....	58
Figure 3.3 Sectional Schematic View of the Optical Layout.....	60
Figure 3.4 Schematic View of Side Windows.....	61
Figure 3.5 Schematic View of the Piston Assembly .....	61
Figure 3.6 Schematic View of the Modified Piston Assembly .....	62
Figure 3.7 LED Position .....	63
Figure 3.8 Schematic Diagram of Common Rail Diesel Injection System .....	64
Figure 3.9 Schematic Diagram of Fuel Injection Control System.....	65
Figure 3.10 Schematic Diagram of Port Fuel Injection System .....	66
Figure 3.11 Ricardo Hydra Engine Intake System .....	68
Figure 3.12 Supercharging System .....	69
Figure 3.13 Intake Heating System.....	70
Figure 3.14 Schematic diagram of the EGR System .....	71
Figure 3.15 High Speed Camera and Copper Vapor Laser Arrangement [170] .....	75
Figure 3.16 Schematic of a single-stage image intensifier [171].....	76
Figure 3.17 High Speed Camera and Intensifier Arrangement.....	76
Figure 3.18 Schematic Diagram of NDIR Analyser [172] .....	77
Figure 3.19 Schematic Diagram of a Magneto-Pneumatic Oxygen Analyser [172] ....	79
Figure 3.20 Schematic Diagram of a FID Analyser [173] .....	80
Figure 3.21 Schematic Diagram of a Chemiluminescence Detector [174] .....	81
Figure 3.22 Schematic Diagram of AVL 415 Smoke Meter Measuring Principle [192] .....	82
Figure 3.23 Teledyne Hastings Laminar Flow Element Flowmeter .....	83

Figure 3.24 Four-Stroke Engine p-V Diagram [176].....	85
Figure 3.25 Definitions of Flame-development Angle, $\Delta\theta_d$ , and Rapid-burning Angle, $\Delta\theta_b$ , on A Mass Fraction Burned Curve [178]. .....	87
Figure 3.26 Definitions of Efficiencies [179] .....	91
Figure 3.27 Injection Rate Profile for Delphi VOC Injector .....	93
Figure 3.28 Injection Rate Profile for Delphi VOC Injector with Split Injections.....	94
Figure 3.29 Effect of First Injection on Second Injection in Split Injection Operations .....	95
Figure 3.30 Injection Rate Profile for Bosch EV 14 Injection Valve.....	96
Figure 4.1 Comparison of Engine Performance, Emission and Combustion Characteristics at Different Intake Conditions, with 60% Ethanol Substitution Ratio and Single Diesel Injection .....	104
Figure 4.2 In-Cylinder Pressure and HRRR at Different Single SOI with 100°C Intake Temperature, and 60% Ethanol Substitution Ratio.....	105
Figure 4.3 In-Cylinder Pressure and HRRR at Different Intake Conditions when SOI is 25° CA BTDC, and 60% Ethanol Substitution Ratio .....	106
Figure 4.4 In-Cylinder Pressure and HRRR at Different Intake Conditions when SOI is 5° CA BTDC, and 60% Ethanol Substitution Ratio .....	107
Figure 4.5 In-Cylinder Pressure and HRRR with the Optimized SOI at Different Intake Conditions .....	108
Figure 4.6 Engine Performances and Emission with the Optimized SOI at Different Intake Conditions.....	109
Figure 4.7 Comparison of Engine Performance, Emission and Combustion Characteristics Between Single and Split Diesel Injection with 60% Ethanol Substitution Ratio, 150°C Intake Temperature, and No EGR.....	111

Figure 4.8 In-Cylinder Pressure and HRRR with Single and Split Diesel Injection when SOI of Single is 30° CA and the SOI of Split is 30°-65° CA BTDC, 150°C Intake Temperature, and 60% Ethanol Substitution Ratio ..... 112

Figure 4.9 In-Cylinder Pressure and HRRR with Single and Split Diesel Injection when SOI of Single 5° CA and the SOI of Split is 5°-40° CA BTDC, 150°C Intake Temperature, and 60% Ethanol Substitution Ratio ..... 112

Figure 4.10 Comparison of Engine Performance, Emission and Combustion Characteristics at Different Ethanol Substitutions Ratio, when Single Diesel Injection Timing is Sweeping and Constant 150°C Intake Temperature ..... 114

Figure 4.11 In-Cylinder Pressure and HRR with at Different Ethanol Substitution Ratios when Diesel SOI is 5° CA BTDC, with Constant 150°C Intake Temperature ..... 116

Figure 4.12 In-Cylinder Pressure and HRR with the Optimized SOI at Different Ethanol Substitution Rratio ..... 116

Figure 4.13 Engine Performances and Emission with the Optimized SOI at Different Ethanol Substitution Ratio ..... 117

Figure 5.1 Comparison of engine performance, emission and combustion characteristics at different intake conditions when gasoline substitution ratio is 60% and diesel injection is single injection ..... 126

Figure 5.2 In-cylinder pressure and HRRR at different single SOI when intake temperature is 100°C and gasoline substitution ratio is 60% ..... 127

Figure 5.3 In-cylinder pressure and HRRR at different intake conditions when SOI is 5 CA BTDC, gasoline substitution ratio is 60% ..... 127

Figure 5.4 in-cylinder pressure and HRRR with the optimized SOI at different intake conditions, gasoline substitution ratio is 60%..... 128

Figure 5.5 Engine performances and Emission with the optimized SOI at different intake conditions ..... 129

Figure 5.6 comparison of engine performance, emission and combustion characteristics between single and split diesel injection, as well as EGR effect, when substitution ratio is 60%, intake temperature is 150°C..... 132

Figure 5.7 in-cylinder pressure and HRRR with single injection and split injection when SOI of the single and the split are 5 and 40-5 CA BTDC respectively, intake temperature is 150°C and gasoline substitution ratio is 60%, at 0 and 40% EGR .... 133

Figure 5.8 in-cylinder pressure and HRRR with single injection and split injection when SOI of single and split are 5 and 40-5 CA BTDC respectively, intake temperature is 150°C and gasoline substitution ratio is 60% ..... 133

Figure 5.9 in-cylinder pressure and HRRR at different split SOI when intake temperature is 150°C and gasoline substitution ratio is 60% with 40% EGR..... 134

Figure 5.10 comparison of engine performance, emission and combustion characteristics at different gasoline substitutions without EGR, when single diesel injection timing is sweeping and intake temperature is constant 150°C ..... 137

Figure 5.11 in-cylinder pressure and HRR with the late SOI at different gasoline substitution ratio..... 139

Figure 5.12 in-cylinder pressure and HRR with the early SOI at different gasoline substitution ratio..... 139

Figure 5.13 Engine performances and Emission with the optimized SOI at different gasoline substitution ratio ..... 140

Figure 6.1 Comparison of engine performance, emission and combustion characteristics between diesel-ethanol and diesel-gasoline operations at different intake conditions when substitution ratio is 60% with single diesel injection. .... 145

Figure 6.2 In-cylinder pressure and HRRR for both diesel-ethanol and diesel-gasoline operations when diesel SOI is 5°CA BTDC at 100°C intake temperature and 60% of substitution ratio without EGR. .... 146

Figure 6.3 In-cylinder pressure and HRRR for both diesel-ethanol and diesel-gasoline operations when diesel SOI is 5°CA BTDC at 150°C intake temperature and 60% of substitution ratio without EGR. .... 147

Figure 6.4 In-cylinder pressure and HRRR with early diesel SOI at 150°C intake temperature and 60% of substitution ratio without EGR. ....	148
Figure 6.5 Engine performances and Emission with the optimized SOI at 150°C intake temperature and 60% of substitution ratio without EGR. ....	149
Figure 6.6 Comparison of engine performance, emission and combustion characteristics between diesel-ethanol and diesel-gasoline operations when substitution ratio is 60%, intake temperature is 150°C and no EGR with single diesel injection.....	152
Figure 6.7 Comparison of engine performance, emission and combustion characteristics between diesel-ethanol and diesel-gasoline operations when substitution ratio is 60%, with different intake temperature, and no EGR, in relation to Ignition delay. ....	153
Figure 7.1 Sectional Schematic View of the Optical Layout.....	160
Figure 7.2 High Speed Imaging using High Speed Intensifier .....	161
Figure 7.3 High Speed Imaging using Copper Vapor Laser .....	162
Figure 7.4 Image of combustion chamber through the glass piston without combustion .....	163
Figure 7.5 Direct combustion Image of diesel combustion without intensifier at 5CA BTDC of SOI.....	165
Figure 7.6 Direct combustion Image with intensifier when substitution ratio is 60%, diesel SOI is 5CA BTDC .....	167
Figure 7.7 Direct combustion Image with intensifier when substitution ratio is 60%, diesel SOI is 28CA BTDC .....	168
Figure 7.8 Direct combustion Image with intensifier when substitution ratio is 60%, diesel injection is split injection and SOI is 63-28CA BTDC .....	170
Figure 7.9 Direct combustion Image with intensifier when substitution ratio is 60%, diesel injection is split injection and SOI is 30-5CA BTDC .....	171

Figure 7.10 Direct combustion Image with intensifier when substitution ratio is 45%, diesel SOI is 42CA BTDC .....	173
Figure 7.11 Direct combustion Image with intensifier when substitution ratio is 75%, diesel SOI is 15CA BTDC .....	174
Figure 7.12 Direct combustion Image with intensifier when substitution ratio is 60%, diesel SOI is 5CA BTDC .....	176
Figure 7.13 Direct combustion Image without intensifier when substitution ratio is 60%, diesel SOI is 5CA BTDC .....	177
Figure 7.14 Direct combustion Image with intensifier when substitution ratio is 60%, diesel SOI is 50CA BTDC .....	178
Figure 7.15 Direct combustion Image with intensifier when substitution ratio is 60%, diesel injection is split injection and SOI is 40-5CA BTDC .....	179
Figure 7.16 Direct combustion Image without intensifier when substitution ratio is 60%, diesel injection is split injection and SOI is 40-5CA BTDC .....	181
Figure 7.17 Direct combustion Image with intensifier when substitution ratio is 75%, diesel SOI is 40CA BTDC .....	182
Figure A1.0.1 Screenshot of EC-Lab Software .....	219
Figure A1.0.2 Screenshot of Data Acquisition Software .....	219
Figure A2.0.1 Hydra Airflow Rate Graph [169] .....	220
Figure A3.0.1 Diesel fuel specification.....	221
Figure A4.0.1 Diesel fuel analysis .....	222
Figure A5.0.1 Ethanol fuel specification .....	223

## List of Tables

Table 1.1 EU Emission Standards for Diesel Passenger Cars [5] .....	3
Table 2.1 Euro VI emission limits for different on-road HD engines and vehicles. Source: Regulation No 49 [17] .....	10
Table 2.2 Comparison of Traditional and HCCI Combustion Modes [75] .....	24
Table 3.1 Ricardo Hydra Engine Specifications .....	58
Table 3.2 Diesel Fuel Injector Specification .....	64
Table 3.3 Port Fuel Injector Specification .....	66
Table 3.4 Fuel Properties .....	67
Table 3.5 Copper Vapour Laser Specifications .....	75
Table 4.1 Fixed Testing Parameters .....	101
Table 4.2 Variable Testing Parameters .....	102
Table 5.1 Fixed Testing Parameters .....	121
Table 5.2 Variable Testing Parameters .....	121
Table 6.1 Comparison of gasoline and ethanol fuel properties [187] .....	143
Table 7.1 Optical Setting of Camera, Lens, Intensifier, Lens, Laser .....	160



# Chapter 1. Introduction

## 1.1 Background and Context

These days, internal combustion (IC) engines, and the industries that develop and manufacture them and support their use, play a dominant role in the fields of power, propulsion, and energy. In 1876, Nikolaus Otto first developed the spark-ignition (SI) engine, and Rudolf Christian Karl Diesel invented the compression-ignition (CI) engine in 1892 [1]. Ever since their invention, as our knowledge of engine processes has grown, new technologies become available, demand for new forms of engine increase, and environmental limitations on engine use changed, these engines have continued to advance. The past three decades have seen an accelerated development in engine research and development as the issues of air pollution, fuel cost, and market competitiveness have become more and more significant [2].

In more recent years concern over exhaust gas CO<sub>2</sub> emissions from motor vehicles has been increasing. To battle this, the automotive industry has been endorsing diesel cars as the cleaner choice compared to gasoline cars in Europe, because of their superior efficiency due to their overall lean-burn mixture, lower pumping loss as well as the greater compression ratio [3]. The efficiency of a typical SI engine can go up to 38%, compared to Diesel engines efficiency of up to 45% in a passenger car and up to 50% in large diesel engines [4]. Because of their superior fuel economy, diesel engines are the dominant powerplant for commercial vehicles, off-road vehicles and marine applications. Although diesel engines can produce less emissions of the regulated pollutants, such as carbon monoxide, hydrocarbons and nitrogen oxides, than a SI gasoline engine, they produce much more soot/Particulate Matter (PM). However, gasoline vehicles fitted with high efficiency 3-way catalyst to the stoichiometric SI engine, produce less NO<sub>x</sub> emissions than diesel vehicles. With the increased number of vehicles and the heightened concern with air quality, the ever more stringent vehicle emission standard has been introduced as shown in Table 1.1

imposed by the European Commission since 1992 for compression ignition (Diesel) passenger cars.

*Table 1.1 EU Emission Standards for Diesel Passenger Cars [5]*

Stage	Date	CO	HC+NOx	NOx	PM	PN
		g/km				
Euro I	1992.07	2.72	0.97	–	0.14	–
Euro II, IDI	1996.01	1.0	0.7	–	0.08	–
Euro II, DI	1996.01	1.0	0.9	–	0.10	–
Euro III	2000.01	0.64	0.56	0.50	0.05	–
Euro IV	2005.01	0.50	0.30	0.25	0.025	–
Euro Va	2009.09	0.50	0.23	0.18	0.005	–
Euro Vb	2011.09	0.50	0.23	0.18	0.005	6.0x10 <sup>11</sup>
Euro VI	2014.09	0.50	0.17	0.08	0.005	6.0x10 <sup>11</sup>

While Figure 1.1 below illustrates the percentage of change in these regulations since their first iteration.

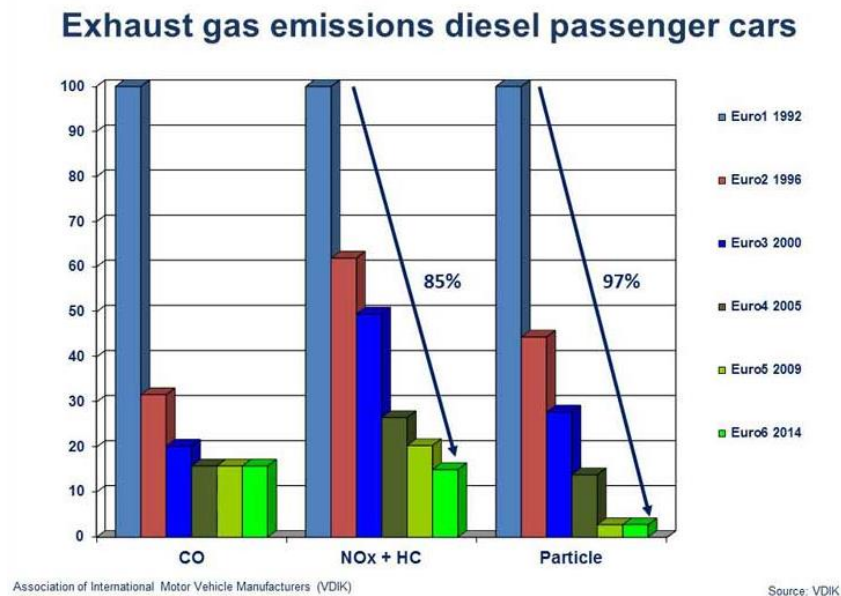


*Figure 1.1 The Change in Euro Emission regulations [6]*

In addition to operating direct injection diesel fuel, the CI engine can be adopted to operate with more volatile fuel premixed with air through port-fuel injection to reduce the pollutant emission, known as the dual fuel operation. When a low carbon fuel is used as the port-injection premixed fuel in the dual fuel operation, they can produce both lower pollutant emissions and CO<sub>2</sub> emission, e.g. diesel-CNG/LNG dual fuel engine [7]. In order to minimise the total life-cycle CO<sub>2</sub> emissions, it would be desirable to use renewable fuels, such as ethanol which is mostly produced from sugar canes, or corn, in significant quantities in some regions of the world, especially in Brazil and United States as illustrated in Figure 1.2 below [8].

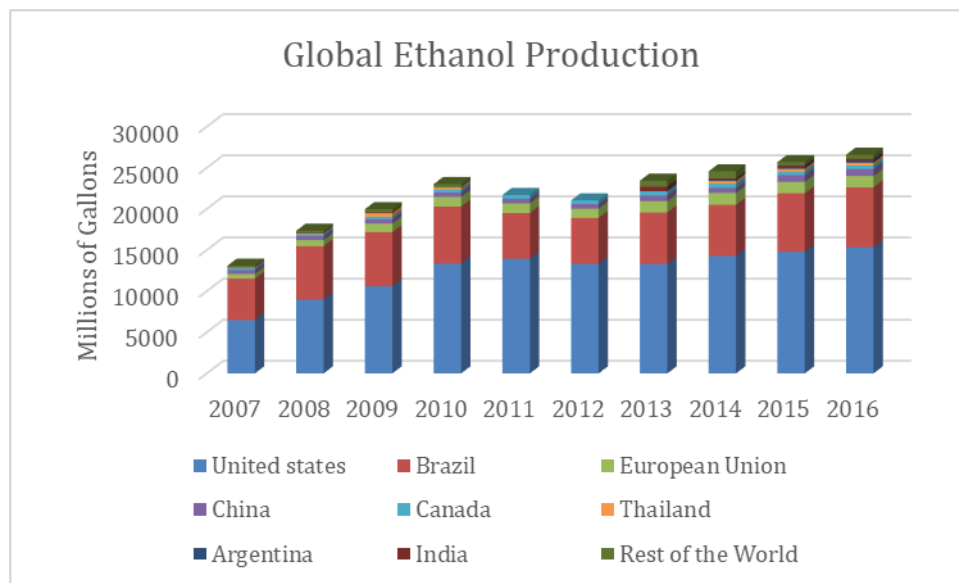


*Figure 1.2 Global Ethanol Production [8]*

However, in order to minimise the emissions and fuel consumptions from the dual-fuel engines, better understanding of the in-cylinder mixture formation, autoignition and combustion of the dual-fuel operation is required. The single cylinder optical engine is well suited for such studies it allows the application of both qualitative and quantitative, non-intrusive, optical diagnostic methods to gain a detailed insight of the mixing, combustion and other in-cylinder processes.

## 1.2 Scope and Objectives

The main aim of this research project is to study the combustion, engine performance and emission characteristics of the diesel-gasoline and diesel-ethanol dual fuel engine operations by means of collecting and comparing thermodynamics, and emission data,

as well as in-cylinder optical analysis of the fuel injection, mixture, and combustion, using high speed video processing. The objectives of this study include

1. Investigation of combustion and heat release characteristics and engine performance of the diesel-ethanol and diesel-gasoline dual fuel operation by means of in-cylinder pressure measurements.
2. Characterisation of the engine exhaust emissions when operating in dual fuel operations under different premixed/direct injection fuel ratio (substitution) and fuel injection strategies.
3. Determination of the optimum fuelling and injection strategies for the diesel-ethanol and diesel-gasoline dual fuel operations for the single cylinder optical engine.
4. Investigation of the in-cylinder fuel injection, mixture, and combustion in Dual fuel operations using optical techniques.
5. Comparison of the engine's performance, exhaust emission, and thermodynamic properties, between standard diesel fuel operation and the two dual fuel operations.

This study allowed for the collection of not only the thermodynamic properties and emission output of two variety of dual fuel operation, namely diesel-ethanol and diesel-gasoline, in a compression ignition diesel engine, it also resulted in a collection of high-speed images from the combustion process from injection, start of combustion, combustion duration, and combustion flame intensity, for both of the two dual fuel operations under investigation.

### 1.3 Overview of Thesis

Following the brief introduction in Chapter 1, a review of the most recent work and literature on the relevant research is provided in Chapter 2. The basics of CIDI diesel engine, its combustion process, and emissions are presented, and furthermore, an explanation of variety of advanced combustion techniques and concepts reviewed. After that, discussion is given to the benefits and the need for dual fuel technology and alternative fuels in today's world, the range and availability of different fuels to replace fossil fuels. This is followed by describing the techniques available in performing optical analysis on the fuel injection, mixture and combustion.

In Chapter 3, the experimental facilities and measurement equipment employed in this research are described and discussed. The single cylinder optical research engine and its components, the intake and exhaust system, the fuel injection system, the data acquisition system, and the emission sampling equipment, are defined in detail. The data analysis procedure is clarified prior to the description of fuel injector calibration process and its results, as well as the method used for the calculation of the equivalence ratio of engine operation at different conditions.

Chapter 4 details the setup and the procedure for collecting the required data for thermodynamic and emission analysis of the engine in diesel-ethanol dual fuel operation under several testing conditions, substitution ratios, and injection strategies, as well as discussing the results, and some complications faced and their resolution.

Chapter 5 presents the setup and the procedure for collecting the required data for thermodynamic and emission analysis of the engine in diesel-gasoline dual fuel operation under several testing conditions, substitution ratios, and injection strategies will be discussed in detail, as well as discussing the results, and some complications faced and their resolution.

Chapter 6 focuses on the comparison of the thermodynamic and emission data and the results from the previous two chapters, diesel-ethanol and diesel-gasoline dual fuel operations, and their results with diesel only engine operations.

Chapter 7 presents all the data collected from the high-speed videos of optical experiments performed on various engine settings and selected different fuels mixtures used, as well as the procedure for collecting this data, and the comparison and discussion of their results.

Finally, Chapter 8 concludes all the experimental results and findings, as well as discussing the possible and recommended work to be performed in this subject matter.

# Chapter 2. Literature Review

In this chapter, some of the available literature related to the subject of this study will be reviewed in order to allow for better understanding of the latest techniques available and the procedures required for the testing, as well as the results and the outcomes of each test.

## 2.1 History of Diesel CI Engine

The engineer Rudolf Diesel filed a patent with the Imperial Patent Office in Berlin for a “new rational heat engine” on February 27<sup>th</sup> of 1892, and a year later, on February 23<sup>rd</sup> of 1893, the patent DRP 67207 was granted to him, for the “Working Method and Design for Combustion Engines” dated 28<sup>th</sup> of February, 1892.

Direct-injection diesel engines of today, are more tough, powerful, robust, and dependable than gasoline engines, and they are also more efficient in fuel consumption. Diesel engines are workhorse engines. That’s why they can be found powering heavy duty trucks, buses, tractors, and trains, as well as large ships, bulldozers, cranes, and other construction machinery. Diesel engines of today, and in the future, will show even further improvements. They will be more fuel efficient, much cleaner in terms of emissions, as well as more flexible in the fuels they can use [4] [9].

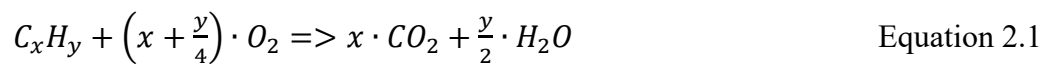
Current diesel engines, inject fuel directly into the engine’s cylinder using very small computers to deliver exactly the right amount of fuel that is needed. All functions in a modern diesel engine are controlled by an electronic control module that communicates with a complex collection of sensors placed at calculated locations throughout the engine to monitor and control all things such as engine speed, coolant and oil temperatures, as well as the piston position. Close electronic control means that fuel burns more carefully, delivering more power, better fuel economy, and less emissions than initial diesel engines could accomplish.

Modern direct injection diesel engines produce low amounts of carbon dioxide (CO<sub>2</sub>), carbon monoxide(CO), and unburned hydrocarbons (UHC), as well as reactive

nitrogen compounds (NO<sub>x</sub>) and particulate matter (PM) have been reduced by more than 90% in the past three decades. However, NO<sub>x</sub> and PM emissions remain at relatively high levels. NO<sub>x</sub> contributes to acid rain and smog, while serious health effects have been related with exposures to high levels of PM [4] [9].

## 2.2 Emissions

All internal combustion engines operate by converting chemical energy in the fuel to mechanical power. Fuel is a mixture of hydrocarbons, which during an ideal combustion process would produce water vapor (H<sub>2</sub>O) and carbon dioxide (CO<sub>2</sub>) only. Exhaust gases are primarily made up of CO<sub>2</sub>, H<sub>2</sub>O and the portion of engine charge air left unused. Diesel fuel and gasoline fuel may both be specified with the empirical formula C<sub>x</sub>H<sub>y</sub>, where an ideal stoichiometric combustion process would yield:



The following, shows the typical range of volumetric concentrations of these gases in the exhaust:

- CO<sub>2</sub> : 2% to 12%
- H<sub>2</sub>O : 2% to 12%
- O<sub>2</sub> : 3% to 17%
- N<sub>2</sub> : 79%

The concentration of these exhaust gases depend on the engine load, where increasing the engine load, the concentration of CO<sub>2</sub> and H<sub>2</sub>O increases and the concentration of O<sub>2</sub> decreases. None of these principal diesel emissions, with the exception of CO<sub>2</sub> for its greenhouse gas properties, have harmful environmental or health effects [10] [11].

Diesel emissions also include pollutants that can have harmful environmental and/or health effects, most of which are caused by a variety of non-ideal combustion processes, such as incomplete combustion of the diesel fuel, reactions between components of the mixture, under high pressure and temperature, combustion of the engines oil based lubricants and oil additives, as well as combustion of components of the diesel fuel that are non-hydrocarbon, such as fuel additives and sulphur compounds. Most common pollutants of diesel combustion include, nitrogen oxides (NO<sub>x</sub>), unburned hydrocarbons (HC), particulate matter (PM), and carbon monoxide

(CO) [10] [11]. Pollutant concentrations in diesel engine exhaust gas with a varied air-fuel ratio is illustrated in Figure 2.1 [12].

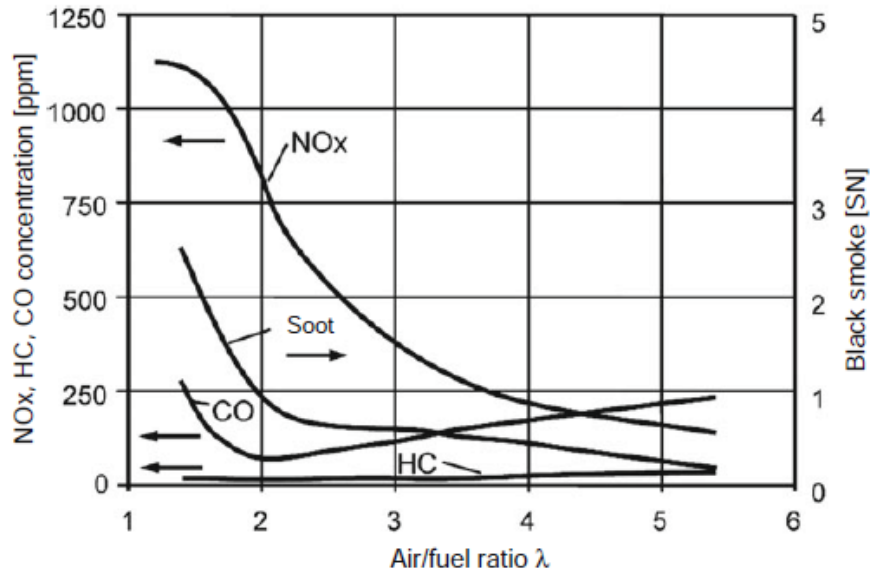


Figure 2.1 Pollutant concentrations in diesel engine exhaust gas with a varied air-fuel ratio [12] [13]

Total concentration of pollutants in diesel exhaust gases typically amounts to some tenths of one percent, which is schematically illustrated in Figure 2.2 [10] [11].

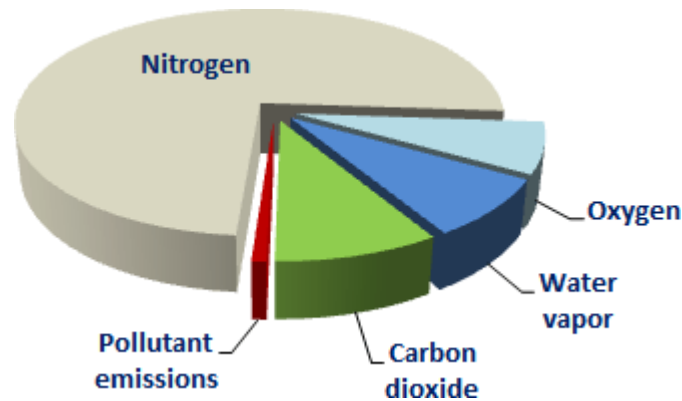


Figure 2.2 Relative concentration of pollutant emissions in diesel exhaust gas before after-treatment [10] [11]

Great demands are made by the market, fuel economy, and regulatory requirements, on diesel engine technology, as well as advanced gasoline concepts and hybrid electric vehicles that are applying pressure in competitive technology, and therefore, diesel engine developers are replying by the use of variety of techniques such as, advanced fuel injection technologies, exhaust gas recirculation (EGR) control, advanced and two-stage turbocharging, variable valve actuation, closed-loop

combustion control, and advanced model-based control. Modern diesel engines are also equipped with emission after-treatment devices like NO<sub>x</sub> reduction catalysts and particulate filters, produce much lower levels of pollutants [10] [11].

Advanced diesel engines [14] are now approaching a specific power output of 70 kW per litre of fuel (70 kW of mechanical power for every litre of diesel fuel combusted) along with 24 bar of brake mean effective pressure (BMEP), where some of these diesel engine developments are allowing these engines to approach Euro VI (Table 2.1) compliant engine exhaust emission levels [15] [16].

*Table 2.1 Euro VI emission limits for different on-road HD engines and vehicles. Source: Regulation No 49 [17]*

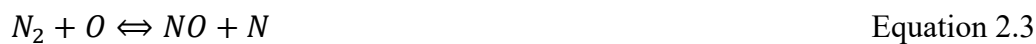
Pollutant	Unit	WHSC (CI)	WHTC (CI)	WHSC (PI)
Nitrogen oxides (NO <sub>x</sub> )	g/kWh	0.40	0.46	0.46
Carbon monoxide (CO)	g/kWh	1.50	4.00	4.00
Total unburnt hydrocarbons (HC)	g/kWh	0.13	0.16	n/a
Non-methane hydrocarbons (NMHC)	g/kWh	n/a	n/a	0.16
Methane (CH <sub>4</sub> )	g/kWh	n/a	n/a	0.50
Particulate matter (PM) mass	g/kWh	0.010	0.010	0.010
Particulate number (PN)	#/kWh	8.0x10 <sup>11</sup>	6.0x10 <sup>11</sup>	6.0x10 <sup>11</sup>
Ammonia (NH <sub>3</sub> )	ppm	10	10	10

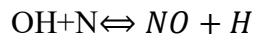
### 2.2.1 Nitrogen Oxides (NO<sub>x</sub>)

Only the combinations NO and NO<sub>2</sub> (nitrogen monoxide and nitrogen dioxide) from the different nitrogen oxides, including NO, NO<sub>2</sub>, N<sub>2</sub>O, N<sub>2</sub>O<sub>3</sub>, N<sub>2</sub>O<sub>5</sub>, are produced in considerable quantities and the description NO<sub>x</sub> (nitrogen oxides) is commonly used as short for the total NO and NO<sub>2</sub>.

The formation of thermal NO, is the main mechanism for the production of NO<sub>x</sub>. Zeldovich described it for the first time in 1946 [12] [18].

Particularly, the following elementary reactions take place:





Equation 2.5

The Zeldovich chain reaction is describe by equations 2.3 and 2.4, with the presence of elementary oxygen (O),  $\text{N}_2$  produces NO and N, where the molecular nitrogen ( $\text{N}_2$ ) formed, becomes NO and O by reacting with  $\text{O}_2$  in the following stage, which completes the cycle and the reaction chain starts once more. Equation 2.5 defines the formation of NO in fuel rich zones, such as the areas located behind the flame front.

The basic condition for the start of the Zeldovich reactions, is the presence of atomic oxygen formed from molecular oxygen at temperatures beyond 1927°C, see equation 2.2, which follow equations 2.3 and 2.4. Therefore, one requirement for the formation of NO is highest temperatures, more accurately, local highest temperatures, not average combustion chamber temperatures. The presence of excess oxygen is the second requirement for the formation of NO, that is local excess air [12] [18].

In gasoline engines, ideal conditions for the formation of  $\text{NO}_x$  are present when  $\lambda=1.1$ . In diesel engine exhaust gas, maximum concentration of  $\text{NO}_x$  moves to a rather higher air fuel ratio. Figure 2.1 [12] [13] illustrated the concentrations of the different pollutants, as a function of the air fuel ratio  $\lambda$ . As  $\lambda$  drops, the  $\text{NO}_x$  concentration curve rises continuously, which can be associate with the exhaust gases increasing temperature. Although the amount of oxygen is reducing, the increasing process temperature enables the increase of the  $\text{NO}_x$  concentration to values as high as  $\lambda=2$ . Free oxygen is no longer sufficiently available below  $\lambda=2$  as the exhaust gas temperature continues to increase. A local maximum is produced as the gradient of the  $\text{NO}_x$  concentration decreases as a function of the air fuel ratio.

The Zeldovich reactions are equilibrium reactions and their equilibrium limits are created as a function of temperature. Though, engine combustion processes are so instant that the equilibrium concentrations are usually not achieved and the actual  $\text{NO}_x$  concentrations are lower than what would be achieved at thermal equilibrium. Conversely, according to equations 2.3 and 2.4, the temperature drop in combustion chamber during the expansion stage causes reverse reactions to “freeze”. NO does not change considerably below approximately 1727°C anymore. Consequently, in the actual exhaust gas, the  $\text{NO}_x$  concentrations are greater than the equilibrium concentrations. Subsequently, equilibrium reactions alone cannot predict  $\text{NO}_x$

emissions, but only by the aid of the reaction kinetics and by including the time order of the combustion that actually occurs.

In diesel engines, the process order can significantly affect NO<sub>x</sub> emissions. Therefore, the combustion temperature could be limited by cooling the charge air and recirculated exhaust gas, and also by retarding injection and combustion after TDC. Exhaust gas recirculation (EGR) lowers the oxygen supply and, therefore, reduces the formation of NO<sub>x</sub> directly. Simultaneously, the rate of combustion is reduced by the lower oxygen concentration, which in turn limits the local highest temperatures. The local highest temperatures are further reduced during exhaust gas recirculation by the higher specific heat capacity of the triatomic gases (CO<sub>2</sub> and H<sub>2</sub>O) in the recirculated exhaust gas.

1% to 10% of the total NO<sub>x</sub> emissions in gasoline engines is made up of NO<sub>2</sub>, and 5% to 15% in diesel engines. Higher concentrations are also evident in the lower part load range at similarly low exhaust gas temperatures [12] [13]. NO<sub>2</sub> forms in an engine from NO by reacting with HO<sub>2</sub> and OH radicals. The most likely equation is:



The chemical equilibrium for NO<sub>2</sub> is practically complete at ambient temperature. NO reacts in the atmosphere with ozone, when there is incident light, to become NO<sub>2</sub>. Depending on the ambient conditions, equilibrium is achieved after a few hours to days. For diesel engine combustion, other mechanisms of NO formation, such as rapid NO from the reaction of N<sub>2</sub> with fuel radicals, NO from fuel based nitrogen, or the formation of NO from N<sub>2</sub>O have a tendency to be of secondary importance.

### **2.2.2 Particulate Matter (PM)**

A motored vehicle's particulate matter emissions, are the total mass of solids and attached volatile or soluble elements, as stated by the legislative test conditions. The test conditions are defined precisely: an exhaust gas sample is diluted with filtered ambient air and cooled to a maximum of 528<sup>o</sup>C [12] [19]. The total mass of the particulate matter is concluded by weighing under distinct conditions, after it is divided onto a defined and conditioned sample holder. Figure 2.3 illustrates the average composition of particulate matter [12] [20]. The particulates primarily consist of soot. The second largest fraction of particulate matters, comprises of organic

compounds comprising of unburned hydrocarbons, which may arise from the fuel itself or the lubricating oil [12].

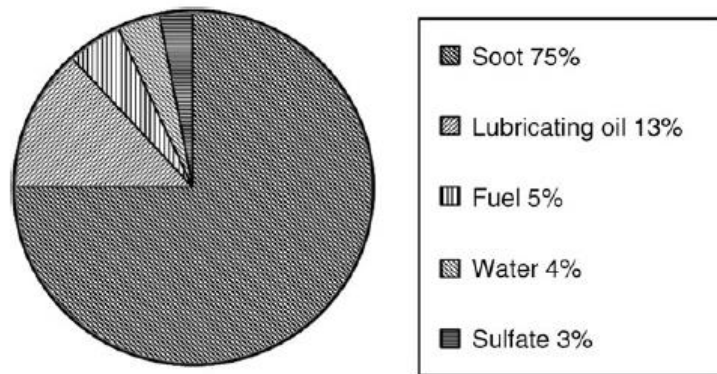


*Figure 2.3 Typical particulate composition with an standard oxidation catalyst [12] [20]*

The sulphur content of the fuel and the engine oil, essentially determines The particulates' sulphate fraction. The sulphur oxidizes into  $\text{SO}_2$  during combustion, and into  $\text{SO}_3$  at exhaust gas temperatures above  $450^\circ\text{C}$ . The downstream exhaust gas after treatment in an oxidation catalytic converter can also enabled the latter oxidation procedure [12] [21]. The development of sulphate ions to create sulfuric acid ( $\text{H}_2\text{SO}_4$ ), is triggered by interaction with water, which condenses on the particulates in the cooled exhaust gas. Lubricating oil or fuel additives produce metal oxides, which are only present in particulate emissions in traces. When an additive is combined into the fuel for particulate filter regeneration, these oxides can take on a substantial percentage of the particulate mass.

Figure 2.3 illustrates the composition of particulate matter, which corresponds to the average value of measurements in a variety of cars and can differ greatly depending on the vehicle type and operation. Therefore, a commercial vehicle engine running at high load has a greater portion of elementary carbon. The portion of hydrocarbons in cars running at part load can considerably exceed the value stated in Figure 2.3. Relative to mass, soot comprises the largest portion of particulate matter. Soot is mainly created in zones lacking air. In older pre chamber engines models, fuel coking partly creates large soot particulates, in areas such as the wall films [12], which are then visible in the exhaust gas. In modern direct injection diesel engines, the particulates are typically considerably smaller and therefore no longer visible in the exhaust gas. The production processes is also noticeably different.

### **2.2.3 Hydrocarbons (HC)**

In diesel engines, when poorly prepared fuel reaches areas where the temperature is no longer sufficient for combustion, may produce unburned hydrocarbons (HC). These type of conditions happen in the lower part load range, when there is considerable excess air. Atomizing the fuel is the main purpose of an injection system in order to prepare the fuel adequately so that even at low temperatures it can evaporate completely.

Other sources of HC emissions can be locally highly rich mixture regions, such as when fuel sprays make contact with the combustion chamber wall. HC emissions increase during cold start as complete evaporation cannot be guaranteed. Similar to the combustion of leaner mixtures in gasoline engines, misfires are usually not observed in diesel engines, since a range with approximately stoichiometric mixing is always established when using direct injection, and therefore, with ideal conditions for auto-ignition.

Another source of HC emissions is the fuel contained in the nozzle holes as well as the injection nozzle's sac hole after the end of injection. This fuel evaporates during the expansion phase at temperatures far below the limit necessary for oxidation and is forced into the exhaust system unburned. Although in recent years, by minimizing the volume of the sac hole, this source of HC emissions has been significantly reduced [12] [22]. An oxidation catalytic converter can further reduce both hydrocarbons and carbon monoxide [12] [21].

### **2.2.4 Exhaust Gas Recirculation**

Diesel engines have characteristically high thermal efficiencies, as a result of their high compression ratio and operating with low fuel consumption. The auto-ignition is achieved from the high temperatures produced by the high compression ratio, and less thermal energy from the engine is discharged in the exhaust due to the resulting high expansion ratio. In order to enable complete combustion, the extra oxygen in the cylinders is essential, as well as compensating for the non-homogeneity in the fuel distribution. Nevertheless, as locally stoichiometric air fuel ratios overcome in such heterogeneous combustion procedures, high flame temperatures are more dominate [23]. Subsequently, due to the high flame temperature in the presence of abundant

oxygen and nitrogen, diesel engine combustion outputs high levels of NO<sub>x</sub> emissions [24] [25] [26].

Keeping the combustion chamber temperatures down, is the most effective way of lowering levels of NO<sub>x</sub> emission. While practical, it also reduces the thermal efficiency of the engine, which makes it a very unsuccessful method in reducing NO<sub>x</sub> levels. Diluting the air fuel mixture with a non-reacting parasite gas is possibly the simplest practical way of decreasing maximum flame temperature. During combustion, this gas absorbs energy, without adding any energy input. Any non-reacting gas would work as a diluent, and the outcome of this process is a lower flame temperature [27].

Exhaust gas recirculation, or EGR for short, is the procedure of introducing exhaust gas into the fresh air from the intake, in order to dilute the air and fuel charge, and thus lowering the combustion temperature. LTC engines typically use a large amount, more than 20%, of EGR, in order to keep combustion temperatures low as well as increasing combustion duration.

EGR has been widely recognised as a powerful tool for reducing NO<sub>x</sub> emissions. It significantly lowers in-cylinder temperature and reduces oxygen concentration which suppresses the NO<sub>x</sub> formation. Therefore, wide-ranging studies [28] [29] [30] have been focusing on reducing NO<sub>x</sub> emission by means of utilizing EGR. In a turbocharged medium speed diesel engine, Six and Herzele [31] used cooled and high pressure loop EGR to reduce NO<sub>x</sub> emissions. It was found that NO<sub>x</sub> emissions were substantially reduced by the use of EGR. However, there were penalties in terms of CO emissions and fuel consumption. In order to overcome excessive CO and HC emissions when operating under a high level of EGR, Lee and Choi [32] applied a main-post injection strategy to improve combustion efficiency as well as soot emissions. Consequently, a noticeable improvement of CO, THC and soot emission could be obtained, without penalty in NO<sub>x</sub> emissions. In Li's [33] work, the combination of a pilot injection strategy and cooled EGR was utilized to improve NO<sub>x</sub> emissions in a single cylinder diesel engine. The results showed that pilot injection could suppress NO<sub>x</sub> emissions as well as maximum pressure rise rate [34].

The influence of exhaust gas recirculation on brake specific fuel consumption, noise, HC, and PM emission levels, as a function of the NO<sub>x</sub> emissions, is illustrated in Figure 2.4 below [12].

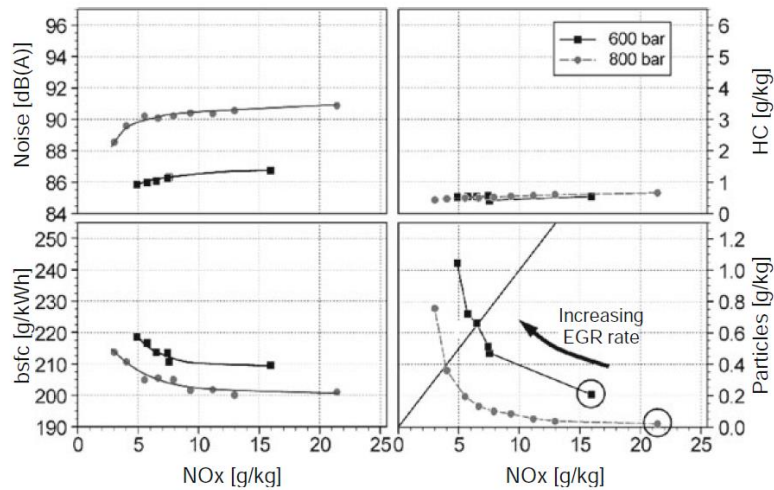


*Figure 2.4 influence of the exhaust gas recirculation rate on noise, specific fuel consumption and HC and PM emissions as a function of the NO<sub>x</sub> emissions for different injection pressures at 2,000 rpm and 50% load [12] (g/kg : grams of emission per kilo grams of fuel mixture combusted)*

## 2.2.5 Exhaust Gas Aftertreatment

Exhaust gas after treatment is another widely utilized technology in engines for the main purpose of reducing the emission output from the engine, in order to meet strict emission regulations. Diesel oxidation catalyst (DOC), diesel particulate filter (DPF), and selective catalytic reduction (SCR) system are the main aftertreatment technologies fitted to modern diesel engines [35]. The diagram of Figure 2.5 below, illustrates the exhaust aftertreatment system, highlighting the exhaust gas flow and main chemical reactions that occur in each stage [36].

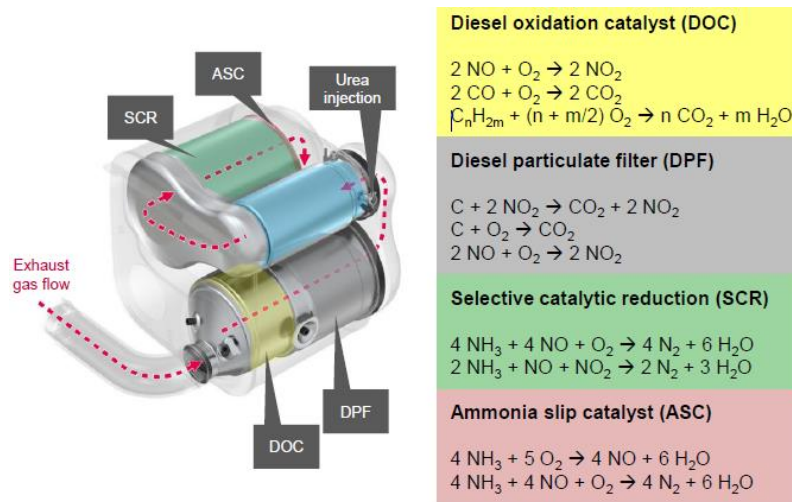


*Figure 2.5 Exhaust gas flow and chemical reactions in the aftertreatment system of a modern diesel engine. Adapted from [37] [36]*

The exhaust coming from the engine first passes through the DOC. It is mainly used for oxidizing nitrogen oxide to nitrogen dioxide, substances that together create NO<sub>x</sub>. However, the DOC also has another important function, which is related to regeneration of the DPF. Regeneration of the filter needs to be done in order to empty the filter from soot. The DPF comes after the DOC in the exhaust aftertreatment system. The DPF removes most of the particles, more than 99%, from the exhaust gases as soot accumulates in a ceramic honeycomb monolith. The device requires periodical “active” and/or “passive” regeneration to burn off the trapped soot and prevent it from blocking [38]. The DOC oxidises hydrocarbons, carbon monoxide, and organic fractions of PM produced by incomplete combustion and fuel injected into the exhaust gas during “active” DPF regeneration. Depending on the engine-out NO<sub>x</sub> to PM ratio, the “passive” filter cleaning process is achieved through the heat and NO<sub>2</sub> produced by the engine and chemical reactions in the DOC [39] [35]. The exhaust gases pass through the filter, which collects particles from the gases. The particles eventually turn into a soot cake. The increasing amount of soot will create a high pressure in the DPF, which means the soot needs to be removed. After collecting the particles from the gases in the DPF and incinerating the soot in the filter, there is still nitrogen oxide and nitrogen dioxide left in the gases. In order to reduce the NO<sub>x</sub> levels even further, Urea, also known as AdBlue in the European market and as Diesel Exhaust Fluid in the North American market, is injected in the exhaust stream. Urea is originally an organic salt that is dissolved in water. Urea contains two amino groups and when disintegrating in heat, they turn into ammonia, carbon dioxide and water.

After urea has been injected in the exhaust aftertreatment system, the exhaust stream enters the SCR where most of the NO<sub>x</sub>, usually more than 98%, is removed. Together with active substances in the SCR, the ammonia coming from the urea injection turns NO<sub>x</sub> to nitrogen gas and water. The ASC is the final component in the exhaust aftertreatment system. In order for as much NO<sub>x</sub> as possible to be removed in the SCR, the amount of urea being injected in the system is often slightly overdosed. However, the leftover ammonia must not be released into the environment. Therefore, ammonia that was not used in the SCR process is removed in the ASC. The ASC oxidizes the ammonia into water and nitrogen gas [40] [36].

Recent research have been focused on reduced pressure drop across exhaust aftertreatment system, increased NO<sub>x</sub> conversion efficiency, and lower NH<sub>3</sub> and N<sub>2</sub>O slip [41] [42]. Studies have also been exploring the SCR catalyst properties, such as volume, effective temperature range, thermal stability, exhaust NO<sub>2</sub> to NO<sub>x</sub> ratio sensitivity, N<sub>2</sub>O emissions, and sulphur tolerance [43] [35]. These characteristics vary significantly with the catalytic coating applied to the SCR honeycomb substrate. Moreover, the use of cooled EGR along with an SCR catalyst have been investigated to minimise aqueous urea solution consumption in the SCR system and reduce the NO<sub>x</sub> conversion efficiency requirements [44] [45] [46]. Further investigation is required to improve the effectiveness of the SCR system under relatively low temperature conditions [47] [48], such as engine start-stops and low load operation [36].

### 2.3 Modern Direct Injection CI Combustion

In the direct injection compression ignition engines, only air is introduced to the cylinder from the intake. Then fuel is injected directly into the engine cylinder before the combustion starts. Load can be controlled by means of varying the amount of fuel injected at each cycle, while the air flow at a given engine speed is basically unaffected. There are many variety of CI engine designs in use in a varied range of applications such as automobile, truck, locomotive, marine, power generation. There are naturally aspirated engines, where atmospheric air is inducted, and there are turbocharged engines, where the inlet air is compressed by an exhaust driven turbine compressor combination, as well as supercharged engines, in which the air is compressed by a mechanically driven pump or blower are common. Turbocharging

and supercharging increase engine output by increasing the air mass flow per unit displaced volume, thus allowing an increase in fuel flow. These methods are used, usually in larger engines, to reduce engine weight and size, also known as downsizing, for a given power output [2].

The engine cycle consists of four phases or strokes, compression stroke, combustion stroke, and the exhaust stroke. During induction, air is drawn into the combustion chamber, then, during compression, air is compressed to a high pressure and temperature, then fuel is injected, often close to top dead centre (TDC) with high injection pressure, directly into the cylinder. Then it is the combustion stroke, which consists of two different stages, premixed combustion and mixing controlled combustion. The exhaust stroke purges the gases out of the combustion chamber by the piston moving back up. The combustion process results in heat generation, the rate in which it generates heat, is used as an instrument to characterise different phases of combustion. The combustion process also comprises of numerous phases such as ignition delay (ID), premixed combustion, mixing controlled combustion and late combustion.

Figure 2.6 illustrates these phases in the operation of a conventional compression ignition diesel engine.

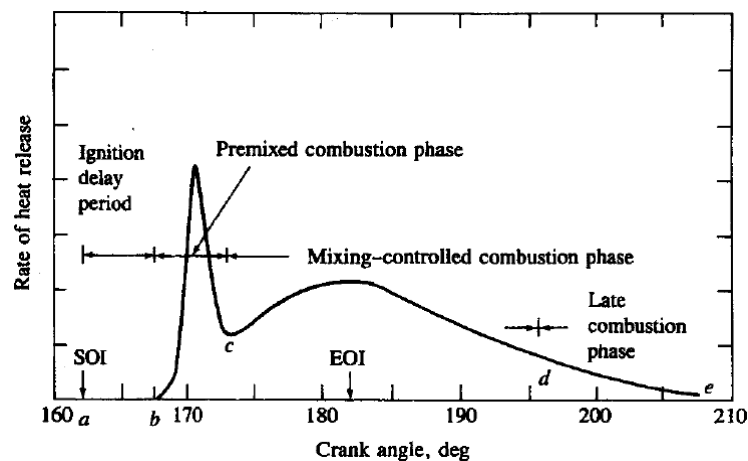


*Figure 2.6 Typical DI Engine Heat Release Rate Diagram Identifying Different Diesel Combustion Phases [2]*

Where ignition delay represents the crank angle between the start of injection (SOI) and the start of combustion (SOC), and premixed combustion phase, which is the mixing of the evaporated injected fuel with the surrounding air during the preignition stage of combustion, usually during the ignition delay. The fuel and air mixture is

close to stoichiometric ratio and thus auto-ignite because of the temperature of the charge, is higher than the flash point of the fuel. The combustion related to this stage is rapid and intense because of the availability and stoichiometric, or slightly rich mixture, while occurring at a high temperature. The subsequent heat release rate spike is accompanied by rapid rise of in-cylinder pressure, which is accountable for the typical diesel engine noise. The NO<sub>x</sub> production occurs mainly at this stage, due to the high temperature; and this stage is followed by mixing controlled combustion, which is normally referred to as diffusion combustion as well. The remaining fuel, and sometimes (in split injection setting) freshly injected fuel burns with a diffusion flame, resulting in a rich combustion because of the limited availability of oxygen. This combustion is limited by the mixing rate, and therefore, it is a slower combustion, and thus, it takes place at lower temperatures. This stage is accountable for the most of the soot produced, because of the fuel rich combustion; and late combustion occurs post the majority of the diffusion combustion has completed and the remaining fuel is partly oxidised. During this stage of combustion, the in-cylinder temperature is fairly low, which leads to the reducing and the end of combustion.

In order to meet the current emission regulations for diesel engines, it has become necessary to develop a thorough understanding of the in-cylinder processes of diesel compression ignition. To achieve this, many studies have been taking place, using innovative laser imaging diagnostic techniques. These studies have provided a significantly enhanced understanding of the diesel combustion, which is illustrated in the schematic of Figure 2.7 [49] [50].

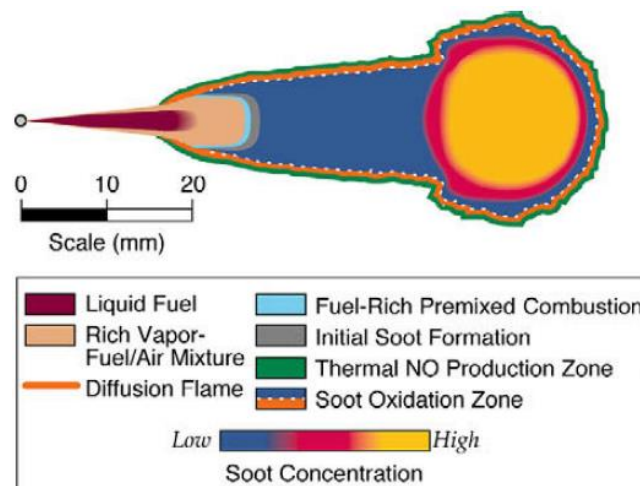


*Figure 2.7 Conceptual Schematic of Conventional diesel Combustion [49] [50]*

## 2.4 Alternative diesel engine combustion technologies

In a conventional diesel engine, there is a trade-off between NO<sub>x</sub> and soot emissions, where reducing one leads to the increase of the other. Though emissions from exhaust gas have been greatly reduced by the introduction of after-treatment equipment and high fuel injection pressure, advanced combustion concepts are still vital to improve engine emissions, in order to meet the ever increasing strict emissions legislation. Thus, due to these regulations, many manufacturers are required to adapt alternative combustion techniques. In the past three decades, extended effort in research has been made in CI diesel engines, with the main goal of reducing NO<sub>x</sub> and soot levels at the same time. homogenous charge compression ignition (HCCI), reactivity controlled compression ignition (RCCI), premixed charge compression ignition (PCCI), low temperature combustion (LTC), and transonic combustion (TSCi), are different types of advance CI diesel combustion techniques discussed here.

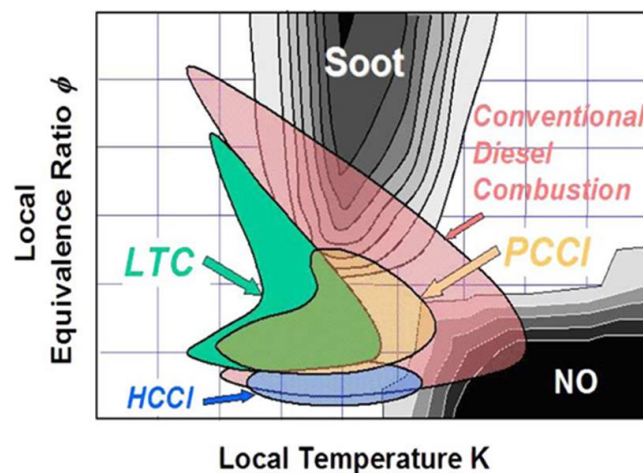


*Figure 2.8 In-cylinder fuel-air equivalence ratio versus temperature range for Conventional Diesel Combustion as well as alternative Diesel Combustion strategies such as LTC, HCCI and PCCI. Adapted from [51]*

As Illustrated in Figure 2.8, there are other combustion concepts that are being investigated in order to allow more efficient and cleaner combustion. Homogeneous charge compression ignition (HCCI) is a low temperature combustion that in the past years has given understandings that have resulted the development of many other combustion methods, such as Reactivity controlled compression ignition (RCCI) as well as partially premixed combustion (PPC).

A shared feature of the new combustion techniques is that they all allow for new ways for new and existing alternative fuels to be utilized. Basically, by modifying

compression ratio and intake temperature, any fuel can be run on HCCI, and RCCI utilizes two different fuels with varying ratios, meanwhile, by altering fuel injection and other some parameters, any liquid fuel can be used efficiently when running on PPC, which has also proved exceptional efficiency as well as very low exhaust emissions for flammable liquid hydrocarbon mixture, which has an octane rating of around 70, or basically, a fuel that has ignition properties somewhere between diesel and gasoline. Figure 2.9 illustrated how the new engine combustion techniques RCCI and PPC relate to conventional SI engine operation and direct injection compression ignition (DICI) engine operation, with regards to how appropriate the engine operation concepts are to reactive fuels like diesel and none-reactive fuels like gasoline [52] [53].

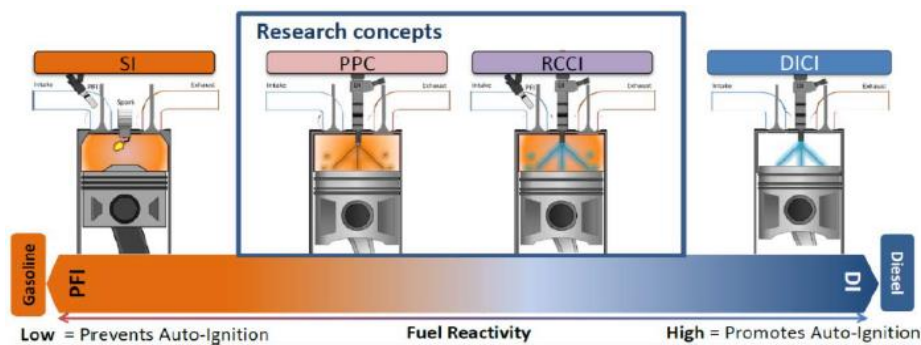


*Figure 2.9 Engine combustion research concepts compared to conventional spark ignition (SI) and Direct Injection Compression Ignition (DICI). Blue indicates a reactive fuel like diesel while orange indicates a none-reactive fuel like gasoline [52] [53].*

### 2.4.1 Homogeneous Charge Compression Ignition (HCCI)

A typical example of this approach is a technique commonly known as homogeneous charge compression ignition (HCCI) [54]. In HCCI, the fuel and air are premixed and compressed to ignite. Though, the mixture is made very dilute either by being lean with fuel-air equivalence ratios, typically less than 0.45, or through the use of high levels of EGR for equivalence ratios up to stoichiometric [54] [55] [56] [57]. While these mixtures are typically very dilute to support flame type combustion, as they are compressed to autoignition temperatures by the piston, they respond and burn volumetrically. Due to the high dilution, combustion temperatures are low, and therefore resulting in low NO<sub>x</sub> emission levels, also, the charge is adequately well mixed to avert soot formation, thus, thermal efficiencies are characteristically similar to those of a diesel engine [54] [56] [57] [58] [59]. Due to these advantages,

considerable research and development efforts on HCCI are happening using a variation of fuels, including gasoline, diesel fuel, ethanol, natural gas, and others [50] [54] [55] [56] [57] [58] [59] [60] [61] [62].

The HCCI or controlled autoignition (CAI) combustion has frequently been known as a new combustion process among the several research papers published over the last decade and a half. Nevertheless, it has been around possibly as long as the spark ignition (SI) combustion in gasoline engine and compression ignition (CI) combustion in diesel engines [63].

Based on the previous work in two-stroke engines [64], Najt and Foster extended the work to four stroke engines in 1983, and attempted to achieve added understanding of the fundamental physics of HCCI combustion [65]. They were the first to apply HCCI combustion idea in a four stroke gasoline engine. In their work they considered that HCCI is controlled by chemical kinetics, with insignificant effect of turbulence and mixing. They performed experimentations using primary reference fuels (PRF) and intake air heating, and with the use of heat release analysis and engine cycle simulation, they demonstrated that HCCI combustion process was dominated by low temperature, less than 950<sup>0</sup>K, hydrocarbon oxidation kinetics. They also determined that HCCI combustion is a chemical kinetic combustion process controlled by the temperature, pressure, and the composition of the in-cylinder charge.

Thring further extended the work done by Najt and Foster in four-stroke engines, in 1989, by investigating the performance of an HCCI engine operating by a full-blended gasoline [66]. The operating procedure of a single cylinder engine was mapped out as a function of air fuel equivalence ratio, EGR rate, and the compression ratio.

Studies on four stroke engines have demonstrated that it is possible to achieve high efficiencies and low NO<sub>x</sub> levels of emission by means of a high compression ratio and a lean mixtures [67]. In four stroke engines, numerous experiments have been carry out, where the HCCI combustion on its own is examined. This has mainly been done on single cylinder engines, which generally do not provide brake values. Nevertheless, Stockinger demonstrated brake efficiency of 35% on a 4-cylinder 1.6 litter engine at 5 bar Brake Mean Effective Pressure (BMEP) [68]. Later studies have revealed brake thermal efficiencies of over 40% at 6 bar BMEP [69] [70].

While HCCI combustion was established well over two decades ago [66], only the current developments like, intake air charge, varying the compression ratios and exhaust gas recirculation (EGR) have made it controlled combustion and reduced knocking. HCCI operation has been effectively applied to spark ignition (SI) as well as compression ignition (CI) engines, and demonstrated to be fuel adaptable, as mentioned, using with gaseous fuels such as propane or natural gas and liquid fuels like traditional gasoline or diesel fuels. The HCCI process operates on the basis of having a lean, premixed, homogeneous charge that responds and burns volumetrically in the cylinder as it is compressed by the piston [71] [72].

In HCCI engines, a lean homogeneous flammable mixture, basically fuel and air mixture with equivalence ratio of  $<1$ , is created before the start of ignition and is auto ignited as a result of increasing pressure and temperature in the compression stroke [73]. The HCCI operation is similar to SI engine operation, since both use the homogeneous charge for combustion and it is also similar to CI engine since they both rely on the auto ignition of the mixture. Therefore, HCCI combustion can be viewed as the mixture of SI and CI combustion processes [74].

*Table 2.2 Comparison of Traditional and HCCI Combustion Modes [75]*

Fuel	SI	CIDI	HCCI
$\lambda$	$\approx 1.0$	$\approx 1.2-2.2$	$>1.0$
Mixture preparation	PFI, GDI	DI	DI, PFI & DI+PFI
Ignition	Spark ignition	Auto-Ignition	Auto-Ignition
Combustion form	Premixed	Diffusion	Diffusion but dominated by chemical kinetics
Combustion rate limitation	Flame propagation	Mixing rate	Multipoint or spontaneous
Flame front	Yes	Yes	Without
Combustion temperature	High	Partially high	Relatively low

Table 2.2 gives a brief comparison of typical features of SI, CIDI and HCCI combustion modes. The advantages of HCCI combustion can be summarized as follows:

1. HCCI combustion uses a higher compression ratio, lacks a threshold value and has a shorter combustion period and faster combustion rate. Therefore, it almost achieves constant volume combustion and a higher thermal efficiency because of lower combustion temperature and lower radiation loss.
2. There is no flame front or flame spread or local regions of excessively high temperature and rich mixture, thus reducing soot and NO<sub>x</sub> generation to a very low level.
3. Different variety of fuel types can be used in this mode of combustion [75] [76].

The air fuel mixture can be prepared either internally, by direct injection, or externally, by port fuel injection. The latter prevents the well-known drawbacks of mixing by controlled combustion that lead to soot formation in DI diesel engines. Additionally, as the combustion occurs without flame propagation, it leads to lower gas temperatures, and therefore reducing NO<sub>x</sub> emission levels [77].

Since HCCI combustion offers the potential for reducing NO<sub>x</sub> and soot emissions simultaneously while maintaining high efficiencies, it is a very desirable choice for compression ignition diesel engines. But it suffers from problems such as very advanced ignition, requirements for higher temperatures, and an excessive heat release rate at high load operations. In order to overcome these problems, several investigations and developments have been carried out on HCCI combustion in three main categories, premixed HCCI [78] [62], early direct injection HCCI and late direct injection HCCI. Suzuki and Odaka [79] [80] used a gasoline type injector to introduce diesel fuel into the intake manifold. Knocking was suffered at high load operation and HC emissions were excessive, due to overmixed diesel fuel. In subsequent work, efforts were made to resolve the problem of overly advanced combustion phasing. It was achieved by using iso-octane as the premixed fuel at some conditions [81] [82]. By injecting the fuel early during the compression stroke, the mixing process can be promoted due to higher in-cylinder temperature and pressure. Iwabuchi [83] studied early injection HCCI by investigating several key parameters in both experimental and CFD works. It was found that NO<sub>x</sub> emissions were suppressed to low levels,

while soot and HC were very high. Higher fuel consumption was reported compared to conventional diesel combustion. In order to improve combustion, an impinging-spray-nozzle injector was introduced to generate wider dispersion angles and reduce penetration [84]. Consequently, fuel consumption was improved by 10%, soot and HC emissions were considerably reduced. The similar research in terms of early injection HCCI can be found in New ACE Institute [85] [86] [87], Hino Motors [88], and IFP [89]. Nissan Motor [90] [91] [92] has carried out numerous studies on late injection HCCI. They reported 4 to 5 times less NO<sub>x</sub> emissions and improved PM emissions and fuel consumption compared to conventional operation [34].

#### **2.4.2 Premixed Charge Compression Ignition (PCCI)**

HCCI engines promise efficiency similar to diesel engines without the high NO<sub>x</sub> and particulate matter emissions that is involved with diesel engine combustion. Nevertheless, significant difficulties have kept HCCI engines from being widely available in commercial vehicles. The main challenges include control of combustion timing and low specific power output [93], with the combustion control matter being particularly difficult for transportation applications.

Premixed charge compression ignition (PCCI) could be solution to the combustion control and specific power obstacles involved with HCCI engines. PCCI is a simplified version of HCCI combustion in which the fuel and air mixture may be partially stratified at the time of ignition. There are different examples of PCCI engines such as, direct injected engines with early injection [94], and controlled autoignition (CAI) engines, which use high residual fraction and variable valve timing to control the combustion [95]. In PCCI engines may use equivalence ratio stratification for extending the duration of burn, thus, permitting for the engine to run with a higher specific power. Direct injection of fuel into the combustion chamber may also assisted engine control, particularly in the case of injection of highly reactive fuel, like diesel fuel. In contrast, high emissions of NO<sub>x</sub> and PM may be produced due to fuel stratification. Meeting the control and high power output requirements of modern engines is the main challenge for PCCI engines, while meeting the current and future emissions standards, by keeping the NO<sub>x</sub> and PM emission levels low enough [96].

Since PCCI combustion for diesel engines are capable of providing both high efficiency and extremely low particulate emission levels, it is more attractive to auto makers recently. In contrast to conventional diesel combustion, to avoid soot emissions, PCCI combustion approach, uses early in-cylinder, or direct, fuel injection. Nevertheless, as previously mentioned, because of the low volatility of diesel fuel, and its high ignitability, numerous technical obstacles, like mixture preparation and control of combustion phasing, has to be resolved prior to the availability of PCCI diesel engine commercially [2].

In the PCCI combustion approach, fuel can be introduced into the combustion chamber through either, early direct injection, port fuel injection, or even late direct injection. Early direct injection and port fuel injection frequently have incomplete fuel vaporization, as well as fuel spray impact on the cylinder walls, which causes high levels of hydrocarbon and carbon monoxide emissions along with fuel/oil dilution [50]. Use of narrow spray cone angle injectors, as a tactic to decrease fuel-wall impact has been investigated in the past. Late direct injection avoids fuel-wall impact and provides adequate control over combustion phasing. Lechner et al. [97] assessed the possibility of using the injector nozzle with narrow spray cone angle for diesel PCCI combustion by advanced injection timing, and by changing the spray cone angle. It is observed that carbon monoxide (CO) emissions rise drastically and combustion efficiency drops considerably as the fuel starts to miss the piston bowl. Mie-scattering technique was employed to examine the in-cylinder combustion and spray development processes by Fang et al. in a diesel PCCI engine using a 70-degree spray angle injector [98] [99].

Figure 2.10 illustrates the structure and the shape of the chamber for the PCCI engine compared to those of direct injection diesel engine and direct injection compression ignition gasoline engine.

Gas oil is compressed to above 200 bar In DI diesel engines, and then, in the second half of the compression stroke, it is injected into the high pressure, high temperature combustion chamber by a diesel injection nozzle, and lastly, it is burned by compression ignition. The combustion process for direct injection compression ignition gasoline engine, is the similar except that gasoline is utilized instead. As seen in Figure 2.10 the chamber wall shape is pointing inward.

In the PCCI engine however, gasoline is compressed to about 3 bar and injected by an electromagnetic gasoline injector into the air intake port at atmospheric condition. The gasoline is subject to compression in the cylinder, and is combusted by compression ignition. The combustion chamber the shape of an open shallow dish. There are no inlet throttling and ignition equipment such as spark plug in the PCCI engine, but instead, in order to achieve compression ignition, it has a compression ratio practically same as that of the diesel engines [100].

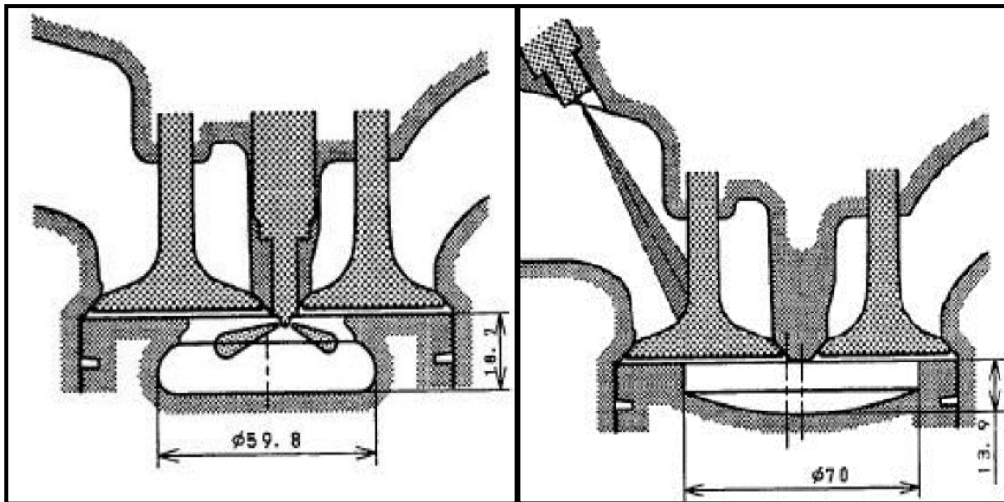


*Figure 2.10 Combustion systems of direct injection diesel engine and direct injection compression ignition gasoline engine (Left) and PCCI (Right) [100]*

### **2.4.3 Reactivity Controlled Compression Ignition (RCCI)**

Reactivity controlled compression ignition (RCCI) uses two types of fuel with varying auto ignition properties or reactivity that are injected separately, generating charge stratification. Such as a lower reactivity fuel, like gasoline, can be injected early into the intake manifold using a port fuel injector, whereas a more reactive fuel, like diesel, can be injected directly into the combustion chamber. This combustion method offers a high fuel economy with low emission levels compared to conventional diesel combustion. Nevertheless, as a down fall, this method calls for the added expense of an additional fuel injection system, in addition to low reception from consumers. Related studies in this subject matter can be found in various publications [101] [102] [103] [34].

As an evolution of HCCI and PCCI, RCCI aims to provide more control over combustion phasing, by means of multiple fuels of differing reactivity in a compression ignition engine. In detail, multiple injections of various fuels at planned

intervals, provides control over the reactivity of the charge in the combustion chamber, in order to provide optimum combustion duration and intensity. A comparatively low reactivity fuel is injected, early in the engine cycle, and creates a homogeneous mixture with the air. Later in the cycle, a higher reactivity fuel is injected into the combustion chamber. This method produces pockets of varying air fuel ratios and reactivity, thus, causing the combustion to take place at different times and at different rates. Therefore, multiple injection systems are needed in order to run an RCCI engine. Variations of this method have been validated with different combinations of diesel, gasoline, natural gas, as well as numerous biofuels and boutique fuels [104].

#### 2.4.4 Low Temperature Combustion (LTC)

Classic HCCI is not willingly applied with diesel fuel, due to the fuel's low volatility and the ease with which it auto ignites (high cetane number) [54] [58] [62] [71] [105] [83]. Consequently, many diesel engine researchers and manufacturers are pursuing substitute methods to achieve combustion similar to HCCI, generally referred to as diesel low temperature combustion (LTC). With diesel LTC, numerous methods are employed in order to obtain sufficient premixing, so that combustion temperature and equivalence ratio combinations that cause soot and NO<sub>x</sub> formation are prevented. This can easily be understood by the means of the equivalent ratio-temperature diagram in Figure 2.11 [106] [107] [108].

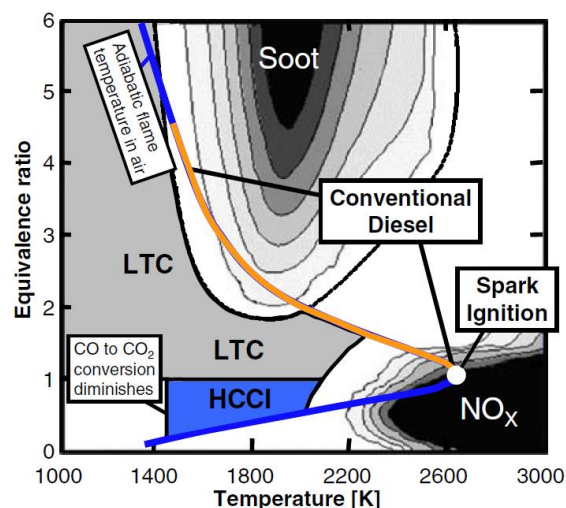


Figure 2.11 Diagram showing the temperature ranges for soot and NO<sub>x</sub> formation and the regions for conventional diesel, SI, HCCI, and diesel LTC engines [106] [107] [108].

Nevertheless, it is not essential for combustion to take place entirely in the HCCI region in order to avoid soot and NO<sub>x</sub> formation. LTC diesel operation takes advantage of this by permitting the combustion to take place anywhere in the grey shaded area, as it is attempting to insure that most of the fuel is mixed to equivalent ratio of less than or equal to stoichiometric (equivalent ratio  $\leq 1$ ), which is the HCCI region, before the reactions are quenched by the expansion, so that good combustion efficiency is sustained. Therefore, diesel LTC basically uses the same principles as HCCI in order to obtain low emissions, although its combustion is not entirely premixed [50].

Basically, the goal of an LTC engine is to achieve high levels of fuel efficiency without producing harmful emissions, such as NO<sub>x</sub> and particulate matter (PM), or soot. Figure 2.11 illustrates the relationship between flame temperature and pollutant formation, where NO<sub>x</sub> formation is reduced as flame temperature is reduced, as well as PM, which are reduced with lean combustion. So it could be concluded that LTC engines burn cool enough and lean enough, meaning low equivalence ratio, to stay out of the high soot and NO<sub>x</sub> formation regions, yet they still have the ability to take advantage of the high thermal efficiency of typical CI engines, which means they have high compression ratios and ideally operate without a throttle [104].

Mainly because of breakthrough work done in the 1980s and 1990s at Sandia's Combustion Research Facility (CRF) in California, researchers already understand how pollutants are created throughout the conventional diesel combustion. Details of how conventional diesel combustion works, with research that took advantage of special optical engines and optical diagnostic techniques with lasers and scientific high speed cameras to examine the combustion processes, were combined into a highly referenced theoretical model that was developed by Sandia's John Decimeter of 1997 [49]. The laser based optical diagnostics demonstrated that one pollutant, soot or PM, was formed in areas where fuel concentrations were very high. Another serious pollutant, namely NO<sub>x</sub>, resulted from high-temperature flame inside the combustion chamber. NO<sub>x</sub> emissions are not just toxic, but once released into the atmosphere, and exposed to sunlight, they react with other pollutants to create ground level ozone, also known as smog [49].

LTC tackles the NO<sub>x</sub> emissions by means of EGR. With this dilution influence, the combustion temperatures are reduced so NO<sub>x</sub> formation is considerably decreased.

According to Musculus, another part of the LTC approach, is to spray in the fuel earlier in the engine cycle in order to allow the fuel more time to mix with air prior to it burns. Thus, LTC avoids much of the fuel rich areas which lead to PM as well as the high temperature areas which lead to NO<sub>x</sub> formation [104] [109].

Although LTC engines have the potential of increased efficiency and low emissions for IC engines, controlling the combustions in the combustion chamber can be a tough challenge to overcome. With the advance of processor and field-programmable gate array (FPGA) technology, LTC and other engine operation techniques are being controlled and researched in major universities and laboratories worldwide [104].

#### **2.4.5 Transonic Combustion (TSCi<sup>TM</sup>)**

In 2010, a new combustion concept named transonic combustion (TSCi<sup>TM</sup>) was proposed by Chris De Boer [110] [111]. This combustion procedure is based on the direct injection of fuel into the combustion chamber as a supercritical fluid. Supercritical fluid or SCF is any substance at a temperature and pressure above its critical point where distinct liquid and gas phases do not exist [112]. Fuel at this state achieves rapid mixing with the contents of the cylinder, and after a small delay period, spontaneous ignition takes place at multiple locations. The combination of multiple ignition sites and rapid combustion, causes high cycle efficiency and high rates of heat release. Essentially, the pressurized fuel, at approximately 250 bar, requires to be heated up to nearly 370°C using a TSCi<sup>TM</sup> injector. When tested in a 1.6 L CI engine, by De Boer, it was reported to produce high thermal efficiency of 42% with the use of EGR and supercritical fuel at 2000 rpm engine speed and 2 bar Brake mean effective pressure (BMEP), which achieved low brake-specific NO<sub>x</sub> (BSNO<sub>x</sub>) at 0.5 g/kWh, and low soot emissions at 0.17 filter smoke number (FSN), at the same time, as well as low HC and CO emissions [34] [110] [111].

Heat loss to the surrounding surfaces is reduced under part load conditions, due to the stratified nature of the charge, thus resulting in further improvements to efficiency. The ignition and combustion events take place after TDC, which is due to the short combustion delay angles that allow for late injection timing. This late injection timing creates an advantage by allowing work resulting from heat release produces positive work on the piston. Other advantages include the removal of droplet burning and

increased combustion stability, which is a result of having multiple ignition sources [113].

## 2.5 Dual Fuel Diesel Engine Technology

The main concept of a dual-fueled reciprocating engine is not new. In the 1890s, Rudolf Diesel experimented with this idea during his development of the diesel engine. He introduced a pipeline of natural gas into the air intake and observed the improvements in the engine performance. Since then, dual-fuel engines have been available in many markets, including stationary applications in the gas compression industry. These types of engines were in use as early as the 1930s. Today, the topic of reducing dependency on oil is a recurring issue. Emissions regulation and the effort for cleaner technologies are the main concern of many governments, as well as the rising price of fossil fuels. Diesel engines can be designed to operate interchangeably between dual-fuel or pure diesel fuel operations. Modern dual-fuel systems incorporate electronic controls that enhance system performance even further [114].

In a dual-fuel engine the primary fuel is mixed relatively homogeneously with the air in the intake, similar to a SI engine. However, unlike the SI engine, the air fuel mixture is ignited by injecting a small amount of diesel fuel, known as the pilot fuel, as the piston approaches the top of the compression stroke or TDC. This diesel pilot fuel, quickly induces autoignition reactions and ignites due to the heat of compression, just as it would in a regular CI diesel engine. The combustion of the diesel pilot then ignites the air fuel mixture in the rest of the combustion chamber [115].

### 2.5.1 Diesel-Gas Dual Fuel

Natural gas is the most popular fuel used in the dual fuel engine primarily because of its lower cost in industrial applications, such as mine trucks, diesel power generation systems, marine vessels, and railroad locomotives. In addition, the low carbon content of natural gas leads to lower CO<sub>2</sub> emissions and much less soot emissions than other fossil fuels [116]. In addition to natural gas, bio fuels, such as bio-methane, bio ethanol, can also be used as the premixed fuel in a dual fuel engine. The disadvantage is the requirement of having two separate fueling systems for the dual-fuel engine operation.

The combustion processes in CI engines running on pure diesel fuel can be divided into four stages as shown in Figure 2.12. They are, A– B: period of ignition delay; B– C: premixed (rapid pressure rise) combustion; C–D: controlled (normal) combustion; and D–E: late combustion. Point ‘A’ is the start of fuel injection and ‘B’ for start of combustion.

However, the combustion processes in gas-fumigated dual-fuel engines using pilot injection have been identified to take place in five stages as shown in Figure 2.13. They are the pilot ignition delay (AB), pilot premixed combustion (BC), primary fuel ignition delay (CD), rapid combustion of primary fuel (DE) and the diffusion combustion stage (EF).

Ignition delay (AB) of injected pilot fuel exists longer than the pure diesel fuel operation. This is due to the reduction in oxygen concentration resulting from gaseous fuel substitution for air. The pressure rise (BC) is moderately low as compared to pure diesel fuel operation due to the ignition of small quantity of pilot fuel.

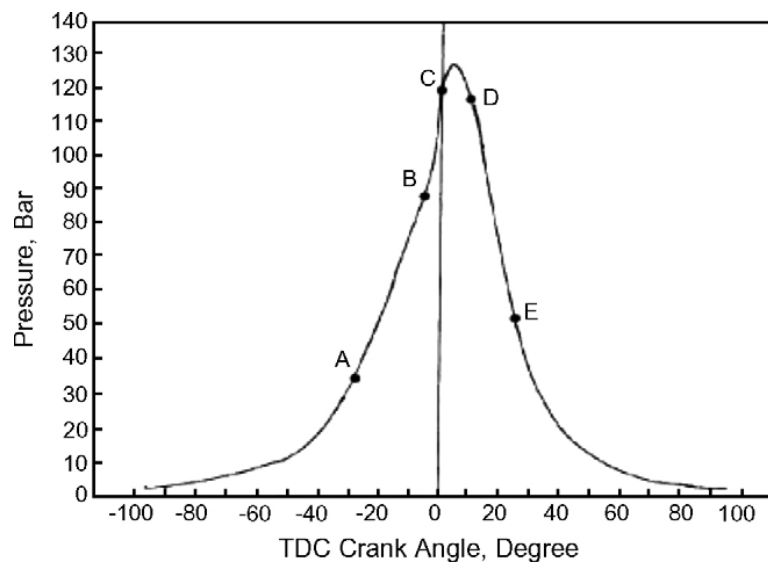


*Figure 2.12 Details of combustion processes in diesel engine [117]*

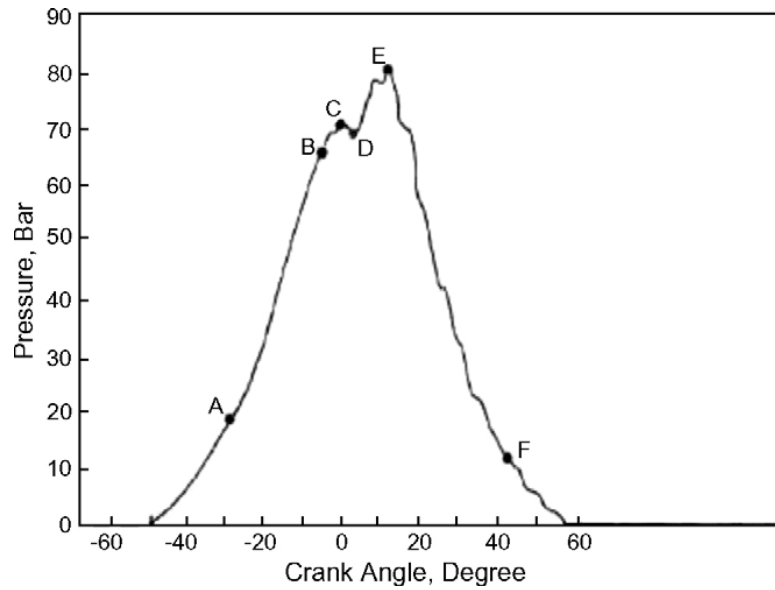


*Figure 2.13 Dual fuel pilot injection pressure-crank angle diagram [117]*

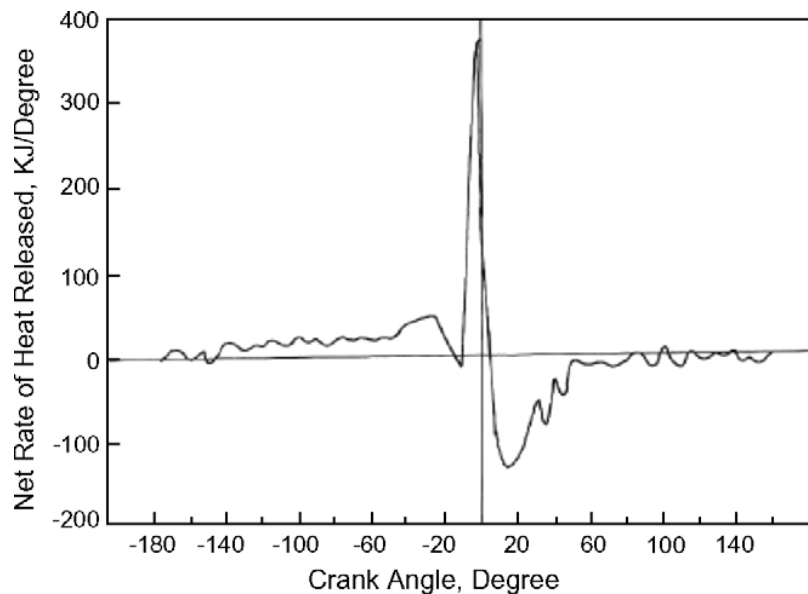


*Figure 2.14 Heat release diagram of diesel fuel operation (engine speed 3000 rpm, engine torque 9.65 N-m) [117]*

There is a finite time lag between the development of the first and second pressure rises due to a longer ignition delay of gas-air mixture, a result of the high self-ignition temperature. However, this ignition delay is short as compared with the initial delay period due to the pilot fuel injection. The pressure decreases slowly (CD) until the actual combustion of the fumigated gas starts. The phase of combustion (DE) is very unstable because it started with flame propagation that has been initiated by the

spontaneous ignition of pilot fuel. The pressure rise here does not cause any operating problem since it occurs in an increasing cylinder volume. Diffusion combustion stage (EF) starts at the end of rapid pressure rise and continues well into the expansion stroke. This is due to the slower burning rate of gaseous fuel and the presence of diluents from the pilot fuel. Some gas–air mixture may escape combustion under this phase due to low oxygen concentration, valve overlap, flame quenching on the walls or the effects of crevices. The success of this phase primarily depends on the length of ignition delay.

The heat release diagram of diesel fuel operation (Figure 2.14) shows an apparent negative heat release prior to the main start of combustion. This is due to the cooling effect of the injected liquid fuel. This effect is not apparent with the dual-fuel combustion processes as pre-oxidation of the gaseous fuel starts before pilot fuel injection (Figure 2.15). The pilot fuel is then flattened the heat release rate within this region. Figure 2.15 shows the initial heat release due to pilot injection. This figure also indicates that dual-fuel combustion is continued well into the expansion stroke [118] [117].

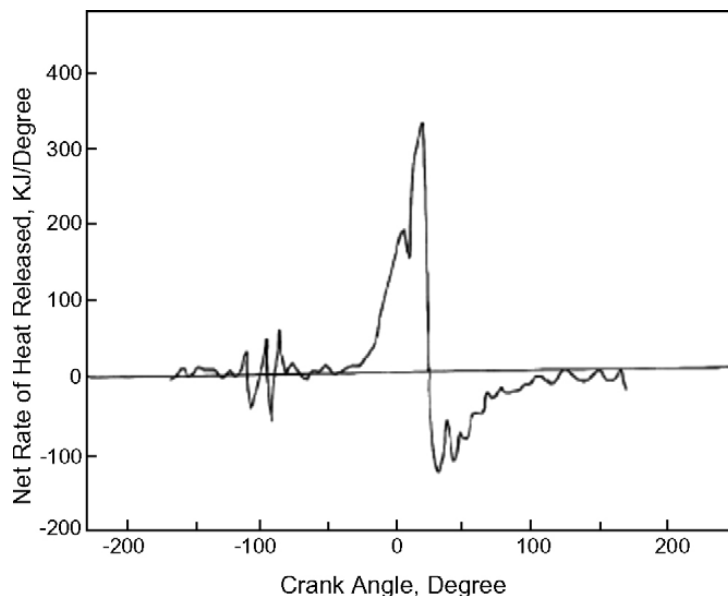


*Figure 2.15 Dual fuel pilot injection heat release diagram (engine speed 3600 rpm, engine torque 5.15 N-m) [117]*

There have been many published works on dual-fuel technology and in particular the use of natural gas in dual fuel diesel engines with diesel used as pilot fuel, including

study of combustion, emissions, performance, thermal loading, temperature distribution and also reduction of diesel knock.

In [119], the effect of dual fuel operation on the exhaust emission and performance characteristics of an existing diesel test engine using natural gas as primary fuel and diesel fuel as a pilot ignition source is examined, and two sets of measurements are collected, one using diesel fuel alone as originally intended for the engine operation, and the other using dual-fuel configuration at different engine operating conditions. Analysis of the cylinder pressure data and the measured emissions data were used to evaluate the effects of dual fuel operation on combustion duration, heat release rate, brake specific fuel consumption and peak cylinder pressure, and the effects of dual-fuel combustion on pollutant formation from.

Analysis of the experimental data revealed that dual fuel operation lowers peak cylinder pressure compared to the normal diesel operation, which is positive, as it opposes no risk to engine structure. Under dual fuel operation at low loads, the combustion duration is longer compared to normal diesel operation, and at high loads, it is shorter.

The total brake specific fuel consumption becomes inferior under dual fuel operation compared to the normal diesel operation at similar engine operating conditions. At high loads, the values of total brake specific fuel consumption under dual fuel operation converge to values under that of normal diesel operation.

Use of natural gas under dual fuel operation has a positive effect on lowering NO<sub>x</sub> emissions compared to normal diesel operation. Meanwhile, there is a considerable decrease in soot emissions under dual fuel operation regardless of engine operating conditions, which is an important finding. On the other hand, CO and HC emissions levels are considerably higher in dual-fuel configuration compared to normal diesel operation.

Therefore, it seems that dual fuel combustion using natural gas is a viable technique for controlling NO and soot emissions of existing DI diesel engines and requires only minor modification of the engine original construction. This is important if we consider the difficulties of controlling both pollutants, NO and soot, on DI Diesel engines. The consequence of Brake specific fuel consumption (BSFC) observed is partly compensated by the low price of natural gas. It is also possible to reduced HC

and CO, especially at low engine loads, by some modifications to engine tuning, such as injection timing of the pilot diesel fuel [119].

In *Effect of pilot fuel quantity on the performance of a dual fuel engine*, Abd Alla, Soliman, Badr and Abd Rabbo (1999) investigate the effect of pilot fuel quantity on the performance of an indirect injection diesel engine fueled with gaseous fuel. With diesel used as the pilot fuel and methane or propane used as the main fuel, inducted into the intake manifold to mix with the intake air, it is shown that, “the low efficiency and excess emissions at light loads can be improved significantly by increasing the amount of pilot fuel, while increasing the amount of pilot fuel at high loads led to early knocking.” [120].

The conclusions show that increasing the amount of pilot fuel, improve the thermal efficiency, because of the corresponding high pressure and temperature while the combustion duration is increased. Also the increase in NO<sub>x</sub> emissions with increasing amount of pilot fuel was contributed to the increases of the maximum temperature of the charge. Meanwhile, due to general improvement in the combustion process, there were reductions in carbon monoxide and unburned hydrocarbon emissions.

It was also observed that increasing the amount of pilot fuel at high loads, lead to early knocking, concluding that increasing the amount of pilot fuel is not effective in dual fuel operation at high loads [120].

### **2.5.2 Diesel-Gasoline RCCI Combustion**

There has been many researches done on dual-fuel engine and variety of fuel mixtures to be utilized. In the past few years, one of the concepts that has been examined by several researchers, is the diesel-gasoline RCCI combustion. Shuaiying Ma et al. [121] investigated the effects of diesel injection strategy on gasoline/diesel dual-fuel combustion, emissions, fuel economy and the operation range with high efficiency and low emissions on a modified single-cylinder diesel engine with port fuel injection of gasoline and direct injection of diesel fuel with rapid in-cylinder fuel blending, employing single and double injection strategies at 1500 rev/min and 50 mg/cycle total equivalent diesel fuelling rate. From their results they reported that this combustion mode had the capability of achieving high efficiency with near zero NO<sub>x</sub> and soot emissions by using an early injection timing of single strategy with high gasoline substitution ratio.

In a similar investigation on a heavy duty diesel engine, Jesús Benajes et al. [122] perform an experimental and numerical study to understand mixing and auto-ignition processes in RCCI combustion conditions, using gasoline and diesel as low and high reactivity fuels, respectively, by the means of three parametrical studies with diesel direct injection and gasoline port fuel injection, as well as a detailed analysis in terms of air/fuel mixing process by means of a 1-D spray model. They report their finding shows that as the Diesel/Gasoline fuel ratio is reduced, the ignition delay increases and thus extending the mixing time and the first combustion stage gets lowered while the second one is enhanced, also that the advance of the diesel injection timing extends these effects over the combustion process. Finally it is stated that compared to conventional neat diesel combustion, a slight reduction in terms of NO<sub>x</sub> and a very important reduction in terms of soot were achieved with the RCCI combustion.

Furthermore in a numerical investigation by J. Li et al. [123] on the effect of reactivity gradient in an RCCI engine fuelled with gasoline and diesel, the role of fuel reactivity gradient was examined numerically by comparing a dual-fuel mode combustion with other hypothetical cases under one specific load condition, where a chemical reaction mechanism was initially developed aiming at a modelling study on dual fuel and blend fuel combustion in internal combustion engines fuelled by gasoline/diesel and gasoline/biodiesel. Ignition delays were validated for 100% diesel, 100% gasoline and 100% biodiesel under 102 conditions in total. They further conducted three dimensional validations under 3 conditions, including pure diesel combustion, and gasoline/diesel combustion, with both single and split injection strategies in the engine. In order to investigate the fuel reactivity gradient, they compared the gasoline/diesel combustion with a single injection, with other three hypothetical cases, one of which was dual fuel mode without fuel reactivity gradient, and the other two were the blend fuel mode but with different injection timings. They report their result illustrates that the fuel reactivity gradient could retard the ignition timing, reduce heat release rate, and ease peak pressure rise rate, as well as resulting in low levels of NO<sub>x</sub> and soot emissions from the diesel-gasoline dual-fuel combustion.

These studies, along with few other show the potential of diesel-gasoline dual-fuel engine combustion in delivering both enhanced performance as well as much improved emission.

### 2.5.3 Dual Fuel PPC

Study has shown [124] that in a 2.44L heavy duty one cylinder compression ignition test engine, with a similar diesel-gasoline fuel delivery system, improving the fuel mixture could result in having increased operational domain for the premixed dual fuel combustion. This resulted in substantial reduction in NO<sub>x</sub> and soot emissions, with net indicated efficiency of 50%, at 11bar IMEP. Further study by means of computer simulation revealed that areas with high concentration of diesel tend to ignite first.

As illustrated in Figure 2.16, study has also shown [125] that different fuel proportions in dual fuel Partially premixed combustion (PPC) effects efficiency and emission and output, where with port injected gasoline to direct split injected diesel ratio of 89 to 11, 53% net indicated efficiency and considerable reduction in soot and NO<sub>x</sub> is attainable.

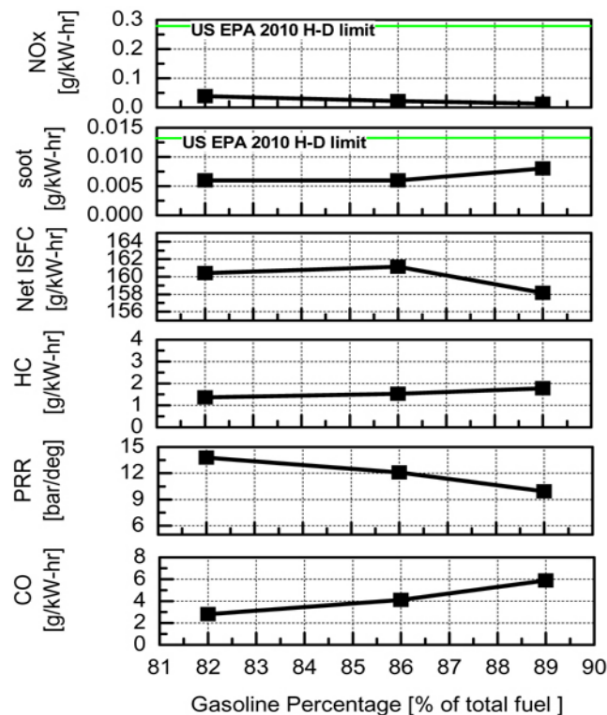


Figure 2.16 Measured Engine Emissions as a Function of Gasoline Percentage [125].

In a study [126] by means of computer simulation of diesel-gasoline dual fuel combustion in a one cylinder compression ignition diesel engine, where the gasoline substitution ratio was increased from 0% to 85%, combustion pressure as well as

temperature were reduced with the increase of gasoline substitution ratio. This was also true for the levels of soot and NO<sub>x</sub> emission output as a result. In addition, the NO<sub>x</sub> emissions could be further repressed by using EGR. uHC emissions were reduced as the premixed ratio increased, and were also related to the EGR rate. The simulation confirmed the experimental results, which can be used to predict the trend of emissions under the dual fuel PPC operation.

A more recent study carried out by Ma and Zheng [127] reported high efficiency and low emissions on a single cylinder diesel engine in a dual fuel PPC operation. They investigated the effects of diesel injection strategies on combustion, emissions and the operation range by using gasoline and diesel dual fuel. At 1500 rpm high load condition, the single injection strategy offered ultra-low NO<sub>x</sub> and soot emissions. However, as NO<sub>x</sub> emissions were sensitive to EGR rate, this injection strategy was appropriate when sufficient EGR was available. In terms of double injection strategy, early 2nd injection timing strategy provided lowest ISFC of 173 g/kWh, NO<sub>x</sub> emission of 0.2 g/kWh and soot emission of 0.003 g/kWh, but with a penalty in terms of maximum pressure rise rate. The results also showed that the combustion phasing could be retarded by using a higher gasoline fuel percentage so that a lower combustion temperature was achieved, resulting in reduced NO<sub>x</sub>, soot emissions and maximum pressure rise rate. In contrast, late 2nd injection timing strategy demonstrated the ability to reduce maximum pressure rise rate due to prolonged combustion duration. Therefore, this injection strategy could be used for extending the high load operation regime. However, high levels of soot emissions could be problematic due to high load operation. This issue might be solved by increasing the diesel injection pressure. The high HC and CO emissions in this dual fuel PPC operation could be suppressed to within EURO VI limits if an appropriately specified oxidation catalyst was utilized [34].

## 2.6 Ethanol For Dual-Fuel Engines

Harmful ecological effects of fossil fuels and fears regarding their supplies, have prompted the search for renewable transportation biofuels. In order to be a feasible substitute, a biofuel should have environmental benefits, deliver a net energy gain, be producible in large quantities while being economically competitive, and without reducing food supplies. Ethanol produces 25% more energy than the energy utilized

in its production when produced from corn grain, where for the ethanol produced from sugar cane, this energy balance is seven times greater [128]. The production and combustion of ethanol reduces greenhouse gas emissions by 12%. None of the biofuels can replace much fuel without affecting food supplies. Reserving all the production of United States corn and soybean crops to biofuels production, would still fulfil only 12% of gasoline demand and only 6% of diesel demand. Up until current rises in fuel prices, high production costs made biofuels unprofitable without financial assistance [129].

Ethanol has advantages as a fuel as well as disadvantages over fossil fuels such as gasoline and diesel. In spark ignition (SI) engines, ethanol can run at a much higher exhaust gas recirculation (EGR) rates as well as higher compression ratios. This alcohol has a high octane rating, at 109 RON (Research Octane Number), 90 MON (Motor Octane Number), (which equates to 99.5 AKI (anti-knock index)) [130]. AKI stands for Anti-Knock Index, which averages the RON and MON ratings  $(RON+MON)/2$ , and is used on United states gas station pumps. Conventional European gasoline is typically 95 RON, 85 MON, equal to 90 AKI. Ethanol creates very little particulates as a compression ignition (CI) engine fuel, but the low cetane number requires that an ignition improver like glycol must be mixed into the fuel with approximately 5%. When used in spark ignition engines as the fuel, ethanol has the potential to decrease NO<sub>x</sub>, CO, HC as well as particulate emissions. A test with E85 fuelled Chevrolet Lumina [131], showed that NMHC (Non-Methane Hydro Carbons) decreased by 20% to 22%, NO<sub>x</sub> by 25% to 32% and CO by 12% to 24% compared to reformulated gasoline [132]. Toxic and harmful emissions of benzene and 1,3-Butadiene were also reduced whereas aldehyde emissions increased, particularly acetaldehyde.

Exhaust gas emissions of CO<sub>2</sub> also decrease due to the lower ratio of carbon to hydrogen in these alcohols, as well as the improved engine efficiency.

Ethanol contains soluble and insoluble contaminants [133]. Halide ions, which are soluble contaminants, for instance chloride ions, have a great effect on the corrosivity of alcohol fuels. Halide ions help increase corrosion in two ways:

1. They chemically attack passivating oxide films on several metals causing pitting corrosion, and;

2. They increase the conductivity of the fuel, where increased electrical conductivity promotes electrical, galvanic and ordinary corrosion in the fuel system.

Soluble contaminants like aluminium hydroxide, which by itself is a product of corrosion by halide ions, obstructs the fuel system over time. To avoid corrosion, the fuel system has to be manufactured from appropriate materials, proper insulation of electrical wires is necessary, while the fuel level sensor requires to be of pulse and hold type, or similar as well. Furthermore, a low concentration of contaminants is expected from high quality alcohol, as well as having an appropriate corrosion inhibitor as an additive.

Ethanol is incompatible with some polymers as well. The alcohol can react with the polymers, resulting in swelling, and over time the oxygen breaks down the carbon-carbon bonds in the polymer affecting the tensile strength by causing a decline in the strength. However, for the past few decades, most engines have been designed and manufactured to have the ability to withstand up to 10% of ethanol (also known as E10) without any problem. This involves both fuel system compatibility and lambda compensation of fuel delivery in fuel injection system of engines that include a closed loop lambda control system. Ethanol could damage some of the compositions of plastic or rubber fuel delivery components in some engines which are designed for conventional gasoline, as well as the disability to appropriately lambda compensate the fuel [134].

One litre of ethanol can produce 21.1 MJ of energy, while a litre of gasoline can produce around 32.6 MJ of energy from burning (or combusting). In other words, 1.6 litres/gallons of ethanol is required, for the same amount of energy content as one litre or one gallon of gasoline. However, the raw energy per volume values create misleading fuel consumption numbers, due to the fact that engines fuelled with alcohol can be made significantly more energy efficient. A greater fraction of the energy available in a litre of alcohol fuel can be transformed into positive work. Depending on the specific engines that are being compared, this difference in efficiency can somewhat, or entirely, compensate for the difference in energy density [134].

Ethanol is already being widely used as a fuel additive, and the use of ethanol fuel, in pure form or as part of a mixture with gasoline, is growing. Ethanol's primary

advantage is that it is less corrosive in comparison to methanol, and additionally, the fuel is also non-toxic, even though the fuel will generate some toxic exhaust gas emissions. Since 2007, the Indy Racing League has been using ethanol as the exclusive fuel of the events, after using methanol for 40 years [135]. Since September 2007 gasoline stations in New South Wales, Australia are mandated to supply all their gasoline products with 2% of ethanol content [136].

Below is the combustion process for both of these alcohol fuels:

Methanol combustion is:  $2\text{CH}_3\text{OH} + 3\text{O}_2 \rightarrow 2\text{CO}_2 + 4\text{H}_2\text{O} + \text{Q}$

Ethanol combustion is:  $\text{C}_2\text{H}_5\text{OH} + 3\text{O}_2 \rightarrow 2\text{CO}_2 + 3\text{H}_2\text{O} + \text{Q}$

Where Q is the quantity of heat transferred to or from the object [134].

Another beneficial aspect of ethanol that makes it desirable as a fuel additive or replacement, is that ethanol is a renewable energy resource. The declining fossil fuel resources and the ever increasing reliance of the United States of America (USA) in particular, on crude oil which is imported, have led to a great appeal in increasing the use of bioenergy and thus biofuels. The current commitment by the America government to increase bioenergy by three times in ten years, has increased the motivation for the pursuit for feasible biofuels. The European Union (EU) had also implemented a proposition for a mandate on the advancement in the use of biofuels, with procedures guaranteeing that biofuels make up at least 2% of the market for gasoline and diesel sold as transport and vehicle fuel back in 2005, which required increasing in stages to a minimum of 5.75% by the end of 2010 [137] and up to a minimum of 10% by 2020 [138].

The carbon dioxide ( $\text{CO}_2$ ) captured when the feedstock crops are grown to make ethanol, offsets the carbon dioxide released by a vehicle when ethanol is burned as its fuel. This varies from gasoline and diesel, which are refined from petroleum extracted from the earth. Emissions are not offset when these petroleum products are burned as fuel. On a life cycle analysis basis, with corn based ethanol made from dry mills, compared with gasoline and diesel production and use, greenhouse gases emissions are reduced on average by 40% and up to as much as 108% if cellulosic feedstocks are used for ethanol production [9].

Ethanol is attracting most attention amongst all the biofuels. It is already produced in large scale in both Brazil and the United States, and it can be easily blended with gasoline to operate in spark ignition (SI) engines. In Brazil, bioethanol is used as neat ethanol in 100% alcohol-fuelled passenger cars (hydrous ethanol) or is blended (anhydrous ethanol) with all the gasoline in proportions of usually about 24% to operate in gasoline engines, or it is still used (as hydrous ethanol) in any proportion in flexible-fuel vehicles (FFV) [139]. In Brazil, sugarcane ethanol, which is already well known as an efficient and renewable biofuel, has promoted rural development, diversification of energy sources, lower dependence on oil imports, reduction in local pollutants from vehicle exhausts and net reductions in greenhouse gas (GHG) emissions. These objectives were attained with the development of the Brazilian Alcohol Program, Proalcool, which was created in 1975 to increase the production of alcohol as a fuel in the face of rising oil prices on the market internationally. The positive results of the ethanol production program were possible due to the technological achievements, infrastructure investments and management in both sugarcane and ethanol production. Due to these developments, Brazil is nowadays the global benchmark in sugarcane based ethanol production. Hydrated ethanol is sold to consumers for less than 70% (by volume) of the gasoline price, corresponding to an ethanol break-even price in energy terms in relation to gasoline. Thus, alcohol is economically competitive with gasoline without any subsidies. These are the two main fuels used in cars in Brazil, since diesel vehicles manufactured in the country are heavy-duty commercial vehicles [140] [141].

Methanol and ethanol can both be derived from biomass, fossil fuels, or possibly most simply, using carbon dioxide and water. Generally in most cases, ethanol has been produced by the fermentation of sugars, and methanol has generally been produced from synthesis gas, also known as Syngas, but there are more contemporary methods of obtaining these fuels. Enzymes can be used as an alternative to fermentation. Ethanol can be made from methanol, since methanol is the simpler molecule. Methanol can be produced from virtually any biomass industrially, including animal waste, or even from carbon dioxide and water or steam, by converting the biomass to syngas initially in a gasifier. It can be produced in a laboratory using enzymes or electrolysis as well [142].

Approaching the 2020 directives laid down in the Renewable Energy Directive (RED), EU bioethanol and biodiesel consumption is forecasted to grow in 2017 and 2018. A new legislative proposal (RED II) was published by the European Commission (EC) in November 30 of 2016, for the period of 2021-2030. The RED II gradually limits the use of food based biofuels. The blending rates for advanced biofuels are increased in a series of distinct stages between 2020 and 2030. This aims to boost the market for these non-food based biofuels. The RED II directive also comprises of additional consistent sustainability standards for products from biofuels to biomass. The planned sustainability requirements are a possible trade barrier for the import of wood pellets [143].

Figure 2.17 below shows the fuel ethanol production in EU by country, where low feedstock prices in 2014, and limitations placed on bioethanol imports benefitted the segment, thus as a result, EU bioethanol production increased to about 5.3 billion litres. In 2016, EU bioethanol production rate declined because of financial problems within the segment, but it is forecasted to recover to approximately 5.4 billion litres [143].

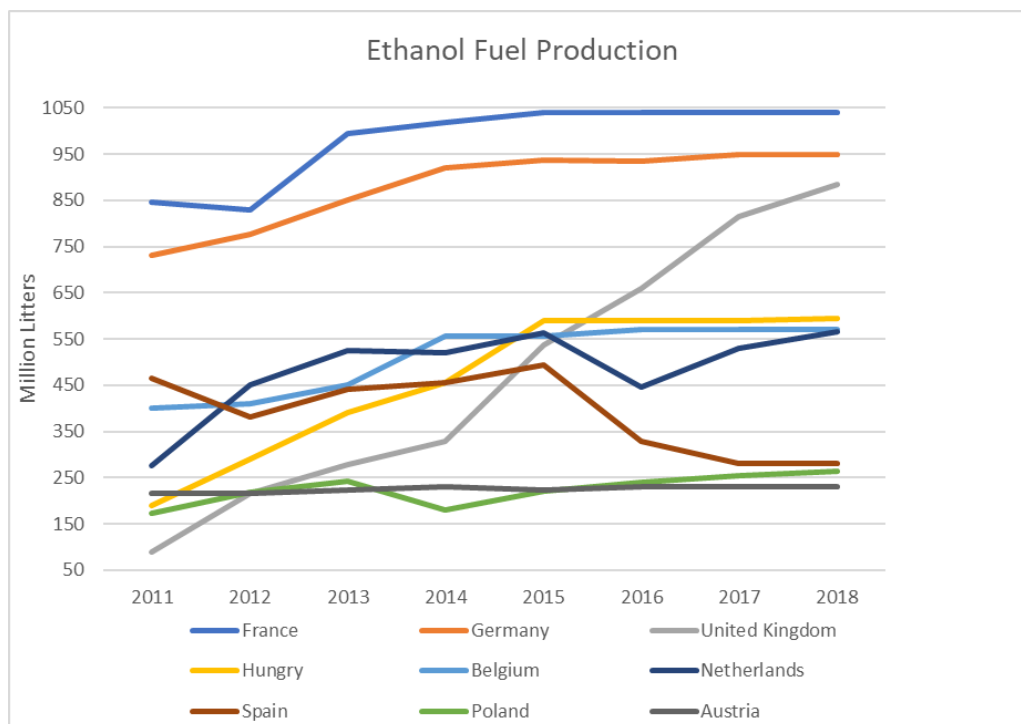
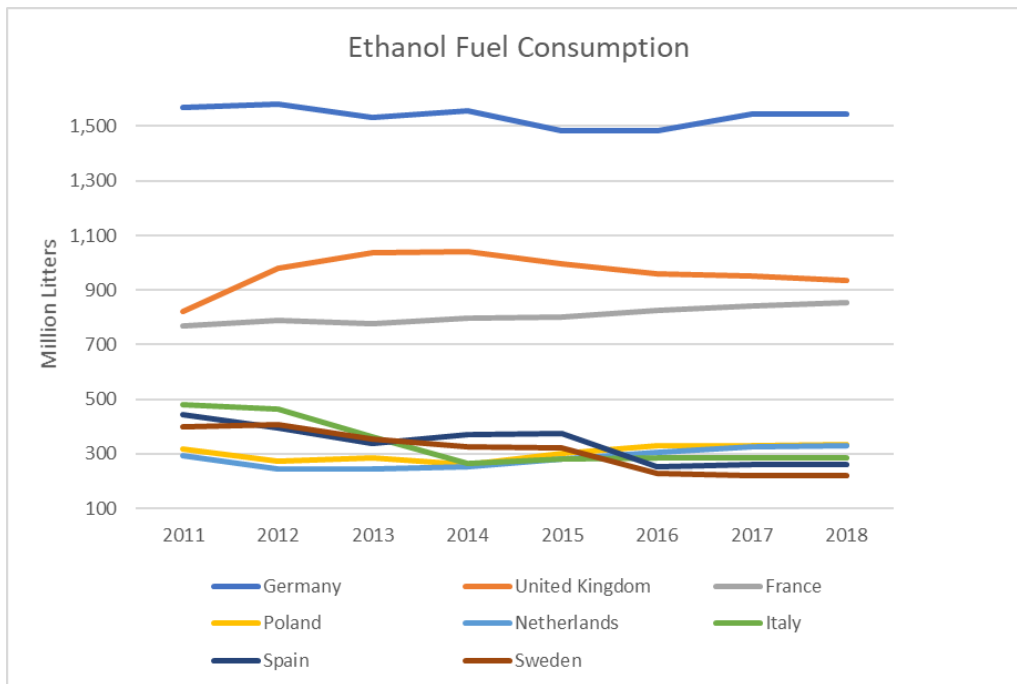


Figure 2.17 EU Fuel Ethanol Production Main Producers (source: EU FAS Posts) [143]

Figure 2.18 below shows the fuel ethanol consumption in EU by country;



*Figure 2.18 EU Fuel Ethanol Production Main Consumption (source: EU FAS Posts) [143]*

Although EU bioethanol production has idled since 2015, consumption of bioethanol has been on the decline since 2011. This tendency can primarily be clarified by lower gasoline use and the adjustment of national blending directives. Another influence is the blending of biofuels, which count twofold towards the directive. In the markets which are regulated by the directives and consumption of biofuels is fixed, the decrease in price of fossil fuels, did not have a noteworthy effect on biofuel consumption. Price increases have been moderated by the decreasing value of the Euro against the united states dollar. The low gasoline prices have considerably influenced the sales of the higher ethanol blends. Bioethanol consumption is projected at approximately 5.3 billion litres in 2016, and is expected to regularly increase to over 5.4 billion litres in 2018 [143].

The use of ethanol blended with diesel as a fuel was a topic of research in the 1980s and it was shown that ethanol blended with diesel were theoretically suitable for diesel engines of the time. However, the rather high cost of ethanol production at that time meant that the fuel could be considered for use, only in situations of fuel shortage risk. Recently, the production of ethanol has become much more favourable economy wise, and therefore, it is able to compete with typical diesel fuel.

Subsequently, the appeal of ethanol diesel fuel blends has reemerged, with distinct importance on reduction in the emissions output [137].

Ethanol fuel has been projected as a future biofuel, and often as a substitute to the hydrogen economy. Biofuel has an extended past as a racing fuel. Blended mixtures as well as in pure form were used as early grand prix racing fuel. After the war, it was mainly used in north America. However, this fuel could not be counted as a biofuel since it has mainly been grounded on production from syngas for use as racing fuel, which has been originated from natural gas and therefore from fossil fuel resources. Nevertheless, when the syngas is originated from biomass, this fuel can be considered as a biofuel. Theoretically, using nuclear power or any renewable energy source, ethanol can also be made from carbon dioxide and hydrogen, although this is improbable to be economically feasible on an industrial level, considering the ethanol economy. The primary advantage of methanol biofuel, compared to bioethanol, is its much superior well to wheel efficiency. In moderate climates where fertilizers are required for growing sugar or starch crops to produce ethanol, this is predominantly relevant, while lignocellulose, or woody biomass can be used to produced methanol from [134].

As discussed before, ethanol is a renewable, domestically produced alcohol fuel that can be produced from plant materials, such as corn, sugar cane, or even grasses. Using ethanol has a great potential to reduce dependency on oil and oil based fuels, as well as reducing greenhouse gas (GHG) emissions. Ethanol fuel use in the united states has increased considerably from about 1.7 billion gallons back in 2001 to around 14.4 billion gallons back in 2016 [144].

Most of the gasoline sold in the united states gasoline stations, contains up to 10% of ethanol. Although this amount varies region by region. All car makers support blends of up to E10 in their gasoline engine vehicles. As of 2011, EPA (Environmental Protection Agency) started permitting the use of E15 in year 2001 model vehicles, as well as more recent gasoline vehicles [145].

As previously mentioned, ethanol contains about a third less energy than that of gasoline. Therefore, vehicles will typically go 3% to 4% fewer kilometres per litre on E10 and 4% to 5% fewer on E15 compared to pure gasoline [146].

E85, also called flex fuel, is an ethanol and gasoline blended fuel, which depending on geography and season, contains 51% to 83% of ethanol. While winter blends have less ethanol in comparison to summer blends which tend to have higher percentage of ethanol [147].

Because of the fact that ethanol has a lower energy content, Vehicles operating on E85 Flex Fuel, get approximately 15%, based on the difference in the energy content of a 51% ethanol blend and that of gasoline, which is usually 10% ethanol, to 27%, based on the difference in official EPA fuel economy tests of current model FFVs (Flex Fuel Vehicle) running on ethanol free or pure gasoline, and running on E85, less kilometres per litre than when running on regular gasoline, subject to the ethanol content. Standard gasoline usually contains approximately 10% of ethanol.

Compared to gasoline, or E10, the cost of E85 can differ based on location, as well as changes in energy markets. Typically, E85 is cheaper per litre compared to gasoline, but somewhat more expensive per kilometre.

Drivers should not notice any loss of performance when using E85. In actual fact, some FFVs perform better, and have improved horsepower and torque when operating on E85 compared to operation with standard gasoline [148] [149] [150] [151] [152].

Flex Fuel vehicles have advanced fuel system and engine components and elements that are designed and manufactured for long life even when using E85 or M85, and the ECU (engine control unit) can adjust to any fuel combination amongst gasoline and E85 or M85. Usual upgrades consist of alterations to fuel tanks, fuel pumps, fuel tank electrical wiring, fuel lines, fuel filters, fuel level sensors, filler tubes, fuel rails, fuel injectors, fuel pressure regulators, inlet valves, valve seats, and seals. Total flex vehicles intended for the Brazilian market have the ability to run on E100 (100% Ethanol) [134].

Many techniques have been assessed to allow for the simultaneous use of diesel and ethanol in CI engines. Some of these techniques include alcohol fumigation, dual injection, alcohol-diesel fuel emulsions, and alcohol-diesel fuel blends. Amongst these methods, only alcohol-diesel emulsions and blends are compatible with most commercial diesel engines. Since emulsions are difficult to achieve and tend to be unstable, blends, either as micro-emulsions or using co-solvents, are the most

common approach as they are stable and can be used in engines with relatively no modifications.

Blends of ethanol with diesel fuel are often referred to as E-Diesel or eDiesel. In E-diesel blends, standard diesel fuel is typically blended, by volume, with up to 15% of ethanol using an additive package that helps maintain blend stability and other properties, most importantly cetane number and lubricity. The additive package may comprise from 0.2% to 5.0% of the blend. The use of E-diesel can bring some reductions in diesel PM emissions, while opposing reports exist on its effect on NO<sub>x</sub>, CO, and HC emissions. Possibly the biggest advantage of E-diesel, if renewable ethanol is used as the blending stock, is its partly renewable character. Bearing in mind its potentially noteworthy operational and safety issues, such as very low flash point, E-diesel will likely remain a niche market fuel of limited applicability. [153] [154]

## 2.7 Optical Diagnostics, Engines and Analysis

Developments in Internal Combustion (IC) engine performance, particularly in terms of improved fuel economy and reduction in engine emissions output, have been mainly as a result of important mutual research and development attempts by automotive industry, research institutes and universities, as well as suppliers. Especially over the last few decades, the development and application of experimental as well as computational research and development tools and instruments, has provided the ability for a more comprehensive understanding of basic and essential physical phenomena occurring in IC engines. Single cylinder, optical access engines, with regards to experimental engine research, have been broadly used as they allow for the application of qualitative and quantitative study at the same time, as well as non-intrusive, optical diagnostic techniques, in order to gain a detailed insight of all the processes taking place within the combustion chamber from fuel injection, mixing, combustion and the formation of emissions. Even though earlier work executed on optical engines offered valuable experimental data, thus providing an enhanced understanding of fundamental in-cylinder physical occurrences and for the authentication of CFD (computational fluid dynamics) representations, from the engine developer's standpoint, the significance of optical engine data was often considered to be relatively imperfect since optical engines were not considered to be

completely representative of typical all metal engines. Specifically since particular compromises are frequently made, for example the use of a more simplified piston bowl structure (Figure 2.19) in order to expand the engine's optical access. Additionally, single component fuels are frequently utilized instead of standard commercial fuels, because of the limitations of laser diagnostic techniques. Also, custom made non-standard piston rings, made from specific specialist materials, are used in optical engines because of the requirement to run these engines dry and without regular lubrication meaning that the upper cylinder liner on an optical engine is not, and cannot be lubricated, which consequently, often results in the assertion that the engine blow-by is considerably more in an optical engine compared to that of a typical engines [155].

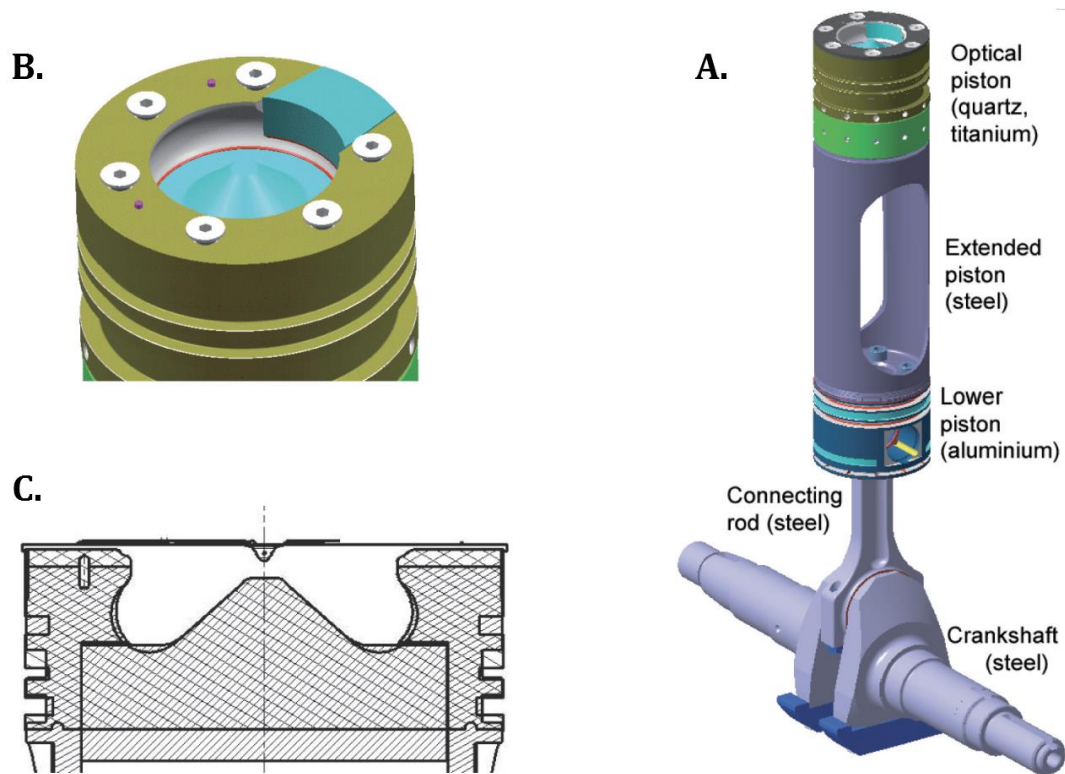


*Figure 2.19 A. 3D schematic showing main components of the optical engine including the extended piston assembly and optical piston. – B. Optical-access Diesel piston bowl showing location of quartz windows. – C. Comparison of optical-access and all-metal engine combustion chamber geometries [155].*

In the more recent years, in-cylinder combustion processes studies are relying on a combined approach more than before, where experiments are performed on an optical

engine as well as an identical, typical, all-metal engine [156] [157] [158]. (Figure 2.20)

There are undoubtedly numerous benefits to this method testing. Primarily, on all-metal engines, experimental data can be attained at a much higher rate, compared to an optical engine, in order to create an extensive set of data in which a variety of engine characteristics can be examined. As for example, these variations may comprise of engine characteristics such as, injection timing/strategies, amount of charge dilution, intake temperature, intake pressure, coolant temperature, and equivalence ratio.

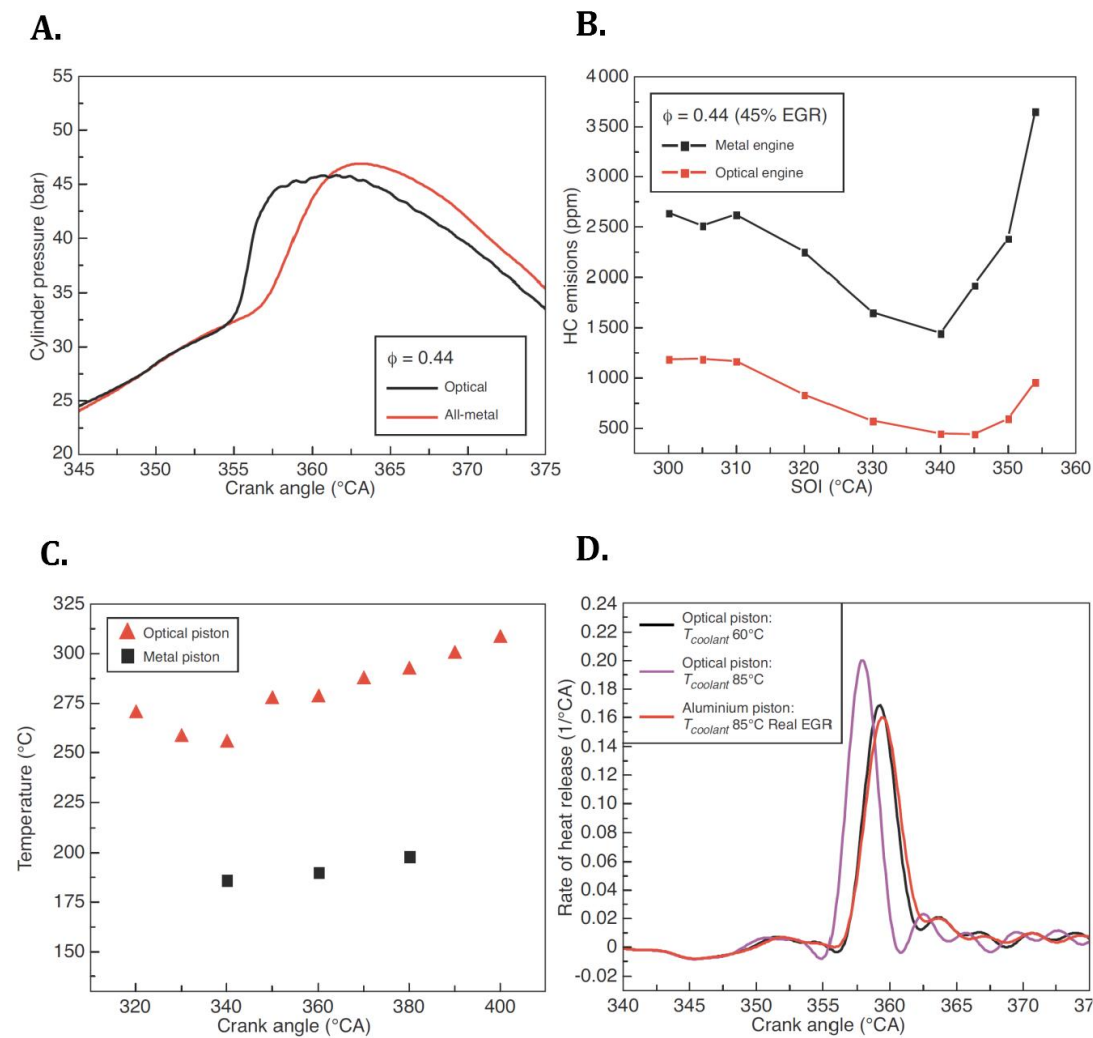


**Figure 2.20 Comparison of:** **A.** Pressure traces obtained on optical and all-metal engine, SOI  $340^{\circ}$ CA, simulated EGR, 1500 rpm, 2 bar IMEP,  $P_{inj}$ . 1000 bar, standard Diesel fuel. – **B.** Measured engine-out HC emissions obtained on optical and all-metal engines for a SOI timing sweep, EGR 45% (simulated EGR on optical engine), standard Diesel fuel. – **C.** Piston wall temperature

*measurements acquired in squish zone for the optical-access (quartz/titanium) and all-metal (aluminium) pistons, 1200 rpm, SOI 350°C, 45% EGR without skip-firing. Ensemble-averaged LIP data over 100 engine cycles at each Crank Angle position. – D. Heat release rates obtained on optical engine with all-metal and optical pistons showing effect of adjusting engine coolant temperature [155].*

Hence, researches on all-metal engines allow for a thorough set of testing data to be collected reasonably quick. A following examination of these data may provide appealing trends, that can be examined with more in depth detail on the optical engine. The application of suitable laser based diagnostic techniques on the optical engine particularly, can present results that could potentially result in enhanced understanding of the physical occurrences taking place in the combustion chamber [155].

In *Optical Engines as Representative Tools in the Development of New Combustion Engine Concepts*. by J. Kashdan and B. Thirouard, a thorough comparison of the thermodynamics and emissions analysis of a single cylinder, optical research engine and a typical all metal engine with the same specifications has taken place under Diesel LTC (low temperature combustion) operating conditions. The main differences between the two engines were noted and the influences of these differences on fuel mixing and combustion, and emissions formation have been discussed, where the results have illustrated the significant effect of properties of different materials on the combustion chamber wall heat transfer characteristics for the optical as well as the all metal engines. The low thermal conductivity materials typically used on optical engines specifically, cause higher wall and bulk gas temperatures, which have a major effect on combustion phasing and engines emission output. Non-intrusive piston surface temperature measurements in the aforementioned study, were accomplished using the Laser Induced Phosphorescence technique. Results of the study were acquired at a 1200 rpm and 2 bar IMEP operating condition, which revealed surface temperatures near to TDC in excess of 300°C for the optical access piston, compared with around 190°C for that of the all metal piston [155].

The application of optical engines and laser based diagnostic techniques as a means of achieving a detailed understanding and an improved perception of in-cylinder fuel mixing and combustion, as well as emissions trends is justly recognised.

Nevertheless, the capability to guarantee an entirely representative combustion and emissions characteristics of optical engines, improves the significance of optical engine data, thus stressing the prominence of using these engines as research instruments for the further improvement of ground-breaking and low emission combustion models.

### **2.7.1 In-cylinder studies of diesel dual fuel combustion**

Where in-cylinder studies and optical diagnostics can provide many insights to any engines operating characteristics by allowing closer examination of in-cylinder activities such as the fuel injection, mixing, and combustion, this is true for all forms of fuels and fuel mixtures, and diesel dual-fuel is of no exception. Many researchers have utilized this technique (Optical Analysis) to examine and study variety of engines, engine modes, and fuels, in terms of performance and fuel consumption, as well as emission production. In *Optical Investigation of Dual-fuel CNG/Diesel Combustion Strategies to Reduce CO<sub>2</sub> Emissions*, Nicolas Dronniou et al. [159] explored the fundamental combustion phenomena occurring when methane is ignited with a pilot injection of diesel fuel, on a single-cylinder optical research engine, typical of modern, light-duty diesel engines, along with a high-speed digital camera which recorded time-resolved combustion luminosity as well as an intensified CCD camera for single-cycle OH\*chemiluminescence Imaging. A wide range of equivalence ratios of the premixed charge were experimented on, showing from the optical engine results that at low equivalence ratios, combustion of the premixed charge of methane gas was dominated by spray entrainment and mixture stratification of diesel fuel, while time-resolved natural luminosity images shown that at higher equivalence ratios, specifically close to stoichiometry, there are significant modifications in combustion behaviour indicating some evidence of flame propagation. Corresponding rates of heat release support the optical measurements in terms of revealing a significant impact on combustion following an increase of equivalence ratio. They also performed planar laser-induced fluorescence tracer experiments in order to investigate the influence of in-cylinder fuel distribution on dual-fuel ignition.

Changzhao Jiang, Xiao Ma and Hongming Xu [160] studied the combustion of DMF and ethanol under dual-injection strategy, where high speed imaging and thermal

investigation were carried out to study DMF and gasoline dual-injection on a single cylinder, direct injection spark ignition optical engine, by combining direct injection and port fuel injection simultaneously, resulting in two different fuels to be blended in the cylinder with any ratio. For all of their tests, gasoline was injected through PFI and different amounts of DMF or ethanol were injected through DI. For each of the predetermined IMEP, 3bar and 5bar, bio-fuel DI fraction was increased from 0% to 100%. The flame morphology was analysed, and normalized flame area data was then used to study the effect of the dual-injection strategy and fuels, showing that DMF-gasoline dual-injection combustion has higher flame propagation speed and shorter combustion duration than baseline 100% gasoline PFI. The flame luminance of DMF-gasoline is much higher than ethanol-gasoline and pure gasoline, and that flame propagation speed of ethanol increases with the increase of IMEP, while the engine load conditions have less influence on DMF-gasoline dual-injection flame propagation speed.

Furthermore, in *An Optical Investigation of Fuel Composition Effects in a Reactivity Controlled HSDI Engine* by Matthew Blessinger, Joshua Stein and Jaal Ghandhi [161], reactivity controlled compression ignition combustion was investigated for three fuel combinations of isooctane-diesel, PRF90-diesel, and E85-diesel, at 1200 rpm, 160 kPa absolute intake pressure, and fixed total fuel energy using optimal operating condition for each fuel combination, chosen based on combustion performance from SOI timing and premixed energy fraction sweeps, where the heat release duration was found to scale with the difference in reactivity between the premixed and directly injected fuel, and a small difference gives rise to short heat release duration, similar to that of HCCI combustion. On the other hand, with increase in the difference, the heat release period increases. The high-speed optical data collected by them confirmed that the combustion happened in a staged manner from the high-reactivity zones, which were located at the edge of the chamber, to low-reactivity zones in the field of view of the camera. Additionally, the range of ignition timing across the imaged area was found to scale with respect to the difference in the reactivity of the two fuels. The ignition took place in a relatively narrow window within the heat release profile in instances where there was a small difference in reactivity. The progression of the ignition front from high- to low-reactivity regions was found to occur over an extended part of the heat release duration in situations

with large enough reactivity difference. Similar integrated luminosity levels in the 310 nm range were observed for the tested fuels, in spite of the difference in combustion characteristics and injection timings. The luminosity levels were comparable to HCCI combustion levels and in excess of two orders of magnitude lower than standard diesel combustion.

These studies and ones similar to them represent the value of in-cylinder study and optical analysis in better understanding and improving various engine operation modes and combustion development.

### **2.7.2 High Speed Imaging**

Within the past decade, new camera and laser technologies have provided the ability for the improvement of high-speed imaging diagnostics for measurements at frame rates corresponding with the time scales of turbulent mixing of the fuel, fuel injection, combustion, and emission formation in internal combustion engines. The capability to study the development of in-cylinder flow, fuel and air mixing, injection, ignition, and combustion within each engine cycles, and for many successive cycles, offers new understanding into the physics and chemistry of internal combustion engine and their performance. Data used for model and device development are acquired with exceptional access to the detection of arbitrary outcomes such as cycle to cycle difference and ignition unpredictability [162].

The application of high speed imaging in IC engines, permits the visualization of sequential and spatial resolution of fuel spray, as well as its combustion. The experimental setup simply requires a source of light, i.e. laser beam, and a device for image capture, i.e. high-speed camera. Essentially, for high speed visualization, the source of light is selected with respect to its brightness, spectral distribution and its repetition rate, as a result of the necessity of a significant amount of light over a short period of time. Likewise, because of their high repetition rate, high-speed cine film cameras are normally used. Herfatmanesh and Lu [163] visualized the fuel injection formation and combustion process, by using a copper vapour laser and a NAC Memrecam FX6000 high speed camera, in a research optical diesel engine. This technique was also widely employed in many studies [164] [165] [166] [167] [34].

## 2.8 Summary

In this chapter, the background on current and future state of emissions legislation was discussed in detail. An in depth look at the current state of dual fuel engines, including the researches completed in this field, as well as a look at a range of alternative fuels available, from natural gas to non-fossil fuel based sources such as biofuels, namely ethanol. The more recent engine diagnostic techniques, namely optical analysis for the visualisation of the entire combustion procedure from injection , to combustion and emissions, and the advantages and disadvantages of employing such techniques were also discussed and elaborated on, as well as ways to overcome the disadvantages brought forward by these techniques. The fundamentals of IC diesel engines combustion with attention to the variety of their operation principles, as well as their possible emissions were explained, detailing their respective mechanism of formation and diminution. Effect of variety of techniques employed in the industry and in research level for improving engine performance as well as exhaust gas emissions, such as using EGR, or different fuel injection systems and strategies, with respect to the researches done in these areas were also discussed.

By and large, diesel-ethanol and diesel-gasoline dual fuel combustion can aid in reducing the carbon footprint of the transport sector, as well as minimising dependency to petroleum based fuels, and while there has been many investigations and publications on variety of alternative fuels and energy sources, including ethanol, and their pros and cons to provide efficiency and effectiveness to reduce emissions, as well as some visual in-cylinder studies to better understand fuel behaviour during combustion, further research and development is required to apply the more recent optical analysis techniques for in-cylinder visualization, to alternative fuels and fuel mixtures, and more specifically, to dual fuel engines, in the effort to aid GHG reduction and to satisfy emission legislations.

# Chapter 3.

## **Experimental Facilities, Methodology and Data Analysis**

### 3.1 Introduction

In this chapter, the experimental setup, the test facilities, data acquisition system, and the data analysis techniques used in this study is explained in detail. A brief description of the test bed, the Ricardo single cylinder optical research engine, and also the fuel injection system, air intake and exhaust system are given. The equipment and the process for high speed imaging are presented. The calibration for both diesel direct injector and the port fuel injector and the air flow measurements are discussed. Furthermore, the data analysis for the heat release and combustion process and emission testing is discussed.

### 3.2 Ricardo Single Cylinder Research Engine with Optical Access

#### **3.2.1 General Description**

All the experimental testing in this study was carried out on a single cylinder Ricardo Hydra Optical engine, with an extended cylinder block, a standard production 4-cylinder engine cylinder head and a common rail fuel injection system, designed to be representative of a typical modern high-speed direct injection (HSDI) diesel engine. The engine specifications are presented in Table 3.1. The engine is mounted on a Cussons Technology's single cylinder engine test bed consisting of a seismic mass engine mounting, 30 kW DC dynamometer and engine coolant and oil circuits, as shown in Figure 3.1 and Figure 3.2 below.

*Table 3.1 Ricardo Hydra Engine Specifications*

Ricardo Hydra Single Cylinder Optical Engine	
Bore	86 mm
Stroke	86 mm
Swept Volume	499 cm <sup>3</sup>
Compression Ratio	16:1
Piston Bowl Diameter/Depth	43.4/11.6 mm, re-entrant bowl with flat bottom
Swirl Ratio	1.4
Engine Speed for Testing	1200 rpm

The upper and lower portions of the extended cylinder block are connected to the cylinder head and the engine crankcase respectively. The cylinder block houses three cut-outs on its wall, where the glass windows can be mounted in order to gain optical access on the side.

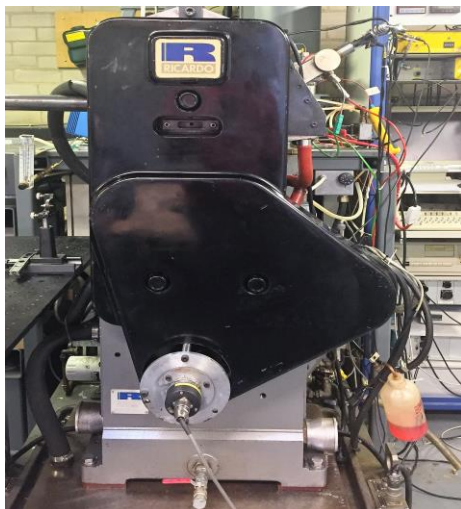


*Figure 3.1 Front View of the Ricardo Hydra Engine*



*Figure 3.2 Side View of the Ricardo Hydra Engine*

Inherently, optical engines have limited operation time. This is due to the considerable mechanical and thermal stresses on the optical components, such as the glass access points, during the combustion cycle. Hence, both the engine oil and the coolant require preheating, to around 90°C and 80°C, respectively, in order to prevent any damage to the optical components. The lubricating system comprises of a wet sump,

mounted on the test bed, gravity-fed pressure pump powered by an electric motor and two immersion heaters in the oil sump. Oil is pumped from the sump and pass through an oil filter before being fed in to the main oil reservoir surrounding the crankcase. This provides lubrication to the crankshaft, the big end bearing in the crankcase, as well as the camshaft in the cylinder head. The lower piston and the piston rings are lubricated by splattered oil, meanwhile the upper part of the piston and the cylinder block are lubricated by two carbon graphite rings made of Le Carbone Lorraine grade 5890 carbon and lubricant paste that is rubbed on the top compression piston ring. The coolant system comprises of a test bed mounted electric water pump and an immersion heater controlled by a thermostat.

The engine is motored using a 30 kW DC dynamometer, and it acts as a brake when the engine is firing. The engine speed is controlled by the dynamometer, allowing a fixed engine speed, which is then automatically maintained by driving or braking the engine as required.

### **3.2.2 Cylinder Head**

The Ricardo Hydra engine in this study was made to permit the use of a standard production four cylinder engine cylinder head. To allow for mounting of such cylinder head on the single cylinder engine block, a platform visible in Figure 3.1 was designed and built. This cylinder head is from a production Ford 2.0 litre ZSD 420 Duratorq turbocharged engine. The aluminium cylinder head comprises of, a double overhead camshaft system, four valves, a central injector, and a glow plug. The valvetrain of the unused cylinders is disabled by removal of the rocker arms. Each of the corresponding oil feed holes on the rocker shafts are obstructed as well in order to prevent the spurting of unwanted oil that could cause a drop in oil pressure. As mentioned above, the engine is preheated prior to the motoring, therefore problems related to the cold start are eradicated, and therefore, the glow plug is replaced by a Kistler 6125 piezoelectric pressure transducer for this study to enable in-cylinder pressure measurement.

### **3.2.3 Optical Configuration**

#### **3.2.3.1 Extended Piston and Cylinder Block**

The Bowditch piston design allows for optical access into the combustion chamber, through a fused silica glass window mounted in the crown of the piston. An extended

piston and cylinder block are required in order to accommodate for this optical configuration, which comprises of a lower and an upper part, with a 45° angled mirror, made from glass with aluminized front surface, between the two sections. Therefore, the combustion chamber and cylinder walls are fully visible through such optical arrangement, shown in Figure 3.3. The lower part of the piston comprises of a standard type piston, modified in a way so that the upper piston can be bolted on. Conventional oil scraper rings are employed to control the excess oil in the lower cylinder wall while the elongated piston has a large cut out slot allowing for the mounting of the 45° mirror around which the piston moves up and down.

Since the lubricating oil could cause rapid contamination of the optical surfaces, the elongated cylinder block and the extended piston cannot be lubricated by oil. Therefore, the upper piston is lubricated by the two carbon graphite rings. In addition to the two carbon graphite rings, two conventional steel compression rings are fitted for sealing, which are lubricated by the carbon particles deposited on the cylinder walls by the carbon graphite rings. To provide additional lubrication between the piston and the cylinder block, high performance dry moly paste, made by Rocol, is applied to the upper cylinder block periodically as well as during each rebuild.

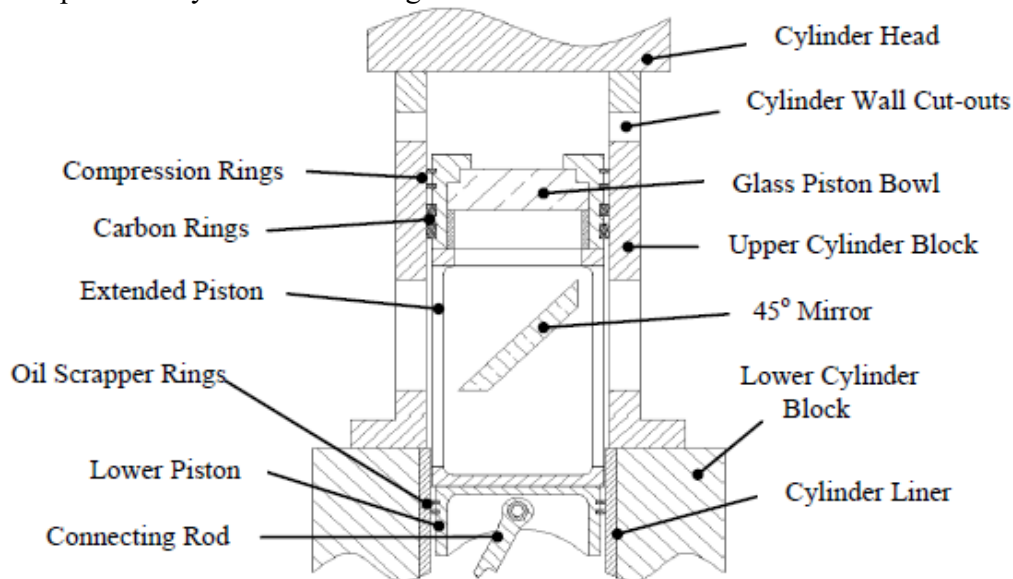


*Figure 3.3 Sectional Schematic View of the Optical Layout*

### **3.2.3.2 Optical windows**

As presented below in Figure 3.4, there are three rectangular cut outs on three side of the upper part of the cylinder wall, that can be fitted with fused silica glass to provide optical access from the side of the combustion chamber. As seen in the figure, two of the three cut outs are positioned along the same axis, while the third is in located

along a perpendicular axis. The former two will provide access for laser sheet imaging, while the latter one, is provided for imaging and/or detection.

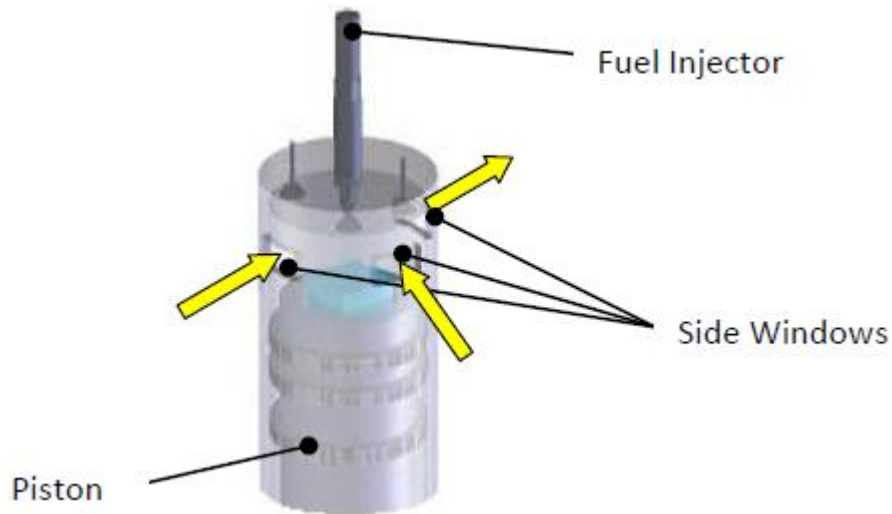


*Figure 3.4 Schematic View of Side Windows*

For this study, the optical access provided through the piston crown is the only one utilised. It is a fused silica glass window of a diameter of 43.4mm placed in the piston crown. Figure 3.5 below visualises the arrangement of sealings, rings, and the crown optical access in the top part of the piston.

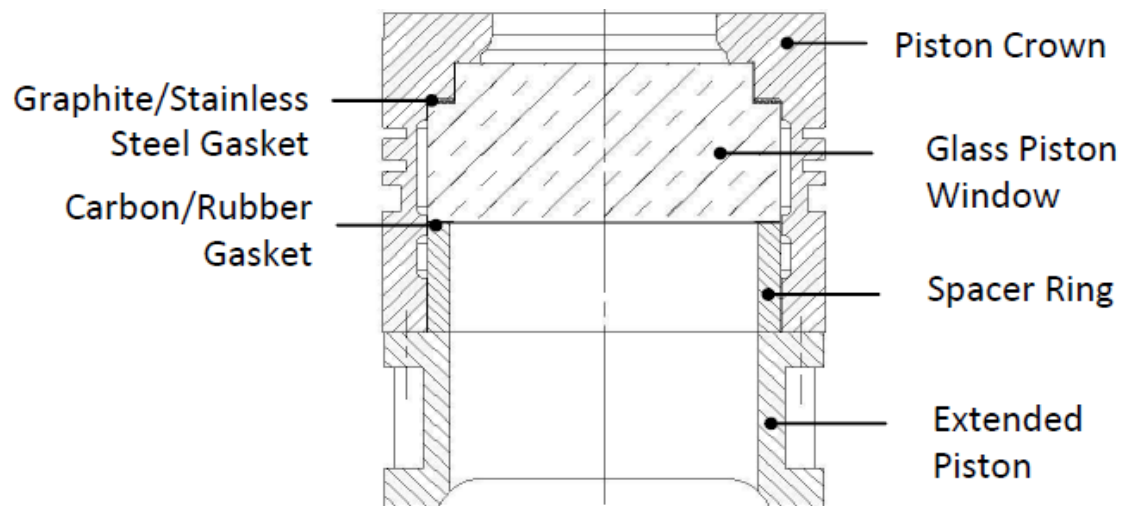


*Figure 3.5 Schematic View of the Piston Assembly*

The spacer ring in the Figure 3.5 above, made from steel, is placed between the upper part and the lower part of the elongated piston in order to ensure a leak proof seal between the window and the gasket. Tight fitting of the spacer ring on the gasket and the window is not recommended, as this could damage the fragile window, especially by the high stress levels created during the engine operation on the window. In order

to eradicate this matter, three raised edges were machined on the surface of the spacer ring, at the point of contact with the carbon graphite gasket, in order to create points of high pressure, thus aiding the seal. An O-ring was also fitted between the inner wall of the piston and the window, as seen in Figure 3.6 below, in order to improve seal and avert additional leakage from the space between the two said parts.

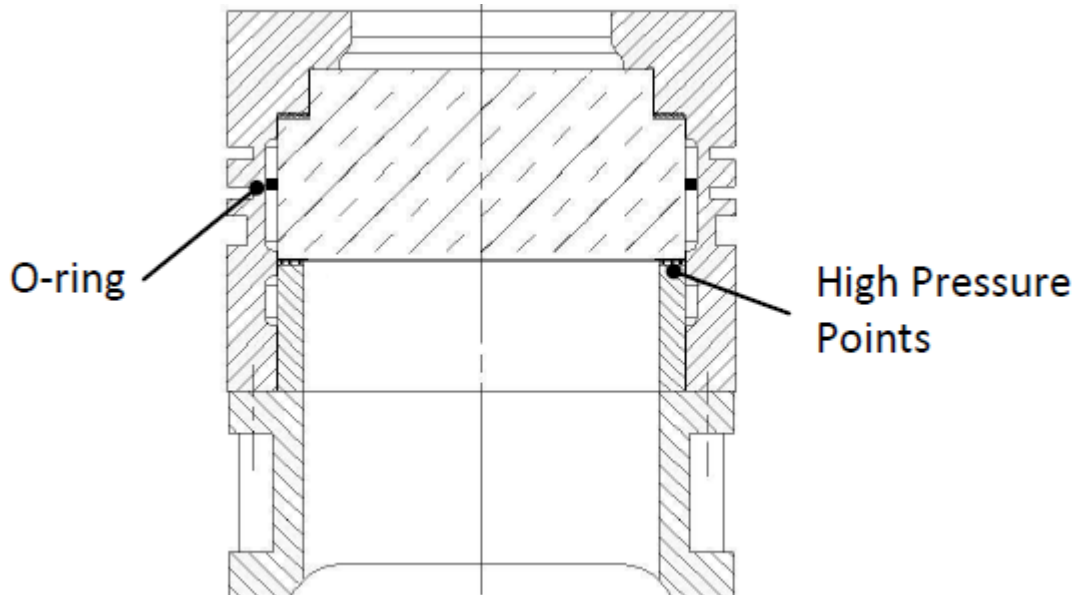


*Figure 3.6 Schematic View of the Modified Piston Assembly*

Additionally, during the compression stroke, the increased in-cylinder pressure pushes the window down against a Klingersil gasket manufactured from carbon and rubber, that improved the sealing between the glass and the metal even further. Thus, reducing the leakage at the glass and metal ring contact point, even further. Though, it should be noted that the piston is replaced with a metal blank during emission and thermodynamic testing, in order to enable more combustion cycles to be performed, by not having to risk damaging or breaking the glass window.

### **3.2.4 Crank Shaft Position System**

A shaft encoder, connected to the crankshaft, aids establishing the angular position of the piston, which generates two separate signals. One of which with 1800 pulse per revolution (ppr), and the other with 1 ppr. The two signals are then sent to the electronic control unit (ECU), where they are used to control the data acquisition system as well as the fuel injection system. The 1ppr signal is used to illuminate a light emitting diode (LED). This LED, located on the left side of the opening where

the 45° mirror is positioned, as seen in Figure 3.7 below, help identify the position of the thermodynamic top dead centre (TDC) in the high speed images by illuminating. This signal is generated on every revolution, and therefore creating two pulses at every engine cycle, one for every TDC. Thus, to be able to identify which TDC is for the compression stroke, and which is for the exhaust stroke, a hall-effect sensor, mounted on a metal disk, connected to the high pressure pump is used, which is driven at half the engine speed. The presence or absence of the signal from the hall-effect sensor allows the fuel injection system to determine which part of the cycle each TDC signal refers to. The signal from the hall effect sensor helps the fuel injection system to identify which TDC signal is being referred to.

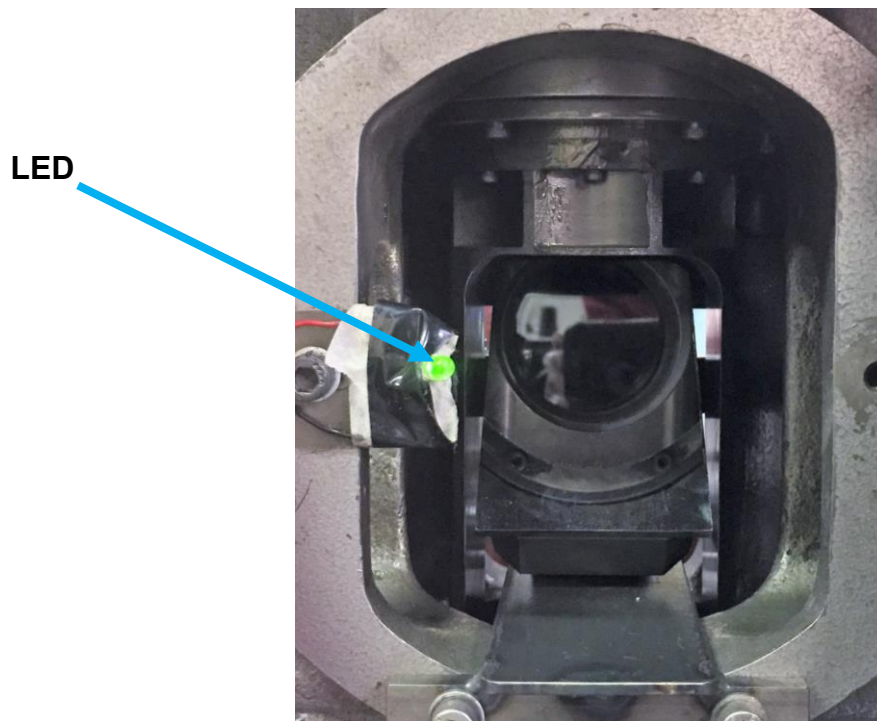


*Figure 3.7 LED Position*

### **3.2.5 Fuel Injection system**

For this study, in order to enable dual fuel operation, two separate fuel injection systems were used; one to deliver diesel, and second one to deliver ethanol/gasoline.

A Delphi HP common rail fuel system was used on the Ricardo single cylinder optical engine. The common rail injection system provides the high injection pressure independent of the engine speed. The pump used in the fuel supply system for this study includes a Powerstar 4 pneumatic high pressure pump, which converts

pressurized inlet air to a hydraulic output pressure of up to 1200 bar. As seen in Figure 3.8 below, this system also includes a fuel filter, a pressure sensor, and a fuel tank.

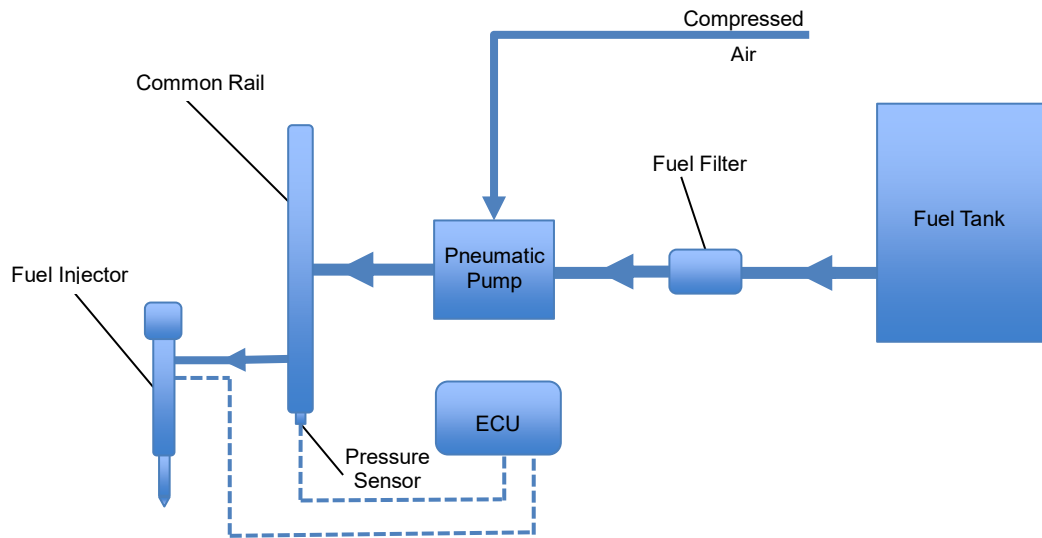


*Figure 3.8 Schematic Diagram of Common Rail Diesel Injection System*

The common rail used here, comes with four outlets, where one of them is connected to the fuel injector through a single thick wall steel pipe, the other three are blocked off. At one end of the common rail, a Delphi rail pressure sensor is connected, sending the signal to the ECU in order to allow for control over injection pressure. The injector used is a Delphi multi-hole Valve Covered Orifice (VCO) injector, detailed in Table 3.2 below.

*Table 3.2 Diesel Fuel Injector Specification*

Delphi Standard Injector	
Number of Holes	6
Hole Size	0.154 mm
Cone Angle	154 degree
Flow Rate	0.697 L/min
Maximum Injection Pressure	1600 bar
Type	VCO

The injector controller used for operating the diesel fuel injection for this study is a EC-GEN 500 ECU manufactured by EmTroniX, while EC-Lab, a computer based software, provides the control interface. The ECU receives the input signals from the shaft encoder, hall-effect sensor and fuel rail pressure. While the number of injections, injection timing, and injection quantity is set in EC-Lab. The injection driver, which is part of the EmTroniX system, converts the pulses to the appropriate current and voltage signals that is required for driving the injector. This is illustrated in Figure 3.9.

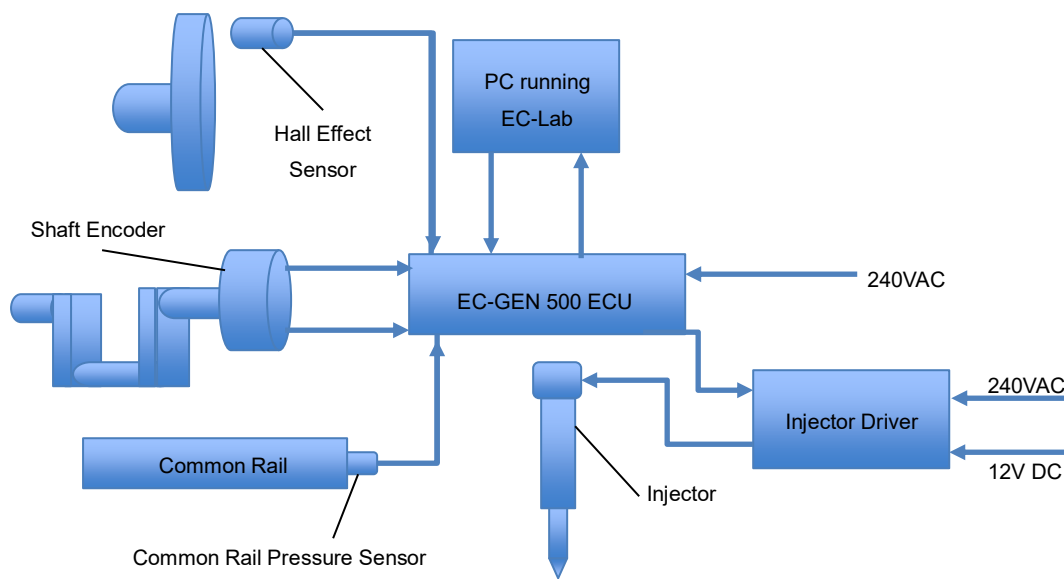


**Figure 3.9 Schematic Diagram of Fuel Injection Control System**

The port fuel injection and fuel delivery system seen in Figure 3.10 below, is comprised of a Bosch Injection Valve EV 14 injector, a gasoline fuel pump, a gasoline fuel filter, a fuel pressure regulator with pressure gauge, and a fuel tank.

A Bosch Injection Valve EV 14 injector provides the fuel delivery of ethanol/gasoline in form of port fuel injection. The factory build intake manifold, made for the Ford production cylinder head was replaced with a custom made intake manifold designed by this researcher and constructed by the lead lab technician, in order to allow for the accommodation of the port fuel injector at the top of the intake valves. The specifications of this injector can be found in Table 3.3 below.

*Table 3.3 Port Fuel Injector Specification*

Bosch EV 14 Injection Valve	
Maximum System Pressure	8 bar
Fuel Input	Top-Feed Injector
Spray Type	C (Conical Spray) or E (2-Spray)
Fuel Compatibility	E85 / M100
Power Supply	6 to 16.5 V
Coil Resistance	12Ω
Spray Angle $\alpha$	15 to 85°
Spray Angle $\gamma$	0 to 15°

The injector is then driven by a driver made in house by the electrical technician, which allows for setting injection duration, while it receives the TDC signal from the shaft encoder at every cycle, meaning that the fuel from the port fuel injector (be it ethanol or gasoline) is delivered in two instances with half of the total required amount being injected while the intake valve is closed, and the rest in the following cycle just before the intake valve opens, hence providing the total required fuel for the next compression cycle.

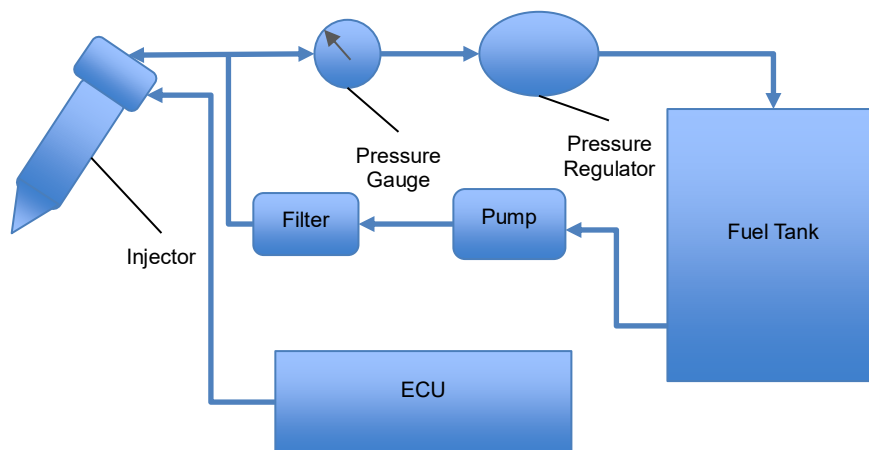


*Figure 3.10 Schematic Diagram of Port Fuel Injection System*

The relevant properties of the diesel and ethanol fuel used in this study is listed in Table 3.4, and additional information on both fuels can be found in Appendixes 3, 4 and 5, respectively.

*Table 3.4 Fuel Properties*

Property	Red diesel (gas oil)	Anhydrous ethanol
Supplier	Advance Fuels	Haymankimia
Product/standard specification	BS 2869 Class A2	Absolute ethanol (F203227)
Density at 293 K ( $\rho$ )	0.827 kg/dm <sup>3</sup>	0.790 kg/dm <sup>3</sup> [167]
Cetane number	> 45	n/a
Research octane number (RON)	n/a [8]	~107 [8]
Alcohol content	n/a	99.9% (> 99.5%)
Fatty acid methyl ester content	< 7.0%	n/a
Water content	< 0.20 g/kg [29]	1.7 g/kg [167] (< 8.2 g/kg)
Sulphur content	< 0.01 g/kg	n/a
Heat of vaporisation	270 kJ/kg [8]	840 kJ/kg [8]
Carbon mass content ( $\%C_{fuel}$ )	86.6%	52.1% [8]
Hydrogen mass content ( $\%H_{fuel}$ )	13.2%	13.1% [8]
Oxygen mass content ( $\%O_{fuel}$ )	0.2%	34.8% [8]
Normalised molecular composition	$CH_{1.825}O_{0.0014}$	$CH_3O_{0.5}$
Lower heating value (LHV)	42.9 MJ/kg	26.9 MJ/kg [8]

### 3.2.6 Intake System

The Ricardo single cylinder optical engine of this study is setup in a way that it could operate either as a naturally aspirated engine or as a supercharged engine. A change over valve allows for changing between the two operations. The setup also allows for the simulation of exhaust gas recycling (EGR) by the use of two pressurised gas tanks providing Nitrogen (N<sub>2</sub>) and Carbon Dioxide (CO<sub>2</sub>) into the intake system, in order to observe the effects of EGR on combustion and emission. The intake system is illustrated in Figure 3.11 below.

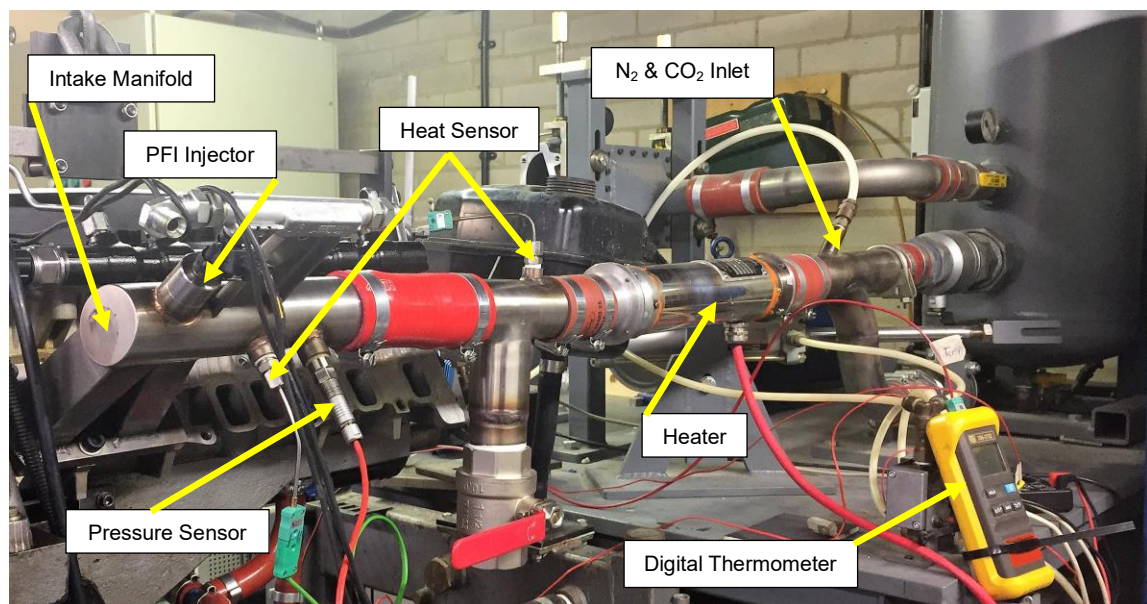


*Figure 3.11 Ricardo Hydra Engine Intake System*

#### 3.2.6.1 Forced Induction

The intake system used for this study also allows for the introduction of boosting to the intake pressure as required, by the virtue of having a forced induction system fitted to it. This boosting system, seen in Figure 3.12 below, consists of a positive displacement roots type blower, an Eaton M45 supercharger, with three lobes and helical rotors driven with an AC motor rotating at 2600 revolutions per minute (rpm). The supercharger on this system is capable of providing a maximum boost pressure of 0.5 bar, which can be manually adjusted by using a bypass valve fitted to the supercharger, where completely closing the bypass, valve will result in the maximum boost pressure. When required, a boost of 25% to 40% bar is used for this study.

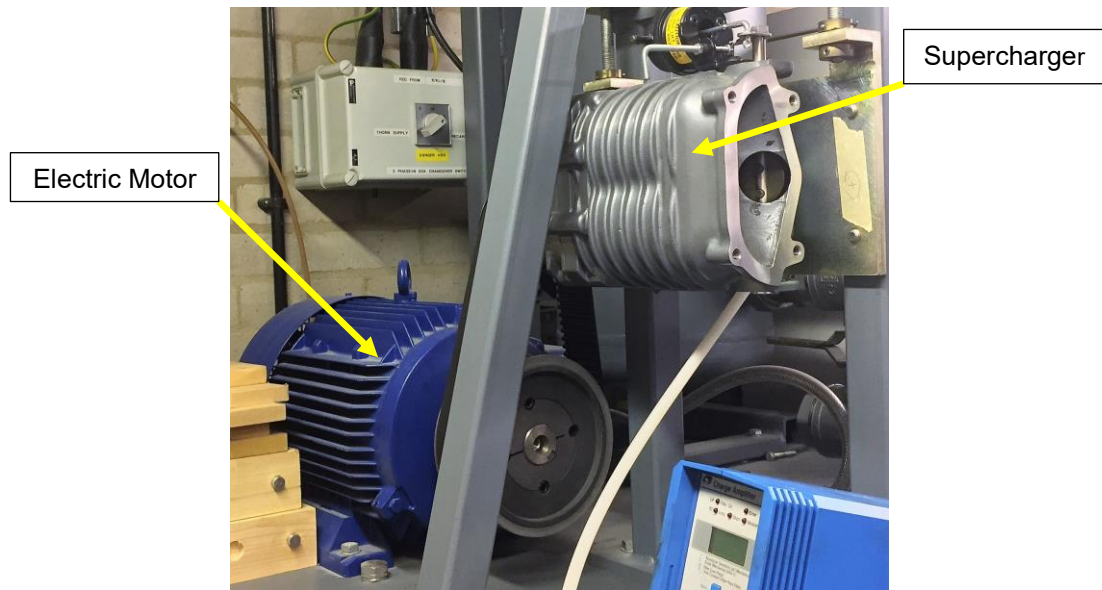


*Figure 3.12 Supercharging System*

A Kistler 4045A5 piezoresistive pressure transducer along with a Kistler 4618A2 piezoresistive amplifier, as seen in Figure 3.11, is fitted to the intake manifold. The signal from the charge amplifier is sent to an oscilloscope where the intake pressure can be monitored.

### **3.2.6.2 Intake Heating**

A 3kW air heater is fitted to the intake system, as illustrated in Figure 3.13, before the intake manifold, in order to allow for the replication of the conditions required for the operation of a typical HSDI diesel engine. A thermocouple attached to the intake manifold and connected to a heater temperature control box, allows for a closed loop control of the heaters temperature, where the box maintains the heater temperature to a set value by powering it on and off. The intake air temperatures used for this study vary between 100°C, 150°C, 180°C, and 200°C, depending on the testing conditions.

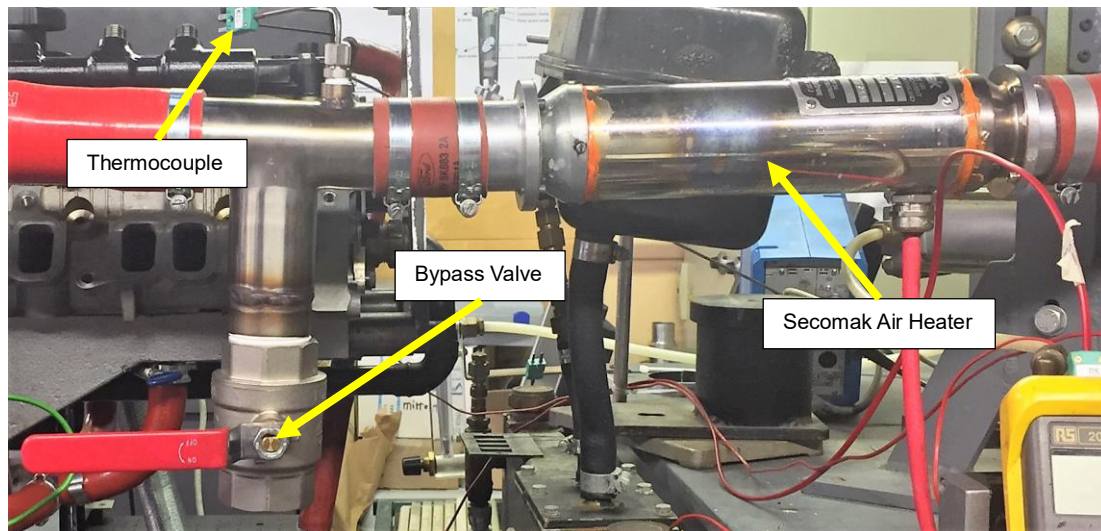


*Figure 3.13 Intake Heating System*

Additionally, a bypass valve along with a thermocouple was also fitted to the intake system, just after the intake air heater and before the intake manifold, which allows for warming up of the intake air heater by starting the supercharger without having to run the engine at all. The addition of this bypass valve aids the longevity of engine operation period between rebuilds, by reducing the time the engine needs to run before the intake air heater has reached the desired temperature for any test condition.

### **3.2.6.3 EGR System**

As illustrated in Figure 3.14, EGR is simulated by using nitrogen ( $N_2$ ) and  $CO_2$  gases provided from two pressurised gas tanks for the purpose of this study. This was mainly due to the fact that the fragile nature of the optical parts of the engine, such as the fused silica window, do not allow for long runs of the engine in order for steady operation of the exhaust gases from the combustion to be recirculated back into the intake system. The  $N_2$  and  $CO_2$  gas flow is measured by a flow meter. The EGR rates used during the experiments was 0%, 25%, and 40% in order to determine whether external EGR has the potential to improve the performance of the dual-fuel combustion process and understanding the effects of the EGR.

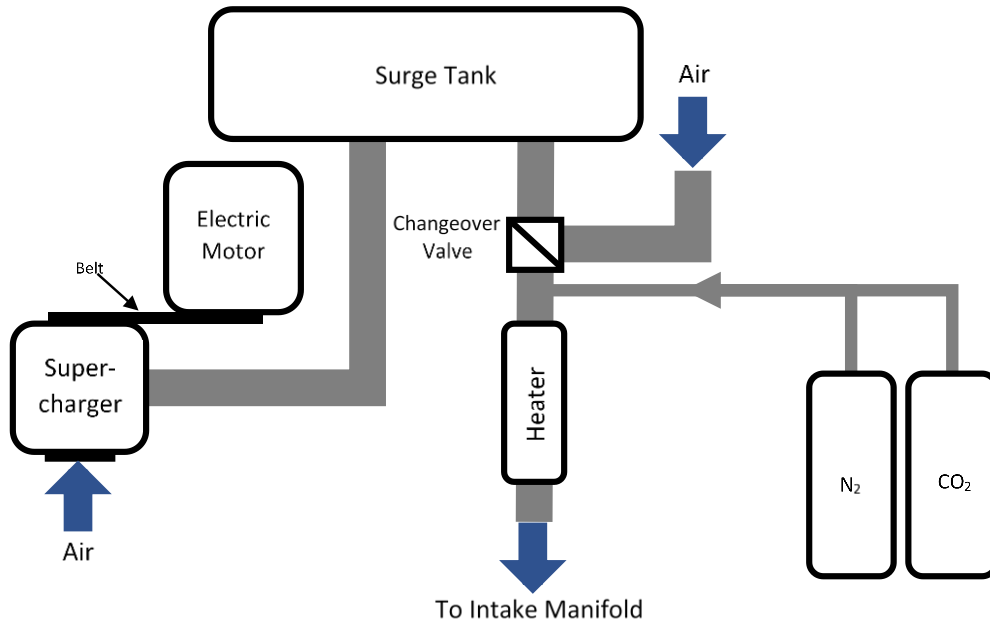


Figure 3.14 Schematic diagram of the EGR System

Level of CO<sub>2</sub> concentration required for each EGR rating was calculated using the equation below:

$$EGR (\%) = \frac{(CO_{2EGR} - CO_{2atm})}{(CO_{2exh} - CO_{2atm})} \quad (\text{Adapted from [168]})$$

Where the fresh intake air contains negligible amounts of CO<sub>2</sub>, while the exhaust CO<sub>2</sub> level was determined using the EGR gas flow rate measured using the flowmeter discussed later in section 3.6.

The level of N<sub>2</sub> concentration required for each EGR rate was determined by the use of the air and N<sub>2</sub> flow rate chart for different engine speeds and temperatures in Appendix 2 [169], and the use of the flowmeter discussed in section 3.6.

### 3.3 In-Cylinder Pressure Data Acquisition System

An important parameter used for combustion analysis of a diesel engine is the heat release rate which is calculated from the in-cylinder pressure. The measurement of the in-cylinder pressure while the engine is motoring, also aids in the detection of any leaks from the seals, particularly when using the optical window. Any drop in the cylinder peak pressure is usually an evidence of some leakage from the combustion chamber. The principle of the in-cylinder pressure measurement and heat release analysis and its implementation are explained in the sections to follow.

### **3.3.1 In-Cylinder Pressure Measurement**

As mentioned in Section 3.2.2, a Kistler 6125A piezoelectric pressure transducer, mounted on top of the cylinder head, in place of the glow plug, coupled with a Kistler 5011 charge amplifier, allows for the measurement of the in-cylinder pressure. The un-cooled transducer has a range of 0-250 bar and a sensitivity of -15 pC/bar. The charge from the transducer is converted and amplified to an output voltage, by passing through the charge amplifier. This signal is then sent to the data acquisition system.

The pressure transducer and the charge amplifier were calibrated using a deadweight tester. To avoid any risk of overloading the charge amplifier, it was calibrated over a range of 0-200 bar and set to produce the maximum output voltage of 10V at 200 bar.

### **3.3.2 Data Acquisition System**

A computer with a LabVIEW programme, created for this system by John Williams, formerly at Brunel University, connected to an interface board with a National Instruments (NI) data acquisition card, is used for collecting and recording the data. The NI BNC-2110 board connected to the NI OCI-MIO-16E data acquisition board collects the signals from the shaft encoder and the in-cylinder pressure transducer amplifier. The 1800 ppr signal from the shaft encoder is used within the software as the clock, giving a 0.2°CA resolution. The 1 ppr signal is used as a reference, indicating the start of recording cycle. The in-cylinder pressure is recorded by the software as a function of crank angle (CA), in real time. The software also has the ability to calculate and record the IMEP, the heat release rate, the mass fraction burned, and the p-V diagram in real time. But for this study, the data acquisition software was used for recording of the in-cylinder pressure only, and the IMEP, and the heat release rate were calculated afterwards using Microsoft Excel. A screenshot of the LabVIEW program is presented in Appendix 1.

### **3.3.3 Experimental Procedure**

The engine was heated by the electrical heaters tailored for the cooling water and the lubricating oil circulation systems preceding to the engine operation for about an hour to imitate the operational conditions of a typical HSDI diesel engine as stated previously in Section 3.2.1. The low pressure pump was turned on before motoring the engine, to ensure that the high pressure pump was being lubricated, although

neither serve any functional purpose, they still require lubrication, as they are still running while the engine is operating and aid the lubrication of the spinning wheel that the hall effect sensor is receiving its reference from. The engine was then motored to 1200 rpm and the intake heater was switched on. The heater could only operate when the engine is running and air is flowing through it, in order to avoid overheating. When the intake air temperature reaches the desired temperature for any test condition, testing can begin. In order to start the combustion, the injection start button in the EC-Lab software was pressed. To finish the testing, the inverse of this process was done. The “Run” button in the LabVIEW data acquisition program was pressed in order to start recording the in-cylinder motoring pressure, which was set to record and save, 20 successive cycles. To record the combustion pressure, the engine was fired for a few cycles to improve the combustion consistency, and regulating the engine speed back down to 1200 rpm, before triggering the data acquisition system. In practicality, the in-cylinder pressure is averaged over several hundred engine cycles, but, this is not possible for optical engines because of excessive window fouling even when operating at low loads. Consequently, the in-cylinder motoring and combustion pressures were recorded for 20 successive cycles, identified to be the optimal number of cycles for optical testing. The glass piston, the cylinder head, and the 45° mirror were cleaned prior to optical testing of each condition to improve the clarity and the quality of the collected in-cylinder footage. The in-cylinder motoring pressure and the combustion pressure were recorded for the optical testing of each condition.

At the start of every day, and regularly during measurements, the motoring pressure was recorded and examined to ensure that all of the seals and gaskets were still intact, and that there were no pressure loss due to any leakage from the combustion chamber. Once the in-cylinder motoring pressure began to decline, anywhere below 31 bar, an engine rebuild and gasket replacement was carried out by the technicians.

It must be noted that some of the data, including high speed images, related to pure diesel combustion is based on the findings of the research done on this setup by a previous research student, Dr. Pin Lu, as cited in [34].

## 3.4 Optical Measurement

The in-cylinder combustion visualisation was performed by high speed imaging of the fuel spray and combustion chemiluminescence using a high speed video camera and high repetition pulsed laser. This technique provides the chronological development of the diesel fuel spray and the combustion process.

### 3.4.1 High Speed Camera

High speed video imaging was used to record video images from the diesel fuel spray during the injection phase and the following combustion. The high speed video camera used for this study was a NAC Memrecam FX 6000, equipped with a high speed colour CMOS sensor. The frame rate set for the high speed camera, where it was used along with a copper vapour laser, was 10,000 frames per second (fps), which means, at the engine speed of 1200 rpm, one frame equates to 0.72 degree crank angle, and where it was coupled with the high speed image intensifier, it was set to 6,000 fps, which means one frame equates to 1.2 degree crank angle. The image resolution is dependent on the frame rate, at 10,000 fps, the image resolution was 512×248 pixels, and at 6,000 fps, the image resolution is 512×384 pixels. A Nikon 60mm f.2.8D lens was used for operations including the laser, and a Nikon 150 mm f.4.5 telescopic lens for operations with the image intensifier.

Collected high speed recordings are processed using the dedicated software from NAC, where the post image processing was done and a MatLab based programme made in house was utilised to remove any noise as well as the background from images, and calculate the relevant properties such as intensity and area of the combustion.

### 3.4.2 Copper Vapour Laser

To visualise the direct diesel fuel spray during the diesel only operations, a copper vapour CU15 Oxford Lasers, was used. The specifications of this copper vapor laser are listed in the Table 3.5 below.

*Table 3.5 Copper Vapour Laser Specifications*

Copper Vapour Laser	
Type	CU15 Oxford Laser
Wavelength (nm)	511
Average Power (W)	8.5
Pulse width (ns)	10 - 40
Pulse Repetition Rate (kHz)	10

In order to redirect the laser beam onto the 45° angled mirror, which redirected the beam into the combustion chamber to illuminate the chamber, an optical fibre was used. The Figure 3.15 below illustrates this arrangement.

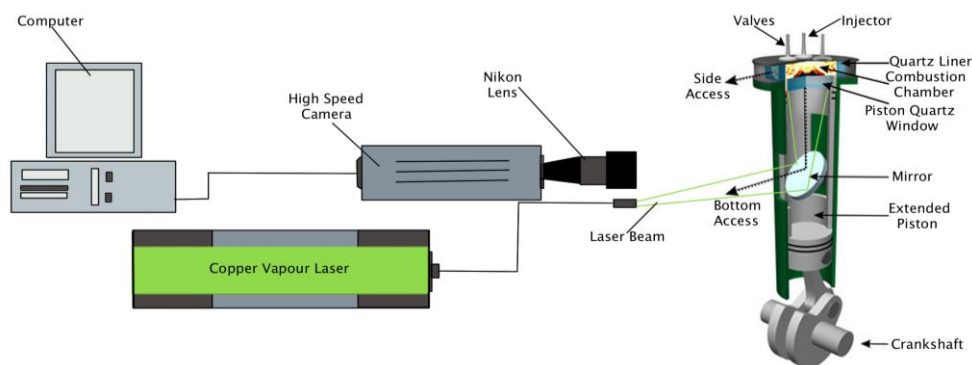


*Figure 3.15 High Speed Camera and Copper Vapor Laser Arrangement [170]*

### **3.4.3 High Speed Image Intensifier**

When performing optical data collection from diesel-ethanol or diesel-gasoline operations, due to the intensity of the combustion flame, using the copper vapor laser for illuminating the combustion chamber, rendered the combustion invisible in the high speed footage. Therefore, for these operations, a DRS Technologies ILS-3-11 High speed video camera intensifier, with 75 lp/mm resolution over 25mm, linear amplification, allowing for gain increase of 60% to 80% depending on the testing condition, was used in line with the high speed camera without the copper vapour laser.

The use of the image intensifier can dramatically improve the ratio of signal to noise for the camera and therefore allows image detection in shorter exposure times at

increased frame rates. It should be noted that the number of primary photons captured is not actually increased by this method, but instead each detected photon is converted into an electron, multiplied and then converted back into a much larger number of photons. Figure 3.16 below illustrates this operation. Figure 3.17 shows the camera and image intensifier arrangement for this study.

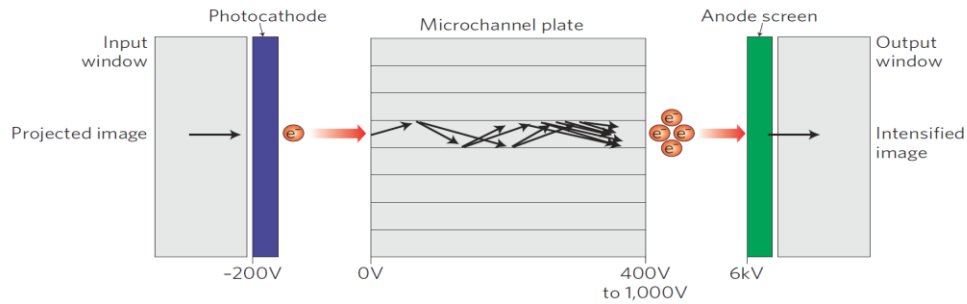


*Figure 3.16 Schematic of a single-stage image intensifier [171]*

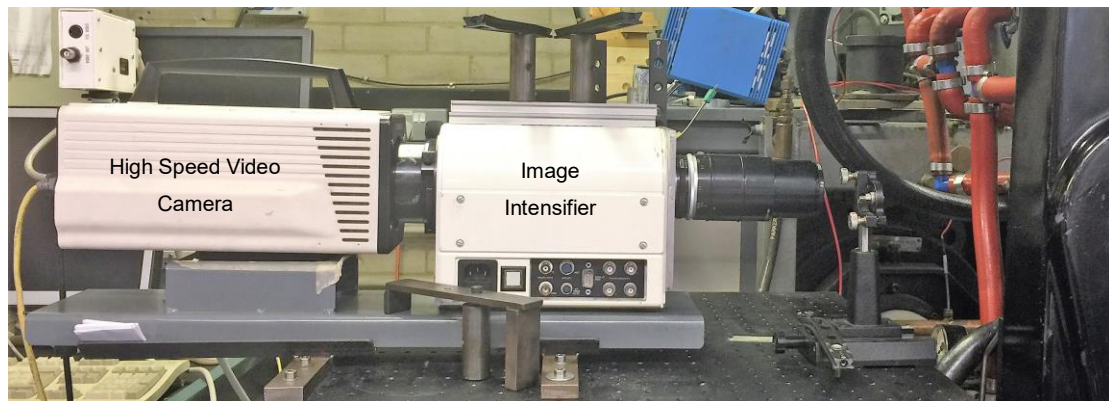


*Figure 3.17 High Speed Camera and Intensifier Arrangement*

### 3.5 Exhaust Emission Measurement

The engine exhaust gas emissions of CO, CO<sub>2</sub>, O<sub>2</sub>, uHC and NO<sub>x</sub> were measured using a Horiba MEXA-7170DEGR Exhaust Gas Analyser. The concentrations of emitted soot was measured by an AVL 415 Smoke Meter.

#### 3.5.1 Horiba MEXA-7170 DEGR Motor Exhaust Gas Analyser

Horiba MEXA-7170 DEGR was used in the measurement of the above-mentioned exhaust emissions. The unit comprises of four analysing modules, all controlled by a PC as the main control unit. Each of the modules operate with a different

measurement principle, which all is explained with details in the following subsections. A touch screen interface, which displays instantaneous or averaged over time measurements of the emissions values in numerical and graphical form.

### 3.5.1.1 Horiba AIA-72X: CO and CO<sub>2</sub> Measurement

For the measurement of CO and CO<sub>2</sub> concentrations, a Horiba AIA-72X analyser module operating based on Non-Dispersive Infrared (NDIR) method was employed. It measures these concentrations based on the fact that infrared radiation is absorb by different molecules at different wavelengths, meaning that each molecules concentration is relative to the level of absorption. Figure 3.18 illustrates an schematic diagram of an NDIR analyser.

The analyser comprises of a chamber divided into two sealed sections of sample cell and comparison cell. The latter of the two is filled with nitrogen gas while the sample gas is pumped through the former of the two cells. An infrared light source is projected into both cells, and the comparison cell, which containing nitrogen, does not absorb radiation in the infrared region, therefore the beam remains unchanged. But, the gas in the sample cell absorbs radiations of specific wavelengths depending on the gases present and their concentrations. The infrared lights are then passed through the detector cells, which contains two sealed cells filled with the sample gas separated by a membrane. The difference in the radiation between the cells causes change in the sample gas temperature resulting in a differential expansion. The movement of the membrane is detected as an electrical signal relative to the concentration of the gas.

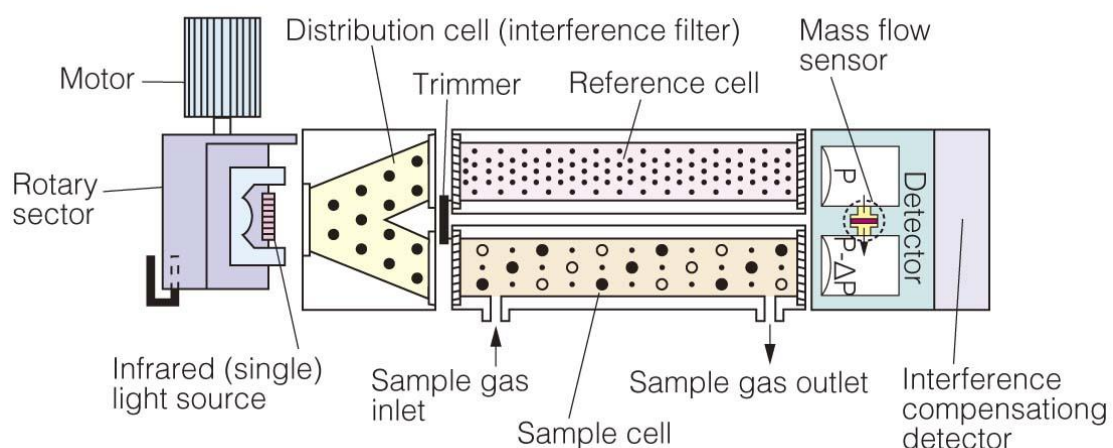


Figure 3.18 Schematic Diagram of NDIR Analyser [172]

A light trimmer is utilised to enable the detection of changes in the gases concentration in the sample cell, by permitting intermittent transmission of infrared light. An optical filter is placed upstream of the detector cell to block the transmission of wavelengths absorbed by unwanted gases, to guarantee that the transmitted signal to the detector cell is only created by the gas types of interest.

### **3.5.1.2 Horiba MPA -720: O<sub>2</sub> Measurement**

to measure the oxygen concentration, the Horiba machine utilises an MPA-720 magneto-pneumatic analyser, which operates based on the principle of paramagnetic, which states, certain materials are magnetic when an external magnetic field is present. Oxygen and oxides of nitrogen namely NO and NO<sub>2</sub>, from all common exhaust gas components, are the only gas types that are affected in the presence of an external magnetic field, while the oxides of nitrogen have negligible effect in comparison. Figure 3.19 below, illustrates the schematic diagram of a magneto-pneumatic oxygen analyser.

The sample gas flows through the magnetic cell, and an electromagnetic field is created around the poles by the flowing AC current. The varying magnetic field attracts the oxygen molecules, which then causes a pressure increase around the poles relative to the oxygen concentration. A condenser microphone within the analyser, generates an electrical signal output when change in pressure is detected.

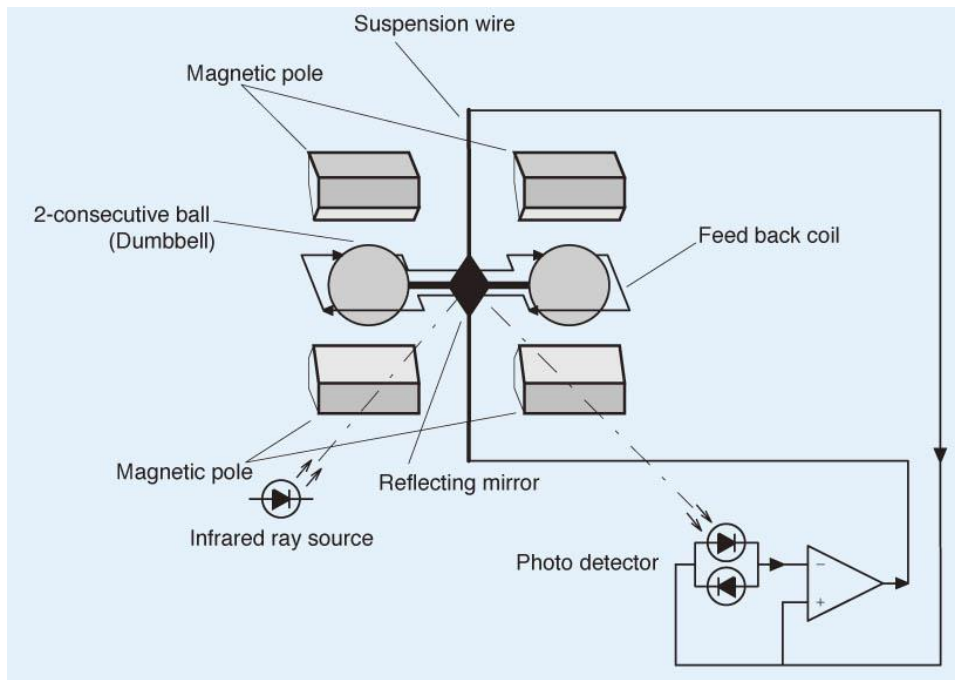


*Figure 3.19 Schematic Diagram of a Magneto-Pneumatic Oxygen Analyser [172]*

### 3.5.1.3 Horiba FIA-720: unburned Hydrocarbon Measurement

To measure the uHC concentration The Horiba FIA-720 Flame Ionisation Detector (FID) module of the Horiba machine was employed. The operation of this module is based on the fact that ions are produced when a hydrocarbon containing gas is burned. The rate of ion production has a direct relation with the hydrocarbon concentration. A schematic diagram of a FID detector is showed in Figure 3.20 below. Since, minimal ionisation occurs during Hydrogens combustion, it is used as the fuel gas, and is burned in the detector using oxygen with high purity. To promote thermal dissociation of hydrocarbons in the mixture, the sample gas is mixed with the hydrogen; during this process, ions are produced. To separate the ions and electrons between the burner jet and the collector around the flame, a high DC voltage is applied between the burner jet and the collector. This creates an electrical current relative to the level of ionisation which is directly relative to the number of carbon atoms present. Therefore, this method can only measure the total hydrocarbons, with no specific information on specific hydrocarbons.

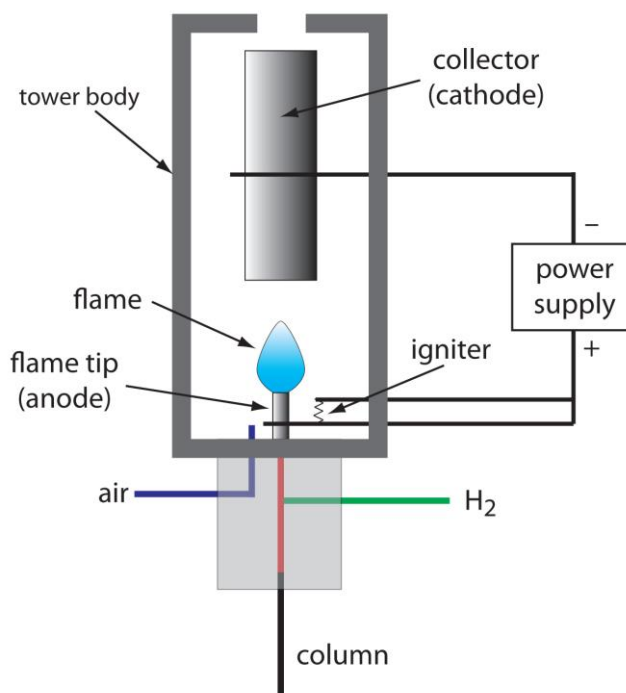
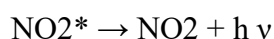
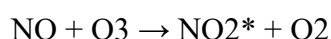


*Figure 3.20 Schematic Diagram of a FID Analyser [173]*

#### **3.5.1.4 Horiba CLA-720: NO<sub>x</sub> Measurement**

For the measurement of NO and NO<sub>2</sub> concentrations, the Horiba CLA-720A chemiluminescence analyser module was utilized. The operational principle of this module is based on the reaction between NO and ozone (O<sub>3</sub>), which results in the oxidation of NO to NO<sub>2</sub>. Some of the NO<sub>2</sub> produced through this process are in an excited state with a raised energy level (NO<sub>2</sub>\*), shown below:



The excited molecules deteriorate to the ground state by the emission of a photon. This process is referred to as chemiluminescence. The intensity of the light emitted is proportionate to the NO molecules concentration in the sample gas.

The sample gas mixes and reacts with the ozone after entering the reaction chamber, and the light emitted through the chemiluminescence process is passed through a bandpass filter in front of a light detector, which upon the detection of light, outputs a voltage signal. Figure 3.21 illustrates the schematic diagram of a chemiluminescence detector.

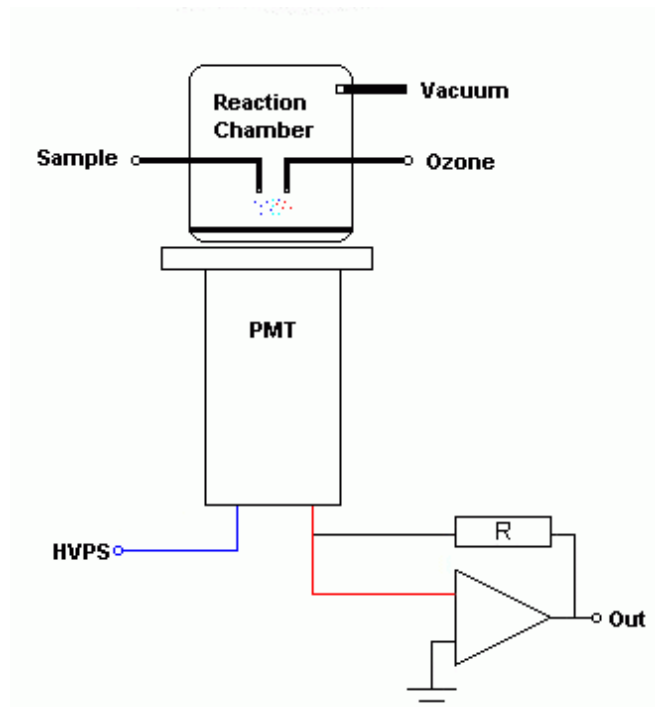


*Figure 3.21 Schematic Diagram of a Chemiluminescence Detector [174]*

Some of the excited molecules lose their energy through collision with other molecules, while the majority emit light by returning to the ground state, such as the molecules of CO<sub>2</sub> and H<sub>2</sub>O present in the exhaust gas. The sample gas is diluted with nitrogen before entering the detector to reduce such interference.

### **3.5.2 AVL 415 Smoke Meter**

For the measurement of soot concentration in the exhaust gas, an AVL 415 smoke meter was employed. The smoke meter is equipped with a diaphragm type pump that sucks the exhaust gas into the sampling line, which is then passed through a paper filter followed by a flow meter. The smoke meter measures the soot concentration by the use of a reflectometer, which measures and compares the reflection from the clean and the smoky filter papers as shown below in Figure 3.22.

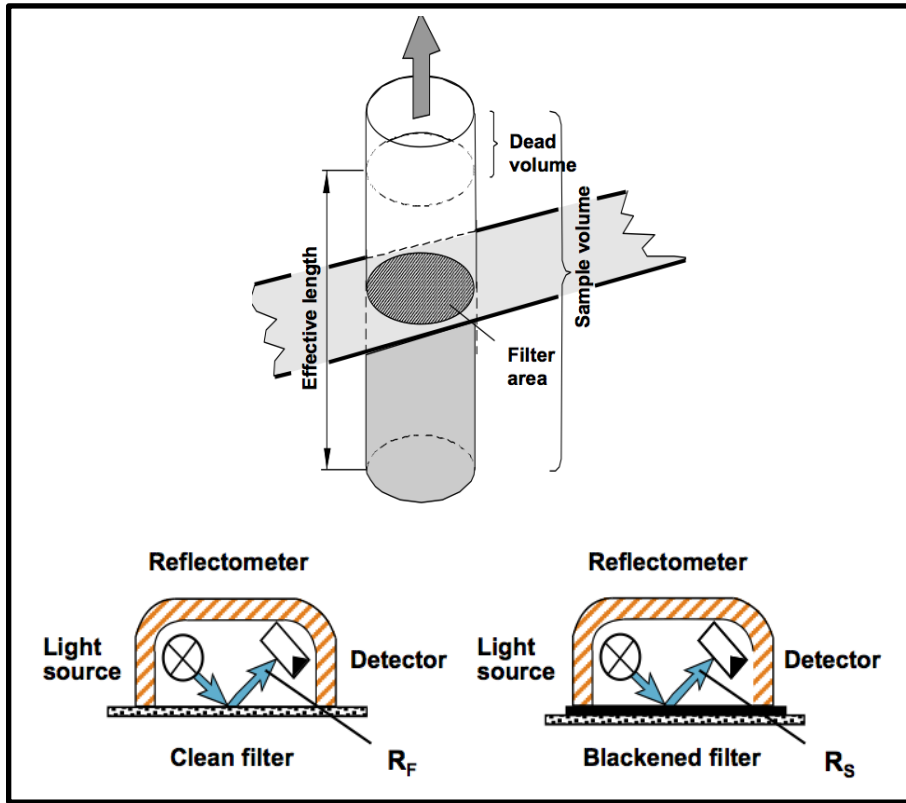


Figure 3.22 Schematic Diagram of AVL 415 Smoke Meter Measuring Principle [192]

The result of this procedure, is the level of blackening on the paper, with a clean white filter paper having the value of zero and a complete black paper having the value of 10, corresponding to soot concentrations of 0, for white, and 32000 mg/m<sup>3</sup>, for black. The governing equation is given by:

$$P_B = \frac{100 - R_R}{10} \quad \text{Equation 3.1}$$

$$R_R = \frac{R_S}{R_F} \times 100\% \quad \text{Equation 3.2}$$

Where:  $P_B$  = Paper Blackening

$R_S$  = Reflectometer Value of the Sample

$R_F$  = Reflectometer Value of the Unblackend Filter Paper

$R_R$  = Relative Brightness of the Sample

The soot concentration is measured in Filter Smoke Number (FSN) throughout this study, where FSN is defined as  $FSN = P_B$  when  $L_{eff} = 405$  mm, based on ISO 10054 standards, and  $L_{eff}$  is given by:

$$L_{eff} = \frac{V_{eff}}{A} \quad \text{Equation 3.3}$$

$$V_{eff} = V_S - V_D - V_L \quad \text{Equation 3.4}$$

Where:  $L_{eff}$  = *Effective Length of Gas Column Drawn Through Filter*

$V_{eff}$  = *Effective Volume of Gas Drawn Through Filter*

$V_S$  = *Sample Volume*

$V_D$  = *Dead Volume*

$V_L$  = *Leak Volume*

(Dead Volume is the volume of clean air between the filter paper and the end of the sampling line sucked through prior to the sample gas, and Leak Volume is the volume of clean air and sample gas lost due to minor leaks.)

This process is done automatically by the smoke meter and the FSN number is displayed on the digital display. For this study, the sample volume was determined automatically, with the smoke meter performing an preliminary test to calculate the sample volume necessary. The smoke meter was programmed to carryout three successive sample measurements, and display the average.

### 3.6 Intake Air Flow Measurement

The air flow rate was measured by attaching a Teledyne Hastings Instruments Flowmeter, shown in Figure 3.23, to the exhaust outlet. The engine was then motored with the intake air heater running, in order to simulate operation conditions as closely as possible.



Figure 3.23 Teledyne Hastings Lamina Flow Element Flowmeter

The Hastings flow controller system comprises of a sensor, electronic circuitry, a valve, and a shunt. The sensor measures the flow rate from 0 to 10 SCCM (Standard Cubic Centimetres per Minute) of the gas to be measured in meters. The shunt divides the flow in a way that the flow through the sensor is an exact percentage of the flow through the shunt. The flow through the sensor and the shunt is always laminar. The sensor output is amplified by the circuit board, and it uses this output to control the position of the valve, which is an automatic metering solenoid valve; The voltage in its coil controls its height off the seat. All of these components working parallel to one another, results in a stable and fast flow controller [175].

### 3.7 Data Analysis

The in-cylinder pressure data was used to determine the heat release rate, mean effective pressure and ignition delay. Additionally, emissions data were analysed quantitatively while the high speed video images served as a qualitative measure in analysing the combustion characteristics.

#### 3.7.1 Cylinder Volume Calculation

The in-cylinder volume is calculated by the engine geometry at any crank angle using the equations below:

$$V = V_C = \frac{\pi B^2}{4} (l + a - s) \quad \text{Equation 3.5}$$

$$S = a \cos \theta + \sqrt{(l^2 - a^2 \sin^2 \theta)} \quad \text{Equation 3.6}$$

Where:  $V = \text{Cylinder Volume}$

$V_C = \text{Clearance Volume}$

$B = \text{Cylinder Bore}$

$l = \text{Connecting Rod Length}$

$a = \text{Crank Radius}$

$s = \text{Distance Between Crankshaft and Piston Pin Axes}$

Compression ratio is defined by the following equation:

$$r_C = \frac{V_d + V_C}{V_C} \quad \text{Equation 3.7}$$

Where:  $r_C = \text{Compression Ratio}$

$V_d = \text{Displacement Volume}$

And the ration of connecting rod length to crank radius is:

$$R = \frac{l}{a} \quad \text{Equation 3.8}$$

Where:  $R = \text{Ratio of Connecting Rod Length to Crank Radius}$

Equation 3.5 can be rearranged to:

$$V = V_c \left\{ 1 + \frac{1}{2} (r_c - 1) [R + 1 \cos \theta - \sqrt{(R^2 - \sin^2 \theta)}] \right\} \quad \text{Equation 3.9}$$

### 3.7.2 Engine Combustion and Heat Release Analysis

The engine efficiencies and combustion characteristics, for various operating conditions, can be calculated from the in-cylinder pressure data, using Microsoft Excel.

#### 3.7.2.1 Indicated Mean Effective Pressure

A theoretical measure of the effectiveness of the engine in producing work, is Indicated Mean Effective Pressure (IMEP), which is a function of the displacement volume of the engine with respect to the maximum pressure produced in the cycle. The gross IMEP is equivalent to the areas between the compression stroke and the expansion stroke, on the pressure versus volume diagram, known as the p-V diagram, and the net IMEP is the subtraction of the negative work from the gross IMEP. The p-V diagram of a four-stroke diesel engine is illustrated below in Figure 3.24.

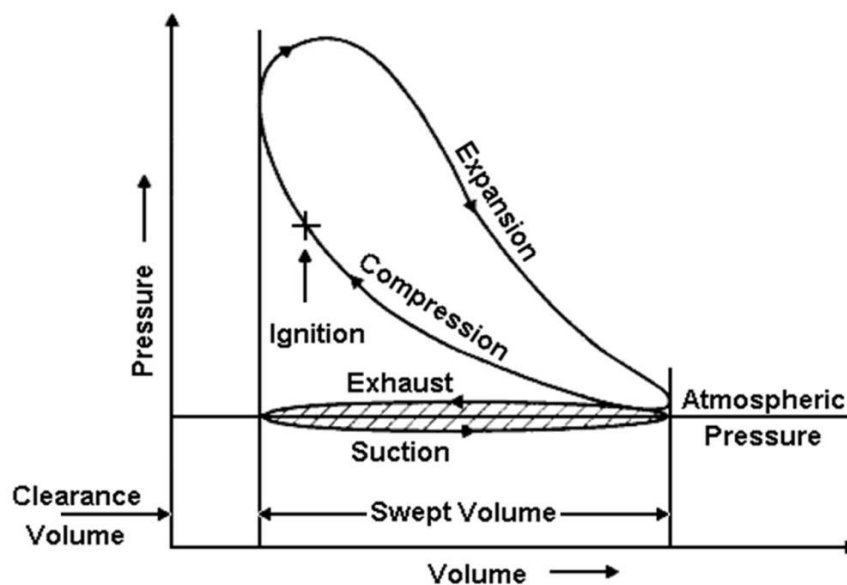


Figure 3.24 Four-Stroke Engine p-V Diagram [176]

A four-stroke engine comprises of four-strokes, induction stroke, compression stroke, expansion stroke and exhaust stroke. The p-V diagram of this type of engine includes two loops, the work loop outlined by the lines of the compression stroke and the expansion stroke and the pumping loop bounded by the lines of the induction stroke and the exhaust stroke, therefore, positive work is done during the combustion process, which takes place in the work loop, while negative work is done during the pumping loop, which is the work done on the engine. The Gross IMEP is represents by the area enclosed by the work loop, but the net IMEP takes the work done during the induction stroke and exhaust stroke into account, thus it is determined by the subtraction of the area of the pumping loop from the work loop.

IMEP is calculated by the numerical integration of the p-V diagram as shown below:

$$IMEP = \frac{1}{V_d} \int_y^x p dV \quad \text{Equation 3.10}$$

Where:  $p = in - cylinder\ pressure$

The in-cylinder pressure sampling rate acts as the step interval in the equation 3.10 above, which is  $0.2^\circ$  CA here. The integration limits, x and y, are from zero to  $720^\circ$  CA, which includes a complete engine cycle, representing the Net IMEP as calculated for purpose of this study.

### 3.7.2.2 Indicated Specific Fuel consumption

Indicated Specific Fuel Consumption (ISFC) is calculated based on the fuel flow rate and the engine work output, which is shown below:

$$ISFC = \frac{\dot{m}_f \times rpm}{IMEP \times V_d} \quad \text{Equation 3.11}$$

Where:  $\dot{m}_f = Mass\ Flow\ Rate\ of\ Fuel$

### 3.7.2.3 Fuel Mass Fraction Burned Analysis

It is necessary to estimate the Mass Fraction Burn (MFB) profile from the cylinder pressure and volume data, as the MFB curve is used to identify the start of combustion (CA of 10% MFB), the combustion phasing (CA of 50% MFB) and the combustion duration (CA 10%-90% MFB). According to analysis developed by Rassweiler and Withrow [177], the rise in in-cylinder pressure, during any crank angle interval,  $\Delta\theta$ , is considered to be caused by the rise in pressure due to the change in volume,  $\Delta p_v$ , and the increase in pressure due to combustion,  $\Delta p_c$ :

$$\Delta p = \Delta p_v + \Delta p_c$$

Equation 3.12

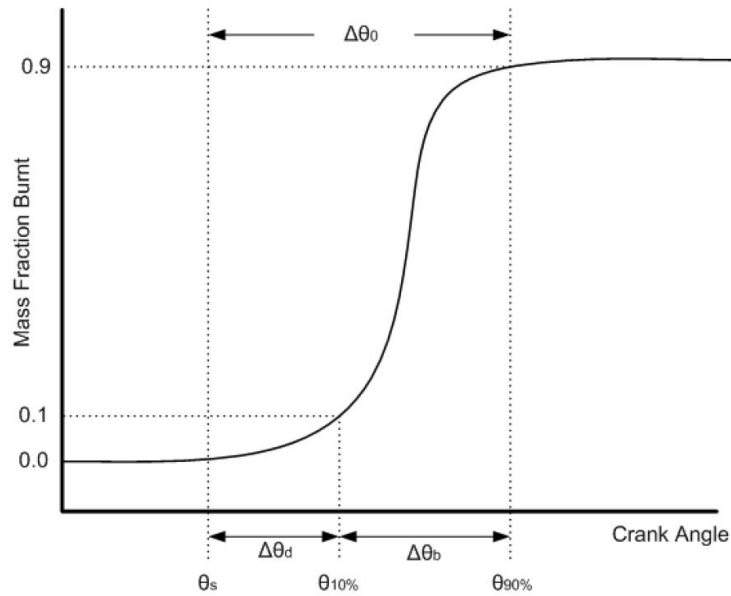


Figure 3.25 Definitions of  $F$  flame-development Angle,  $\Delta\theta_d$ , and Rapid-burning Angle,  $\Delta\theta_b$ , on A Mass Fraction Burned Curve [178].

As the crank angle ( $\theta_i$ ) increments to its next value ( $\theta_{i+1}$ ), the volume changes from  $V_i$  to  $V_{i+1}$ , and the pressure changes from  $p_i$  to  $p_{i+1}$ . The change in pressure, is due to the movement of the piston, which is related to the volume change by the polytropic relationship (Figure 3.25).

$$\Delta p = p_i \left[ \left( \frac{V_i}{V_{i+1}} \right)^n - 1 \right]$$

Equation 3.13

By combination of the equation 3.12 and the equation 3.13:

$$\Delta p_c = p_{i+1} - p_i \left( \frac{V_i}{V_{i+1}} \right)^n$$

Equation 3.14

Where:  $V_i =$  The Cylinder Volume Given by Equation 3.9

As the combustion process does not occur at the constant volume, the mass of fuel burned is not directly proportional to the increase in pressure due to combustion. Thus, the clearance volume at top dead centre,  $V_C$ , is accounted for as the volume effect:

$$\Delta p_c^* = \Delta p_c \left( \frac{V_i}{V_C} \right)$$

Equation 3.15

Assuming that the mass fraction burned ( $\chi$ ), is proportional to the referenced increase in pressure due to combustion, at the end of the interval ( $\Delta\theta$ ) the mass fraction burned is given by:

$$\chi = \frac{m_{b,i}}{m_{b,total}} = \frac{\sum_1^i \Delta p_C^*}{\sum_1^N \Delta p_C^*} \quad \text{Equation 3.16}$$

#### 3.7.2.4 Heat Release Rate

Engine heat release rate, a measure of the amount of heat added or removed from the cylinder contents to achieve the same in-cylinder pressure, is calculated using the in-cylinder pressure and volume. This method is unable to measure the accurate amount of heat release rate, since the in-cylinder charge leakage in optical engines due to the use of optical components, therefore it is termed “apparent heat release rate”. to calculate the heat release rate, one-zone thermodynamic model is used by seeing the cylinder as an open system, thus:

$$\frac{dQ}{dt} - p \frac{dV}{dt} + \sum_i \dot{m}_i h_i = \frac{dU}{dt} \quad \text{Equation 3.17}$$

Where:  $\frac{dQ}{dt}$  = Rate of Heat Transfer into System Across Boundary

$p \frac{dV}{dt}$  = Rate of Work Transfer by System

$\dot{m}_i$  = Mass Flow Rate into System at Location  $i$

$h_i$  = Enthalpy of Flux  $i$

$U$  = Internal Energy of Cylinder Contents

When both intake and exhaust valves are closed, the mass flows across the system boundary. This includes the mass of the fuel injected into the combustion chamber as well as the mass of air lost due to the flow in the crevices. Nevertheless, when using the engine in optical setup, in-cylinder leakage caused by the sealing of optical window needs to be considered, but this is almost impossible to calculate. Because of the complicated calculations required, and since the heat release rate is utilised as an estimated quantity, the effects of the in-cylinder leakage are neglected. So the, Equation 3.17 can be simplified to:

$$\frac{dQ}{dT} - p \frac{dV}{dt} + \dot{m}_f h_i = \frac{dU}{dt} \quad \text{Equation 3.18}$$

U is considered the sensible internal energy of the in-cylinder charge,  $U_s$ , while  $h_f$  is considered the sensible enthalpy of the fuel injected. Therefore,  $dQ/dt$  turn into the net heat release rate, and  $dQ_n/dT$  is the difference between the heat release rate due to fuel combustion and the system heat transfer. Since  $h_{s,f} \approx 0$ , Equation 3.18 can be written as:

$$\frac{dQ_n}{dt} + p \frac{dV}{dt} + mc_v \frac{dT}{dt} \quad \text{Equation 3.19}$$

By assuming the in-cylinder charge to be considered as an ideal gas, Equation 3.19 can be rewritten as:

$$\frac{dQ_n}{dt} + p \frac{dV}{dt} + mc_v \frac{dT}{dt} \quad \text{Equation 3.20}$$

Where:  $c_v = \text{Specific Heat at Constant Volume}$

$T = \text{Absolute Temperature}$

Based on the law of ideal gases,  $pV = mRT$ :

$$V \frac{dp}{dt} + p \frac{dV}{dt} = mR \frac{dT}{dt} \quad \text{Equation 3.21}$$

Where:  $R = \text{Ideal Gas Constant}$

Additionally, the gas temperature, T, can be eradicated by merging the two Equations, 3.20 and 3.21, as illustrated below:

$$\frac{dQ_n}{dt} = \left(1 + \frac{c_v}{R}\right) p \frac{dV}{dt} + \frac{c_v}{R} V \frac{dp}{dt} \quad \text{Equation 3.22}$$

With  $\gamma = \frac{c_p}{c_v}$  considered as the of specific heat ratio, Equation 3.22 can be rewritten as:

$$\frac{dQ_n}{dt} = \frac{\gamma}{\gamma-1} p \frac{dV}{dt} + \frac{1}{\gamma-1} V \frac{dp}{dt} \quad \text{Equation 3.23}$$

This equation, as a simplified form of Equation 3.17, is utilised for the heat release rate calculation for this study.  $\gamma$  is not a constant for different stages of engine cycle, however, for diesel heat release analysis, it is common to take a single suitable value, and for the purpose of this study  $\gamma = 1.3$ .

### 3.7.2.5 Cumulative Heat Release

The cumulative heat release can be calculated from the heat release rate using the following expression:

$$CHR_n = HR_{n-1} + (HR_n \times \Delta\theta) \quad \text{Equation 3.24}$$

Where:  $HR = \text{Heat Release Rate}$

$\Delta\theta = \text{Change in Crack Angle, } 0.2^\circ\text{CA in this case}$

### 3.7.2.6 Ignition Delay

If SOI is the timing of the first injection and SOC is the point where the heat release rate initially begins to increase, ignition delay or ID, is defined as the delay between the start of ignition SOI and SOC. During the initial stages of combustion, the rate of heat transfer is more dominant than the first positive heat release prior to the onset of more substantial heat release, still the start of combustion is considered as the point where the first combustion happens.

### 3.7.2.7 Combustion Efficiency

The combustion efficiency is calculated from the cumulative heat release and the heating value of the fuel:

$$\eta_c = \frac{\sum \frac{dQ_n}{dt}}{\dot{m}_f Q_{HV}} \quad \text{Equation 3.25}$$

Where:  $\frac{dQ_n}{dt} = \text{Heat Release Rate}$

$Q_{HV} = \text{Lower Heating Value of Fuel}$

## 3.7.3 Engine Efficiencies Calculation

In order to evaluate the source of losses during engine work cycles, analysis of engines efficiencies is used. This is as shown in Figure 3.26 below.

These efficiencies can be calculated as shown below:

$$FuelMEP = \frac{m_f \cdot LHV_f}{V_d} \quad \text{Equation 3.26}$$

$$Q_hMEP = \eta_c FuelMEP \quad \text{Equation 3.27}$$

$$IMEP_{gross} = \frac{W_g}{V_d} = \frac{1}{V_d} \int_{compression}^{expansion} p dV \quad \text{Equation 3.28}$$

$$IMEP_{net} = \frac{W_n}{V_d} = \frac{1}{V_d} \oint p dV \quad \text{Equation 3.29}$$

$$BMEP = \frac{4\pi T}{V_d} \quad \text{Equation 3.30}$$

$$\eta_t = \frac{IMEP_{gross}}{Q_h MEP} \quad \text{Equation 3.31}$$

$$\eta_t = 1 - \frac{\sum_i x_i \cdot LHV_i \cdot (m_f + m_a)}{m_f \cdot LHV_f} \quad \text{Equation 3.32}$$

$$\eta_g = \frac{IMEP_{gross}}{FuelMEP} ; \eta_n = \frac{IMEP_{net}}{FuelMEP} ; \eta_b = \frac{BMEP}{FuelMEP} ;$$

$$\eta_{ge} = \frac{IMEP_{net}}{IMEP_{gross}} ; \eta_m = \frac{BMEP}{IMEP_{net}} \quad \text{Equation 3.33}$$

Where:  $m_f$  = Mass of Fuel in One Cycle

$m_a$  = Mass of Intake Air in One Cycle

$W_g$  = Gross Work in One Cycle

$W_n$  = Net Work in One Cycle

$T$  = Break Torque

$x_i$  = The Mass Fraction of CO and HC Respectively (H2 is ignored)

$LHV_i$  = Low Heating Values for CO ( $10.1 \frac{MJ}{kg}$ ) and HC ( $44 \frac{MJ}{kg}$ )

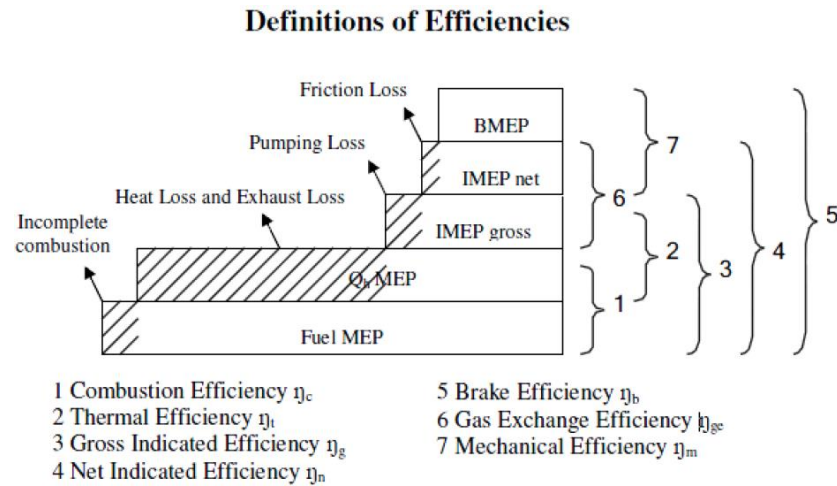


Figure 3.26 Definitions of Efficiencies [179]

### 3.8 Fuel Injection Calibration

For this study, two different injectors are used simultaneously for majority of test conditions, a Delphi multi-hole Valve Covered Orifice (VCO) injector, detailed in Table 3.2, as a diesel direct injector, and a Bosch EV 14 Injection Valve, detailed in

Table 3.3, as a port fuel injector for delivering ethanol/gasoline. Therefore, both of these injectors required calibration.

### **3.8.1 Diesel Direct Injector Calibration**

Here the setup and the procedure for the calibration of the Delphi VCO diesel injector is explained and the results from this calibration is presented.

#### **3.8.1.1 Setup**

For the calibration of the diesel direct injector, the injector was removed from the engine, and the tip was placed into a container while it was still connected to the rail. A fluid measuring burette replaced the diesel fuel tank in the diesel fuel delivery system, and the fuel return hose was placed on top of the burette in order for the returned fuel to return back into the burette, for more accurate measurement of fuel flow.

Once the burette was filled with diesel fuel, while the engine was running at 1200rpm and the rail pressure of 500 bar, the time required for injection of a set amount of fuel (25cc) at a set injection duration was recorded using a stopwatch. This was repeated for various injection durations, while testing single diesel injections, with 3 injections per engine cycle in order to speed up the procedure, as well as split diesel injections with 50/50 fuel distribution between first and second injections, for the total diesel amount required for all three different substitution ratios used in this study (45%, 60%, and 75%), with various dwell angles between the first and second injection.

#### **3.8.1.2 Results**

Figure 3.27 below illustrates the result of the calibration for the single diesel injection procedure in form of injection amount in mm<sup>3</sup> per cycle versus injection signal duration in microseconds. A linear equation for the injection rate can be defined as shown in equation 3.34 below:

$$y = 0.0481x - 13.3787 \quad \& \quad R^2 = 0.9959 \quad \text{Equation 3.34}$$

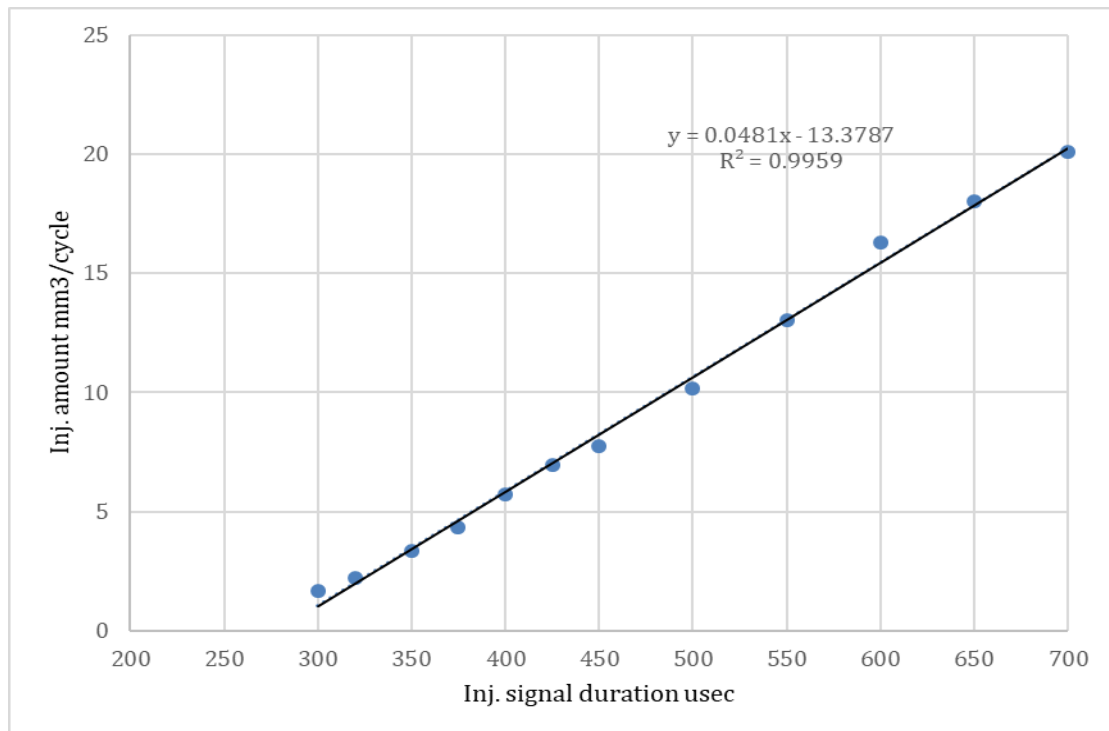


*Figure 3.27 Injection Rate Profile for Delphi VOC Injector*

Figure 3.28 below, illustrates the injection rate of the Delphi diesel injector for split injection operations with 50/50 fuel distribution between the two injections for dwell angles between 30° CA to 80° CA at 5° CA intervals, while all the first injections occur at the same cam angle .

It is apparent from the graph of Figure 3.28, that the injection duration and thus the amount of fuel injected at the second injection, is greatly affected by the first injection, and this is more apparent for conditions where the dwell (or the crank angle lag between two injections) angle between the first and second injection is smaller, and as this dwell angle increases, the effect becomes less apparent. Therefore in order to achieve an equal fuel amount from both injections, either the dwell angle needs to be beyond a certain amount to reduce the effect of the first injection on the second injection, or the injection duration, and thus the injection amount for the second injection needs to be adjusted, in order to match that of the first injection.

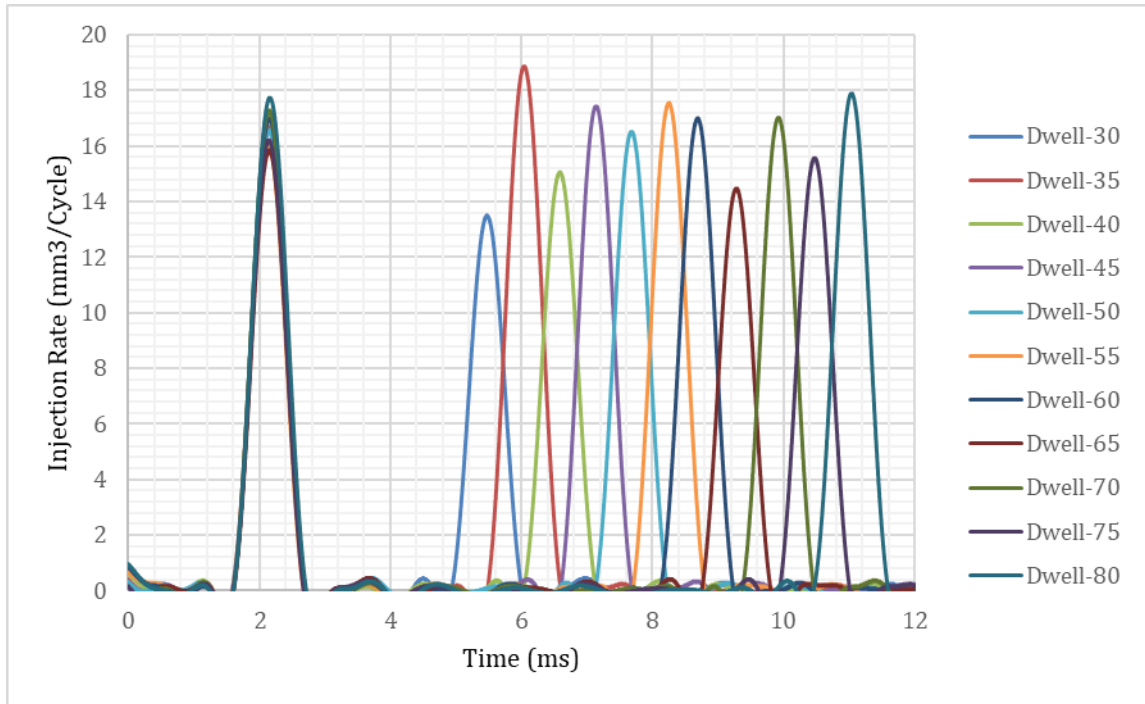


*Figure 3.28 Injection Rate Profile for Delphi VOC Injector with Split Injections*

It should be noted that this interference between the first and second injection is due to the high pressure waves in the fuel lines and the injector nozzle, residual of the first injection.

This effect, mentioned above, is illustrated in Figure 3.29 below in form of comparison between single injection operation, and the second injection of split injection operations, as injection amount versus injection duration graphs, for all substitution ratios used in this study, which are 45%, 60%, and 75%, for different smaller dwell angles, namely 25° CA, 30° CA, and 35° CA.

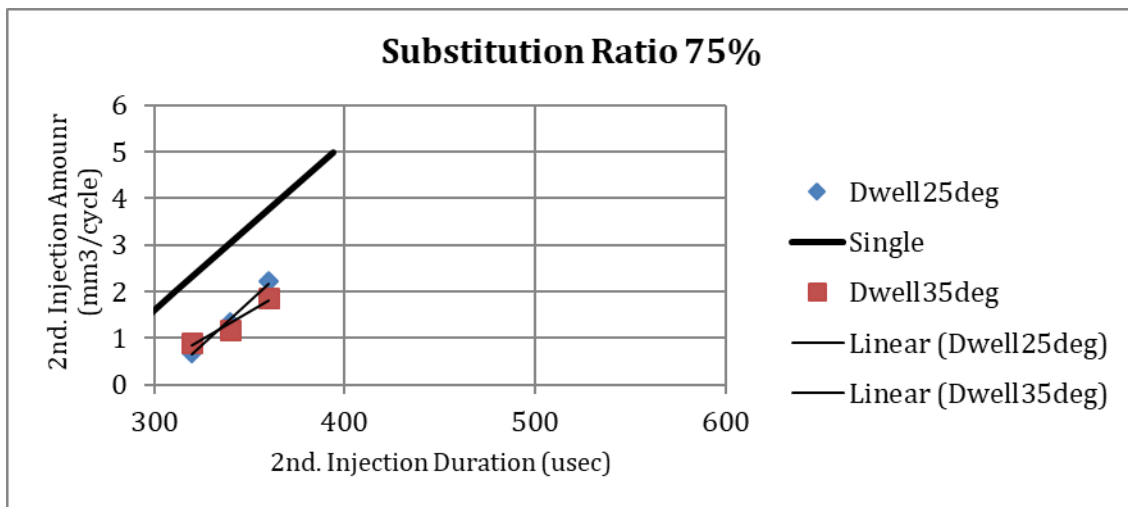
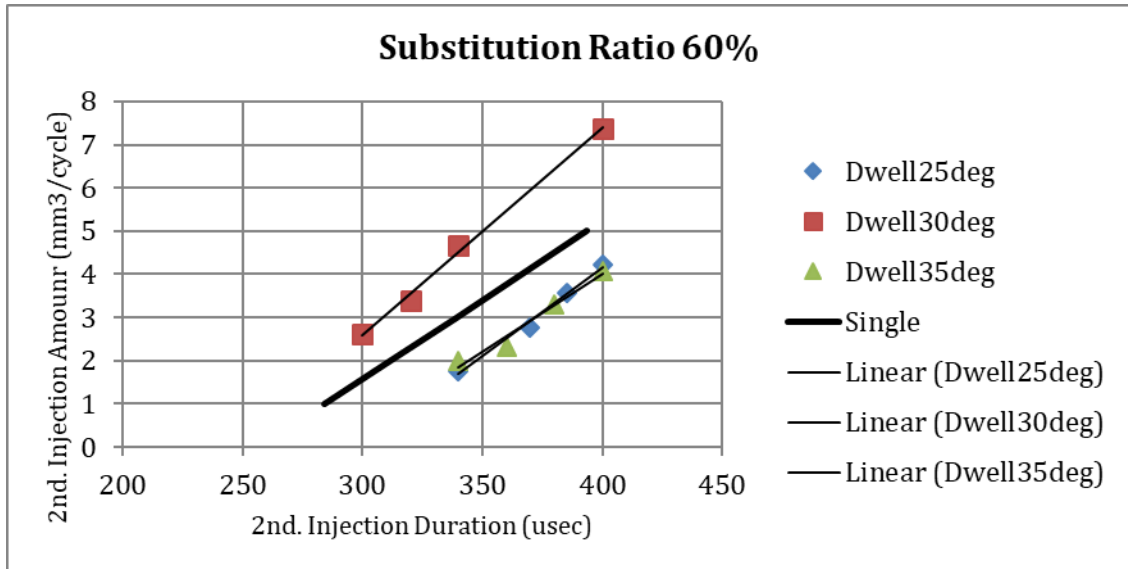
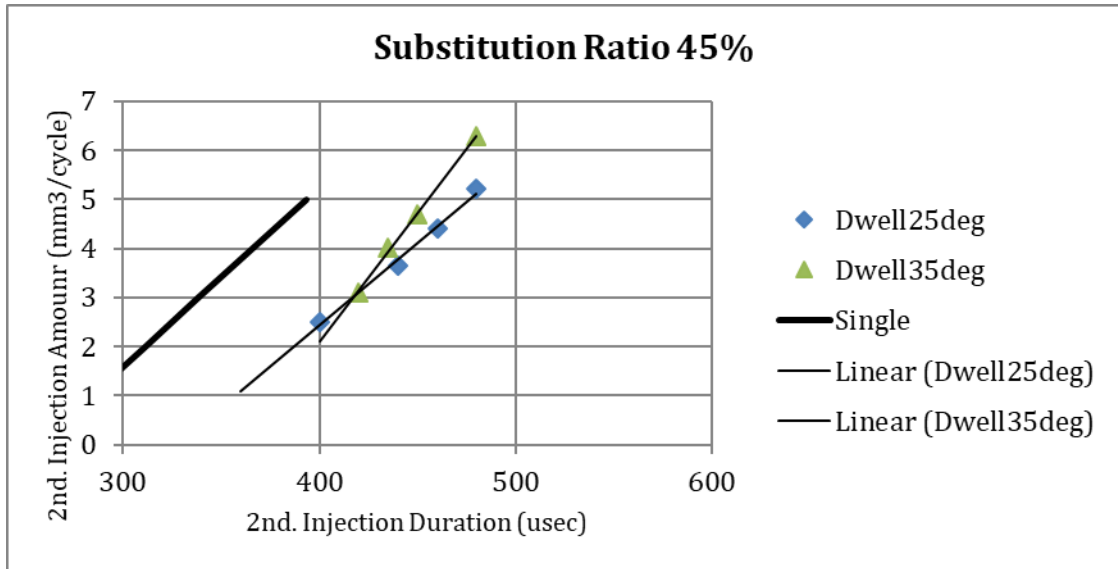


Figure 3.29 Effect of First Injection on Second Injection in Split Injection Operations

### 3.8.2 Port Fuel Injector Calibration

In this section the setup and the procedure for the calibration of the Bosch injection valve used as a port fuel injector is explained and the results from this calibration is presented.

#### 3.8.2.1 Setup

The injector was calibrated using a power source at  $12.0 \pm 0.2$  Volts, with ambient pressure of 1.02 bar, and ambient temperature of  $27^{\circ}\text{C}$ . for the purpose of this study, this injector will be used for the injection of two different fuel types, gasoline and ethanol; and the injection pressures used for the calibration were 3 bar and 4 bar. To activate the injector, the crank angle and reference signal were taken from the encoder, while the engine was motoring at 900 rpm.

The fuel was injected into a sealed dish and was weighted by a Sartorius Research R200D Electronic Semi-Microbalance scale, with a standard deviation smaller than  $\pm 0.1$  mg and a maximum linearity of  $\pm 0.2$  mg.

#### 3.8.2.2 Results

The The equation that determined the mass of ethanol injected at 3 bar was:

$$m_{Ethanol\ at\ 3\ bar} [g/s] = 0.0431 \times Inj \cdot Duration [ms] + 0.0868 \quad \text{Equation 3.35}$$

Figure 3.30 below, shows the result of the calibration of the a Bosch EV 14 Injection Valve for both ethanol and gasoline at 3 bar and 4 bar of injection pressure.

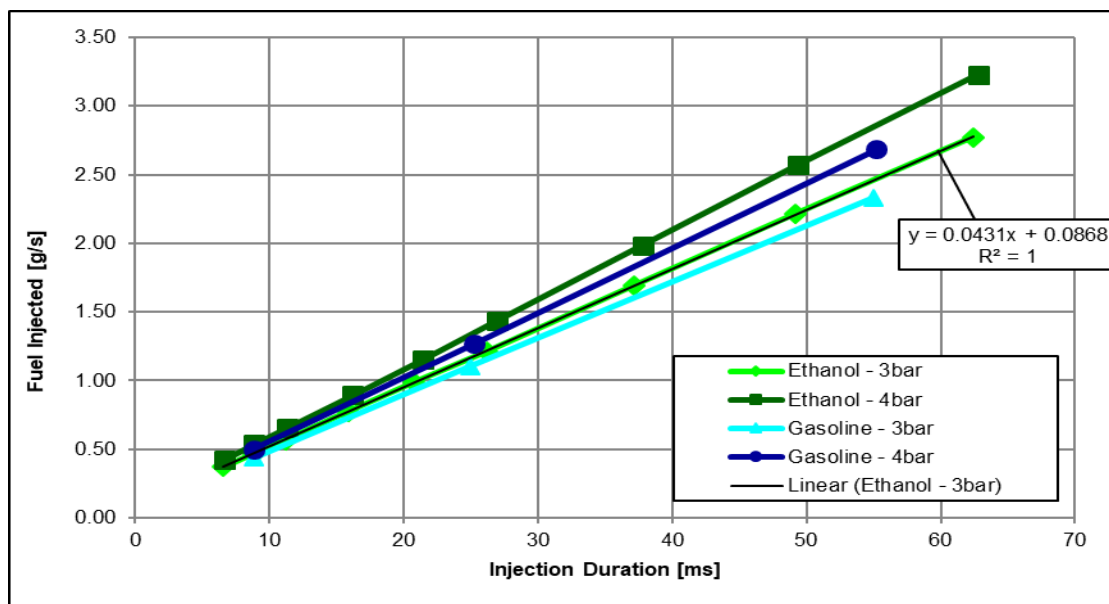


Figure 3.30 Injection Rate Profile for Bosch EV 14 Injection Valve

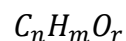
### 3.9 Lambda Calculation Based on Exhaust Gas Composition

The composition of the exhaust gas is generally determined by the ratio of the fuel and the air delivered to the engine, as well as the composition of the fuel being used, and how complete the combustion of the air fuel mixture is. Knowing these information, and the relation between them, will allow for the calculation of the correct ratio between the fuel and the air delivered to the engine.

There are several studies on the way the air to fuel ratio is calculated based on the composition of the exhaust gas. One of the earliest studies in this matter is by D'Alleva [180] in this study, the air to fuel ratio is calculated using charts of the exhaust gas concentration based on the fuels H to C ratio. Elting [181] made it possible to use these charts without the need to measure O<sub>2</sub> and also included cases of incomplete combustion. A formula was created by Spindt [182], which allows for the calculation of the air to fuel ratio without the need to assume the occurrence of a complete combustion. An improvement to the Spindt's equation was done by Brettschneider [183], which took the water in ambient air and the water absorbed by the measured NO<sub>x</sub> into account, and added the oxygenated fuel to the equation. Calculation of an equilibrium constant, K, was proposed by W. Simons [184], using the measurement of oxygen, where this K could have different values, usually less than 3.5. The equilibrium constant, K, changes by the act of the catalyst, which was discovered by Fukui, Tamura, Omori, Satoh in Mitsubishi [185], and also that the water in ambient air affects the water-gas equilibrium.

The Brettschneider method is the most common one used for the analysis of the exhaust gases and determining the air to fuel ratio, and thus, it is the one used for the purpose of this study.

General formula for the fuel composition is:



Because some of the fuels used for this study are petroleum based fuels, oxygen is absent from their composition. Therefore, exhaust production of CO<sub>2</sub>, H<sub>2</sub>O, CO, H<sub>2</sub>, O<sub>2</sub>, NO<sub>x</sub>, N<sub>2</sub>, uHC and soot particles (to be absent when it is adequately trivial) are considered, and the overall combustion reaction can be written as:

$$C_n H_m O_r + \frac{n_{O_2}}{\phi} (O_2 + 3.773 N_2) = n_p (\tilde{x}_{C_a H_b} + \tilde{x}_{CO} CO + \tilde{x}_{CO_2} CO_2 + \tilde{x}_{O_2} O_2 + \tilde{x}_{N_2} N_2 + \tilde{x}_{NO} NO + \tilde{x}_{NO_2} NO_2 + \tilde{x}_{H_2O} H_2O + \tilde{x}_{H_2} H_2) \quad \text{Equation 3.36}$$

Where:  $C_n H_m O_r = \text{The Fuel}$

$(O_2 + 3.773 N_2) = \text{The Oxidizer}$

$\phi = \text{The Measured Equivalence Ratio}$

$\tilde{x}_i = \text{The Mole Fraction of "I"th Component}$

$n_p = \text{The Total Number of Moles of Exhaust Products}$

The number of  $O_2$  Moles required for the complete combustion of one mole of the  $C_n H_m O_r$  fuel is:

$$n_{O_2} = n + \frac{m}{4} - \frac{r}{2} \quad \text{Equation 3.37}$$

The association between moles of exhaust products, (HC), (CO), (CO<sub>2</sub>) mole fractions, hydrocarbons assuming the same composition as fuel, is:

$$n_p = \frac{n}{(n_{HC}) + (n_{CO}) + (n_{CO_2})} \quad \text{Equation 3.38}$$

“H<sub>2</sub>“ mole fraction is:

$$(H_2) = \frac{(CO)(H_2O)}{K(CO_2)} \quad \text{Equation 3.39}$$

“H<sub>2</sub>O” mole fraction is determined using Equation 3.39 and the H balance and it is:

$$(H_2O) = \frac{m \left( \frac{1}{n_p} (HC) \right)}{2 \left( 1 + \frac{(CO)}{K(CO_2)} \right)} \quad \text{Equation 3.40}$$

(O<sub>2</sub>) mole fraction is driven from  $\sum \text{mol fraction} = 1$ , using N and O balance, with NO considered negligible, and it is:

$$(O_2) = \frac{(1 - (HC)) - \left(1 - \frac{\phi}{2}\right) ((CO) + (H_2O)) - (H_2) - (1 + \phi)(CO_2) + \frac{r\phi}{2n_p}}{(1 + \phi)} \quad \text{Equation 3.41}$$

The ratio between the total amount of oxygen in exhaust, to the amount of oxygen required for a stoichiometric combustion is:

$$\lambda = \frac{n_p ((CO) + 2(CO_2) + 2(O_2) + (H_2O)) - r}{2n_{O_2}} \quad \text{Equation 3.42}$$

### 3.10 Summary

In this chapter, the details of all experimental facilities employed for this study are presented. The specifications of the diesel single cylinder optical engine and all its components, such as the intake and exhaust systems, the fuel delivery system and the injectors, the data acquisition system for the in-cylinder pressure data are described. Also, the details of the equipment used for collecting exhaust emissions data, as well as the optical equipment and their setup are given. The experimental procedure as well as the techniques used for data analysis, and injector calibrations are presented and explained.

# Chapter 4.

## **Thermodynamic and Emission Analysis of Diesel-Ethanol Dual Fuel Operation**

### 4.1 Introduction

Thermodynamic analysis of an engine by means of the in-cylinder pressure and temperature as a function of crank angle, will allow for better understanding of an engine's characteristics, such as the transfer of heat and work to and from engine, resulting in the work produced by the engine, the Indicated mean effective pressure (IMEP), effect of injection timing on ignition, as well as the power output, and the engine efficiencies.

In this chapter, the thermodynamics of the engine under diesel-ethanol dual fuel operation is examined, and the effects of various intake air temperatures, injection strategies and injection timings, exhaust gas recirculation or EGR, and boosting of the intake air, on the combustion quality and the engine outputs, as well as their effect on the systems emission output, is detailed, along with the procedure applied for collecting the required information and data for this purpose.

### 4.2 Experiments

All tests were carried out on the Ricardo single cylinder optical diesel research engine detailed in Table 3.1. The Delphi solenoid injector was used for diesel fuel direct injection and a Bosch injector valve at 3.0bar for ethanol injection in the intake port, as given in Table 3.2 and Table 3.3. The intake air was heated by a Secomak electric air heater, and EGR was simulated by the supply of N<sub>2</sub> and CO<sub>2</sub> gas from high pressure gas tanks. All tests detailed in this chapter use commercially available diesel and anhydrous ethanol 100% as the premixed fuel.

In order not to risk damaging the fused silica glass window in the piston crown, all of the thermodynamics and emission testing were performed with the metal blank

piston crown, in order to allow for more extended testing procedures and combustion periods.

IMEP and other combustion characteristics are calculated from 20 cycles of in-cylinder pressure using an in-house made code in visual basic for applications (VBA). In this research, apparent heat release rate is calculated with a constant heat specific ratio of 1.3 for analysis, not gross heat release; this is due to the difficulty of accurately estimating the heat loss.

Finally, gaseous emission is measured by a Horiba MEXA-7170, detailed in section 3.5.1, and smoke level by an AVL 415 smoke meter, detailed in section 3.5.2.

### 4.3 Test Conditions

*For the diesel ethanol dual fuel operation testing, the engine speed and total fuel energy were kept constant. With fuel energy of 5.2kJ/sec, the total equivalent ratio is about 0.4 at 150°C of intake temperature and 1 bar of intake pressure. The diesel fuel injection pressure was fixed at 500bar and the engine was operated at ambient intake pressure but varying ethanol fractions and intake temperatures. These parameters are listed in Table 4.1 and*

Table 4.2 respectively. In addition, the experiments were repeated without and with 25% of EGR. The effect of injection strategy was evaluated by single and split injections at a fixed dwell angle of 35 CA.

*Table 4.1 Fixed Testing Parameters*

Fixed Testing Parameters	
Parameter	Value
Engine Speed (rpm)	1200
Diesel Rail Pressure (bar)	500
Total Fuel Energy (kJ/sec) Constant	5.2
Target IMEP (bar)	3.0
Intake Pressure (bar)	≈ 1.0

*Table 4.2 Variable Testing Parameters*

Variable Testing Parameters	
Parameter	Value
Intake Temperature (°C)	100, <u>150</u>
Substitution Ratio (%)	0 (Diesel only), 45, 60, 75
EGR Rate (%)	0, 25
Diesel Injection Strategy	<u>Single</u> , Split (50/50, 35°CA Dwell)

## 4.4 Results and Discussion

The measured in-cylinder pressure was used to determine the IMEP values and the heat release process. The start of combustion (CA10) was calculated from the 10% mass fraction of fuel burnt and combustion phasing (CA50) were calculated from the 50% mass fraction of fuel burnt. The number of crank angles between 10% and 90% of mass fraction of fuel burnt, defined combustion duration, and the crank angle between the start of second injection (SOI) and onset of combustion (CA10) determined the ignition delay.

While the exhaust gas and soot emissions were measured for all the strategies, the NO<sub>x</sub> and uHC emissions were measured in Parts per Million (ppm), and soot emission was measured in Filtered Smoke Number (FSN)

### 4.4.1 Effect of Intake Air Temperature and EGR with 60% Substitution Ratio

Figure 4.1, from top-left to bottom-right, illustrates Combustion Efficiency, Soot, CO, THC, and NO<sub>x</sub> levels, Indicated Thermal Efficiency,  $P_{max}$ , CA10-90 (Combustion Duration), CA50 (combustion centre), Ignition Delay (from Injection Signal to CA5), PHRR (Peak Heat Release Rate), PPRR (Peak Pressure Rise Rate), start of injection signal timing of diesel fuel.

As indicated in the bottom left graph of the indicated efficiency vs SOI (start of injection) of diesel, data at 150°C of intake temperature without EGR could not be

collected between 10° CA to 20° CA BTDC SOI due to the presence of violent combustion. In addition, when SOI of diesel was retarded beyond 5 CA BTDC or advanced before 28 CA BTDC misfire occurred at 100°C of intake temperature and at 150°C of intake temperature with 25% of EGR. Therefore, direct comparison could only be made between the results of 150°C of intake temperature with 25% EGR and 100°C of intake temperature without EGR.

Results in Figure 4.1 show that the variation of the thermal efficiency with SOI of diesel is quite similar but the peak efficiency of each is obtained at different SOIs because of the difference in ignition delay, combustion duration and heat loss. Higher intake temperature increases NO<sub>x</sub> at the same SOI and EGR decreases NO<sub>x</sub>. The lowest NO<sub>x</sub> was obtained with 25% EGR. Soot emission is very low in all conditions. Soot levels peaked at around 25° CA BTDC injection when the CA50 was most advanced. Higher combustion efficiency was achieved at higher intake temperature with EGR when both uHC and CO were lower due to more complete combustion. The lower NO<sub>x</sub> obtained with higher intake temperature and EGR indicates that the dilution and heat capacity effects of EGR was more dominant over the increase in the intake temperature. The greater effect of EGR is further evidenced by the longer ignition delay, slower combustion (CA10-CA90), retarded CA50, lower P<sub>max</sub>, and lower PRRR.

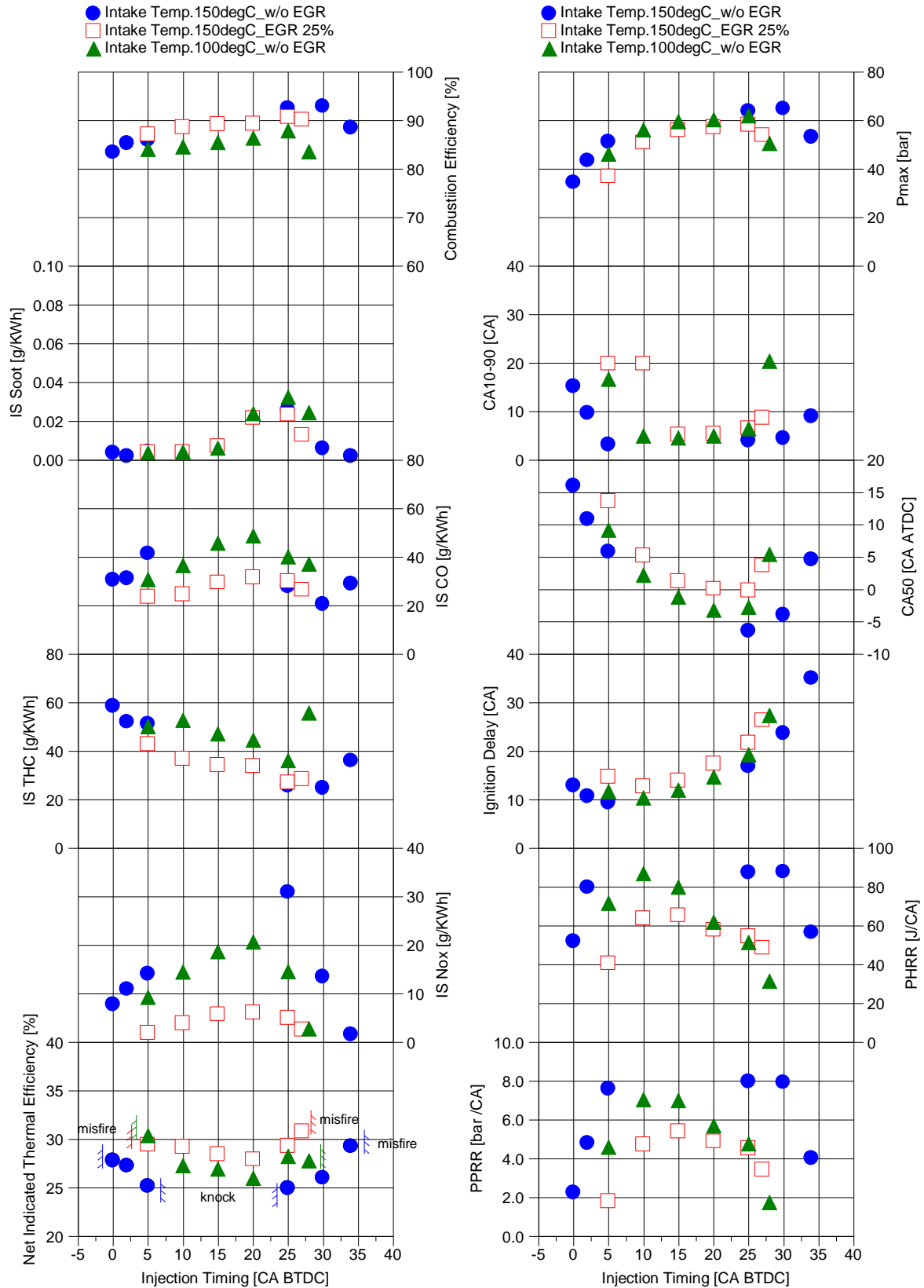
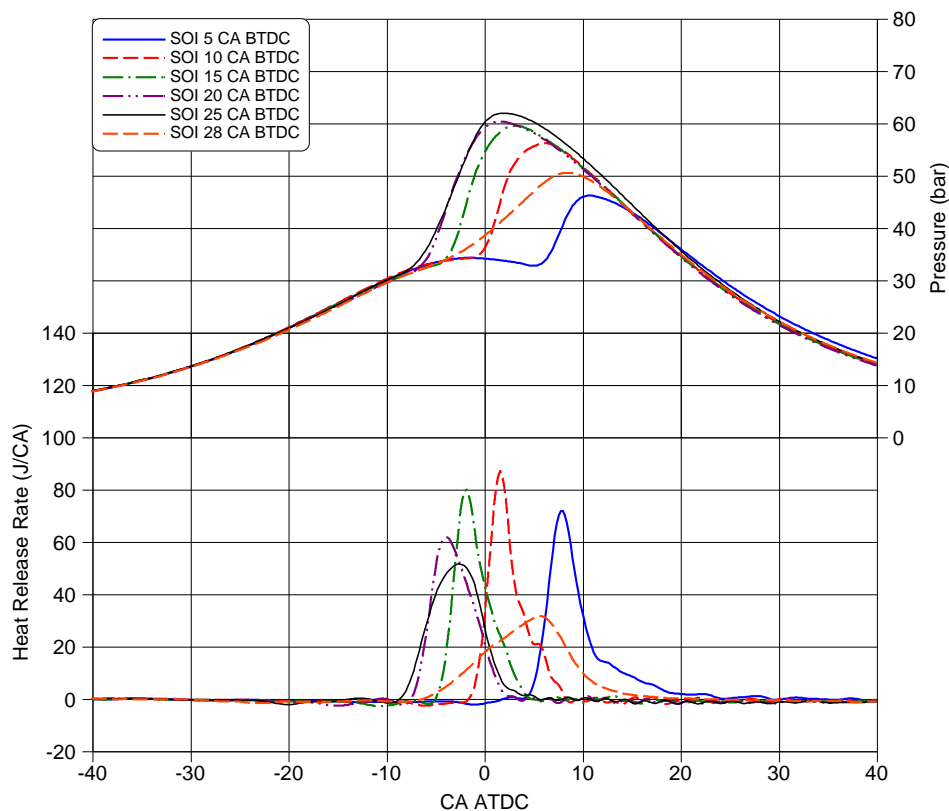


Figure 4.1 Comparison of Engine Performance, Emission and Combustion Characteristics at Different Intake Conditions, with 60% Ethanol Substitution Ratio and Single Diesel Injection

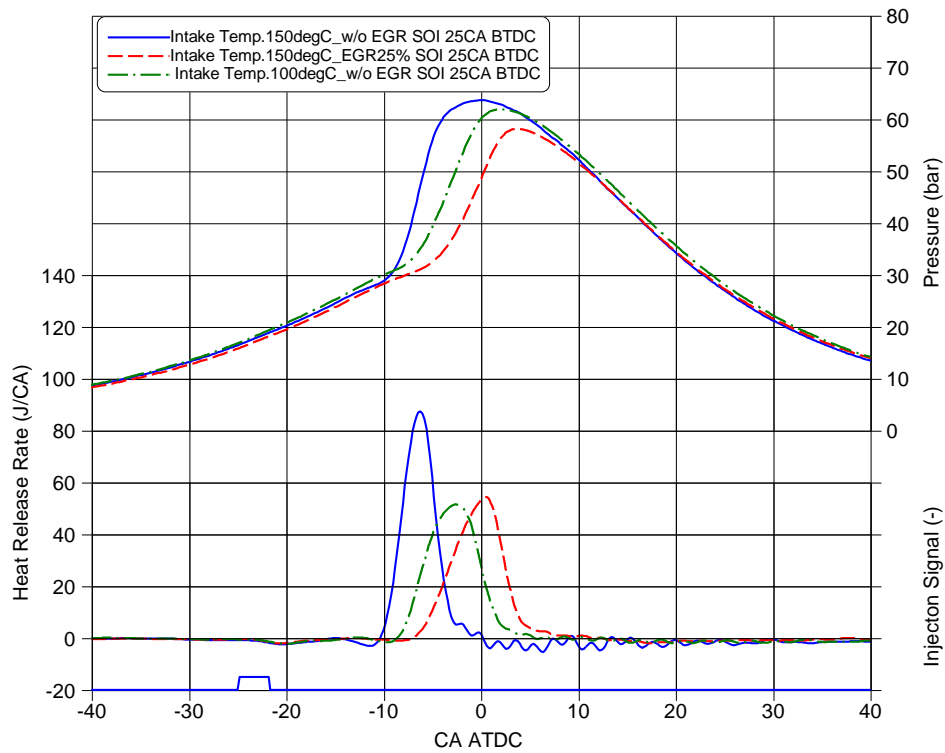
Figure 4.2 shows the in-cylinder pressure and HRRR at 100°C intake temperature and 60% of ethanol substitution ratio without EGR when the SOI of diesel was changed. The start of heat release and combustion timing are advanced with the SOI of diesel as expected, except at 28° CA B TDC of SOI. Among these SOI conditions, 10° CA BTDC of SOI has the highest PHRR and shortest combustion duration when most combustion occurs around TDC. The beginning of HRRR at 28° CA BTDC of SOI is slower than others, due to more diluted mixture and lower charge temperature. This combustion, appears to be an RCCI-like combustion. On the other hand, it is also observed that at 5° CA BTDC of SOI, the heat release of late combustion, is more like diesel combustion. Optical measurements will be presented and analysed on the in-cylinder conditions at such operating conditions.



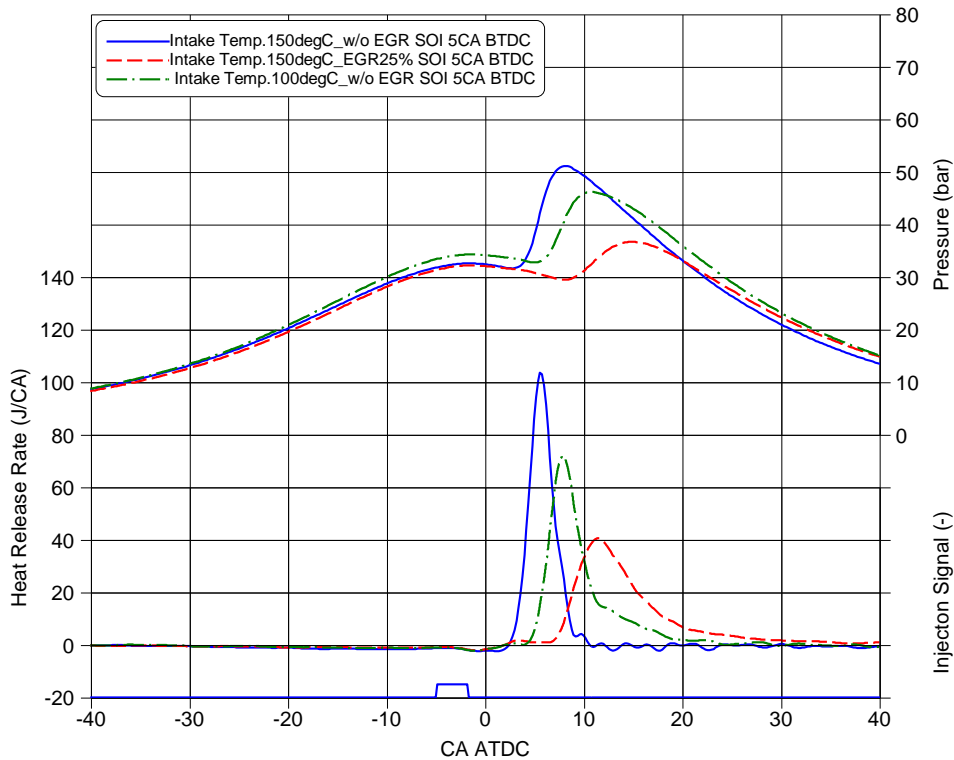
**Figure 4.2 In-Cylinder Pressure and HRRR at Different Single SOI with 100°C Intake Temperature, and 60% Ethanol Substitution Ratio**

Figure 4.3 and Figure 4.4 show in-cylinder pressure and HRRR at different intake conditions at 25° CA and 5° CA BTDC SOI, respectively. Both of these graphs show

that, at higher intake temperature, PHRR is higher, combustion duration is shorter and ignition delay is shorter. EGR has greater effect on slowing down the heat release process than the cooler intake temperature. It is also noted that compression pressure is decreased as the intake air temperature is increased from 100 °C to 150 °C without EGR and it becomes the lowest with EGR, because of the decreased polytropic constant of slightly richer mixture at higher intake temperature and then the presence of EGR.



*Figure 4.3 In-Cylinder Pressure and HRRR at Different Intake Conditions when SOI is 25° CA BTDC, and 60% Ethanol Substitution Ratio*



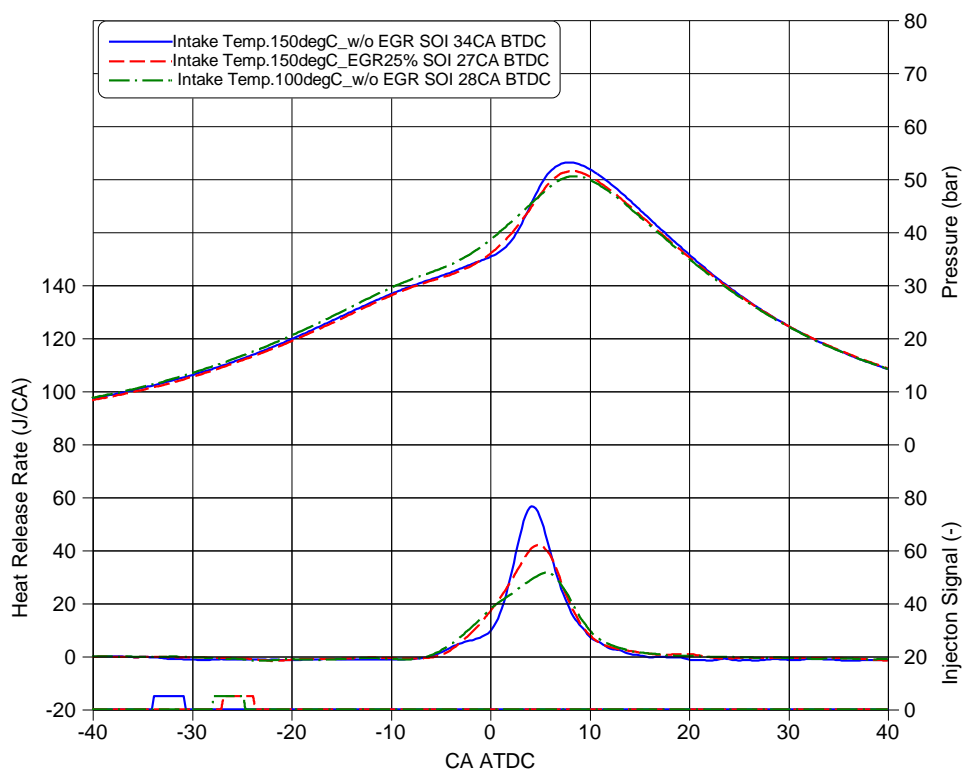
**Figure 4.4 In-Cylinder Pressure and HRRR at Different Intake Conditions when SOI is 5<sup>o</sup> CA BTDC, and 60% Ethanol Substitution Ratio**

Figure 4.5 shows in-cylinder pressure and HRR results at the optimised SOI of diesel for thermal efficiency. They are 34<sup>o</sup> CA BTDC of SOI at 150<sup>o</sup>C of intake temperature without EGR, 28<sup>o</sup> CA BTDC of SOI at 150<sup>o</sup>C of intake temperature with 25% of EGR and 27<sup>o</sup> CA BTDC of SOI at 100<sup>o</sup>C of intake temperature without EGR. Figure 4.6 presents the engine performances, emission and combustion characteristics at the optimized SOI conditions, while displaying the effect of the injection timing for the same exact condition with a later injection as well. The results illustrate that increased intake temperature leads to a higher thermal efficiency because of higher combustion efficiency, due to lower THC. EGR increases the thermal efficiency because of lower heat loss from lower combustion temperature. Combustion efficiency or THC is not decreased by EGR due to higher overall equivalent ratio, caused by less fresh air. NO<sub>x</sub> is lower at 150<sup>o</sup>C of intake temperature without EGR because the fuel mixture is more homogeneous with longer ignition delay, by hotter intake condition without EGR gas.

Increasing intake temperature decreases soot when not using EGR. Combustion duration (CA10-90) is longer with higher intake temperature, or with EGR condition.

The starts of combustion are pretty similar to each other in Figure 4.5. The slope of HRR in the condition with 150°C intake temperature and no EGR, changes around TDC when ethanol combustion is accelerated by diesel combustion.

As reported by Vinícius [186], the use of internal EGR at low loads, for ethanol and diesel dual fuel engine, is effective for reducing emission and increasing thermal efficiency. This matches the results from this study where increasing in-cylinder temperature and using EGR which have the similar effect as using internal EGR, are shown to simultaneously reduce emission and increase thermal efficiency at the low load operations.



*Figure 4.5 In-Cylinder Pressure and HRRR with the Optimized SOI at Different Intake Conditions*

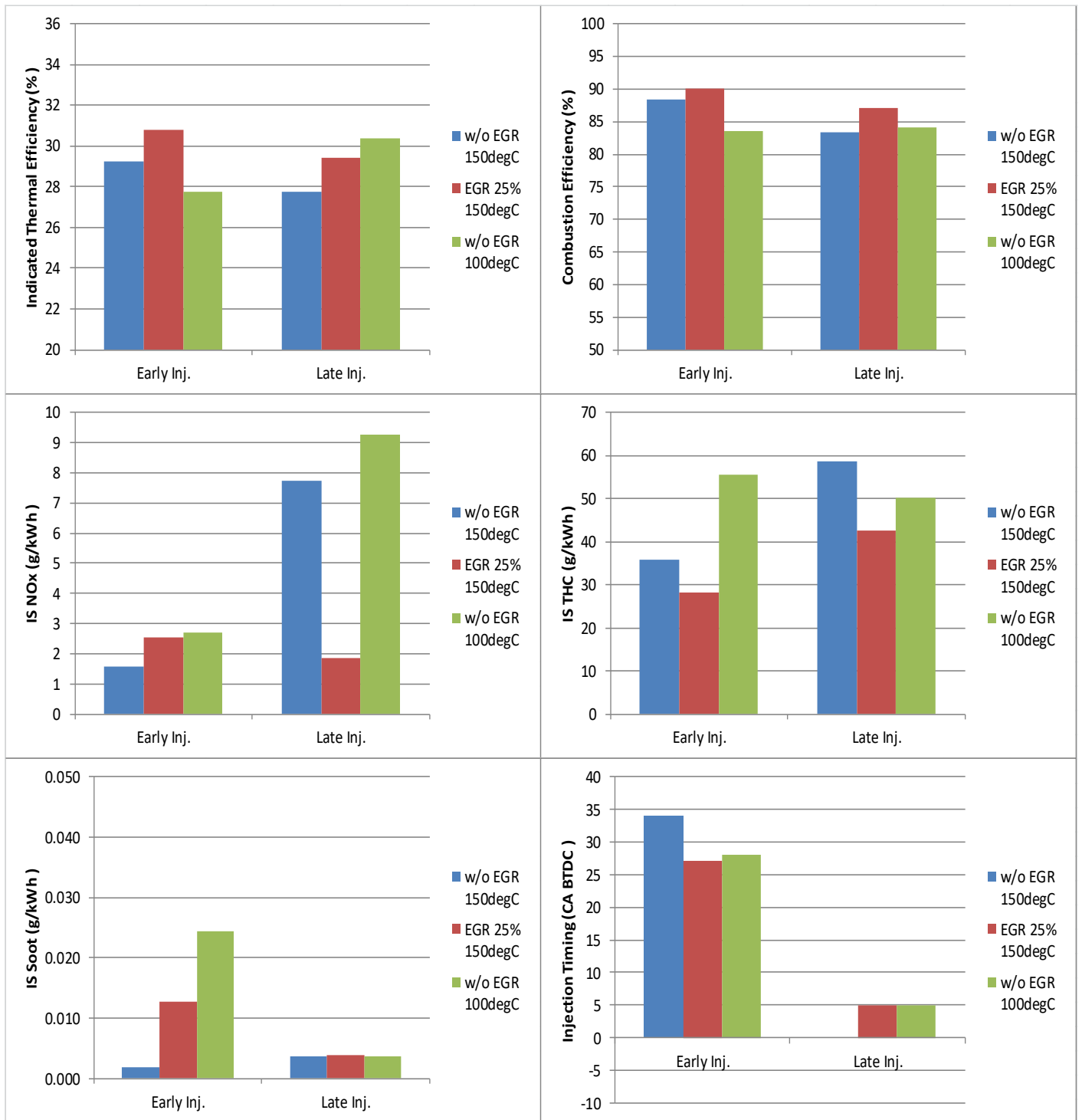


Figure 4.6 Engine Performances and Emission with the Optimized SOI at Different Intake Conditions

#### **4.4.2 Comparison of Single and Split Diesel Injection with 60% Substitution Ratio and Intake Air Temperature of 150°C**

Figure 4.7 illustrates the effect of single and split injections with a fixed dwell angle of 35° CA. For split injection operations, second injection timing is applied to the graphs. From top-left to bottom-right are the Combustion Efficiency, Soot, CO, THC, and NO<sub>x</sub> levels, Indicated Thermal Efficiency,  $P_{max}$ , CA10-90 (Combustion Duration), CA50 (combustion centre), Ignition Delay (from Injection Signal to CA5), PHRR (Peak Heat Release Rate), PPRR (Peak Pressure Rise Rate) .

All of combustion characteristics are quite similar between the single and split injection strategies. The combustion with the split injection strategy is controlled by the second injection. In particular, split injections enable the dual fuel operation to be achieved without the knocking combustion between 10° CA to 20° CA BTDC of second SOI. Misfire limit with split injection is slightly narrower than the single injection.

Figure 4.8 show the in-cylinder pressure and HRRR with 30° CA BTDC of SOI for single injection of diesel and 30° CA to 65° CA BTDC of SOI for split injection of diesel. This shows that split injection has later, lower PHRR and slower combustion because of leaner premixed fuel mixture given by earlier 1st injection and less amount of second injection. Figure 4.9 shows the opposite trend to those in Figure 4.8 about the start of the combustion when 5° CA BTDC of SOI for single injection and 5° CA to 40° CA BTDC of SOI for split injection are used. This is because the 1st injection reduces the ignition delay and assist the start of combustion of the second injection. The combustion can start during or just soon after the second injection has started. In this case, split injection cause more diffusion-like combustion.

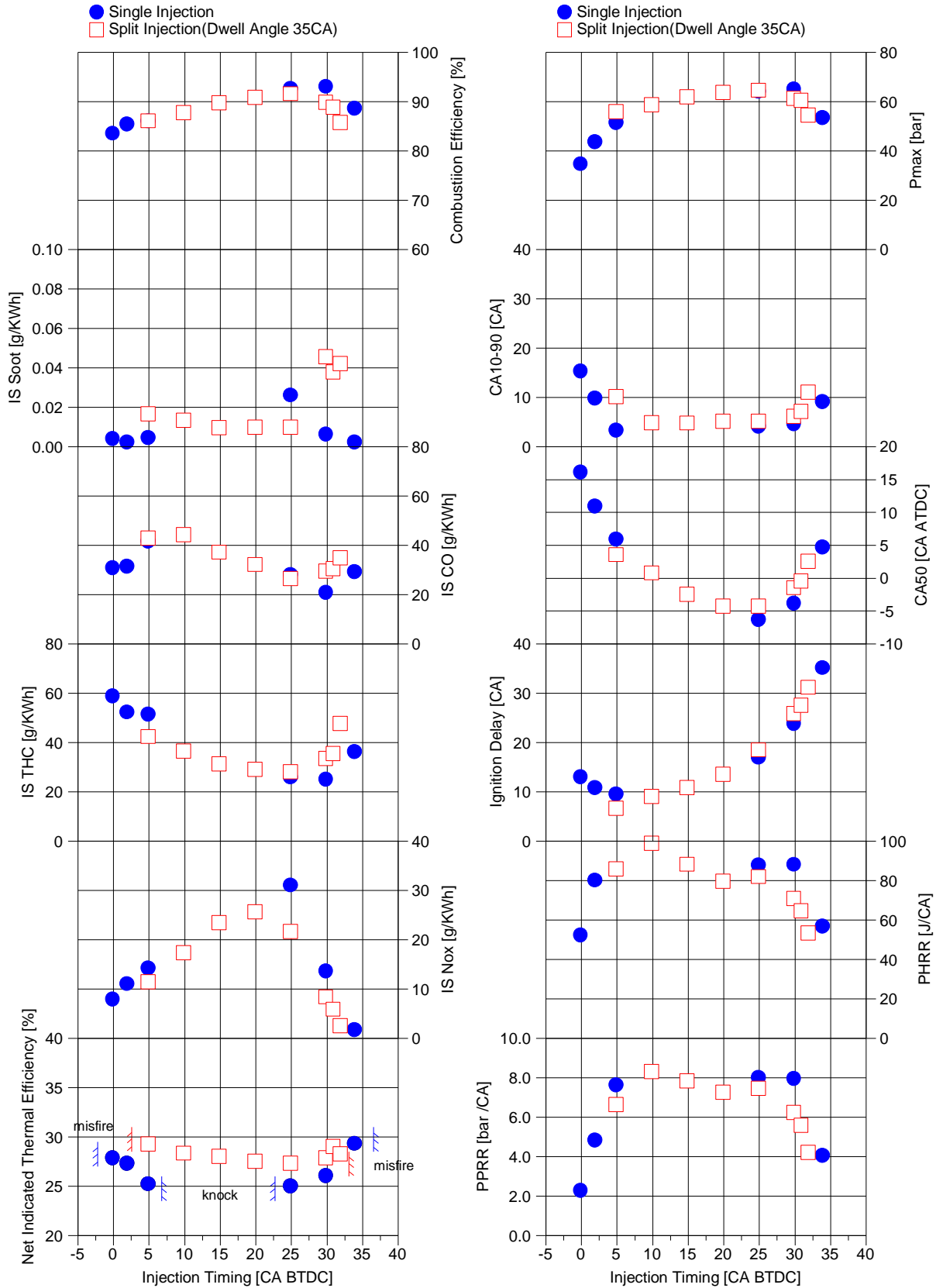


**Figure 4.7 Comparison of Engine Performance, Emission and Combustion Characteristics Between Single and Split Diesel Injection with 60% Ethanol Substitution Ratio, 150°C Intake Temperature, and No EGR.**

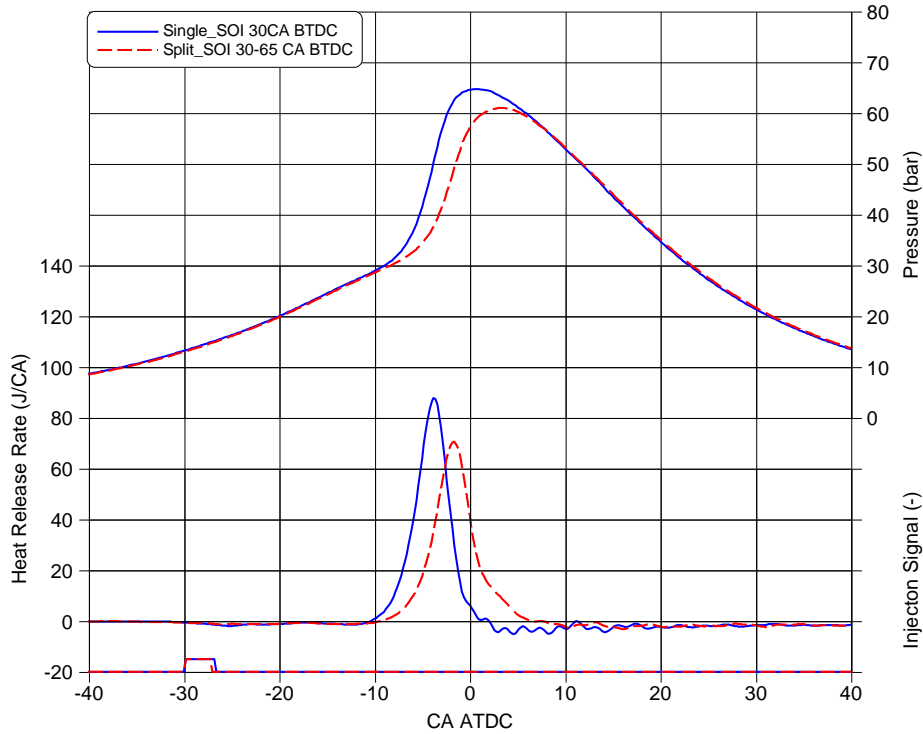


**Figure 4.8** In-Cylinder Pressure and HRRR with Single and Split Diesel Injection when SOI of Single is 30° CA and the SOI of Split is 30°-65° CA BTDC, 150°C Intake Temperature, and 60% Ethanol Substitution Ratio

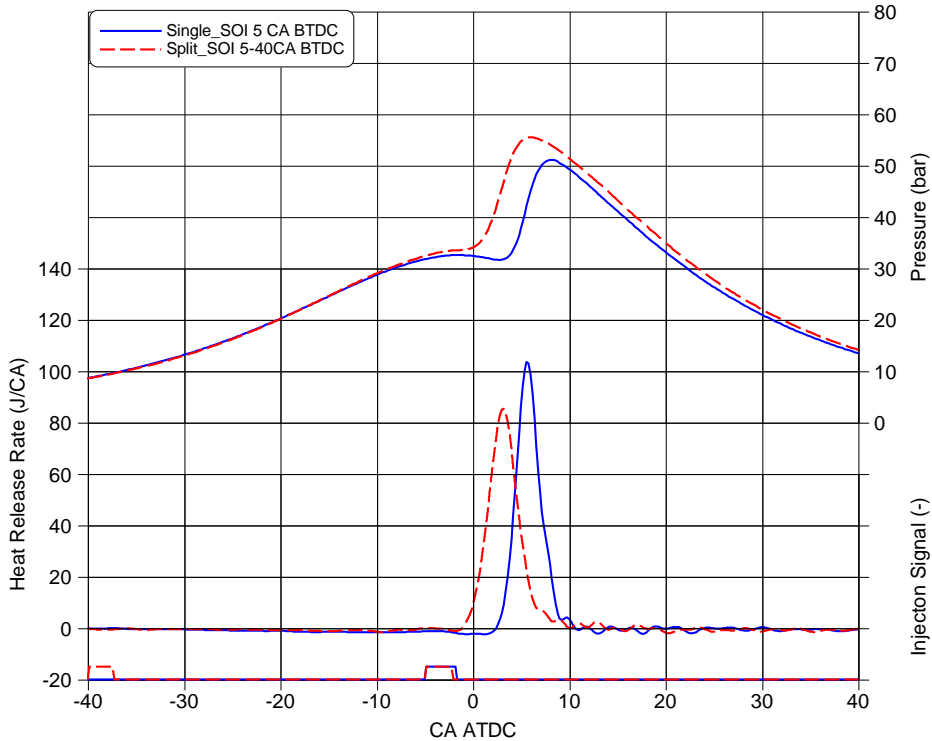


**Figure 4.9** In-Cylinder Pressure and HRRR with Single and Split Diesel Injection when SOI of Single 5° CA and the SOI of Split is 5°-40° CA BTDC, 150°C Intake Temperature, and 60% Ethanol Substitution Ratio

#### **4.4.3 Effect of Substitution Ratio with Single Diesel Injection, Intake Air Temperature of 150°C, and no EGR**

The effect of ethanol substitution ratio on combustion and emissions are presented in Figure 4.10. From top-left to bottom-right, it illustrates Combustion Efficiency, Soot, CO, THC, and NO<sub>x</sub> levels, Indicated Thermal Efficiency,  $P_{max}$ , CA10-90(Combustion Duration), CA50, Ignition Delay (from Injection Signal to CA5), PHRR (Peak Heat Release Rate), PPRR (Peak Pressure Rise Rate), as a function of the Injection timing of diesel fuel.

As shown in the bottom-left graph, Diesel baseline operation is limited to very retarded injection timings of 5 CA BTDC by the upper limit of PRRR of 10bar/CA. Even with such delayed injection timing, diesel only operation has a higher thermal efficiency than dual fuel operations with ethanol substitution ratio of 45% and 60% because of their higher combustion efficiency. However, the thermal efficiency of diesel baseline is lower than that of 75% substitution ratio of ethanol in dual fuel operation, which can be achieved over a wider range of injection timings. In comparison, 45% and 60% substitution ratio of ethanol are limited by knock around 15° CA BTDC of SOI. The lower the ethanol substitution ratio, the earlier the SOI of diesel fuel for peak thermal efficiency, due to longer ignition delay made by richer diesel fuel mixture. When SOI is near TDC, NO<sub>x</sub> emissions are similar in all conditions. The lowest NO<sub>x</sub> is obtained with earlier SOI of diesel with lower ethanol substitution ratio, because of longer ignition delay.

Diesel baseline operation produces the lowest THC and CO and hence the highest combustion efficiency. Dual fuel operation produces higher THC and CO due to ethanol fuel trapped in crevices and over lean zones. Baseline diesel operation produces the highest soot. The smoke level decreases with increasing ethanol substitution ratio.

Combustion efficiency of dual fuel condition increases up to a certain point as SOI is advanced, beyond which, it decreases at later SOI.

Diesel condition has higher PRRR and PHRR than dual fuel condition due to higher reactivity of diesel fuel.

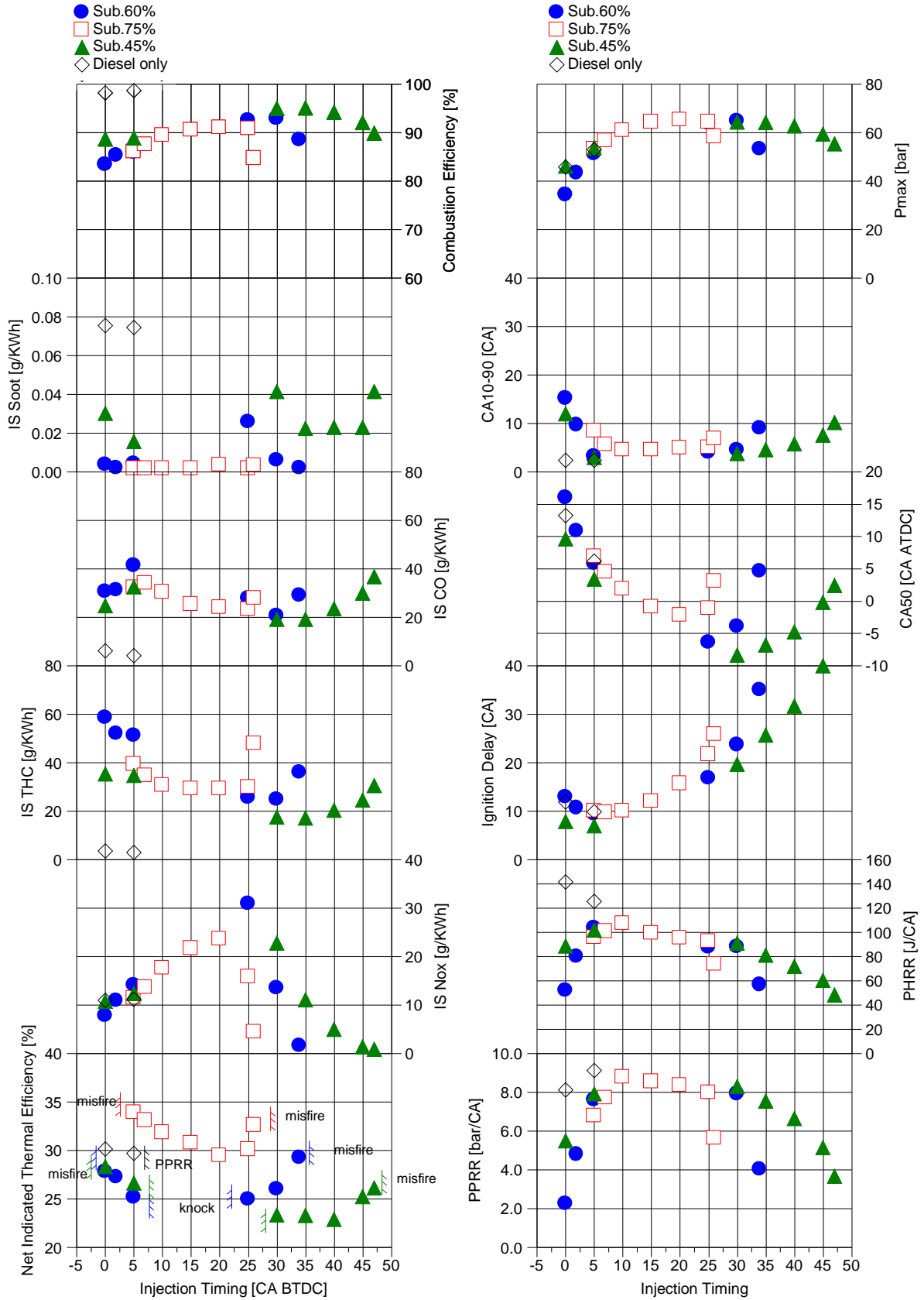


Figure 4.10 Comparison of Engine Performance, Emission and Combustion Characteristics at Different Ethanol Substitutions Ratio, when Single Diesel Injection Timing is Sweeping and Constant 150°C Intake Temperature

Figure 4.11 shows the in-cylinder pressure and HRRR with different substitution ratios of ethanol at the same SOI of 5° CA BTDC. Heat release process begins at similar times at each condition except 45% ethanol substitution ratio. Combustion duration of all conditions are similar, however, that of 75% substitution ratio of ethanol is a bit longer as evidenced by its higher pressure during the expansion stroke.

Figure 4.12 illustrates in-cylinder pressure and HRR with the optimized SOI for emission and efficiency at different ethanol substitution ratios. Figure 4.13 shows engine performance and emission with the same conditions as Figure 4.12, while displaying the effect of the injection timing for the same exact condition with a later injection as well.

When the ethanol substitution ratio is lower, optimized SOI is advanced more, so that richer diesel mixture needs longer ignition delay to have proper combustion timing, and combustion is milder and PHRR is lower. In terms of emission, lower ethanol substitution ratio decreases NO<sub>x</sub> with more homogeneous diesel mixture, and same can be said for THC. The thermal efficiency at lower substitution ratio is worse due to too advanced combustion timing. Only 45% substitution ratio has high level of soot due to overall diesel rich mixture or not enough combustion temperature to oxidise soot.

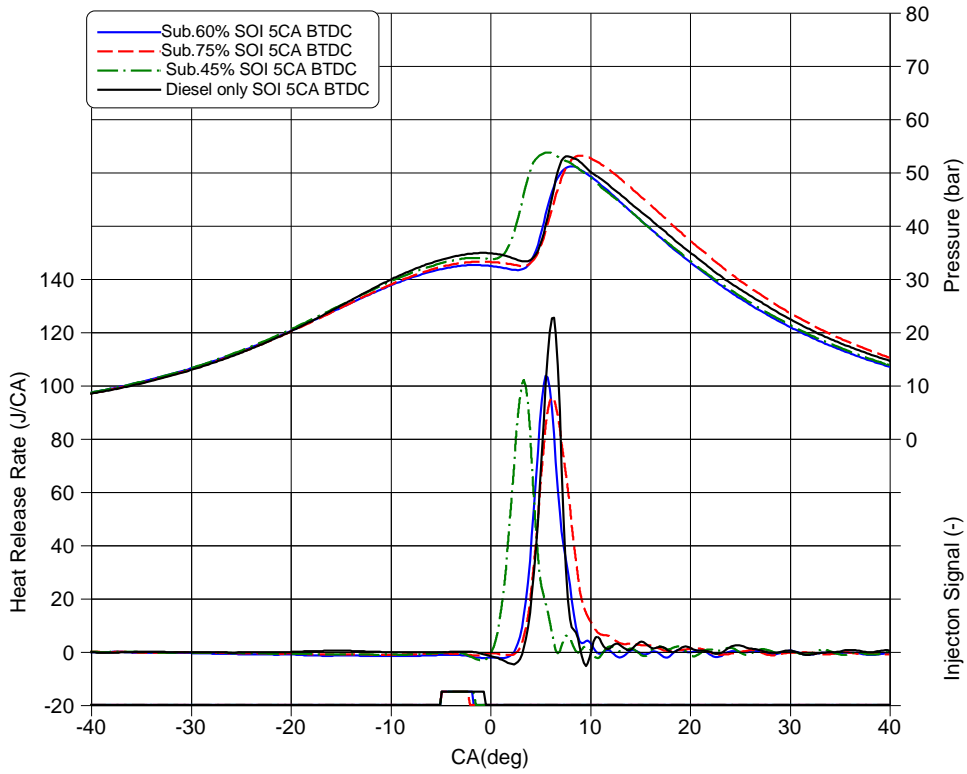


Figure 4.11 In-Cylinder Pressure and HRR with at Different Ethanol Substitution Ratios when Diesel SOI is 5° CA BTDC, with Constant 150°C Intake Temperature

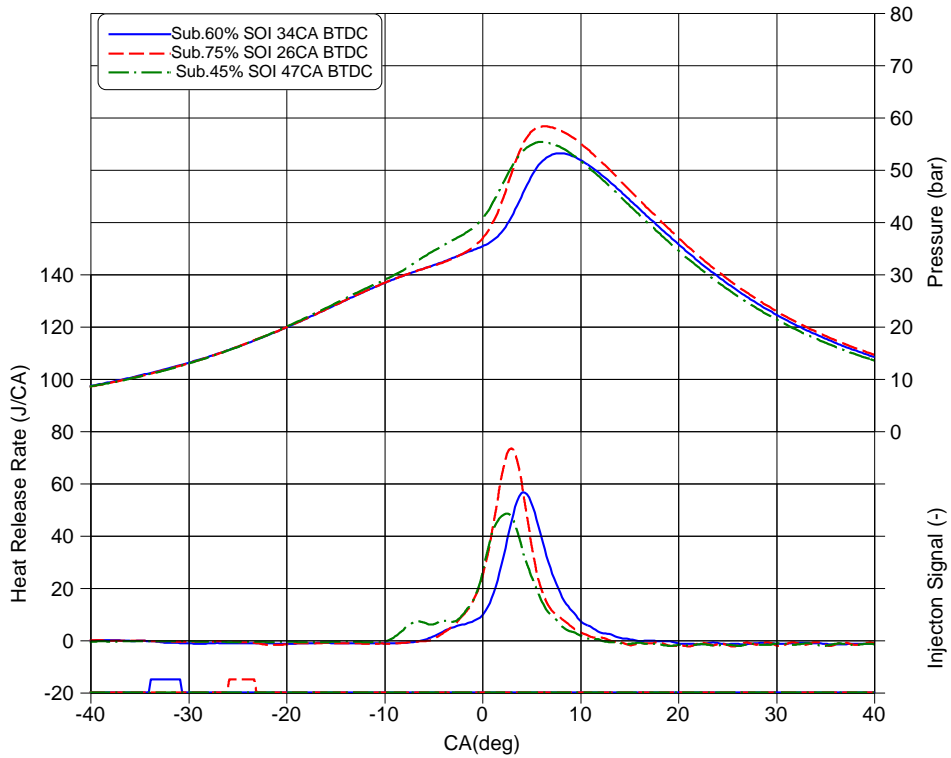


Figure 4.12 In-Cylinder Pressure and HRR with the Optimized SOI at Different Ethanol Substitution Ratio

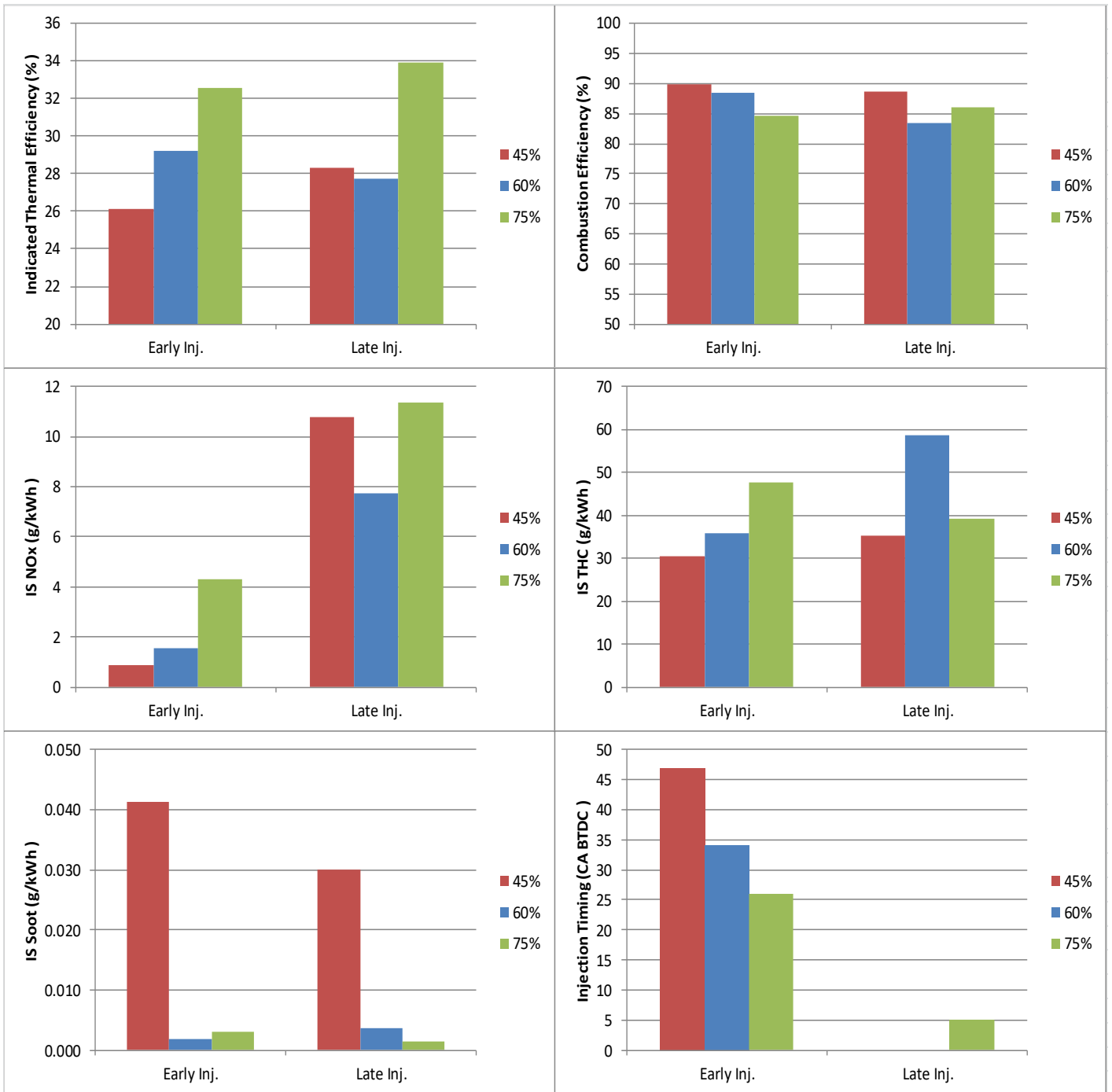


Figure 4.13 Engine Performances and Emission with the Optimized SOI at Different Ethanol Substitution Ratio

## 4.5 Summary

The results obtained from the experiments performed for this chapter demonstrates the effects of different parameters, such as intake air temperature, EGR, different injection strategies including single and split diesel injection, as well as various fuel substitution ratios, on performance, efficiency, and emission output for Diesel-Ethanol dual-fuel engine operations. In terms of the direct diesel fuel injection, injection timing and injection strategies, as well as different Ethanol substitution ratios and intake conditions, all effect the reactivity of the mixture, and show improvements to both efficiency and emissions compared to that of pure diesel operations. However, the addition of ethanol has a greater effect in exhaust gas emission and particulate reduction. The conclusion from these findings is presented in more detail below.

### A. Single injection dual fuel operation at 3.0bar IMEP at 1200rpm:

- In conventional dual fuel combustion that uses a single late diesel injection, EGR is effective in reducing NO<sub>x</sub> produced, because of the lower oxygen concentration and higher heat capacity, and increased thermal efficiency due to less heat loss and less THC. Lower intake temperature has a good effect on NO<sub>x</sub> and thermal efficiency. That suggests that external cooled EGR can have a benefit for emission and thermal efficiency.
- In premixed dual fuel combustion that includes an early diesel injection and a later diesel injection, combined use of EGR and higher intake temperature is effective to reduce THC, and increase thermal efficiency as well as lower NO<sub>x</sub> emissions. Thus external hot EGR or using internal EGR can have a benefit for emission and efficiency at low load dual fuel operations.

### B. Effect of SOI of diesel during the dual fuel operations at 3.0bar IMEP at 1200rpm:

- The split injections enable wider dual fuel engine operation and more optimised performance in efficiency and emissions.

Second injection timing of split injection and injection timing of single injection have similar effects on combustion characteristic, such as ignition delay, CA<sub>50</sub>, PHRR etc.. That means that combustion is primarily controlled by latter (second)

injection timing, but they are slightly different due to the effect of heat release or distribution of diesel fuel mixture of the 1<sup>st</sup> injection.

- when second injection timing and single injection timing are the same, NO<sub>x</sub>, THC and CO trend of both injection strategies are similar but NO<sub>x</sub> of split injection is slightly lower.
- Thermal efficiency of split injection is higher when second injection timing and single injection timing are the same. Late second injection timing improves thermal efficiency compared to late single injection, but produces more soot. This is because late split injection, makes more diffusion-like combustion with shorter ignition delay of second injection since combustion of 1<sup>st</sup> injection starts before or during the second injection, and this combustion makes milder heat release rate with lower heat loss and more soot emission.

C. Comparison of dual fuel single injection operation and baseline diesel combustion at 3.0bar IMEP at 1200rpm:

- Combustion of single diesel injection is more intense than that of dual fuel, with higher PHRR and shorter combustion duration, due to higher chemical reactivity of diesel fuel.
- THC and CO of dual fuel combustion is higher and hence, lower combustion efficiency, because of over lean premixed fuel and air mixtures and their presence in the crevices.
- Dual fuel combustion has a big advantage in reducing soot emission because of leaner fuel mixture.

# Chapter 5.

## **Thermodynamic and Emission Analysis of Diesel-Gasoline Dual Fuel Operation**

### 5.1 Introduction

In this chapter, the thermodynamics of the engine under diesel-gasoline dual fuel operation is examined, and the effects of intake air temperatures, injection strategies and injection timings, exhaust gas recirculation or EGR, and boosting of the intake air, on the combustion quality and the engine outputs, as well as their effect on the systems emission output, is detailed, along with the procedure applied for collecting the required information and data for this purpose.

### 5.2 Experiments

All tests were carried out on the Ricardo single cylinder optical diesel research engine, detailed in Table 3.1. Once again, the Delphi solenoid injector was used for diesel fuel direct injection, and the Bosch injector valve was used this time for gasoline injection at 3.0bar in the intake port, with the details of both injectors given in Table 3.2 and Table 3.3. As before, the intake air was heated by a Secomak electric air heater, and EGR was simulated by the supply of N<sub>2</sub> and CO<sub>2</sub> gas from high pressure gas tanks. All tests detailed in this chapter use commercially available diesel for direct injection and commercially available gasoline as the premixed fuel.

Once more, in order not to risk damaging the fused silica glass window in the piston crown and for extended engine operations, all of the thermodynamics testing as well as all emission testing were performed using the metal blank replacement. IMEP and other combustion characteristics were calculated from 20 cycles of in-cylinder pressure using an in-house made code in visual basic for applications (VBA). As mentioned in previous chapter, in this research apparent heat release rate is calculated

with a constant heat specific ratio of 1.3 for analysis, not gross heat release, due to the difficulty of accurately estimating the heat loss. Gaseous emissions were measured by a Horiba MEXA-7170 and smoke level by an AVL 415 smoke meter, detailed in section 3.5.1 and section 3.5.2 respectively.

### 5.3 Test Conditions

For the diesel gasoline dual fuel operation testing, the engine speed and total fuel energy were kept constant again. The constant and variable engine operating parameters are listed in Table 5.1 and Table 5.2 respectively. Diesel was injected at 500bar by the common rail fuel injector and gasoline in the intake port at 3.0bar. Engine was operated at 1200rpm and supplied with a constant input energy of 5.2kJ/sec, meaning total equivalent ratio is about 0.4 at 150°C of intake temperature and 1 bar of intake pressure. In addition, the experiments were repeated without and with 25% and 40% of EGR. Both single and split injections of diesel were used with a constant dwell angle of 35 CA during the split injections

*Table 5.1 Fixed Testing Parameters*

Fixed Testing Parameters	
Parameter	Value
Engine Speed (rpm)	1200
Diesel Rail Pressure (bar)	500
Total Fuel Energy (kJ/sec) Constant	5.2
Target IMEP (bar)	3.0
Intake Pressure (bar)	≈ 1.0

*Table 5.2 Variable Testing Parameters*

Variable Testing Parameters
-----------------------------

Parameter	Value
Intake Temperature (°C)	100, <u>150</u>
Substitution Ratio (%)	0 (Diesel only), 45, 60, 75
EGR Rate (%)	0, 25, 40
Diesel Injection Strategy	<u>Single</u> , Split (50/50, 35°CA Dwell)

## 5.4 Results and Discussion

The measured in-cylinder pressure was used to determine the IMEP values and the heat release process. The start of combustion (CA10) was calculated from the 10% mass fraction of fuel burnt and combustion phasing (CA50) were calculated from the 50% mass fraction of fuel burnt. The number of crank angles between 10% and 90% of mass fraction of fuel burnt, defined combustion duration, and the crank angle between the start of second injection (SOI) and onset of combustion (CA10) determined the ignition delay.

While the exhaust gas and soot emissions were measured for all the strategies, the NO<sub>x</sub> and uHC emissions were measured in Parts per Million (ppm), and soot emission was measured in Filtered Smoke Number (FSN).

### 5.4.1 Effect of Intake Air Temperature and EGR (Exhaust Gas Recycling) with 60% Substitution Ratio

Figure 5.1 below shows, from left-top to right-bottom, Combustion Efficiency, Soot, CO, THC, NO<sub>x</sub>, Indicated Thermal Efficiency, P<sub>max</sub>, CA10-90(Combustion Duration), CA50(combustion centre), Ignition Delay (from Injection Signal to CA5), PHRR (Peak Heat Release Rate), PPRR (Peak Pressure Rise Rate), injection signal start timing of diesel fuel.

In the bottom left graph, indicated efficiency to SOI (start of injection) is illustrated. The data at 150°C of intake temperature without EGR cannot be collected between 10° CA to 45° CA BTDC SOI due to the presence of violent combustion causing high knocking. Also any injection before 65° CA BTDC at these intake conditions leads to misfire. The same misfire occurs for any injection timing after 5° CA BTDC and before 62° CA BTDC when the intake temperature is at 100°C without any EGR.

When increasing the EGR to 25% with the 150°C intake temperature, some knocking occurs between the SOI timings of 35° CA BTDC and 15° CA BTDC, with any SOI timing after 5° CA BTDC or before 56° CA BTDC leading to misfire. By increasing the EGR to 40% for the same intake temperature of 150°C, there is less chance of knocking but misfire happens at a SOI timings before 50° CA BTDC, excluding, as well as any SOI timing beyond 5° CA BTDC. Higher intake temperature increases NO<sub>x</sub> at the same SOI and EGR decreases NO<sub>x</sub>. Comparing the lowest NO<sub>x</sub> of each intake condition, NO<sub>x</sub> at higher intake temperature is lower and without EGR, NO<sub>x</sub> is lower, because more premixed and leaner mixture of diesel fuel, due to earlier SOI and long ignition delay, decreases NO<sub>x</sub> levels.

Soot emissions are generally lower at earlier SOI with higher intake temperatures and higher levels of EGR. That said, there is an increase in soot levels at SOI timings earlier than 50° CA BTDC, specially for lower intake temperatures and EGR levels. It can be observed that there is a peak in soot levels at SOI timing of 20° CA BTDC without any EGR when the intake temperature is 100°C. This could be caused by the diesel fuel not being injected into the combustion bowl properly at this diesel injection timing.

Combustion efficiency, at higher intake temperature, is higher, and that is due to higher in-cylinder temperature. EGR does not decrease combustion efficiency so much, even though oxygen concentration is decreased, because increasing EGR ratio decreases fresh air flow and increases total equivalent ratio. Ignition delay is longer at lower intake temperature and with EGR because of lower in-cylinder temperature made from lower heat specific ratio and lower oxygen ratio. Both decreasing intake temperature and using EGR, led to later CA<sub>50</sub>, longer CA<sub>10-90</sub>, lower P<sub>max</sub>, and lower PRRR, because of slower chemical reaction in lower temperature or lower oxygen ratio.

Figure 5.2 shows the in-cylinder pressure and HRRR when SOI is sweeping at 100°C intake temperature and 60% of gasoline substitution ratio without EGR. SOI from 5° CA to 30° CA BTDC, advances combustion. As SOI of diesel is advanced, combustion timing is advanced except at 40°, 50° and 60° CA BTDC of SOI, with the SOI of 0° CA BTDC having its combustion much later starting at around 15° CA ATDC. Amongst these SOI conditions, 10° CA BTDC of SOI of diesel, has the highest PHRR and shortest combustion duration, which is because combustion occurs

around TDC, and moderate homogeneity of diesel mixture created, causes the rapid combustion. The beginning of HRRR at 50° CA BTDC of SOI is slower than others and even more so in the case of 60° CA BTDC, due to more diluted mixture and lower charge temperature. This combustion, appears to be an RCCI-like combustion. Optical analysis is required in order to have more detailed analysis. On the other hand, it is also observed that at 5° CA BTDC of SOI, heat release of late combustion, is more like diesel combustion, and as expected the heat release for the SOI of 0° CA BTDC is as low as the heat release rate for SOI of 50° CA BTDC and starts faster but very late in comparison.

Figure 5.3 shows in-cylinder pressure and HRRR with the same SOI at different intake conditions. SOI for all of these intake conditions is at a late injection timing of 5° CA BTDC. This graph shows that, at higher intake temperature, PHRR is lower, combustion duration is shorter and ignition delay is shorter. Increasing EGR to 25% at the same SOI and intake temperature increases the ignition delay as well as the heat release rate with similar combustion duration. At intake temperature of 100°C without any EGR, the start and duration of the combustion, as well as the heat release rate and peak pressure, are almost the same as that of the intake temperature of 150°C with 25% of EGR with the 100°C intake temperature without EGR being slightly higher. But as the EGR increases to 40% with 150°C intake temperature, it also shows the similar effect to cooler intake as to heat release characteristics, with 40% EGR at 150°C intake temperature having the least heat release rate at a much later time in comparison. At the conditions with EGR and the one with 100°C intake temperature, heat release occurs slightly just before main heat release. This may be LTH (low temperature heat release) of diesel fuel due to the longer ignition delay. Similar observations were made when comparing different intake conditions at the same early SOI timing.

Figure 5.5 demonstrates engine performances, emission and combustion characteristics with the optimized SOI as to thermal efficiency and NO<sub>x</sub> at different intake conditions, while displaying the effect of the injection timing for the same exact condition with a later injection as well. Figure 5.4 shows in-cylinder pressure and HRR for the same conditions as Figure 5.5. The intake conditions are: 50° CA BTDC of SOI at 150°C of intake temperature without EGR, 45° CA BTDC of SOI at 100°C of intake temperature without EGR, 40° CA BTDC of SOI at 150°C of intake

temperature with 25% EGR, and 35° CA BTDC of SOI at 150°C of intake temperature with 40% EGR.

The results illustrate that increased intake temperature leads to a higher thermal efficiency because of higher combustion efficiency, due to lower THC. EGR increases the thermal efficiency because of lower heat loss from lower combustion temperature. This is more apparent in later injection timings. Combustion efficiency or THC is not decreased by EGR due to higher overall equivalent ratio, caused by less fresh air. It can be observed that NO<sub>x</sub> is generally low at early SOI timings, but it can be seen from the later diesel SOI timings that NO<sub>x</sub> is lower at 150°C of intake temperature without EGR because the fuel mixture is more homogeneous with longer ignition delay, by hotter intake condition without the EGR gas.

Increasing intake temperature decreases soot when not using EGR, and combustion duration (CA<sub>10-90</sub>) is longer with higher intake temperature, or with EGR conditions.

The starts of combustion are pretty similar to each other in Figure 5.4, with diesel SOI of 35° CA BTDC with 150°C of intake temperature and 40% EGR having the highest heat release rate, at just before TDC, probably due to less time being available for heat loss between start of injection and the start of combustion at this condition. The slope of HRR in the condition with SOI of 45° CA BTDC and 100°C intake temperature

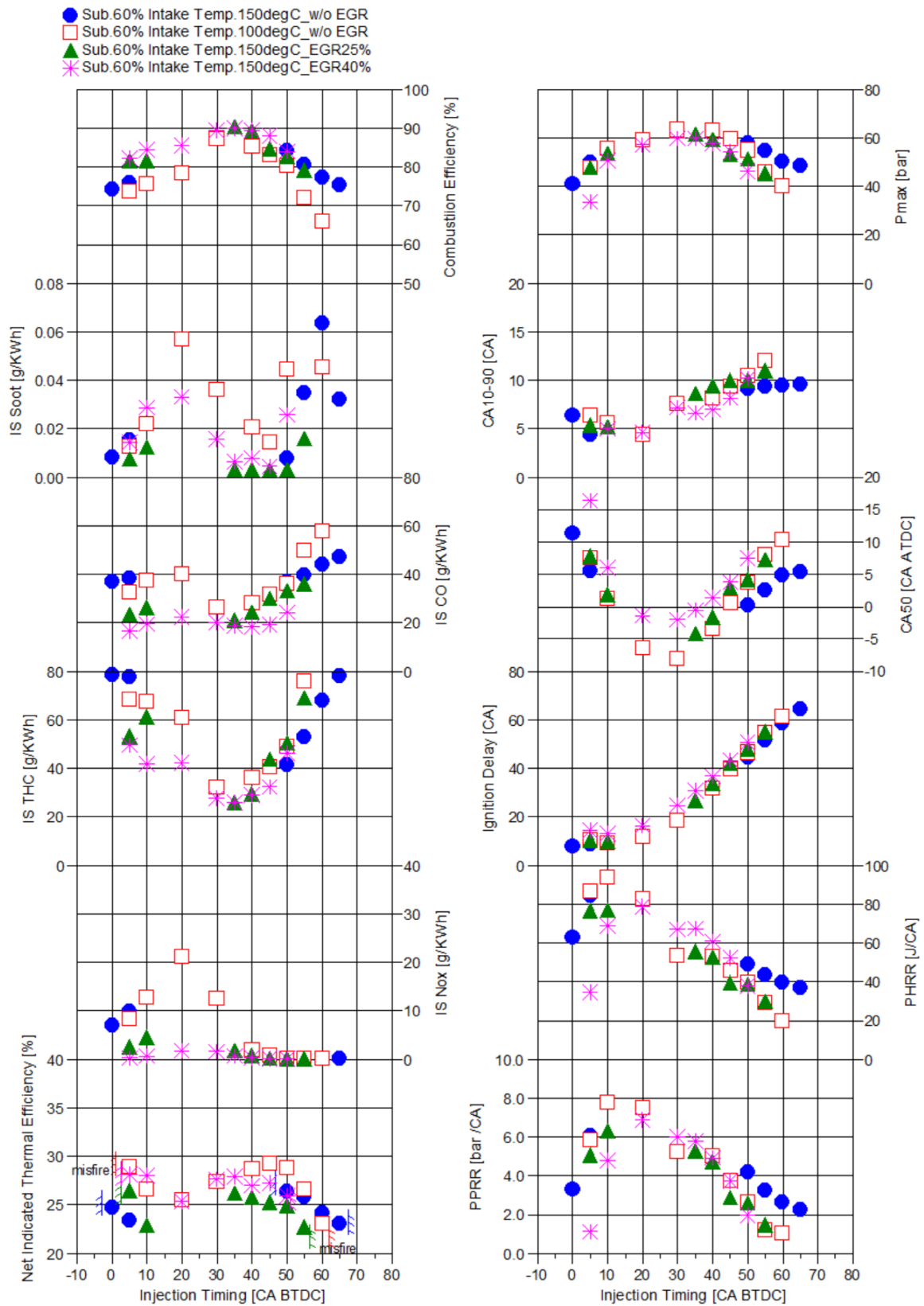


Figure 5.1 Comparison of engine performance, emission and combustion characteristics at different intake conditions when gasoline substitution ratio is 60% and diesel injection is single injection

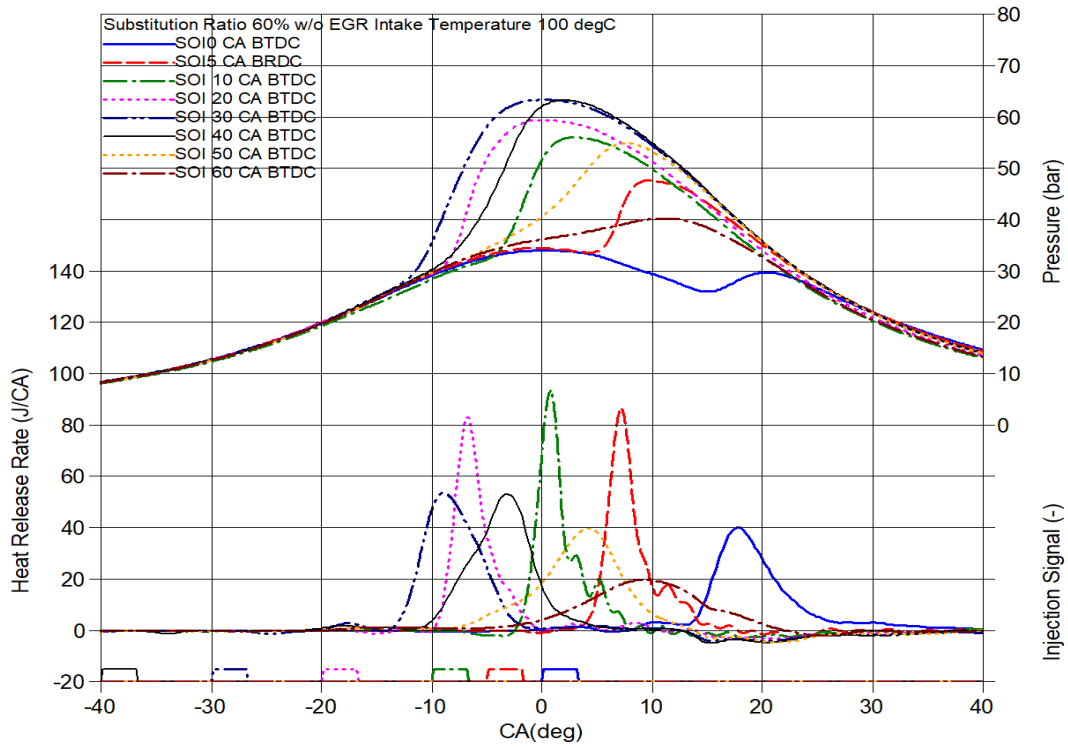


Figure 5.2 In-cylinder pressure and HRRR at different single SOI when intake temperature is 100°C and gasoline substitution ratio is 60%

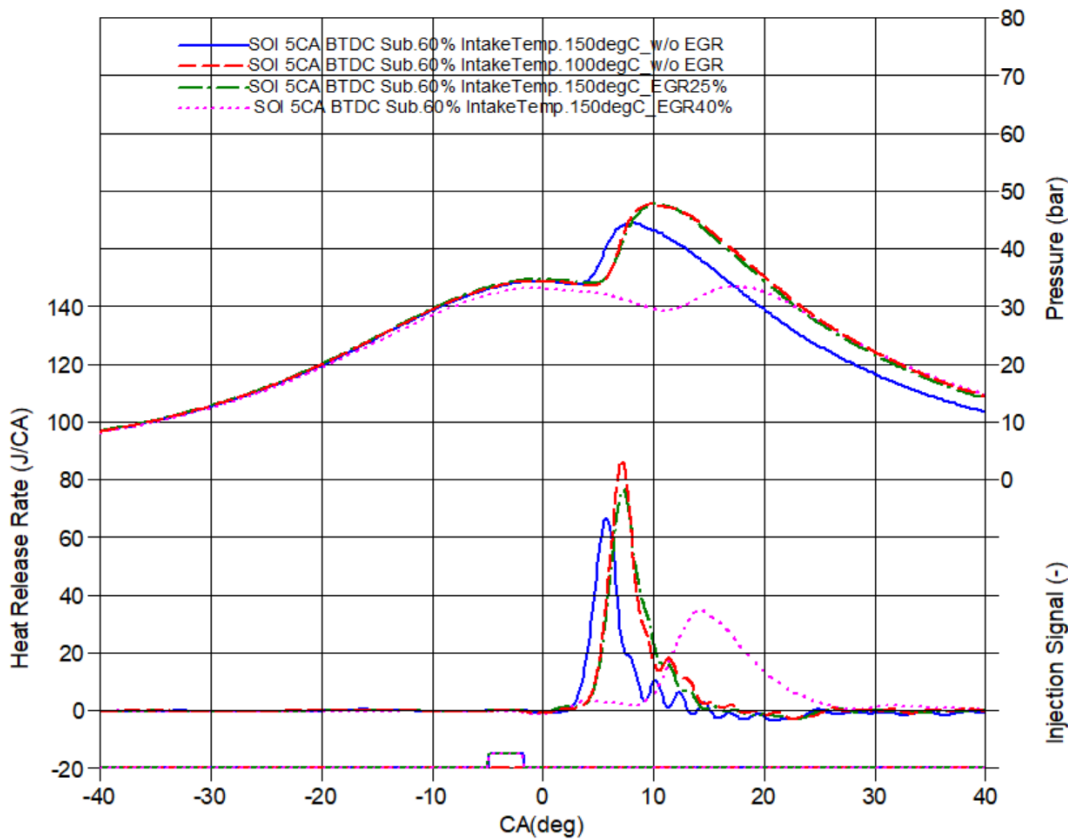
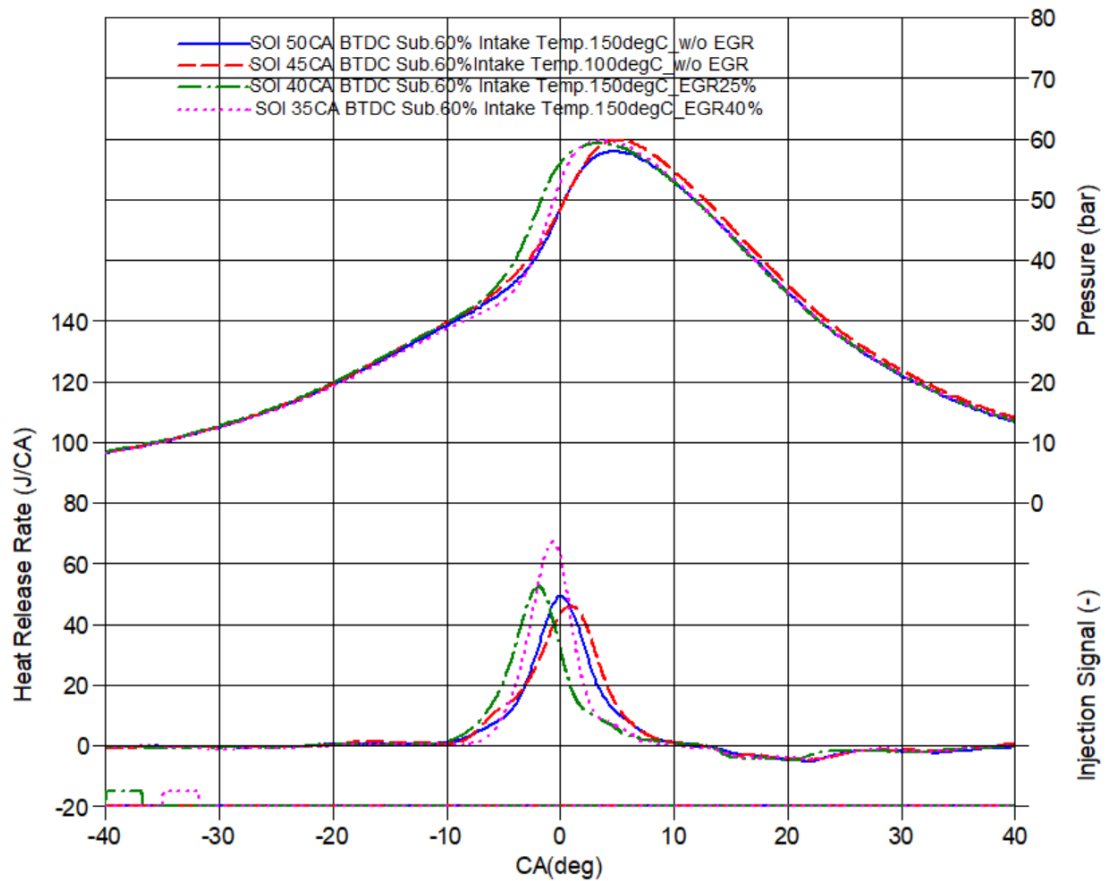


Figure 5.3 In-cylinder pressure and HRRR at different intake conditions when SOI is 5 CA BTDC, gasoline substitution ratio is 60%



*Figure 5.4 in-cylinder pressure and HRRR with the optimized SOI at different intake conditions, gasoline substitution ratio is 60%*

and no EGR, changes around TDC. It is assumed that gasoline combustion is accelerated by diesel combustion at this point.

The results of this section of the study shows that, increasing in-cylinder temperature and using EGR, which has the similar effect as using internal EGR, are effective to simultaneously reduce emissions and increase thermal efficiency.

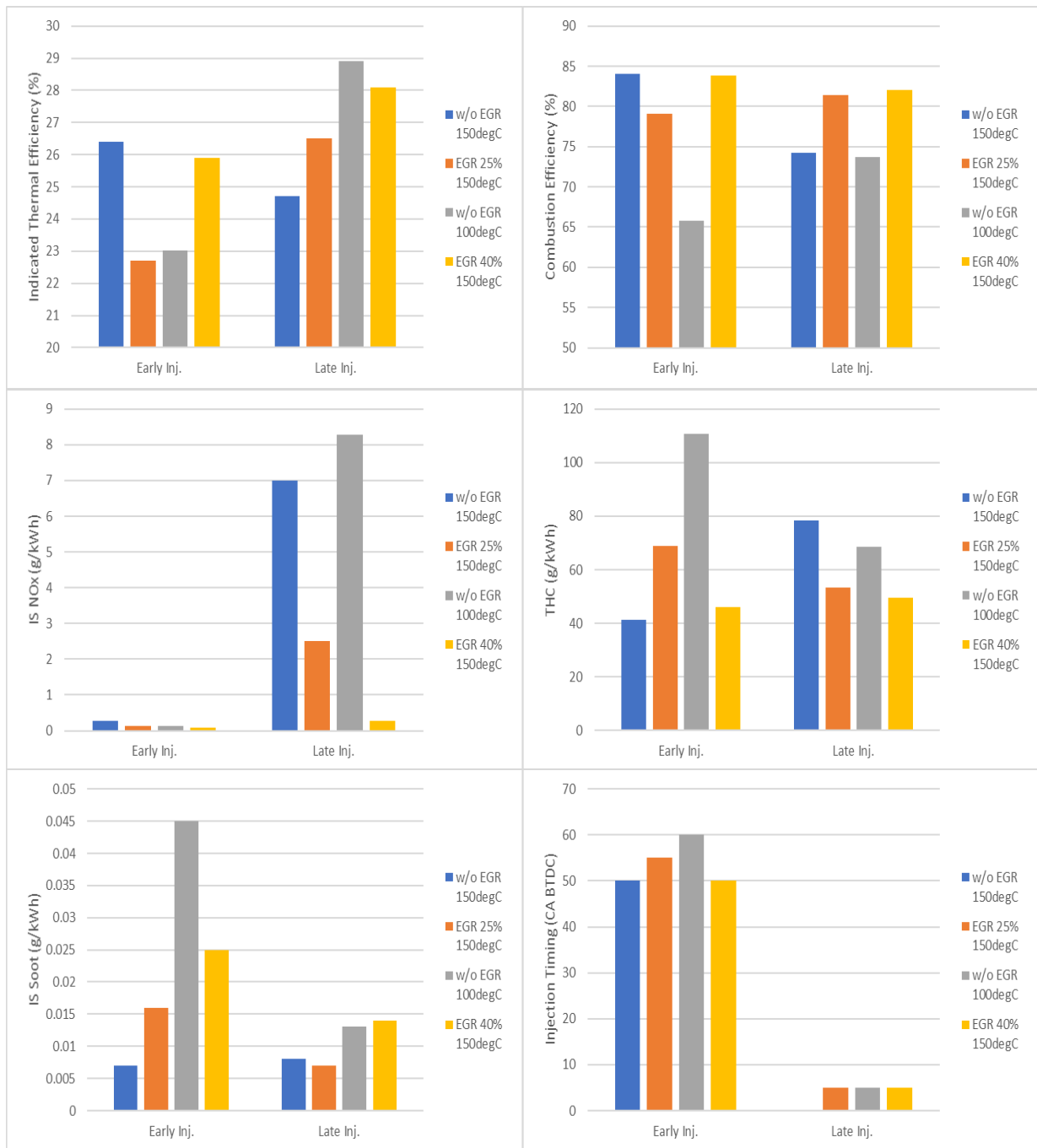


*Figure 5.5 Engine performances and Emission with the optimized SOI at different intake conditions*

#### 5.4.2 Comparison of Single and Split Diesel Injection with 60% Substitution Ratio and Intake Air Temperature of 150°C

Figure 5.6 from top-left to bottom-right, illustrates Combustion Efficiency, Soot, CO, THC, and NO<sub>x</sub> levels, Indicated Thermal Efficiency,  $P_{max}$ , CA10-90 (Combustion Duration), CA50 (combustion centre), Ignition Delay (from Injection Signal to CA5), PHRR (Peak Heat Release Rate), PPRR (Peak Pressure Rise Rate), start of diesel fuel injection signal timing, for split injection operations, second injection timing is applied to the graph.

All of combustion characteristics are quite similar between the single and split injection strategies. The combustion with the split injection strategy is controlled by second injection. Where there is no EGR, split injection prevents knocking from 10° CA to 45° CA BTDC of second SOI, due to more stratified mixture given by split injection. Misfire limit with split injection is slightly narrower than the single injection, due to the smaller amount of second injection, creates leaner diesel mixture.

Figure 5.7 and Figure 5.8 show the in-cylinder pressure and HRRR with the same SOI that are part of the same condition as Figure 5.6, including some of the same SOI with EGR. Figure 5.7 illustrates the 5° CA BTDC of SOI for single injection of diesel and 5° CA and 40° CA BTDC of SOI for split injection of diesel. This figure shows that the split injection strategy has an early, but lower heat release rate with a slow combustion where there is no EGR used compared to single injection at same intake conditions, and when using EGR, comparing single injection strategy with the split injection strategy at the same intake conditions, shows the heat release rate of the split injection to be still earlier than the single injection heat release rate, as well as being slightly higher rate. This is because the retarded 1st injection can assist the combustion start by reducing the ignition delay of the second injection, which results in combustion starting during or just soon after second injection timing.

Figure 5.8 illustrates the in-cylinder pressure and HRRR with the same SOI that are part of the same condition as Figure 5.6 but this time for the SOI of single diesel injection at 50° CA BTDC and 5° CA BTDC, along with split diesel injection at 5° CA and 40° CA BTDC. It is observed that at similar intake conditions, 150°C of intake temperature and no EGR, late single injection of diesel has the highest heat release

rate and shorter ignition delay, with start of combustion at 5° CA ATDC. With a single early diesel SOI timing having the longer ignition delay with combustion starting at around

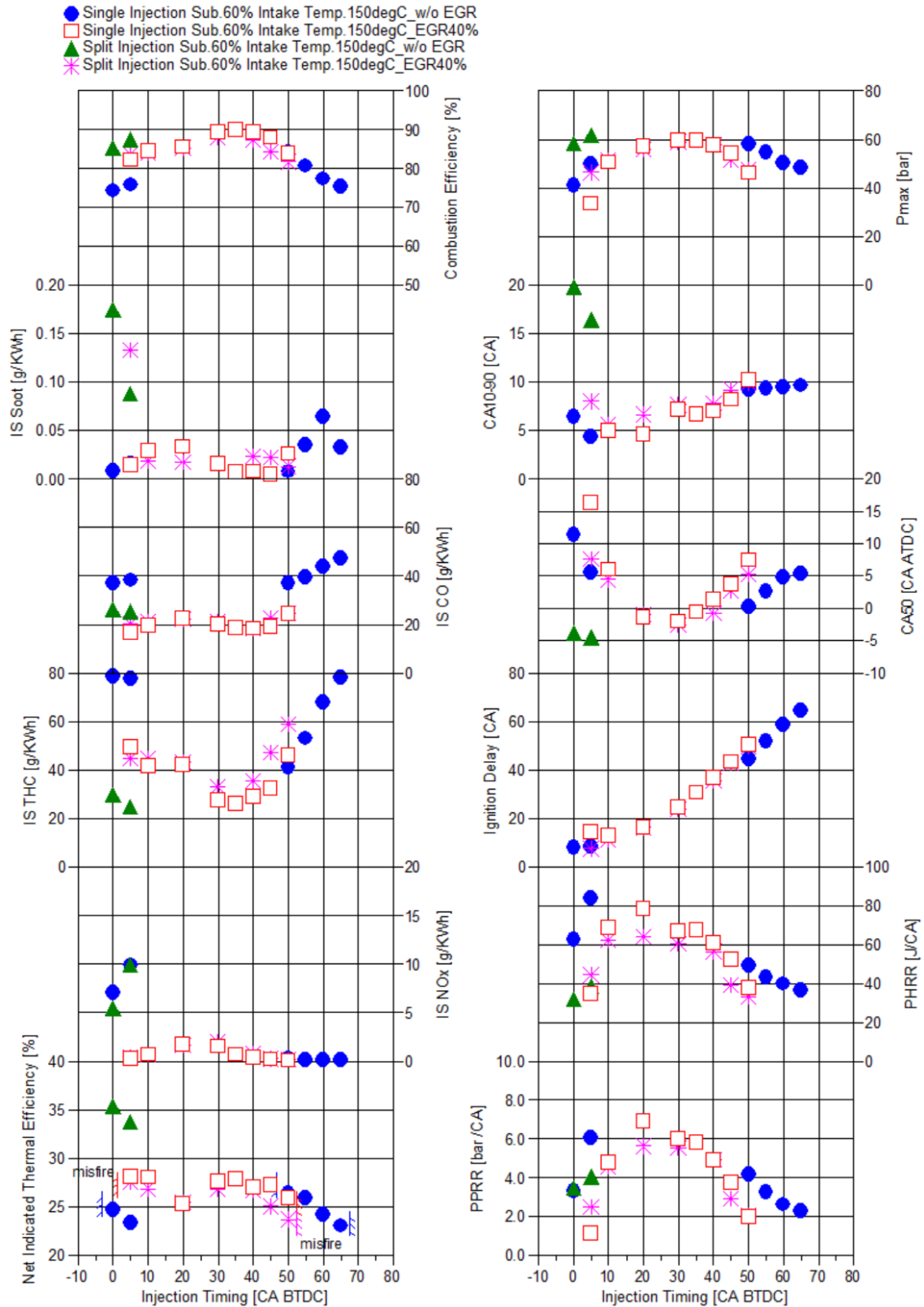


Figure 5.6 comparison of engine performance, emission and combustion characteristics between single and split diesel injection, as well as EGR effect, when substitution ratio is 60%, intake temperature is 150°C.

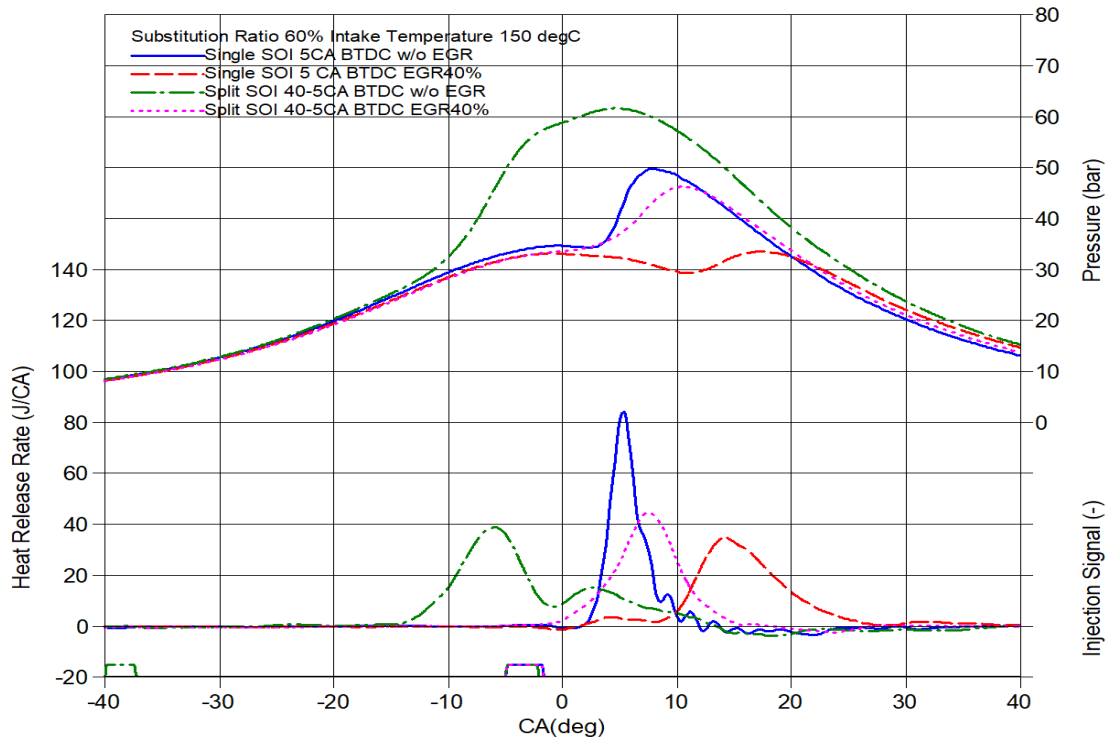


Figure 5.7 in-cylinder pressure and HRRR with single injection and split injection when SOI of the single and the split are 5 and 40-5 CA BTDC respectively, intake temperature is 150°C and gasoline substitution ratio is 60%, at 0 and 40% EGR

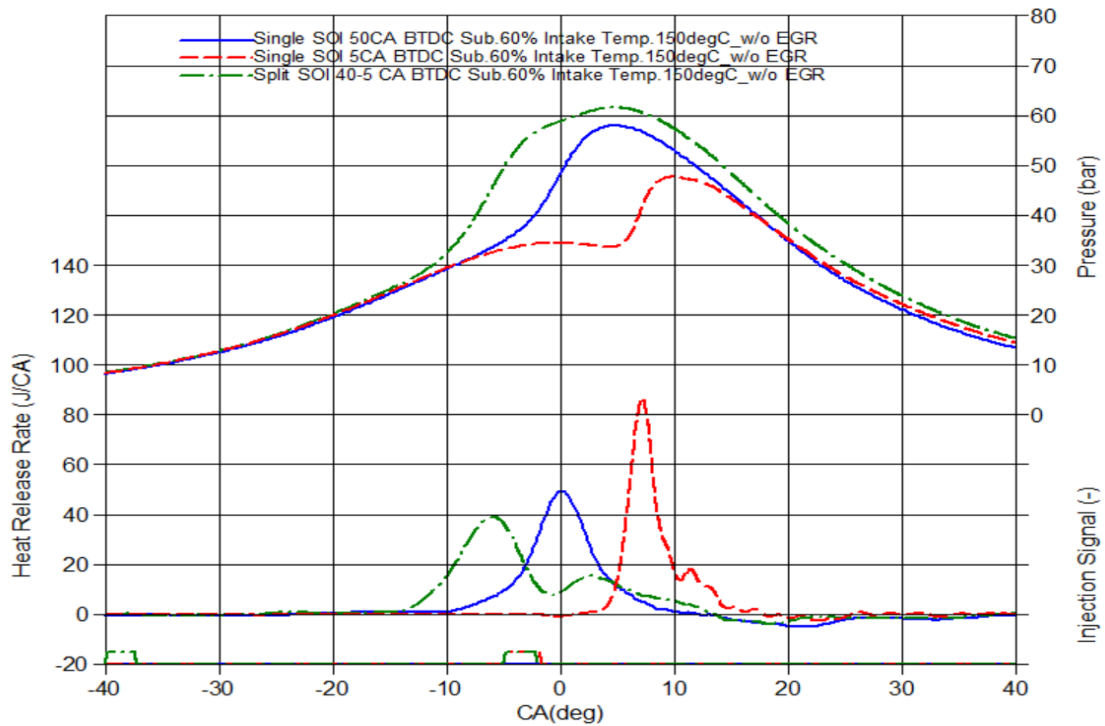
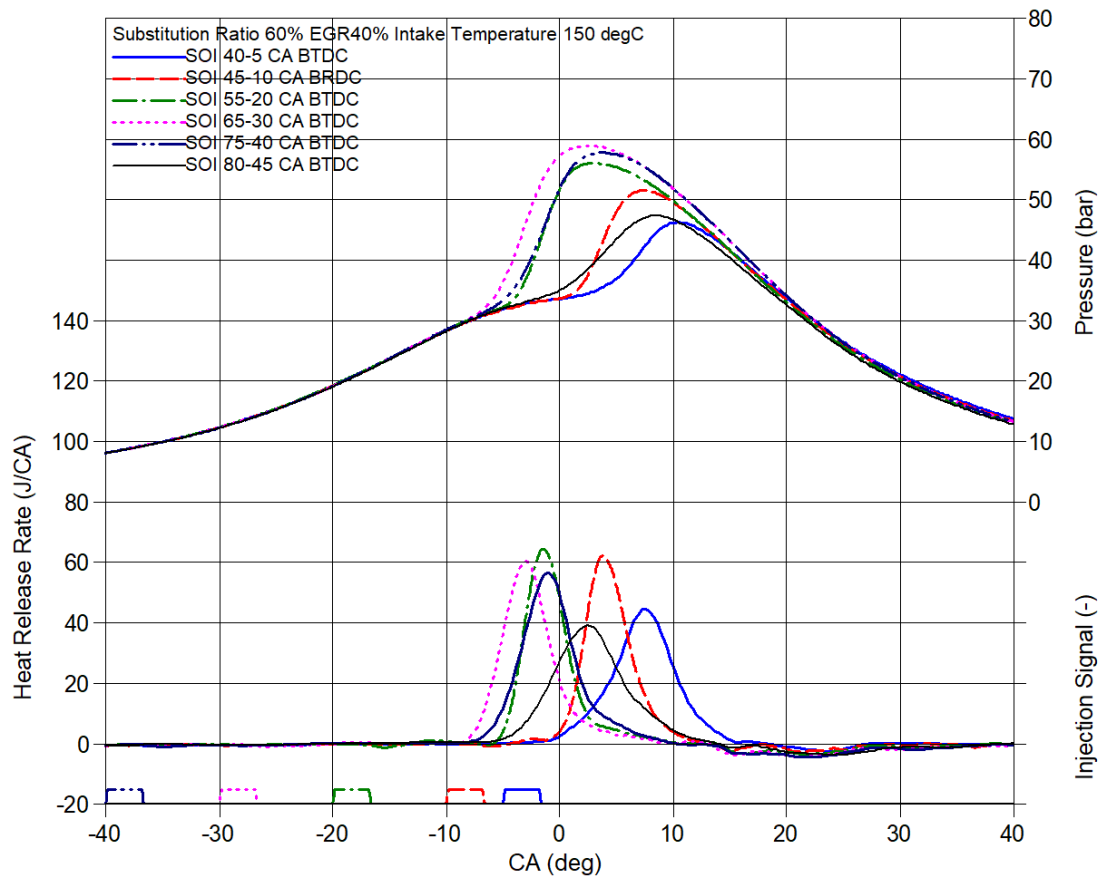


Figure 5.8 in-cylinder pressure and HRRR with single injection and split injection when SOI of single and split are 5 and 40-5 CA BTDC respectively, intake temperature is 150°C and gasoline substitution ratio is 60%



*Figure 5.9 in-cylinder pressure and HRRR at different split SOI when intake temperature is 150°C and gasoline substitution ratio is 60% with 40% EGR*

10° CA BTDC, with the split diesel injection having the later, lower PHRR and slower combustion because of leaner and more premixed fuel mixture given by the earlier first injection and less amount of second injection. Figure 5.9 shows the in-cylinder pressure and HRRR at different split SOI when intake temperature is 150°C and gasoline substitution ratio is 60% with 40% EGR, where with 35° CA dwell between the first and second diesel injection, operation with initial diesel injection at 65° CA BTDC has the shortest ignition delay evident by the early heat release, and also has the highest in cylinder pressure, and the late injection operation with initial diesel injection at 40° CA BTDC has a longer combustion duration with a much lower in-cylinder pressure rise. Therefore, result show that split injection causes more diffusion-like combustion, which might be helpful to enhance thermal efficiency but worsen soot.

### **5.4.3 Effect of Substitution Ratio with Single Diesel Injection, Intake Air Temperature of 150°C, and no EGR**

The effect of gasoline substitution ratio on combustion and emissions are presented in Figure 5.10. From top-left to bottom-right, it illustrates Combustion Efficiency, Soot, CO, THC, and NO<sub>x</sub> levels, Indicated Thermal Efficiency,  $P_{max}$ , CA10-90 (Combustion Duration), CA50 (combustion centre), Ignition Delay (from Injection Signal to CA5), PHRR (Peak Heat Release Rate), PPRR (Peak Pressure Rise Rate), start of diesel fuel injection signal timing.

The bottom-left graph shows the net indicated efficiency variation with SOI of diesel. Looking back at Figure 4.10, diesel baseline operation has higher thermal efficiency than dual fuel operations with gasoline substitution ratio of 60% and 75% because of their higher combustion efficiency.

60% and 75% substitution ratio of gasoline are limited by knock, with 60% substitution ratio having knock between 45° CA BTDC and 10° CA BTDC, and the 75% substitution ratio having knock between 35° CA BTDC and 10° CA BTDC of diesel SOI.

All of dual fuel condition have misfire at early SOI, with 60% substitution ratio having misfire as early as 70° CA BTDC of diesel SOI, and the 75% substitution ratio having misfire as early as 55° CA BTDC of diesel SOI. All condition had also caused misfire for diesel SOI after TDC.

When SOI for diesel is near TDC, NO<sub>x</sub> emissions are similar in all conditions, including diesel only condition (Figure 4.10). The lowest NO<sub>x</sub> is obtained with earlier SOI of diesel with lower gasoline substitution ratio, because of the longer ignition delay for these conditions.

Diesel baseline operation produces the lowest THC and CO and hence the highest combustion efficiency. Dual fuel operation produces higher THC and CO due to gasoline fuel trapped in crevices and over lean zones. Baseline diesel operation produces the highest soot. The smoke level decreases with increasing gasoline substitution ratio. Combustion efficiency of all dual fuel conditions increases up to a certain point as SOI is advanced, beyond which, it decreases at later SOI, with 60% substitution ratio having much higher combustion efficiency than the 75% substitution ratio at the same SOI of diesel injection, for both early and late diesel inject timings.

Diesel condition also has higher PRRR and PHRR than dual fuel condition due to higher reactivity of diesel fuel.

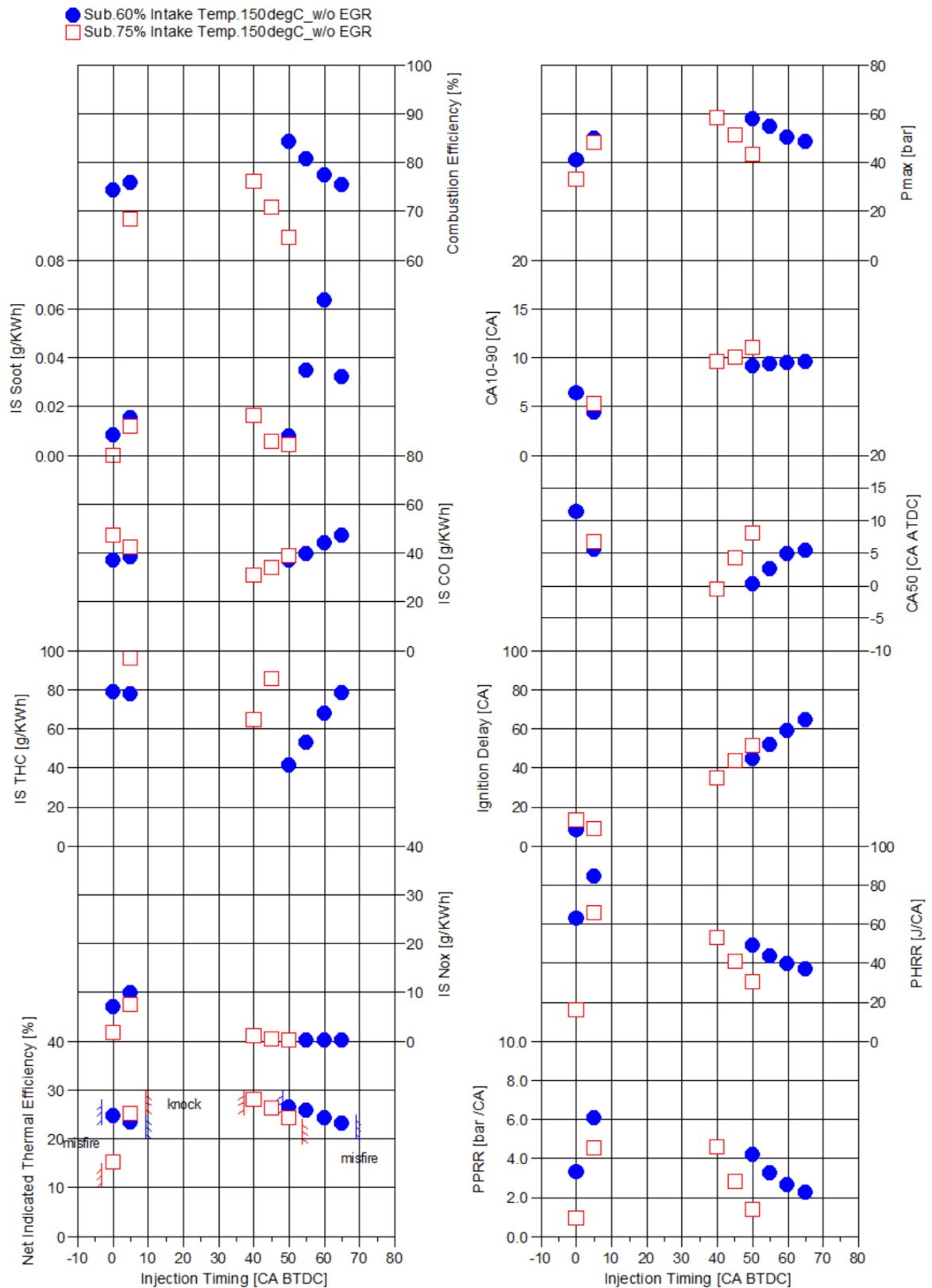


Figure 5.10 comparison of engine performance, emission and combustion characteristics at different gasoline substitutions without EGR, when single diesel injection timing is sweeping and intake temperature is constant 150°C

Figure 5.11 shows the in-cylinder pressure and HRRR with different substitution ratios of gasoline, at the same diesel SOI timing of 5° CA BTDC with 150° intake temperature and no EGR. Heat release process begins at similar times at each condition and to that of diesel only condition illustrated in Figure 4.11, with combustion duration being slightly longer with 75% substitution ratio, as evidenced by its higher pressure during the expansion stroke, while the heat release rate being higher at 60% substitution ratio compared to that of 75% substitution ratio, and the diesel only condition having the highest heat release rate (Figure 4.11). In-cylinder pressure of 60% gasoline substitution ratio has a higher peak pressure, but after that, both substitution ratios have the same pressure.

Figure 5.12 illustrates in-cylinder pressure and HRR with the optimized SOI for emission and efficiency at different gasoline substitution ratios, with 150° intake temperature and no EGR. Figure 5.13 shows engine performance and emission with the same conditions as Figure 5.12, while displaying the effect of the injection timing for the same exact condition with a later injection as well.

It must be noted that the 45% gasoline substitution ratio is ignored for the discussion in this section due to its very low thermal efficiency, and high levels of NO<sub>x</sub> and soot.

When the gasoline substitution ratio is lower, optimized SOI is advanced further, so that richer diesel mixture needs longer ignition delay to have proper combustion timing, and combustion is milder and PHRR is slightly lower due to less local diesel rich mixture area by means of earlier injection timing. In terms of emissions, lower gasoline substitution ratio, decreases NO<sub>x</sub> with more homogeneous diesel mixture, and same can be said for THC. The thermal efficiency at lower substitution ratio is worse, be it very minor, due to too advanced combustion timing. Again, when neglecting the 45% Gasoline substitution ratio, increasing the substitution ratio from 60% to 75%, increases the soot emission, probably due to having a lower combustion temperature in order to oxidise soot. 45% substitution ratio has high level of soot due to overall diesel rich mixture.

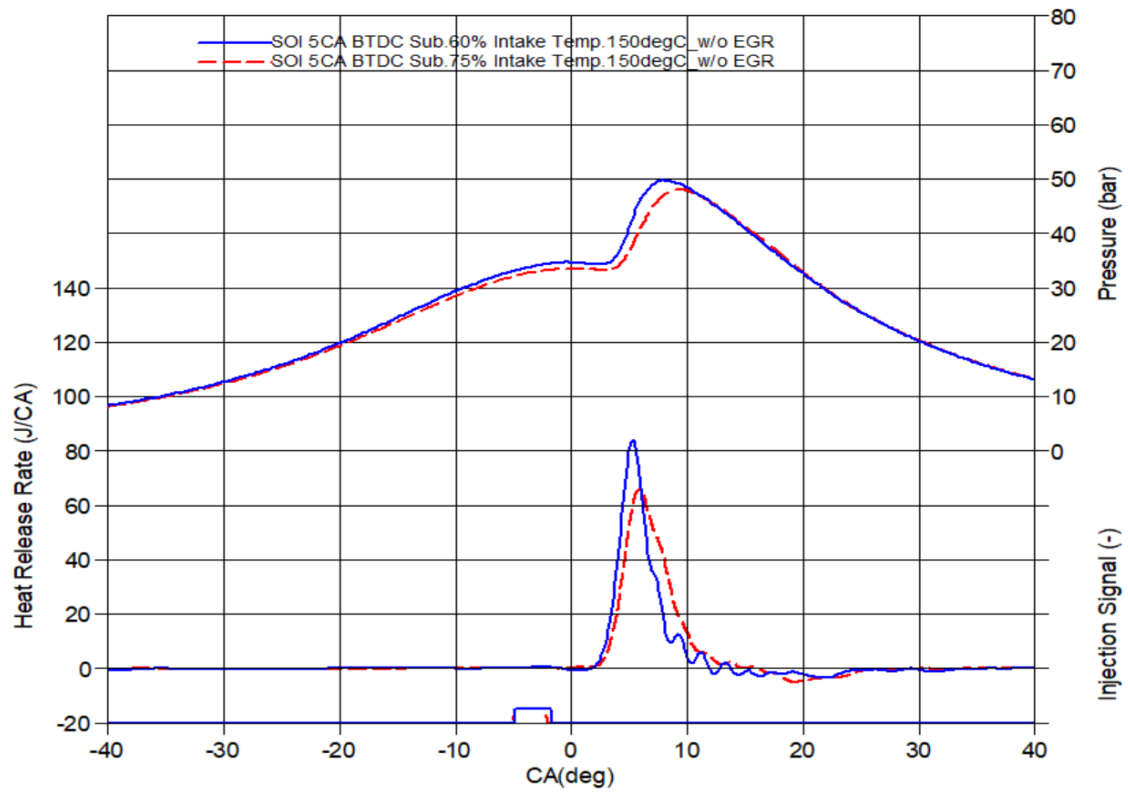


Figure 5.11 in-cylinder pressure and HRR with the late SOI at different gasoline substitution ratio

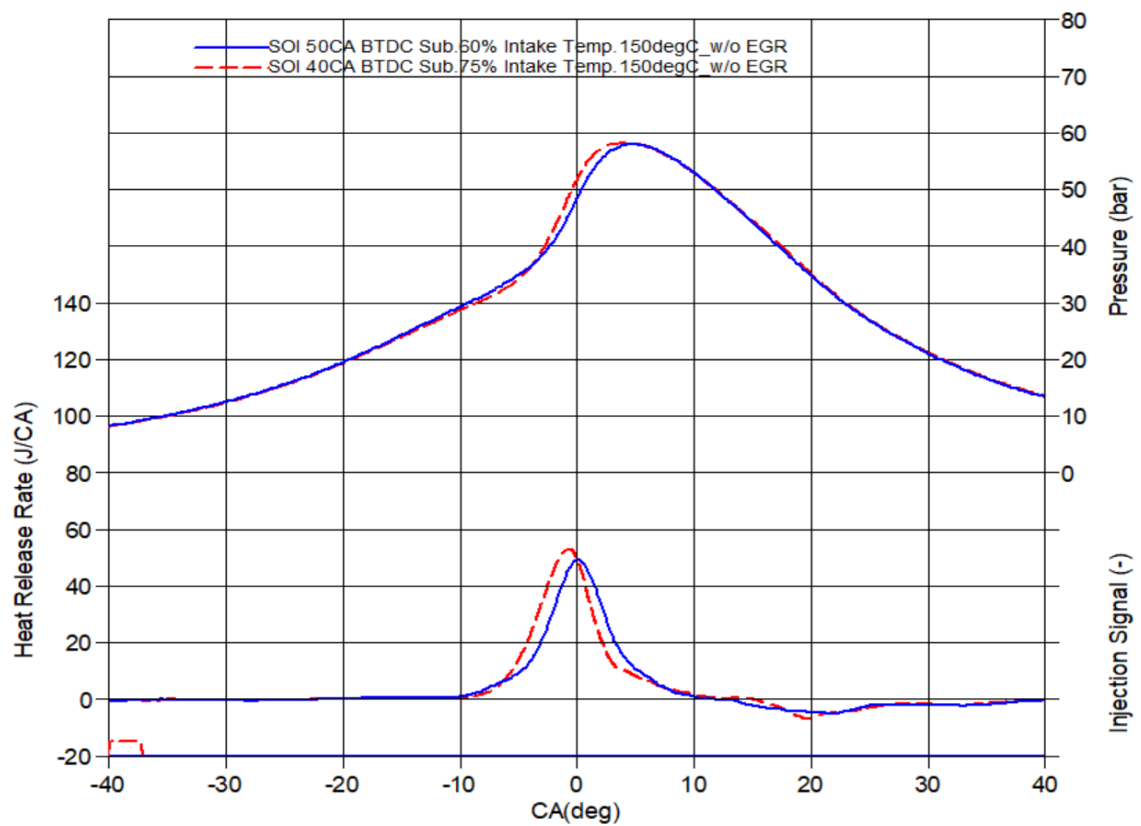
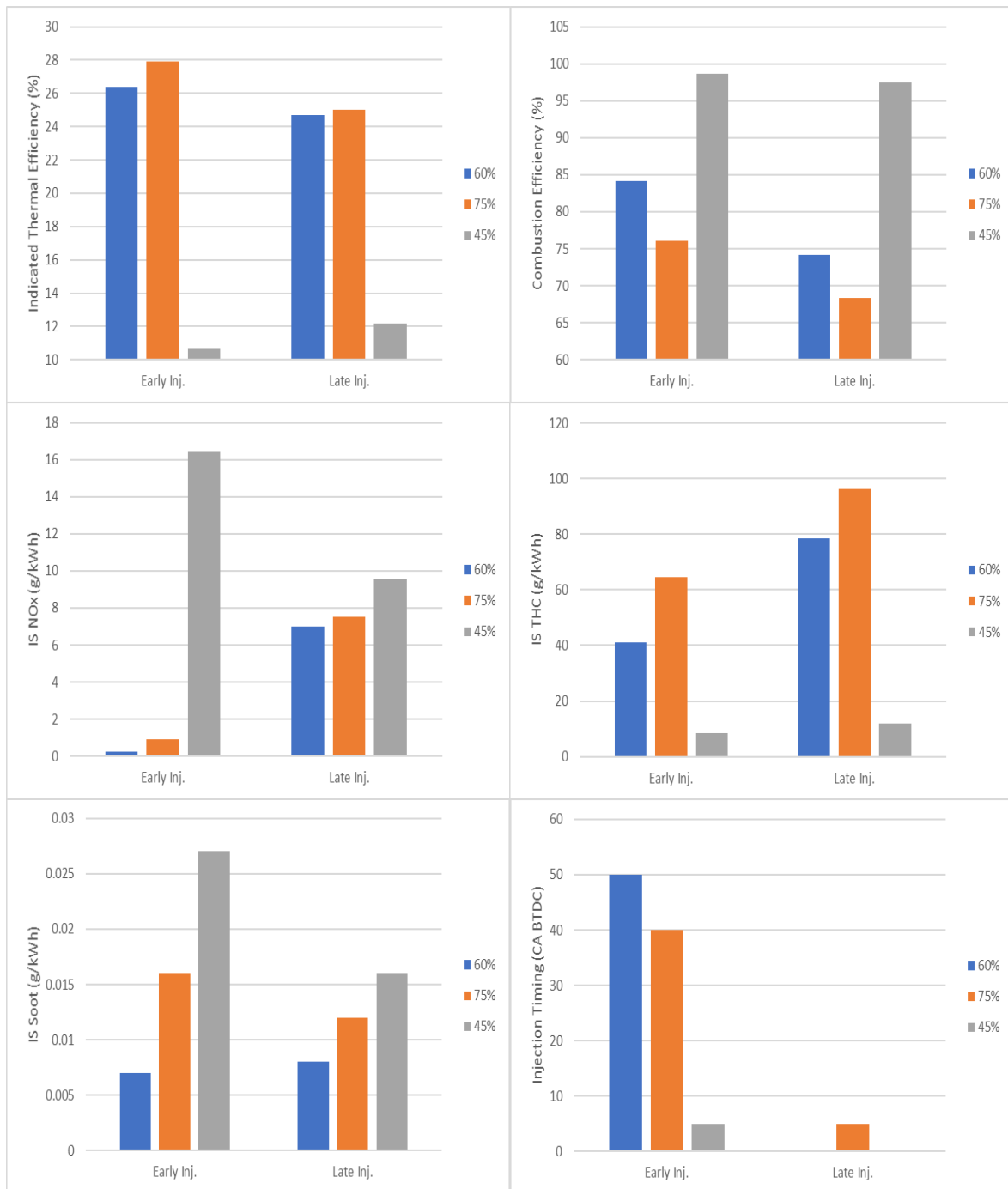


Figure 5.12 in-cylinder pressure and HRR with the early SOI at different gasoline substitution ratio



**Figure 5.13 Engine performances and Emission with the optimized SOI at different gasoline substitution ratio**

## 5.5 Summary

The results obtained from the experiments conducted for this chapter illustrates the effect that different factors, such as intake air temperature, EGR, different injection strategies including single and split diesel injection, as well as various fuel substitution ratios, have on efficiency, performance, and emission output for Diesel-Gasoline dual-fuel engine operations. The diesel gasoline dual-fuel combustion engine operation under certain conditions and parameters tested, has the potential of achieving high efficiency as well as lowered NO<sub>x</sub> and soot emissions. The summary of these conclusion are presented in more detail below.

### A. Single and split injection dual fuel:

- As before, in conventional dual fuel combustion that uses a single late diesel injection, EGR is effective in reducing NO<sub>x</sub> produced, because of the lower oxygen concentration and higher heat capacity, and increased thermal efficiency due to less heat loss an less THC. Lower intake temperature has a good effect on NO<sub>x</sub> and thermal efficiency. That suggests that external cooled EGR can have a benefit for emission and thermal efficiency.
- In premixed dual fuel combustion that includes an early diesel injection and a later diesel injection, EGR is effective to reduce THC, and increase thermal efficiency caused by higher equivalent ratio. Increased intake temperature has the advantage of improving THC, and NO<sub>x</sub> levels, and efficiency as well, because of higher in-cylinder temperature and more homogeneous combustion. That suggests that external hot EGR or using internal EGR can have a benefit for emission and efficiency.

### B. Effect of SOI of diesel during the dual fuel operations:

- Second injection timing of split injection and injection timing of single injection have similar effects on combustion characteristic, such as ignition delay, CA<sub>50</sub>, PHRR etc.. Which means, combustion is primarily controlled by the second injection timing, but they are slightly different due to the effect of heat release or distribution of diesel fuel mixture from the first diesel injection.

- When second injection timing and single injection timing are the same, NO<sub>x</sub>, THC and CO trend of both injection strategies are similar but NO<sub>x</sub> of split injection is slightly lower.
  - Thermal efficiency of split injection is higher when second injection timing and single injection timing are the same. Late second injection timing improves thermal efficiency compared to late single injection, but has worsened soot. This is because late split injection, makes more diffusion-like combustion with shorter ignition delay of second injection since combustion of first injection starts before or during the second injection, and this combustion makes milder heat release rate with lower heat loss and more soot emission.
- C. Comparison of dual fuel single injection operation and baseline diesel combustion:
- Combustion of single diesel injection is more intense than that of dual fuel, with higher PHRR and shorter combustion duration, due to higher chemical reactivity of diesel fuel.
  - THC and CO of dual fuel combustion is higher and hence, lower combustion efficiency. This is because gasoline homogeneous mixture in piston crevice and around cylinder liner, where are gas with low temperature hardly combusts or is quenched by lower temperature zone.
  - Overall, dual fuel combustion has a big advantage in reducing soot emission because of leaner diesel fuel mixture.

# Chapter 6.

## Comparison of Diesel-Ethanol and Diesel-Gasoline Dual Fuel Operations

### 6.1 Introduction

In the last two chapters, the thermodynamic properties and the emissions data from diesel-ethanol dual fuel operation and the diesel-gasoline dual fuel operation were analysed and discussed.

*Table 6.1 Comparison of gasoline and ethanol fuel properties [187]*

<b>Fuel Properties</b>	<b>Gasoline</b>	<b>Ethanol</b>
Molecular weight [kg/kmol]	111	46
Density [kg/l] at 15°C	0.75	0.80-0.82
Oxygen content [wt-%]		34.8
Lower Calorific Value [MJ/kg] at 15°C	41.3	26.4
Lower Calorific Value [MJ/l] at 15°C	31	21.2
Octane number (RON)	97	109
Octane number (MON)	86	92
Cetane number	8	11
Stoichiometric air/fuel ratio [kg air/kg fuel]	14.7	9.0
Boiling temperature [°C]	30-190	78
Reid Vapour Pressure (RVP)* [kPa] at 15°C	75	16.5

\*RVP is a common measure of the volatility of gasoline. It is defined as the absolute vapor pressure exerted by a liquid at 37.8 °C as determined by the test method ASTM-D-323 [188].

Compared to gasoline fuel, ethanol has a higher octane number, wider flammability limits, higher flame speeds and higher heats of vaporisation. But ethanol has a lower energy density and vapour pressure than gasoline. Table 6.1 shows a comparison of the fuel properties of both ethanol and gasoline. The effect of such difference in their properties on the dual fuel combustion and emissions is analysed in the following sections. All the results are carried over from the previous two chapters at 1200rpm and with a constant fuel energy input.

## 6.2 Thermodynamic and Emission Comparison at Various Intake Conditions with 60% Substitution Ratio and Single Diesel Injection

Figure 6.1 from top-left to bottom-right, illustrates Combustion Efficiency, Soot, CO, THC, and NO<sub>x</sub> levels, Indicated Thermal Efficiency, P<sub>max</sub>, CA<sub>10-90</sub> (Combustion Duration), CA<sub>50</sub> (combustion centre), Ignition Delay (from Injection Signal to CA<sub>5</sub>), PHRR (Peak Heat Release Rate), PPRR (Peak Pressure Rise Rate), start of injection signal timing of diesel fuel.

In the bottom left graph, indicated efficiency to diesel SOI (start of injection) is illustrated. It is noted that the diesel-ethanol combustion is more restricted by misfire at early diesel fuel injection, because of the higher octane number of ethanol and slightly lower charge temperature due to its higher enthalpy of evaporation. Where the data are available for both fuel types, it is easy to see that diesel-ethanol operations have slightly better thermal efficiency than diesel-gasoline operation at the same diesel SOI. The best overall thermal efficiency is achieved with diesel-ethanol operation at 5°CA BTDC of diesel SOI with 150°C of intake temperature. In particular, diesel-ethanol dual fuel combustion is characterised with higher combustion efficiency and lower uHC and soot emissions because of the oxygen content in ethanol.

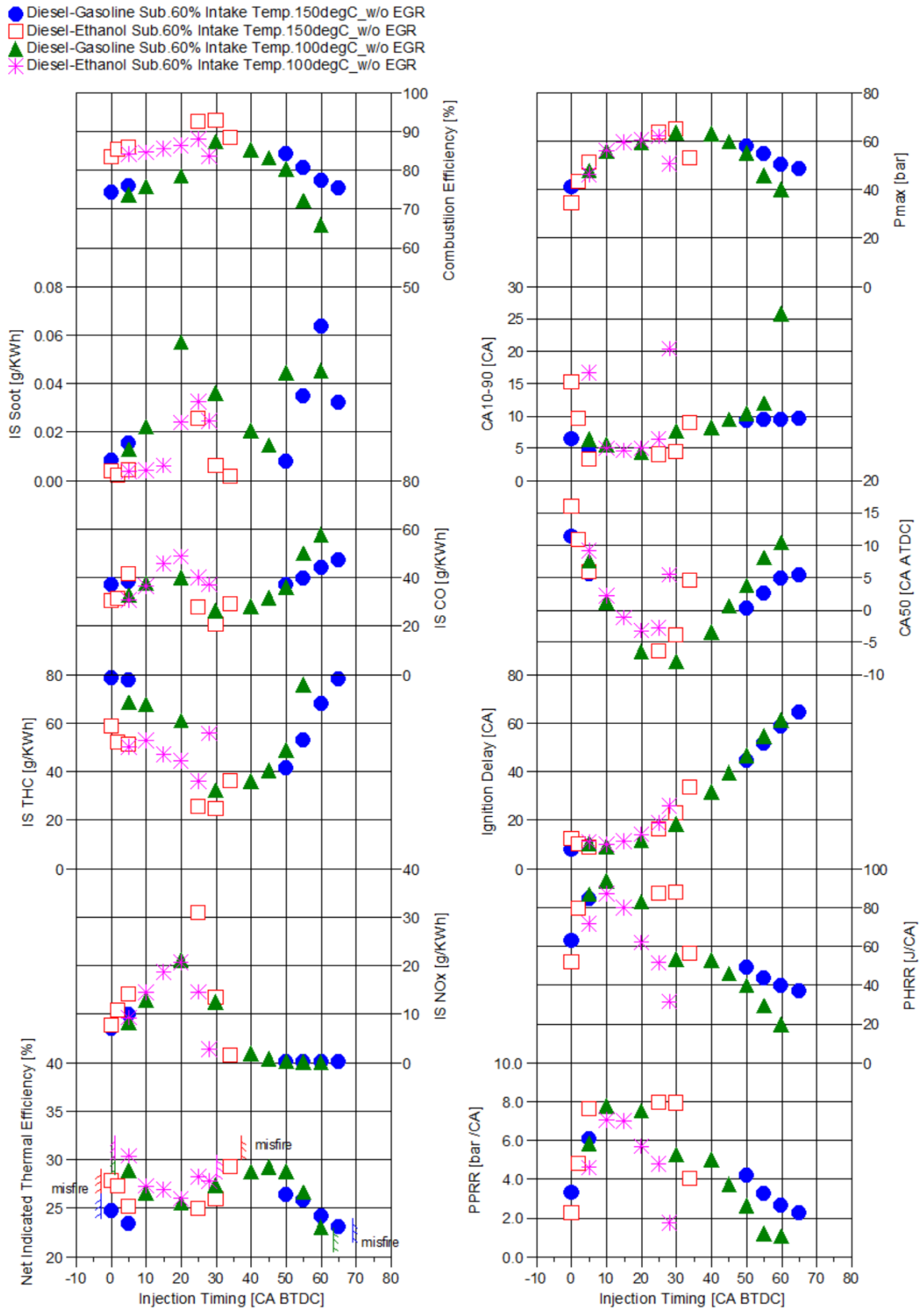
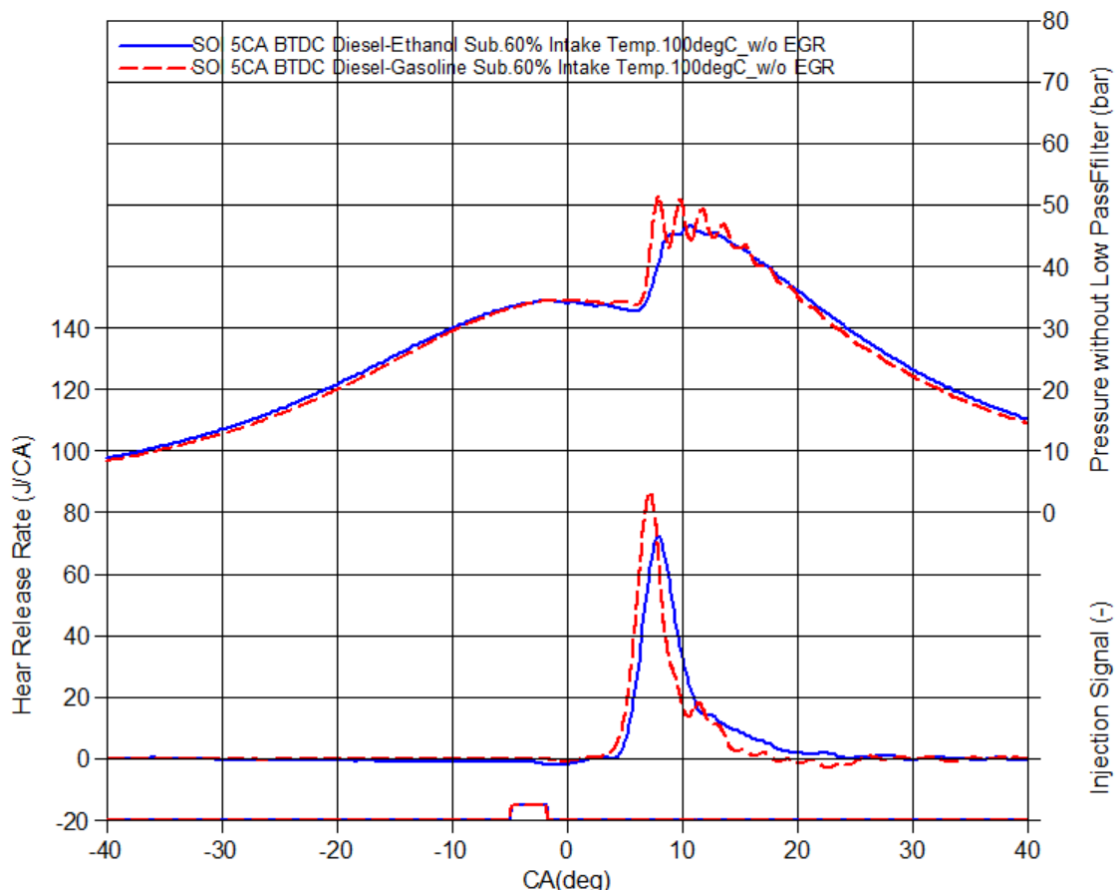


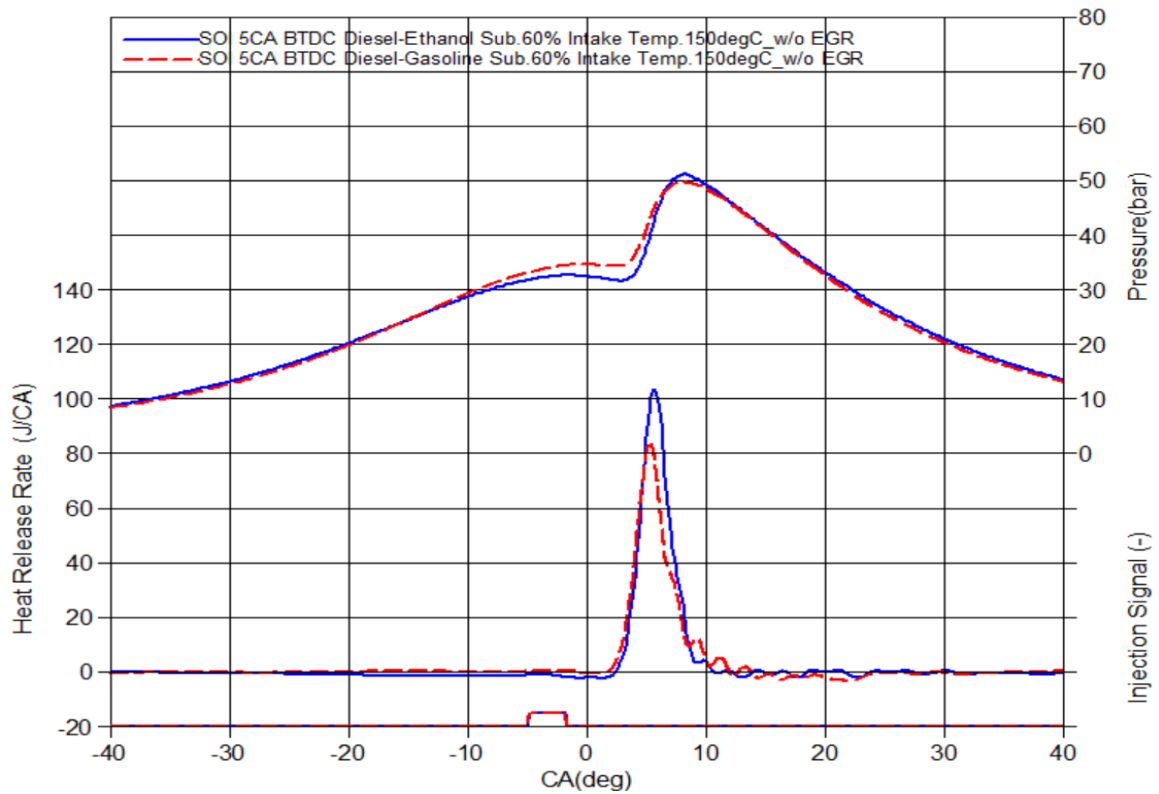
Figure 6.1 Comparison of engine performance, emission and combustion characteristics between diesel-ethanol and diesel-gasoline operations at different intake conditions when substitution ratio is 60% with single diesel injection.

Figure 6.2 and Figure 6.3 compares the in-cylinder pressure and HRRR for both diesel-ethanol and diesel-gasoline operations at 100°C and 150°C intake temperature respectively. In both cases, the start of diesel-gasoline combustion is earlier than that of the diesel-ethanol combustion. However, the effect of fuel properties on the heat release process is different at the two intake temperatures. At the lower intake charge temperature, the diesel-gasoline operation exhibits faster and higher heat release rate than the diesel-ethanol when the ignition delay is relatively long. As the intake temperature is increased, the start of combustion occurs near the TDC and the heat release rate of diesel-ethanol becomes greater than that of diesel-gasoline.

In Figure 6.2, the diesel-gasoline operation with 5°CA BTDC injection timing, is very close to the knocking region as shown in Figure 6.1, and this effect can be seen on the pressure curve of this condition below (Figure 6.2).



*Figure 6.2 In-cylinder pressure and HRRR for both diesel-ethanol and diesel-gasoline operations when diesel SOI is 5°CA BTDC at 100°C intake temperature and 60% of substitution ratio without EGR.*



*Figure 6.3 In-cylinder pressure and HRRR for both diesel-ethanol and diesel-gasoline operations when diesel SOI is 5°CA BTDC at 150°C intake temperature and 60% of substitution ratio without EGR.*

Figure 6.4 illustrates the in-cylinder pressure and HRRR with early diesel SOI, at 34°CA BTDC for the diesel-ethanol operation and at 60°CA BTDC and 50°CA BTDC for the diesel-gasoline operation, at 150°C intake temperature and 60% of substitution ratio without EGR. The diesel-ethanol operation has the shortest ignition delay with the heat release for this operation starting at the same angle as that of the diesel-gasoline operation with diesel SOI of 60°CA BTDC. The diesel-ethanol operation has the highest heat release with the diesel SOI of 50°CA BTDC for the diesel-gasoline operation having the higher heat release and shorter ignition delay of the two diesel-gasoline operations, as well as the highest in-cylinder peak pressure of all three operations discussed here, while the combustion duration for all three is the same. This shows that with optimized early diesel SOI, the diesel-ethanol operation has a higher heat release with a lower in-cylinder peak pressure.

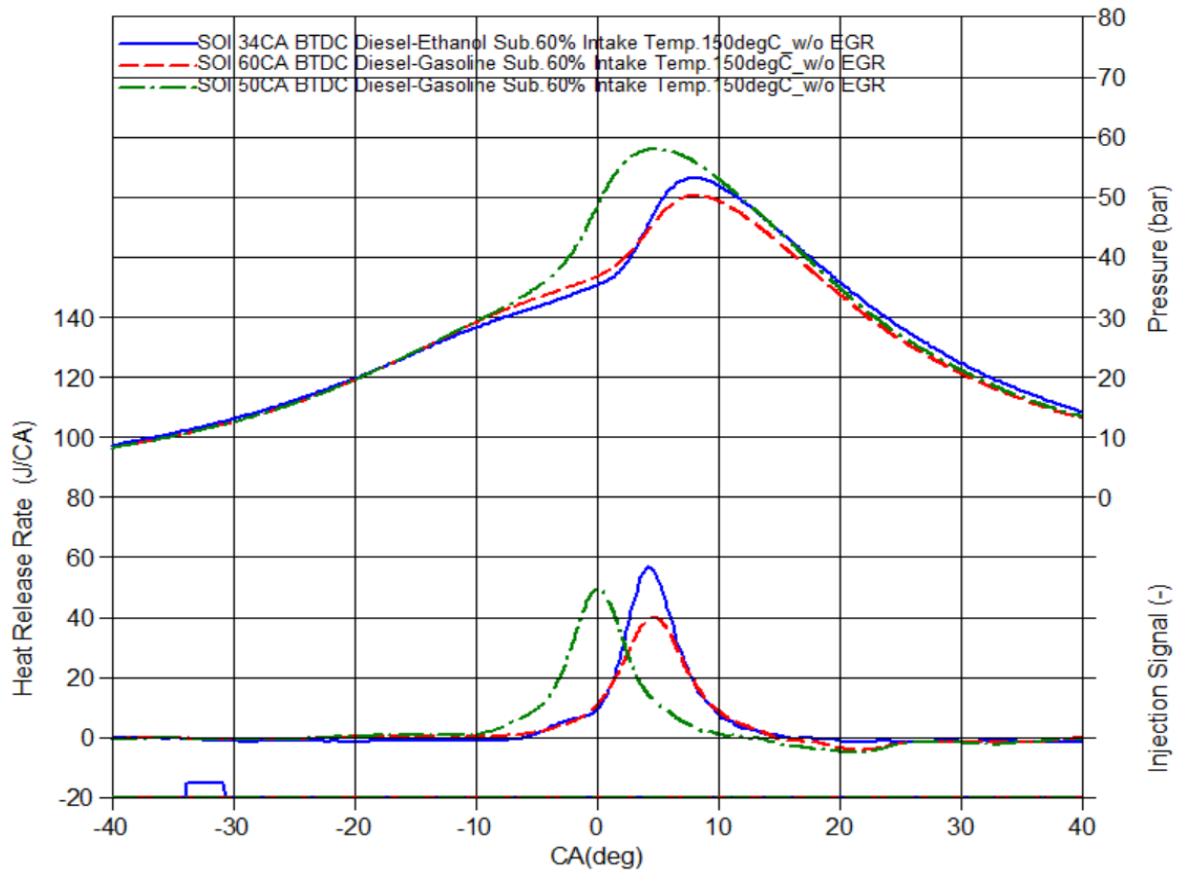
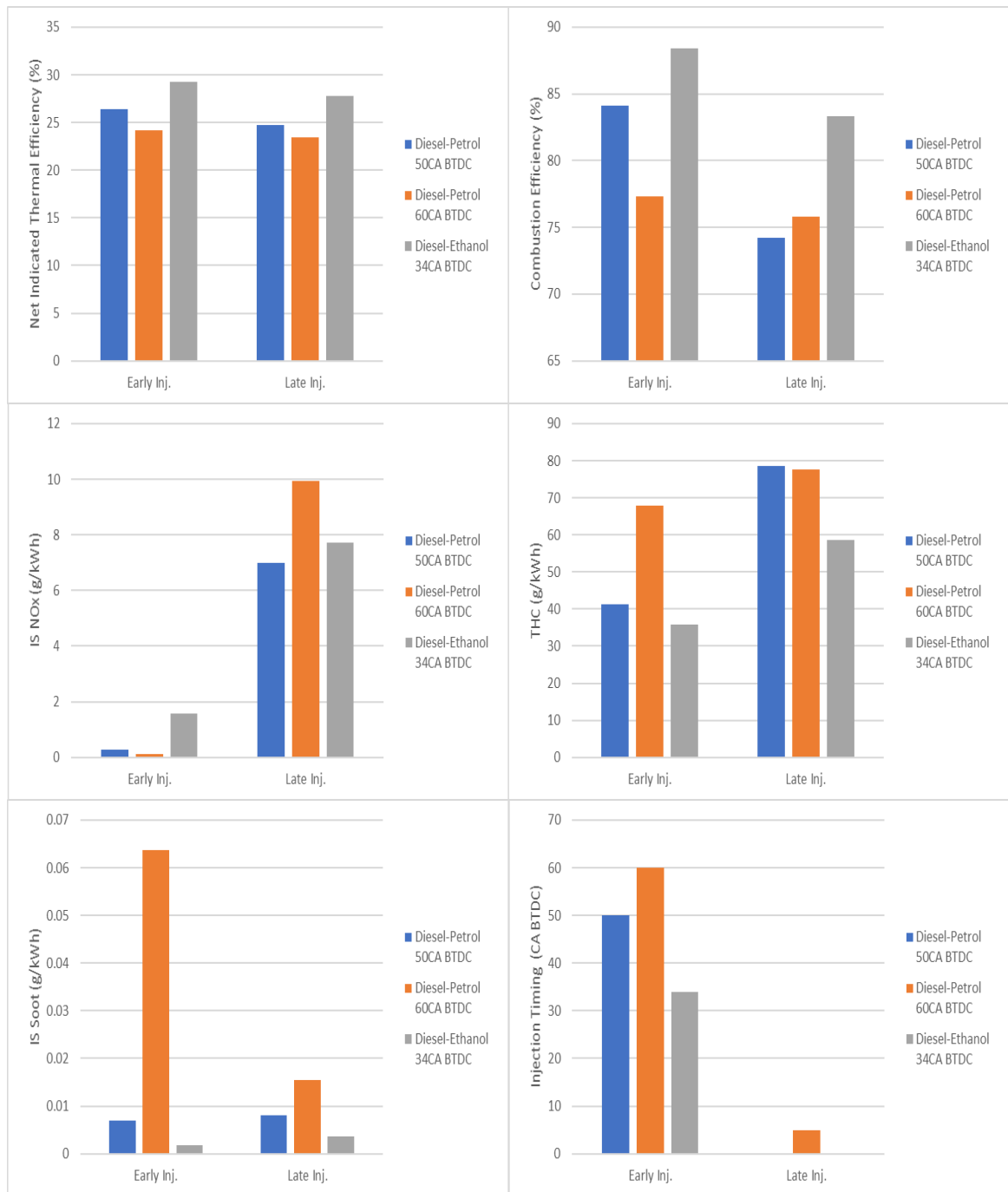


Figure 6.4 In-cylinder pressure and HRRR with early diesel SOI at 150°C intake temperature and 60% of substitution ratio without EGR.



**Figure 6.5 Engine performances and Emission with the optimized SOI at 150°C intake temperature and 60% of substitution ratio without EGR.**

Figure 6.5 demonstrates the engine performances, emission and combustion characteristics with the optimized SOI for diesel-ethanol and diesel-gasoline dual fuel operations at the same conditions as mentioned in Figure 6.4, while displaying the effect of the injection timing for the same exact condition with a later injection as well.

With the highest heat release rate, the results illustrate that the diesel-ethanol operation with optimized diesel SOI and intake conditions, for both early and late diesel injection timings, has the highest net indicated thermal efficiency compared to that of the diesel-gasoline operations. This is also true for the combustion efficiency where the diesel-ethanol operation with early diesel injection timing has the highest combustion efficiency followed by the diesel-gasoline operation with the diesel injection timing of 50°CA BTDC.

However, the diesel-ethanol operation produces the highest amount of NO<sub>x</sub> amongst the three operations under investigation here, but the lowest THC, and very low, close to zero, soot emissions, the higher levels of THC and CO achieved in the diesel-gasoline operations could be due to the fuel, gasoline homogeneous mixture, trapped in piston crevice, cylinder liner, head and other such lower temperature zones hardly combusts or is quenched by these lower temperature zone, and hence the lower combustion efficiency for these operations.

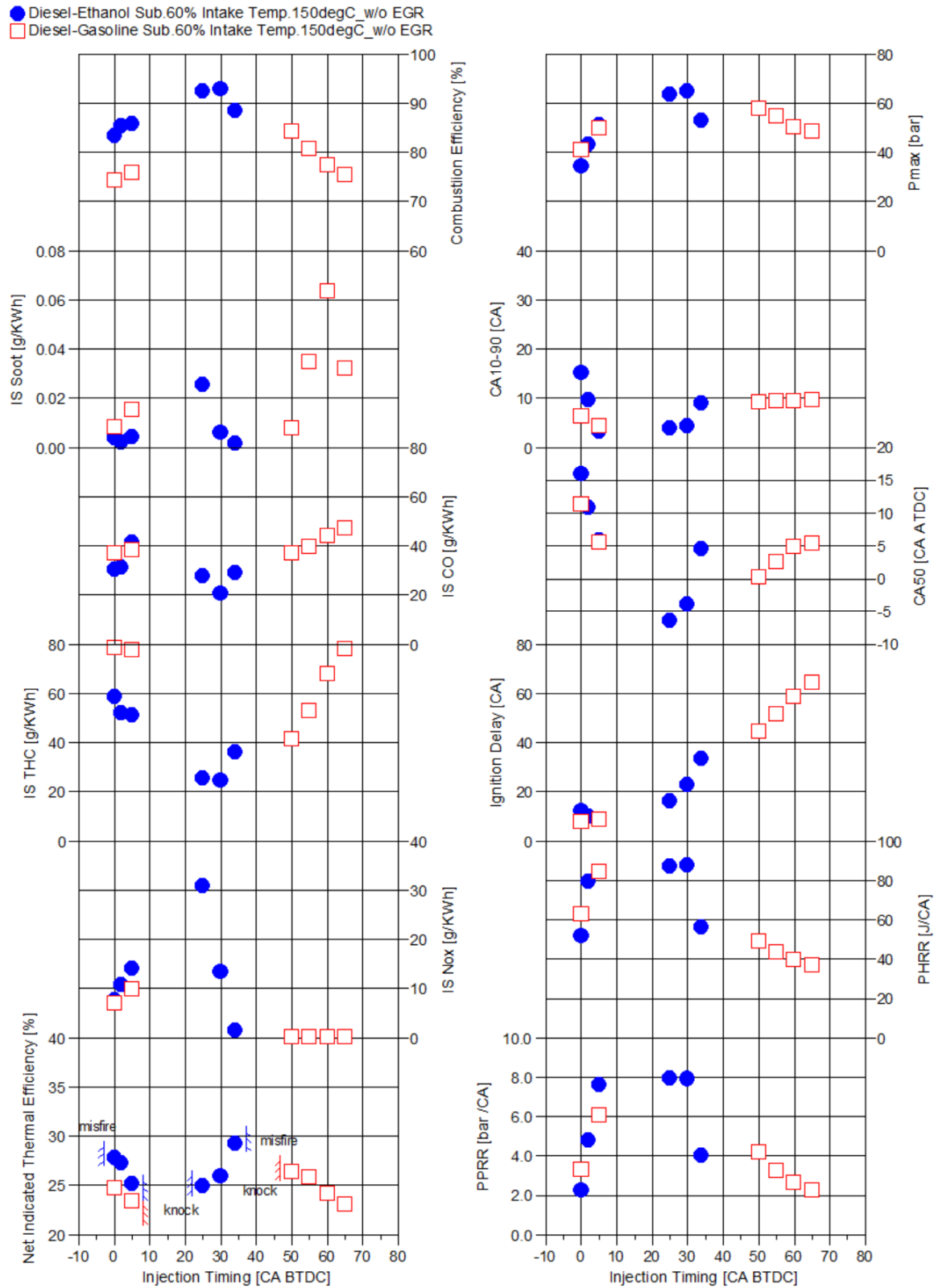
### 6.3 Thermodynamic and Emission Comparison with Varying Injection Timing and Ignition Delay with Constant Intake Conditions

Figure 6.6, from top-left to bottom-right, demonstrates Combustion Efficiency, Soot, CO, THC, and NO<sub>x</sub> levels, Indicated Thermal Efficiency, P<sub>max</sub>, CA<sub>10-90</sub> (Combustion Duration), CA<sub>50</sub> (combustion centre), Ignition Delay (from Injection Signal to CA<sub>5</sub>), PHRR (Peak Heat Release Rate), PPRR (Peak Pressure Rise Rate), with respect to start of injection signal timing of diesel fuel for diesel-ethanol and diesel-gasoline operations when substitution ratio is 60%, intake temperature is 150°C and no EGR.

In the bottom left graph, indicated efficiency to SOI is illustrated. For the diesel-ethanol operation at these intake conditions, 150°C of intake temperature and no EGR, the data cannot be collected between 10° CA to 20° CA BTDC SOI due to the presence of violent combustion and therefore high knocking, and on the other hand, after 5° CA BTDC and before 28° CA BTDC of SOI, misfire occurs. The same can be said for the diesel-gasoline operation, where the data cannot be collected between 10° CA to 45° CA BTDC SOI due to the presence of violent combustion and therefore high knocking. This allows for earlier diesel injection timings for the diesel-gasoline operation, while the diesel-ethanol operation has less chance of knocking when injecting closer to TDC.

Where the data is available for both operations for the same diesel injection timing, the diesel-gasoline operation produces less NO<sub>x</sub> compared to diesel-ethanol operation at the same diesel SOI, with the diesel-gasoline operation with early diesel injection timing, earlier than 50° CA BTDC, showing almost zero NO<sub>x</sub>, and the diesel injection timing of 25° CA BTDC for the diesel-ethanol operation resulting in the maximum NO<sub>x</sub> production among the conditions and timings discussed in this section.

Soot is generally very low across all dual fuel operations, with diesel-ethanol operation having the lowest overall levels of soot production, as well as having lower THC and CO levels compared to the diesel-gasoline operation, and consequently, higher combustion efficiency, with the highest at diesel injection timing of 30° CA BTDC for the diesel-ethanol operation.



**Figure 6.6 Comparison of engine performance, emission and combustion characteristics between diesel-ethanol and diesel-gasoline operations when substitution ratio is 60%, intake temperature is 150°C and no EGR with single diesel injection.**

Where the data for both fuel mixture operations is available for the same diesel injection timing, it can be observed that the diesel-gasoline operation has a slightly higher peak heat release rate as well as higher peak pressure rise rate when diesel SOI is at and very close to TDC, with a slightly shorter ignition delay, which could all be due to the higher reactivity of the gasoline fuel compared to that of the ethanol fuel. This trend is reversed as the diesel injection timing advances and the ignition delay increases, for both fuel mixture operations.

Combustion duration is overall very short for all fuel mixtures and conditions, but at diesel SOI of TDC, diesel-ethanol operation has the longest combustion duration with the diesel-gasoline operation having a shorter combustion duration. Advancing the diesel injection beyond 50° CA BTDC for the diesel-gasoline operation, does not affect the combustion duration.

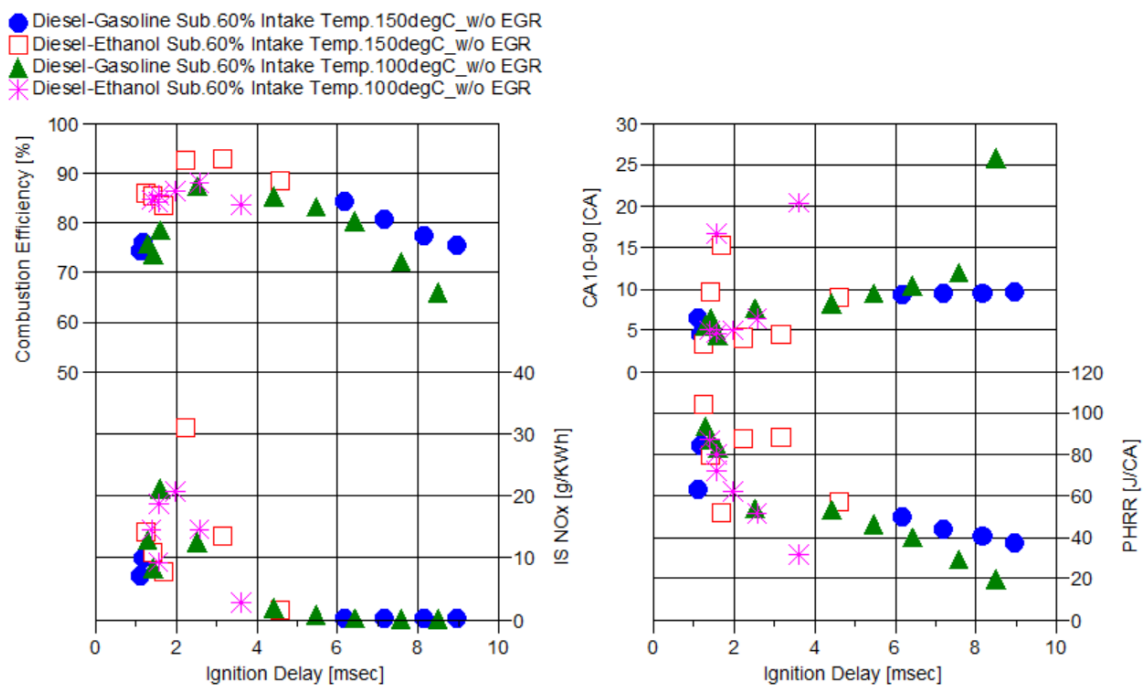


*Figure 6.7 Comparison of engine performance, emission and combustion characteristics between diesel-ethanol and diesel-gasoline operations when substitution ratio is 60%, with different intake temperature, and no EGR, in relation to Ignition delay.*

Figure 6.7 from top-left to bottom-right, illustrates Combustion Efficiency, NOx levels, CA10-90(Combustion Duration), and PHRR (Peak Heat Release Rate, as a function of the Ignition delay of diesel fuel.

The bottom-left graph shows the NO<sub>x</sub> emission level variation in respect to ignition delay. The results show for all conditions, specifically diesel-gasoline operations, that where the ignition delay is longer than 5 milliseconds, there is almost no NO<sub>x</sub> emission, with a small increase between 5ms to 3ms ignition delay. This is due to the fuel mixture becoming more homogeneous with longer ignition delay, especially with the hotter intake condition. As the ignition delay becomes shorter, the NO<sub>x</sub> levels increase, with the diesel-ethanol operation with 150°C intake temperature having the maximum level of NO<sub>x</sub> emission among all of these operation conditions. where the two dual fuel operations with similar intake conditions have the same ignition delay, it is observed that the diesel-ethanol operation usually has a slightly higher level of NO<sub>x</sub> emission. Comparing the lowest NO<sub>x</sub> of each intake condition, NO<sub>x</sub> at higher intake temperature is lower and without EGR, NO<sub>x</sub> is lower, because more premixed and leaner mixture of diesel fuel, due to earlier SOI and long ignition delay, decreases NO<sub>x</sub> levels.

While higher intake temperature improves the combustion efficiency, as the ignition delay increases, so does the combustion efficiency, until a certain point, beyond which, the combustion efficiency begins to decrease. But with the same ignition delay and intake conditions, the diesel-ethanol operations offer higher combustion efficiency.

For diesel-gasoline operations, as the ignition delay increases, so does the combustion duration (CA<sub>10-90</sub>), which is again due to the well mixed and homogeneous fuel mixture. With diesel-ethanol operations however, the relation between ignition delay and combustion duration is a less predictable trend. Although the combustion duration does tend to increase with increasing ignition delay, for both intake conditions, there is a maximum peak in combustion duration at around 1.5ms ignition delay, which drops at 2ms ignition delay, only to increase again as the ignition delay increases beyond 2ms. Both dual fuel operations experience their longest combustion duration with the intake temperature of 100°C, with the longest ignition delay for the said operation. For both dual fuel operations, the operation with lower intake temperature has the longer combustion duration.

The heat release rate in relation to ignition delay, follows the same trend as the combustion duration but in reverse, that is, as the ignition delay increases, the heat release rate decreases, with diesel-ethanol operation with 150°C intake temperature

having the highest heat release rate with 1.5ms of ignition delay. This could be due to the higher volatility of the diesel-gasoline fuel mixture and the better mixing of the fuel with air. For both dual fuel operations, the operation with higher intake temperature has the greater heat release rate.

## 6.4 Summary

In this chapter, the results from the two previous chapters were put together in order to enable the comparison of dual-fuel diesel engine efficiency, performance, and exhaust emissions, under two different dual-fuel operation modes, namely Diesel-Ethanol and Diesel-Gasoline, and the effect of different operation parameters like intake air temperature and EGR, as well as different fuel substitution ratio on each fuel mixture operation. Depending on the testing conditions, such as injection strategy and intake conditions, both dual-fuel operations were able to deliver high efficiency and improved emissions compared to that of a pure diesel engine operation, with the diesel-gasoline operation offering more consistency in improved thermal efficiency, and the diesel-ethanol operation delivering lower emission output. The main conclusions from these comparisons are summarized in detail below.

Efficiency:

- When comparing the two dual fuel operations, diesel-ethanol operation and diesel-gasoline operation, with the same substitution ratio to diesel, 60% for this study, the thermal efficiency of the engine operation is higher for operations with lower intake temperature, 100°C being the lower intake temperature for this study, which is possibly due to the lower heat loss for this conditions. of the two dual fuel operations, the diesel-ethanol operation produces the higher thermal efficiency output, with late diesel injection timings close to TDC. Relatively the same results can be achieved from the diesel-gasoline operation under the same conditions, with early diesel injection timings, creating a more HCCI (Homogeneous Charge Compression Ignition) like combustion, also known as RCCI (Reactivity Controlled Compression Ignition) combustion for dual fuel operations.
- At lower intake temperatures, the diesel-gasoline operation allows for a wider range of diesel injection timing, without incurring any misfire or knocking, compared to the operation range of diesel-ethanol dual fuel operation, which has a smaller diesel injection timing range, thus not allowing for the diesel injection to be advanced much.

- At the same substitution ratio, increasing the intake temperature to higher levels, 150°C being the higher intake temperature for this study, slightly increases the diesel injection timing range before incurring any misfire, allowing for more advanced diesel injection timing, which produces roughly the same thermal efficiency as the lower intake temperature with late diesel injection timing.
- Increasing the intake temperature reduces the diesel injection timing range for the diesel-gasoline operation by increasing the chance of incurring knock, all without improving the thermal efficiency compared to the diesel-ethanol operation with the same intake conditions, nor the diesel-gasoline operation with lower intake temperature.
- However, the same cannot be said about combustion efficiency, as increasing the intake temperature leads to a higher combustion efficiency, with diesel-ethanol operation at 150°C of intake temperature with single diesel injection timing having the best combustion efficiency at diesel injection timing of 30° CA BTDC.

#### Emissions:

- When comparing the two dual fuel operations, diesel-ethanol operation and diesel-gasoline operation, with the same substitution ratio to diesel, 60% for this study, regardless of intake conditions, the operations with diesel injection timings earlier than 35° CA BTDC produce very little, close to zero, levels of NO<sub>x</sub> emissions. This is mainly due to the longer ignition delay with early diesel SOI, creating a more premixed and leaner, more homogeneous mixture of diesel fuel.
- Knowing that higher intake temperature increases NO<sub>x</sub> at the same diesel SOI timing, the highest level of NO<sub>x</sub> emissions is observed in the diesel-ethanol operation with 150°C of intake temperature and diesel injection timing of 25° CA BTDC. This is also true for the diesel-gasoline operation with diesel injection timing of 5° CA BTDC, where the operation with 150°C of intake temperature has a slightly higher level of NO<sub>x</sub> emission compared to that of the operation with 100°C of intake temperature.

- Where the NOx emission level is available for all, or most, operation conditions at the same diesel injection timing, lower intake temperature results in lower NOx with the diesel-ethanol operation having the lowest level with early diesel injection timing, and diesel-gasoline operation having the lowest NOx emission level for late diesel injection timing, suggesting that early diesel injection at lower intake temperature with diesel-ethanol operation, allows for a leaner diesel fuel mixture, resulting in a more RCCI like combustion with lower NOx emission levels.
- When diesel SOI is near TDC, NOx emissions are similar in all conditions, including diesel condition. This is due to the combustion of the diesel fuel mixture being dominant source of NOx formation, as there is not enough time, short ,ignition delay, to create a well-mixed fuel.
- Soot emission is very low in all conditions of the diesel-ethanol dual fuel operation. It is assumed that soot levels peak at around 25° CA BTDC diesel injection timing with 100°C of intake temperature, is caused by the diesel fuel not being injected into the combustion bowl properly.
- Increasing intake temperature decreases soot when not using EGR. This is true for most conditions, and specially at early diesel injection timings, and where the soot levels is available for all conditions at the same diesel SOI, the diesel-ethanol operation with higher intake temperature has the lowest level of soot emission level.

# Chapter 7.

## **In-cylinder Optical Measurements and Analysis of Dual Fuel Combustion**

### 7.1 Introduction

Based on the thermodynamics testing and emission measurements, further studies were carried out on in-cylinder mixture formation and combustion process by means of optical measurements.

First the data collected from the optical testing of the diesel-ethanol dual fuel operation and the diesel-gasoline dual fuel operation will be presented and analysed respectively. A comparison will then be made between the two dual-fuel operations as well as to the images collected from the diesel only operation.

### 7.2 Optical Measurement Setup

The engine has the optical access through the window in the piston crown via a 45° mirror mounted below, whose optical layout for optical test is illustrated in Figure 7.1. Table 7.1 gives the details of the camera, intensifier, lens and high repetition copper vapour laser.

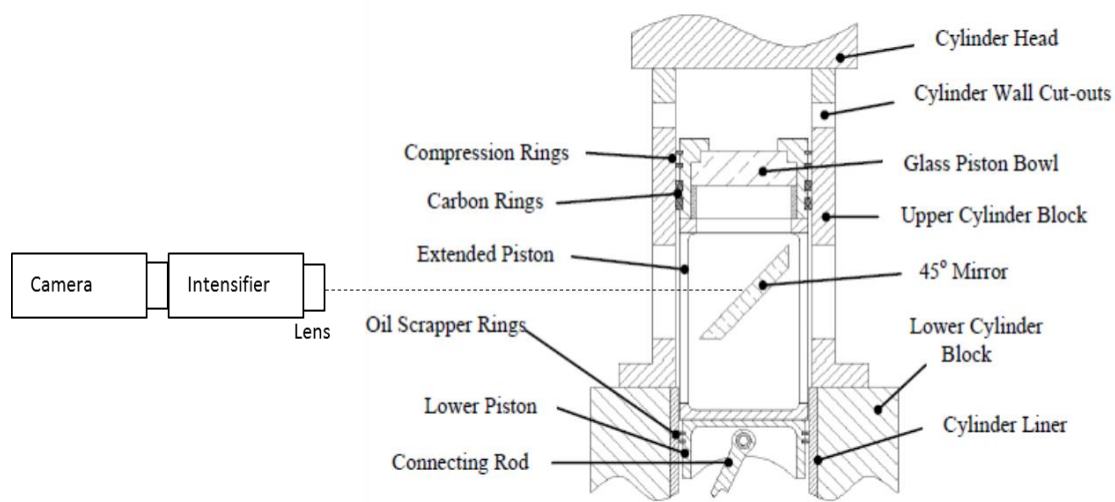


*Figure 7.1 Sectional Schematic View of the Optical Layout*

*Table 7.1 Optical Setting of Camera, Lens, Intensifier, Lens, Laser*

High Sped Camera	NAC Memrecam FX6000
Frame Speed (fps)	6000 (w/ intensifier)
	10000 (w/o intensifier)
Frame Size (pixel)	512 x 384 (w/ intensifier)
	512 x 248 (w/o intensifier)
Intensifier	DRS ILS-3-11
Lens	UV-Nikkor 105mm f/4.5 (w/ intensifier)
	AF Micro-Nikkor 60mm f/2.8D (w/o intensifier)
Laser	CU15 Oxford Wave length 511 nm Pulses Width 10-40ns Pulse Repetition Rate 10 kHz

Due to the different characteristics of the combustion for each of the three different fuel mixture, pure diesel, diesel-ethanol dual fuel, and diesel-gasoline dual fuel, the equipment utilized and their setup to collect in-cylinder injection and combustion high-speed footage varies.

A high speed image intensifier is installed in front of the high speed video camera to detect faint luminosity of dual fuel combustion without laser but not used for diesel combustion to protect intensifier from strong luminosity of diesel diffusion combustion, as shown in Figure 7.2. With the intensifier, the image was recorded as

monochrome images and the same image intensifier level of 80% is used for all dual fuel combustion for direct comparison. The high speed laser is used for diesel combustion to obtain clearer combustion image and fuel spray image as shown in Figure 7.3. In particular, the short laser pulse width of less than 40 ns enables the sharp recording of the high speed fuel spray to be obtained without blur. The high speed video images and in-cylinder pressure from the same cycle are recorded and analysed.

To analyse combustion area and intensity of combustion luminosity, in-house code in MATLAB is used. After combustion images are converted into grey scale images, combustion area is defined by a threshold of intensity and mean intensity is calculated as the average intensity of a whole combustion chamber. Intensity of luminosity is dependent on chemical substance as well as its concentration and its temperature, so higher intensity is related to richer mixture or higher temperature.

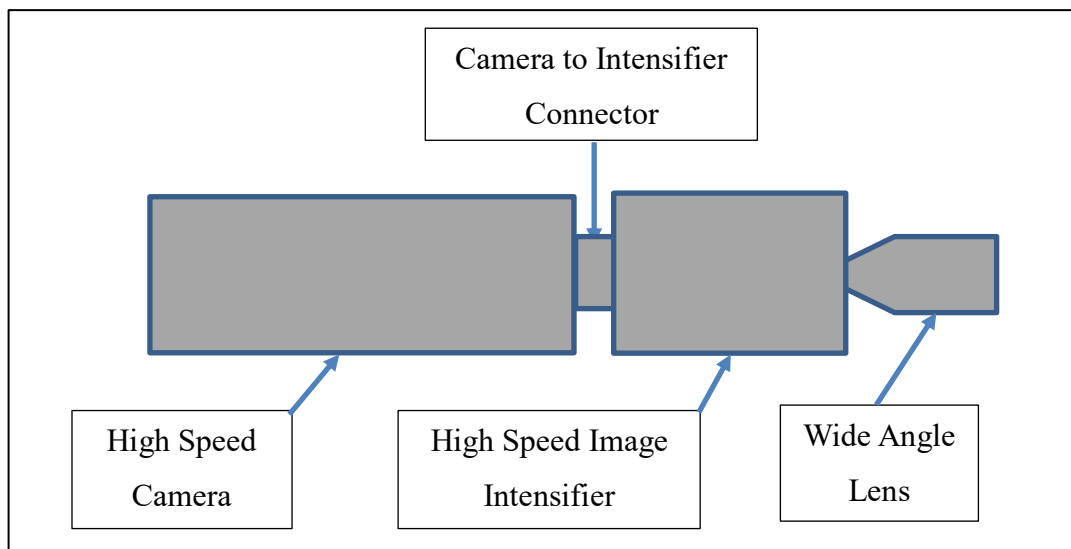


*Figure 7.2 High Speed Imaging using High Speed Intensifier*

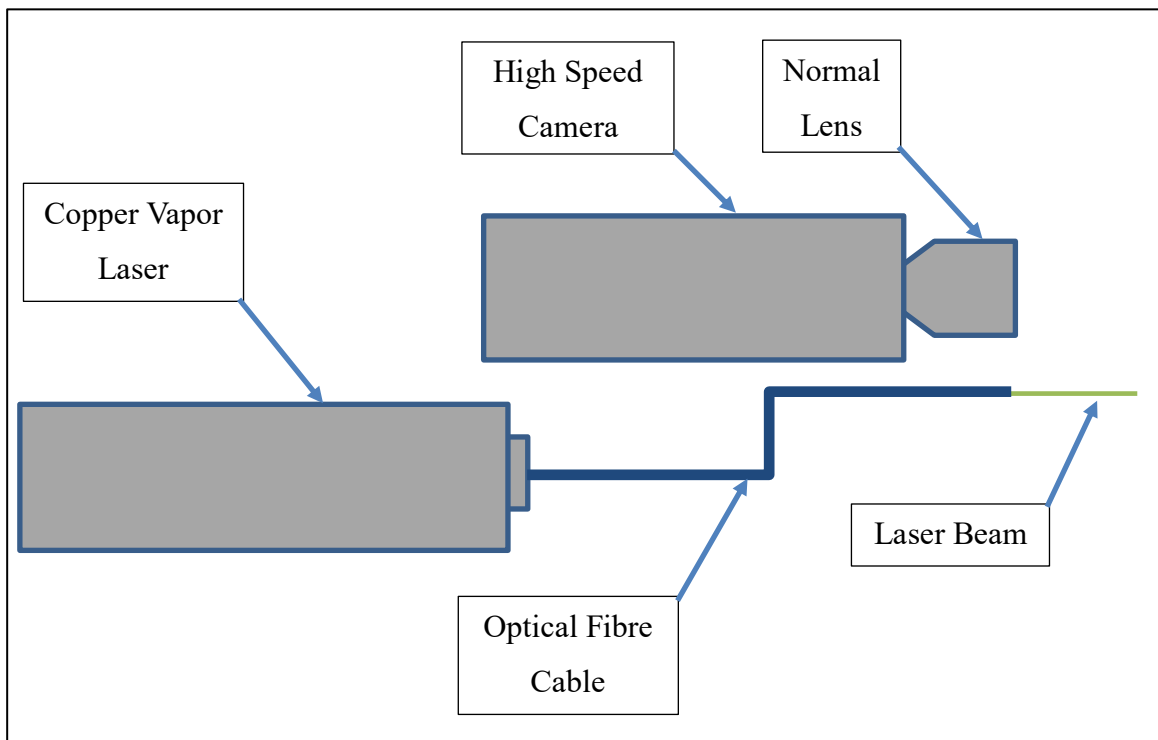


*Figure 7.3 High Speed Imaging using Copper Vapor Laser*

### 7.3 Test Conditions

Due to the greater heat loss and leakage with the glass piston crown, both the intake pressure and intake temperature are raised to higher values than those of the metal piston operation. Other conditions are kept the same as thermal engine test. Table 7.2 below shows the test condition of optical engine experiments. Intake temperature is adjusted to obtain the proper combustion timing. The focus of the in-cylinder study in the optical diesel engine is to understand the difference in mixture formation, ignition and combustion with different diesel injection strategies and ethanol/gasoline substitution ratios.

Figure 7.4 below shows the position of intake and exhaust valve and diesel injection spray angle in image. Dotted lines are injection spray angle.

*Table 7.2 Test condition of optical analysis*

Engine Speed (rpm)	1200
Rail Pressure (bar)	500
Total Fuel Energy (kJ/sec) constant	5.2
Intake Pressure (bar)	1.1 bar
Intake Temperature (°C)	150-200
Substitution Ratio of Ethanol (%)	0(diesel only), 45, 60, 75
Diesel Injection Strategy	Single, Split
EGR Rate (%)	0

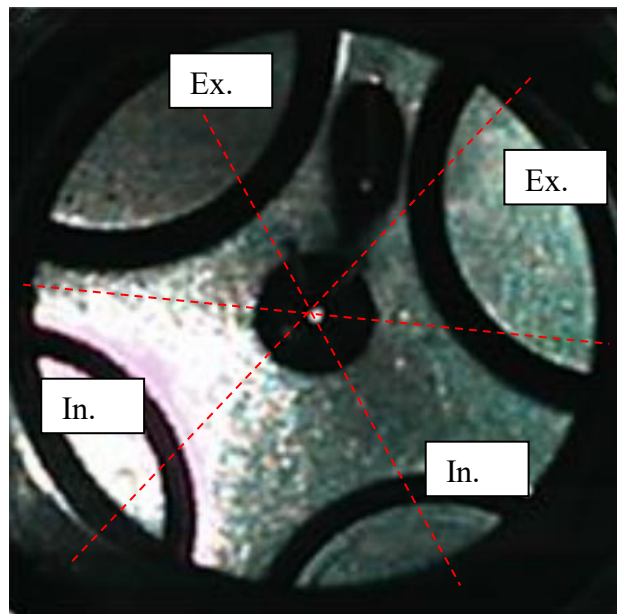


*Figure 7.4 Image of combustion chamber through the glass piston without combustion*

## 7.4 Results and Discussion

In this section the results from the captured images for every fuel mixture operation is presented and discussed.

### 7.4.1 Diesel only and Diesel-Ethanol dual fuel combustion

Figure 7.5 shows in-cylinder pressure, HRR, combustion area and the image sequence obtained simultaneously through high speed video imaging technique without image intensifier during a single diesel injection operation, when SOI is 5 CA BTDC . With in-house MATLAB code, the displayed image is obtained by subtracting the back ground image from the original one.

1<sup>st</sup> picture at -1.2 CA ATDC shows the start of fuel spray jet where fuel sprays are uneven due to uneven pressure inside of injector holes, a characteristic of the VCO type nozzle. The difference in the SOI and the optical image is caused by the delay in actuating the solenoid and lifting of the needle in the injector. At the next image, fuel spray jet developed more and penetration length becomes longer reaching almost the side wall of combustion chamber. 3<sup>rd</sup> image at 8.3 CA ATDC shows the first combustion site at the tip of one of fuel sprays, which matches the beginning of main heat release rate. However, the heat release starts slightly around 5 CA ATDC and is not visible in the combustion image because of the lower temperature. At 4<sup>th</sup> frame, combustion developed primarily with blue flame combustion due to premixed combustion and a little bit luminous flame due to diffusion combustion. Combustion is separated into 6 groups from the 6 fuel sprays. At 5<sup>th</sup> frame at 11.9 CA ATDC, the area of luminous flame spreads around the chamber but the centre of chamber remains dark with no combustion. At 6<sup>th</sup> frame at 14.1 CA ATDC, combustion is still observed even though HRR is finished when more visible light emission is produced by the combustion of soot with much less additional heat released.

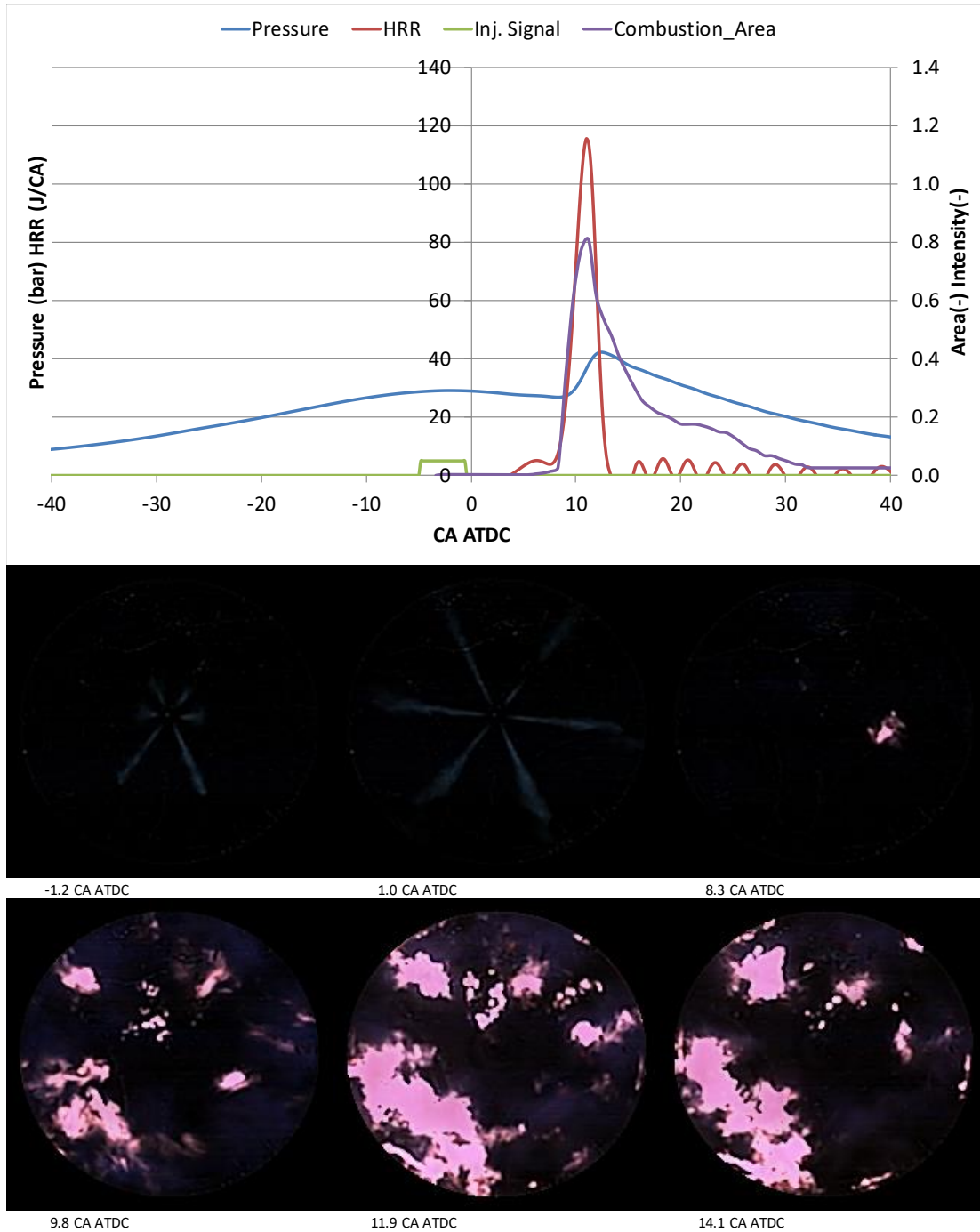


*Figure 7.5 Direct combustion Image of diesel combustion without intensifier at 5CA BTDC of SOI*

Figure 7.6 shows in-cylinder pressure, HRR, combustion area, intensity of combustion luminosity and the image sequence obtained simultaneously through high speed video imaging technique with image intensifier at single dual fuel combustion

when SOI is 5 CA BTDC, substitution ratio is 60%. The HRR graph shows that first small HRR occurs at 5 CA ATDC but combustion is not observed until 6.6 CA ATDC when the main HRR starts. As shown in 1<sup>st</sup> frame of images, combustion starts in the centre and at upper side of the combustion chamber around exhaust valves. At 2<sup>nd</sup> frame, although combustion luminosity increases, combustion does not spread whole combustion chamber. At 3<sup>rd</sup> frame 10.3 CA ATDC, combustion is seen almost in whole combustion chamber except the centre and gaps of each diesel fuel spray which is black area in the image. The timing of peak combustion area and intensity correspond with the peak HRR. From 3<sup>rd</sup> frame, a lot of strong luminosity spots are observed as soot produced from local rich mixture of diesel fuel is burnt. Through all frames at this condition, combustion is not seen to develop to whole combustion chamber. In some area of diesel combustion, combustion luminosity is not seen either in Figure 7.5 because this black area does not have fuel mixture. However, dual fuel has homogeneous ethanol-air mixture even in unburned black area in the images. During diesel only operation fuel-air mixture entrained by diesel fuel sprays exists just along fuel sprays, where combustion occurs. On the other hand, with the dual fuel operation, diesel fuel sprays entrain air and premixed ethanol and then make local rich area along fuel spray but other zone has just lean premixed ethanol distributed, so combustion progresses in the richer area and not spread enough to other lean area. This causes higher THC and lower combustion efficiency of the dual fuel combustion. Later combustion with little heat release is seen at the last frame and in the combustion area and intensity graph as well.

Figure 7.7 shows in-cylinder pressure, HRR, combustion area, intensity of combustion luminosity and the image sequence with image intensifier when SOI is advanced to 28 CA BTDC during the diesel-ethanol dual fuel combustion with 60% substitution rate.

Compared to Figure 7.6, the location of combustion beginning is at exhaust valve side but closer to the wall of combustion chamber in 1<sup>st</sup> and 2<sup>nd</sup> frames due to longer penetration length from longer ignition delay of diesel fuel. Combustion spreads towards the centre from the periphery in 2<sup>nd</sup> to 4<sup>th</sup> frame as HRR and combustion area increase. Combustion luminosity is seen in the whole combustion chamber at 3.0 to 5.0 CA ATDC. Compared to the late single injection in Figure 7.6, little combustion of unburned fuel is present around the centre of chamber. In the last frame, late

combustion is observed around the periphery. Overall, intensity of combustion luminosity is much lower with early injection than that with late injection because of more premixed combustion.

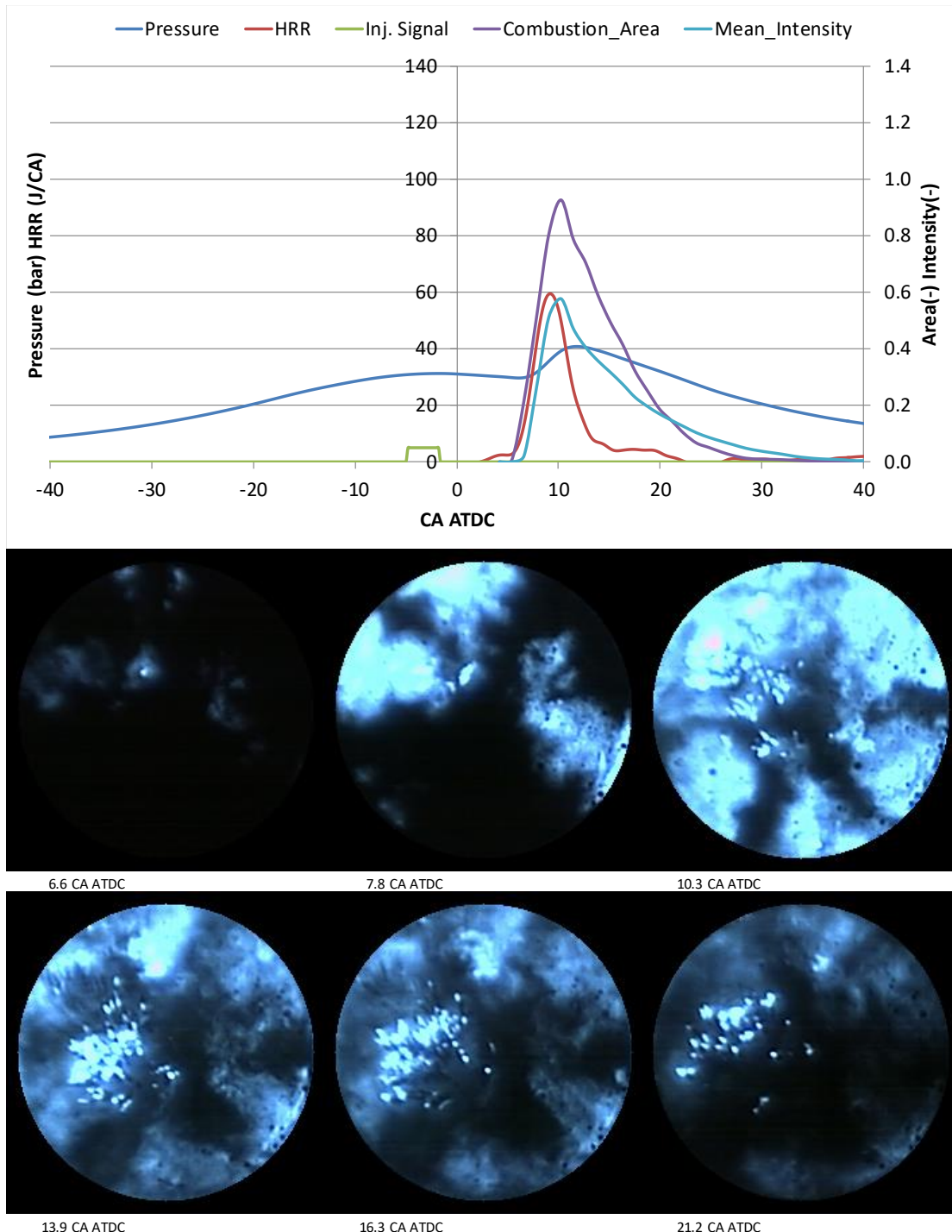
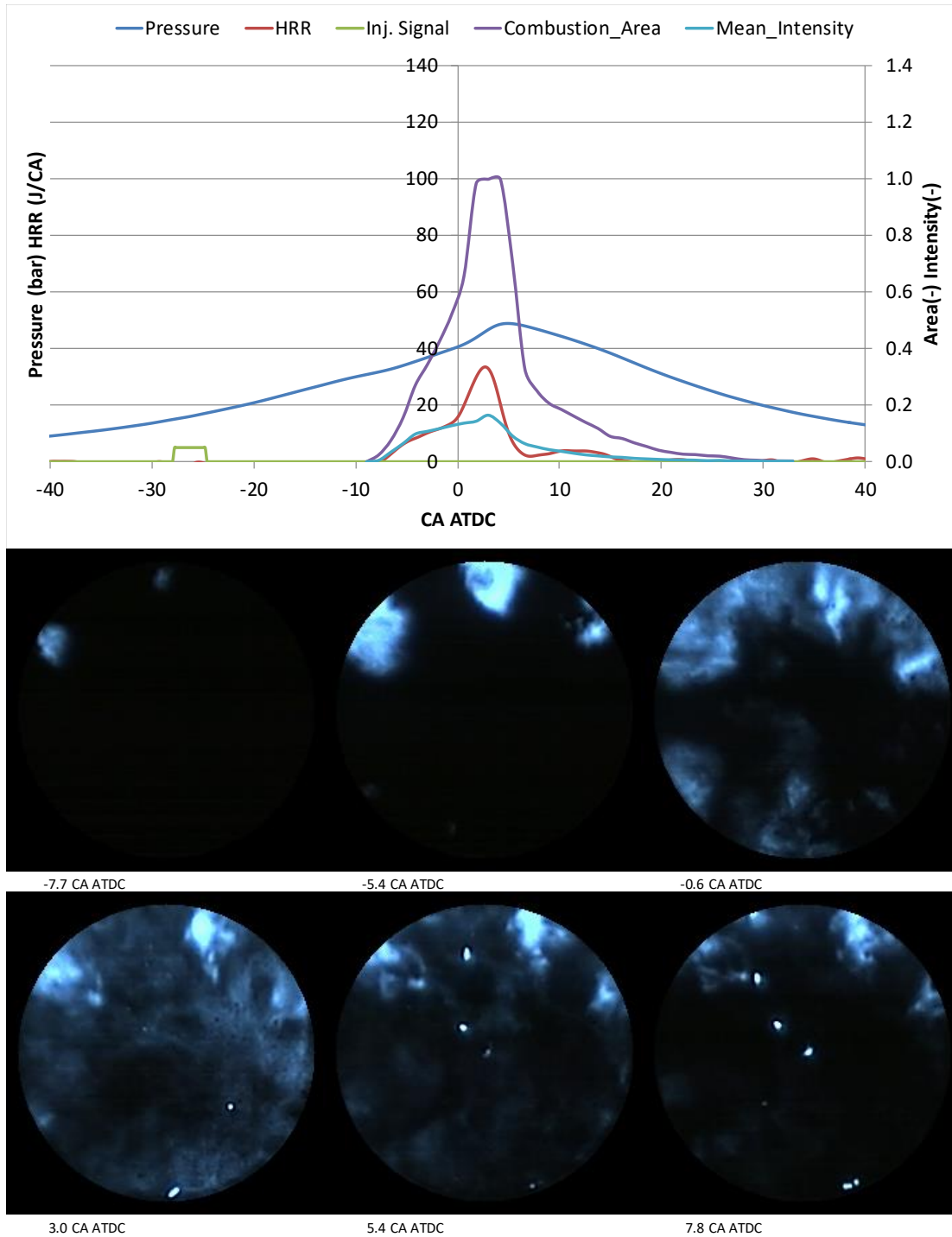


Figure 7.6 Direct combustion Image with intensifier when substitution ratio is 60%, diesel SOI is 5CA BTDC



*Figure 7.7 Direct combustion Image with intensifier when substitution ratio is 60%, diesel SOI is 28CA BTDC*

Figure 7.8 shows in-cylinder pressure, HRR, combustion area, intensity of combustion luminosity and the image sequence with image intensifier at split dual fuel combustion with 60% ethanol when the first and second SOI are at 63 and 28 CA BTDC. 2<sup>nd</sup> injection timing is the same as Figure 7.7. Combustion seems to start at the outer region in 1<sup>st</sup> frame at -7.4 CA ATDC, especially at the lower area and the left

upper area. The first luminosity seen is earlier than HRR start. This is because 1<sup>st</sup> fuel spray at very early timing is injected outside of the piston bowl, and then this fuel mixture starts combustion after long ignition delay. Compared to Figure 7.7, combustion occurs simultaneously in wide regions due to 1<sup>st</sup> very early injection. Combustion spreads towards the centre from the periphery in 2<sup>nd</sup> to 5<sup>th</sup> frame as HRR and combustion area increase. The intensity peak of combustion luminosity is a little bit earlier than peak HRR and peak combustion area, indicating local richer mixture area burns before the combustion of premixed lean ethanol mixture. Throughout whole combustion process, intensity of combustion luminosity is lower than single early injection in Figure 7.7.

Figure 7.9 shows in-cylinder pressure, HRR, combustion area, intensity of combustion luminosity and the image sequence with image intensifier at split dual fuel combustion with 60% ethanol when the split SOI timings are retarded to 30 and 5 CA BTDC, substitution ratio is 60%. 2<sup>nd</sup> injection timing is the same as Figure 7.6. At 1<sup>st</sup> frame -6.8 CA ATDC, combustion luminosity begins faintly at the upper side. In the following frame, the faint luminance spread and strong luminosity occurs around injector nozzle and fuel spray jet is visualized thanks to the strong luminosity. At 3<sup>rd</sup> frame, the area with strong luminosity expands. This strong luminosity is due to diffusion combustion of diesel fuel mixture due to the shorter ignition delay time caused by higher in-cylinder temperature of the combustion of 1st injection. At 4<sup>th</sup> frame, the area of the strong luminosity peaked and then decreased through 4<sup>th</sup> to 6<sup>th</sup> frame. In the graph, intensity peak is earlier than peak HRR, meaning this strong luminosity is not engaged with heat release directly. Combustion area in the graph is not calculated accurately due to too strong luminosity. Such a strong luminosity from diffusion combustion indicates more soot formation, illuminating strongly during combustion. This diffusion combustion can enhance the temperature around the centre of combustion chamber and reduce the temperature around the wall with shorter spray penetration length for combustion beginning before end of injection.

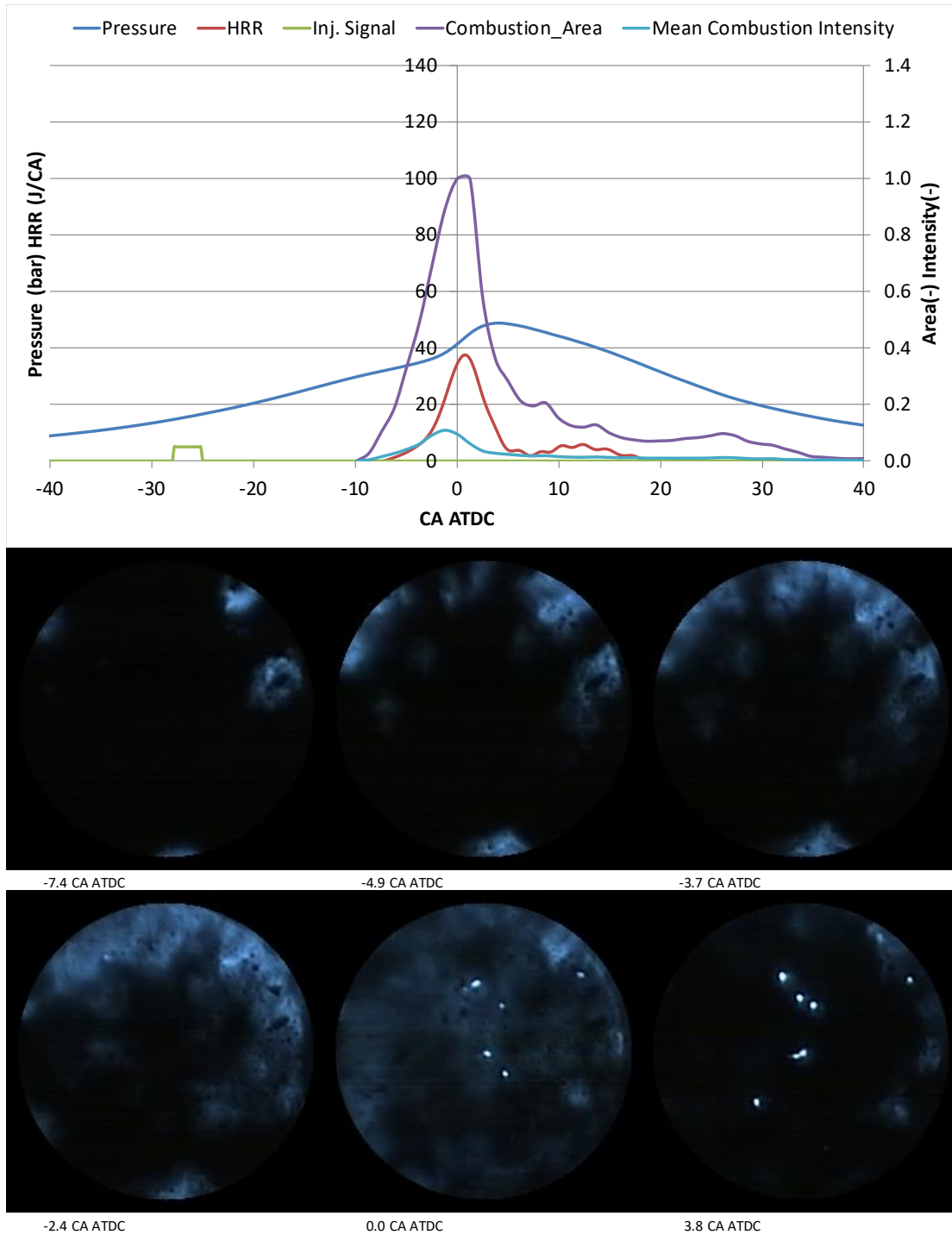


*Figure 7.8 Direct combustion Image with intensifier when substitution ratio is 60%, diesel injection is split injection and SOI is 63-28CA BTDC*

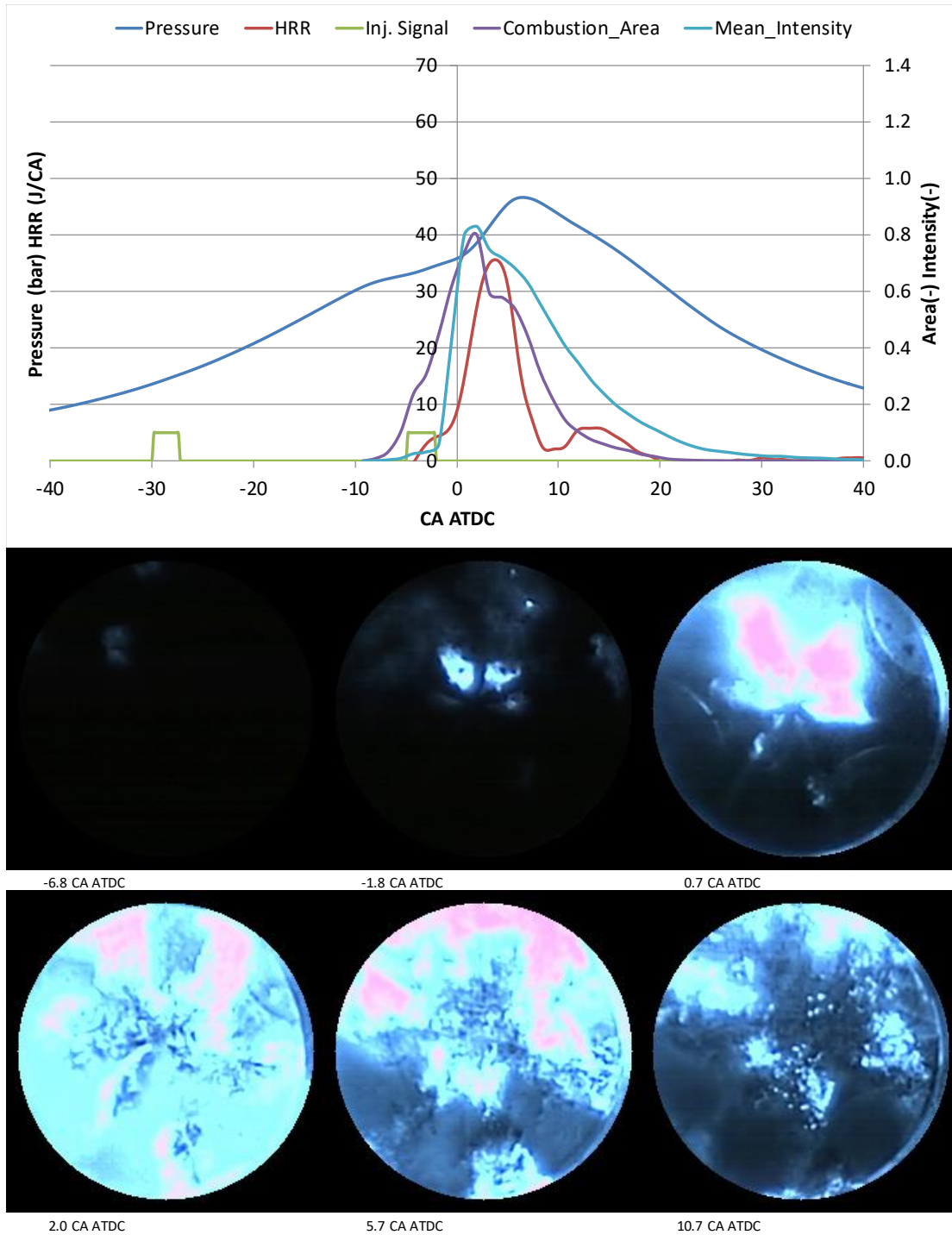


*Figure 7.9 Direct combustion Image with intensifier when substitution ratio is 60%, diesel injection is split injection and SOI is 30-5CA BTDC*

Figure 7.10 shows in-cylinder pressure, HRR, combustion area, intensity of combustion luminosity and the image sequence with image intensifier at single dual fuel combustion when SOI is 42 CA BTDC, substitution ratio is 45%. At 1<sup>st</sup> frame - 2.8 CA ATDC, combustion luminosity begins very faintly around right side and left upper side. At 2<sup>nd</sup> frame, the faint luminance spread. From the 3<sup>rd</sup> frame onward, the area of combustion can be seen to expand to cover the most of the combustion chamber before ending. The lack of high luminous combustion is due to the homogeneous mixture because of the early diesel injection.

Figure 7.11 shows in-cylinder pressure, HRR, combustion area, intensity of combustion luminosity and the image sequence with image intensifier at single dual fuel combustion when SOI is 15°CA BTDC, substitution ratio is 75%. At 1<sup>st</sup> frame, combustion starts at the upper sides near exhaust valves, and then at the next frame, strong luminosity occurs around the centre of upper side due to local richer fuel mixture distributed by later injection and uneven fuel spray. Through frame 2<sup>nd</sup> to 4<sup>th</sup> which is 1.2 to 7.3°CA ATDC, combustion area spreads and mean intensity of combustion luminosity increases in the graph. Even though combustion area, intensity and HRR reach the peak, combustion luminosity is not observed in some area around lower side. At 5<sup>th</sup> frame, some bright spots are seen that seems to be luminous flame of soot caused by injector dribbling. Compared to Figure 7.7 and Figure 7.10, peak intensity of combustion luminosity is higher because of more stratified diesel fuel mixture from later injection timing even though amount of diesel fuel is less. This fact matches the emission results that NO<sub>x</sub> at 75% of substitution is higher than that of lower substitution.

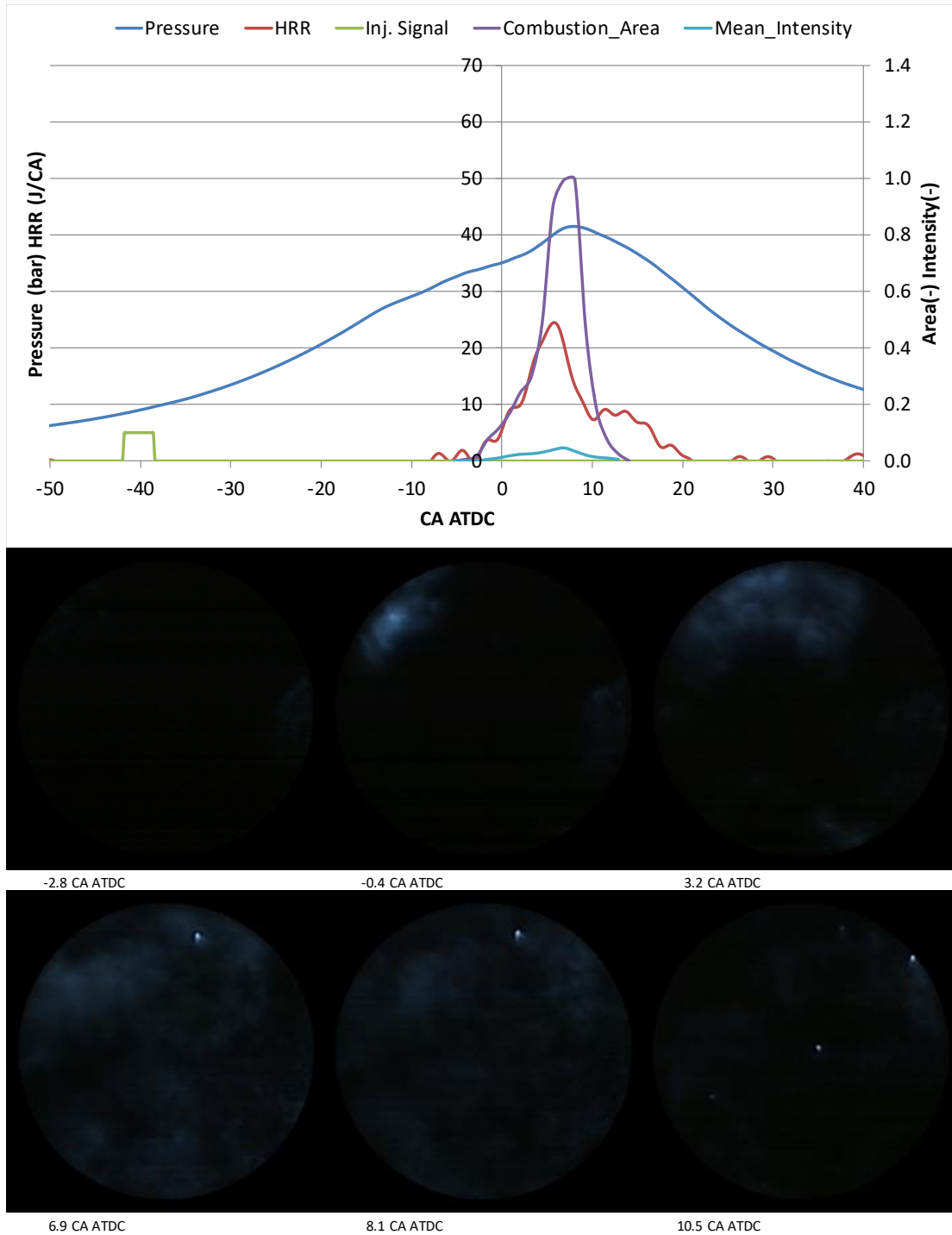


Figure 7.10 Direct combustion Image with intensifier when substitution ratio is 45%, diesel SOI is 42CA BTDC

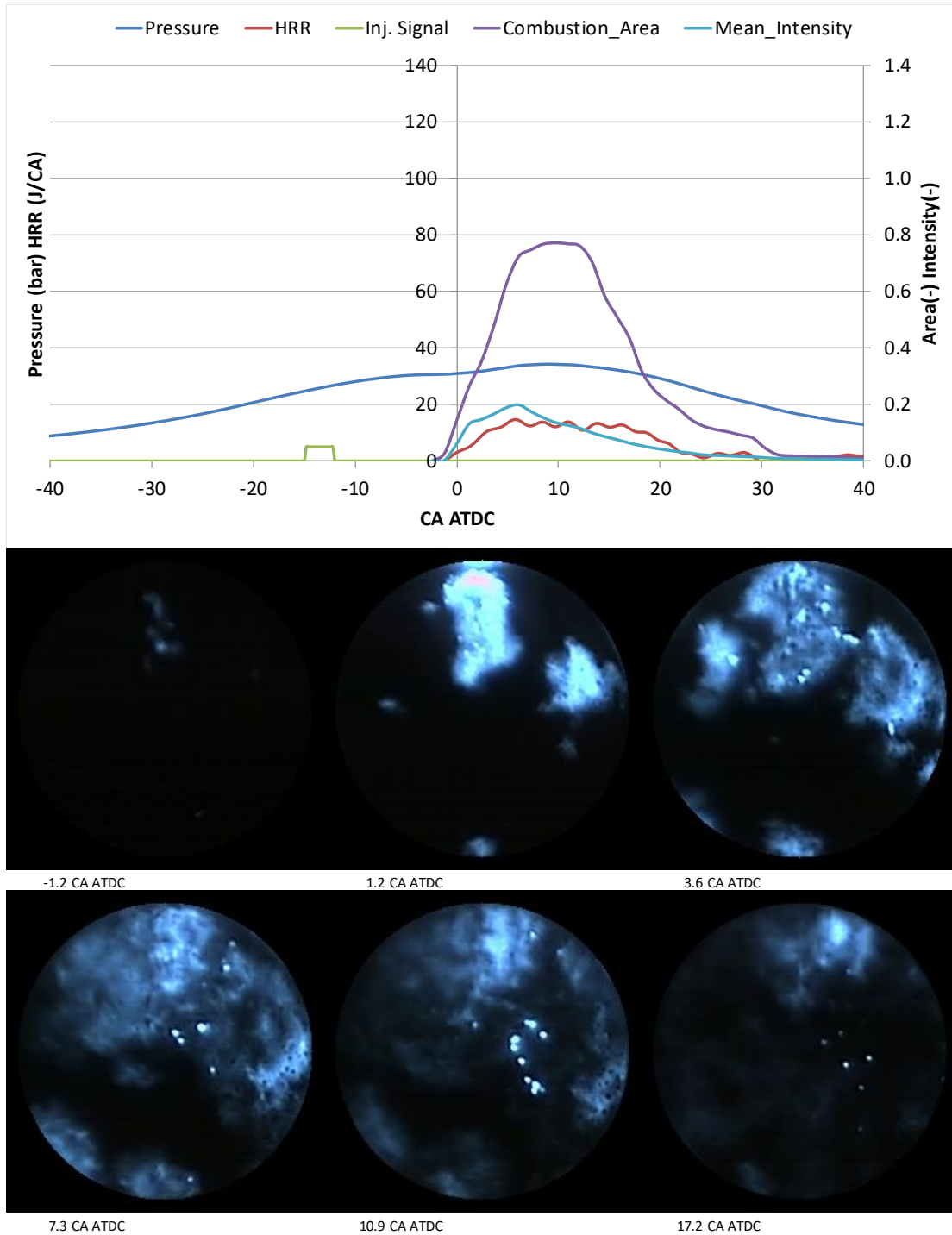
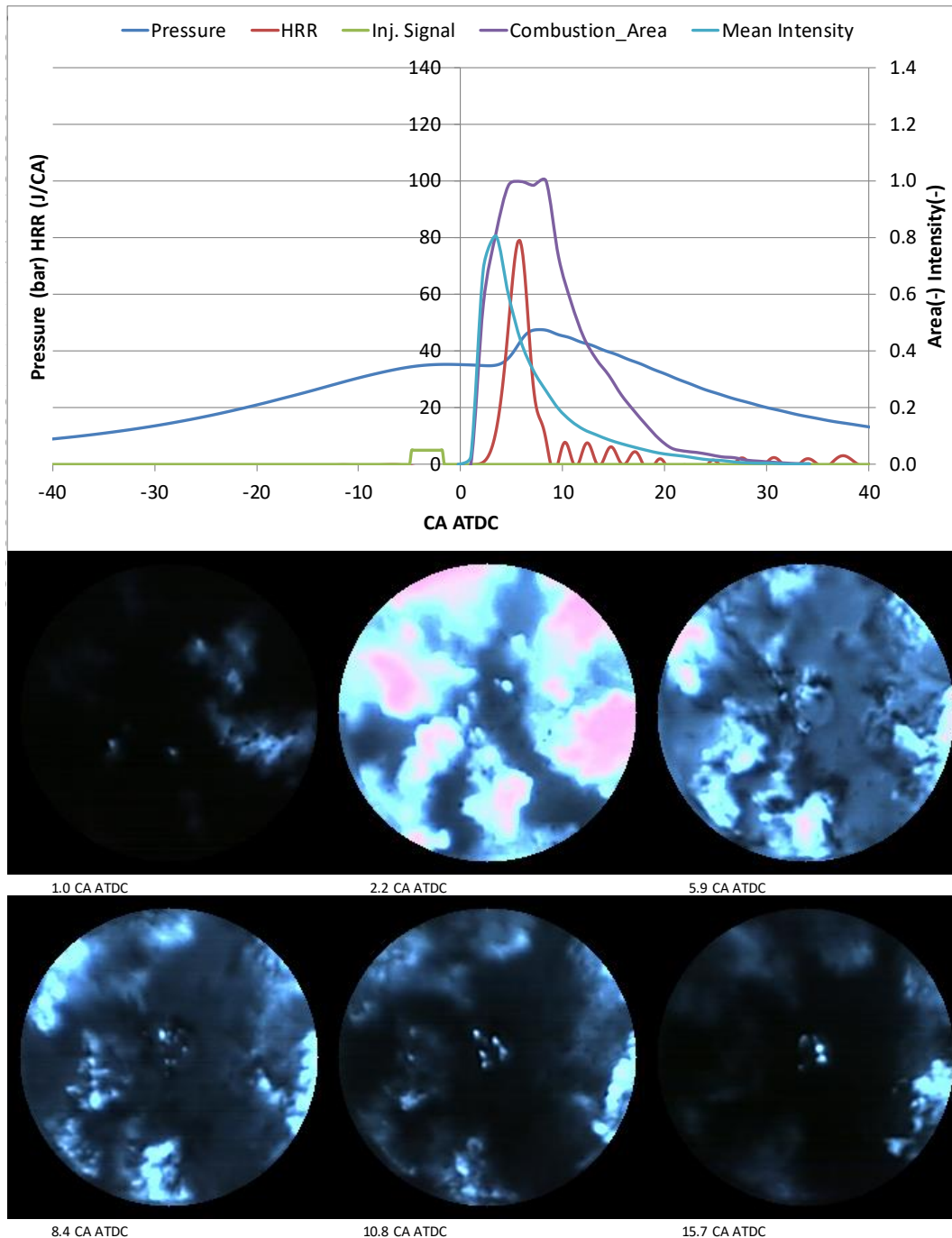


Figure 7.11 Direct combustion Image with intensifier when substitution ratio is 75%, diesel SOI is 15CA BTDC

## 7.4.2 Diesel-Gasoline Operation

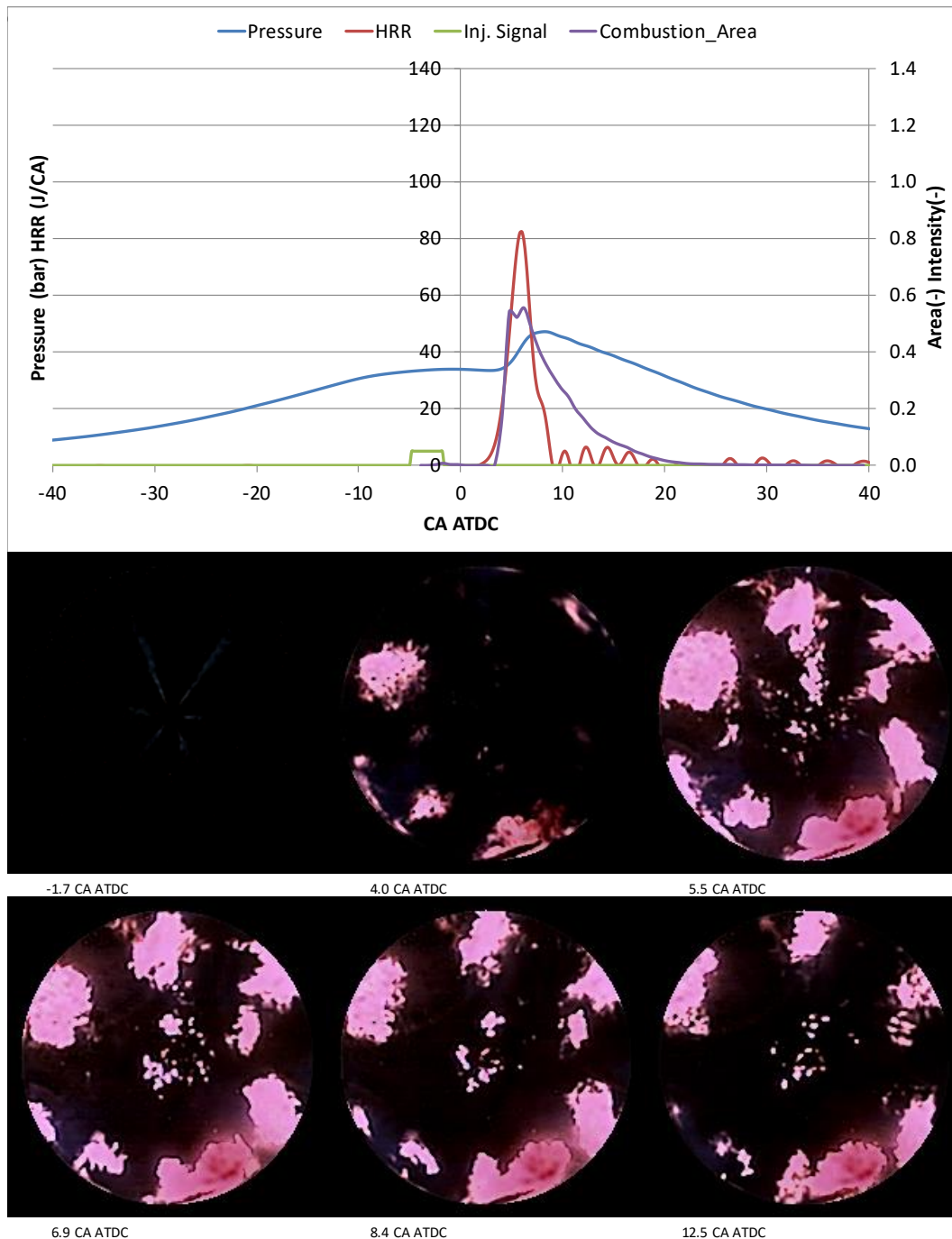
Figure 7.12 shows in-cylinder pressure, HRR, combustion area, intensity of combustion luminosity and the image sequence obtained simultaneously through high speed video imaging technique with image intensifier at single dual fuel combustion when SOI is  $5^\circ$  CA BTDC, substitution ratio is 60%. The HRR graph shows that around  $1^\circ$  CA ATDC HRR occurs, which can be observed from the first frame, where the main HRR start, combustion starts at upper right side of the combustion chamber, possibly due to the higher gas temperature around exhaust valves. At second frame,  $2.2^\circ$  CA ATDC, combustion luminosity is increased, and the combustion almost spread throughout the entire combustion chamber except the centre and gaps between each of diesel fuel spray, which is black area in the image. The timing of peak combustion area and intensity correspond with peak HRR. Here, a lot of strong luminosity spots are observed. This seems to be flame luminosity of soot combustion due to soot made from local rich mixture of diesel fuel or injector dribbling. At this condition through all frames, combustion is not seen to develop to entire combustion chamber. In some area of diesel combustion, combustion luminosity is not seen in Figure 7.5 either, because this black area does not have fuel mixture. However, dual fuel has homogeneous gasoline-air mixture even in unburned black area in the images. At diesel condition fuel-air mixture entrained by diesel fuel sprays exists just along fuel sprays, where combustion occurs. On the other hand, at dual fuel operation, diesel fuel sprays entrain air and premixed gasoline and then make local rich area along fuel spray but other zone has just lean premixed gasoline distributed, so combustion progresses in the richer area and not spread enough to other lean area. This cause unburned fuel, meaning high THC and low combustion efficiency at dual fuel condition compare to diesel combustion. Later combustion like diesel combustion is seen at the last frame and in the combustion area and intensity curve as well.

Figure 7.13 shows the images from the same condition when no image intensifier is used for collecting the high-speed video, and therefore, only the luminosity from the diesel combustion is recorded. When compared with Figure 7.12, it shows a much smaller value of the total combustion area, with the same pressure and HRR curve. At the first frame at  $1.7^\circ$  CA BTDC, the spray from the diesel injection can also be observed.



*Figure 7.12 Direct combustion Image with intensifier when substitution ratio is 60%, diesel SOI is 5CA BTDC*

Figure 7.14 illustrates in-cylinder pressure, HRR, combustion area, intensity of combustion luminosity and the image sequence with image intensifier when the single diesel SOI is 50° CA BTDC, with gasoline substitution ratio of 60%.



*Figure 7.13 Direct combustion Image without intensifier when substitution ratio is 60%, diesel SOI is 5CA BTDC*

Compared to Figure 7.12, the location of combustion beginning is at exhaust valve side but closer to wall of combustion chamber in first and second frames due to longer penetration length from longer ignition delay of diesel fuel. Combustion spreads towards the centre from the periphery in second to fourth frame as HRR and combustion area increase. Combustion luminosity is seen in the entire combustion chamber at 3.9° to 1.5° CA BTDC. Compared to late single injection, less unburned

fuel is present around the centre of chamber. In the last frame , late combustion is observed around the periphery. Overall, intensity of combustion luminosity is much lower with early injection than that with late injection because of lower combustion temperature and more uniformed mixture during combustion.

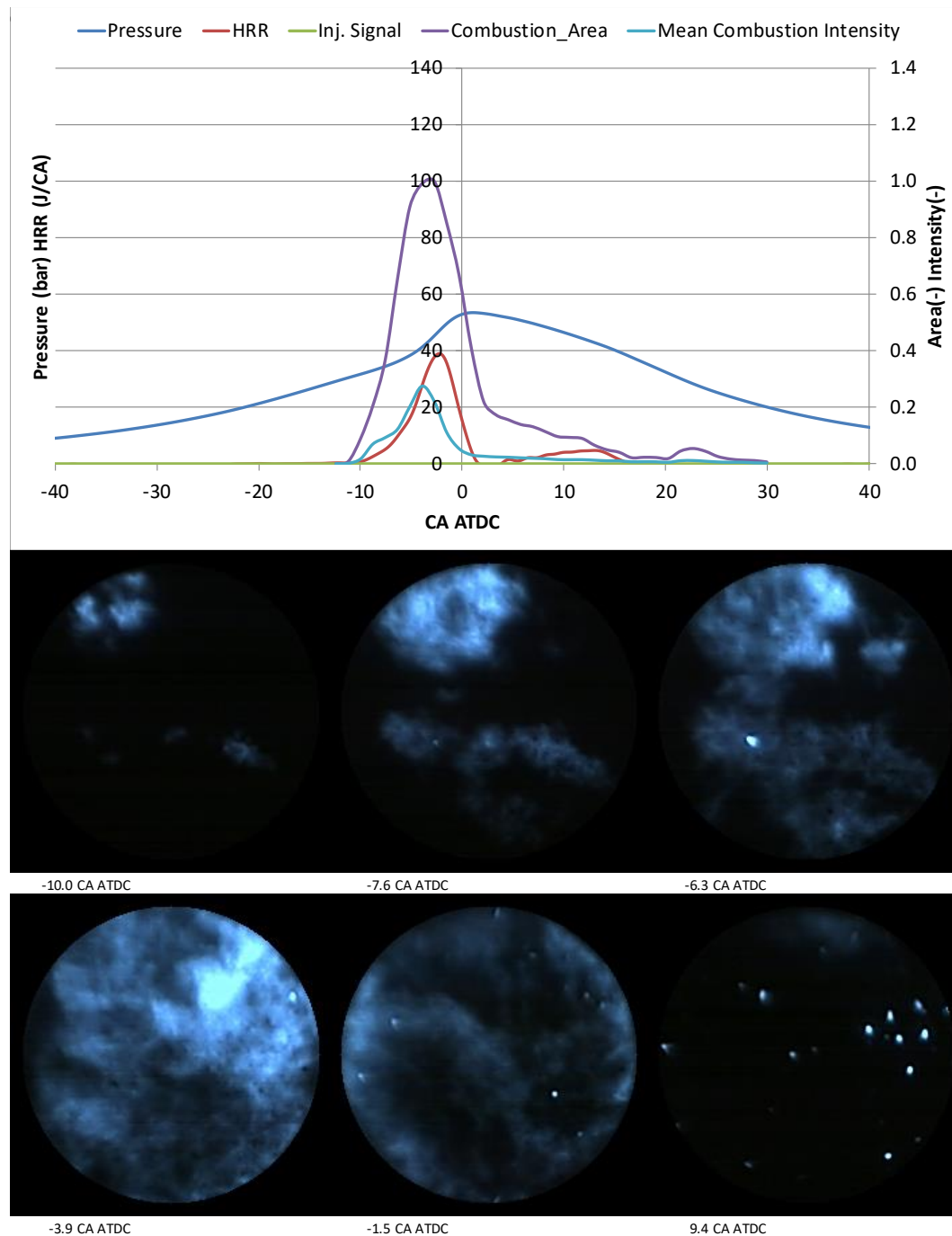
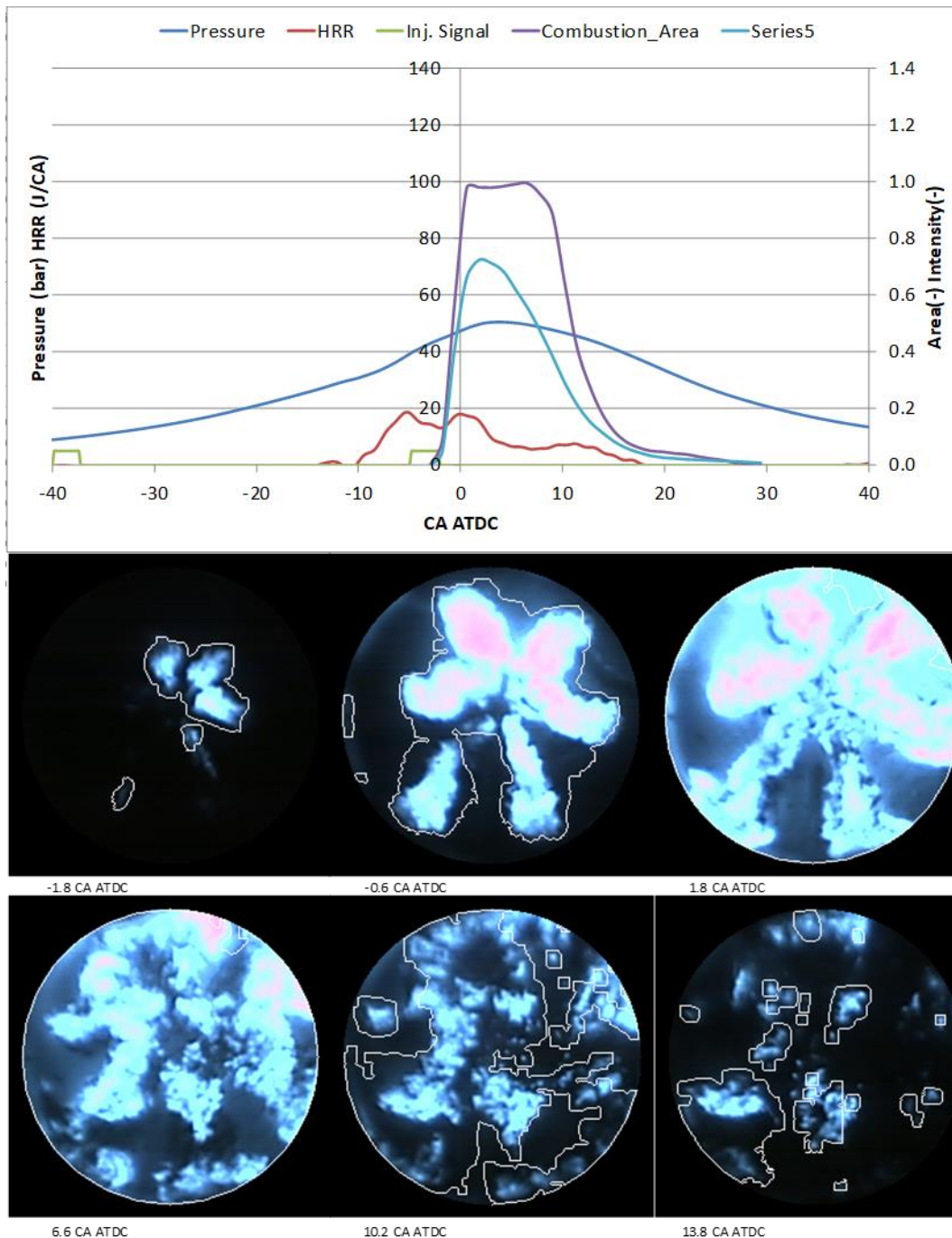


Figure 7.14 Direct combustion Image with intensifier when substitution ratio is 60%, diesel SOI is 50CA BTDC



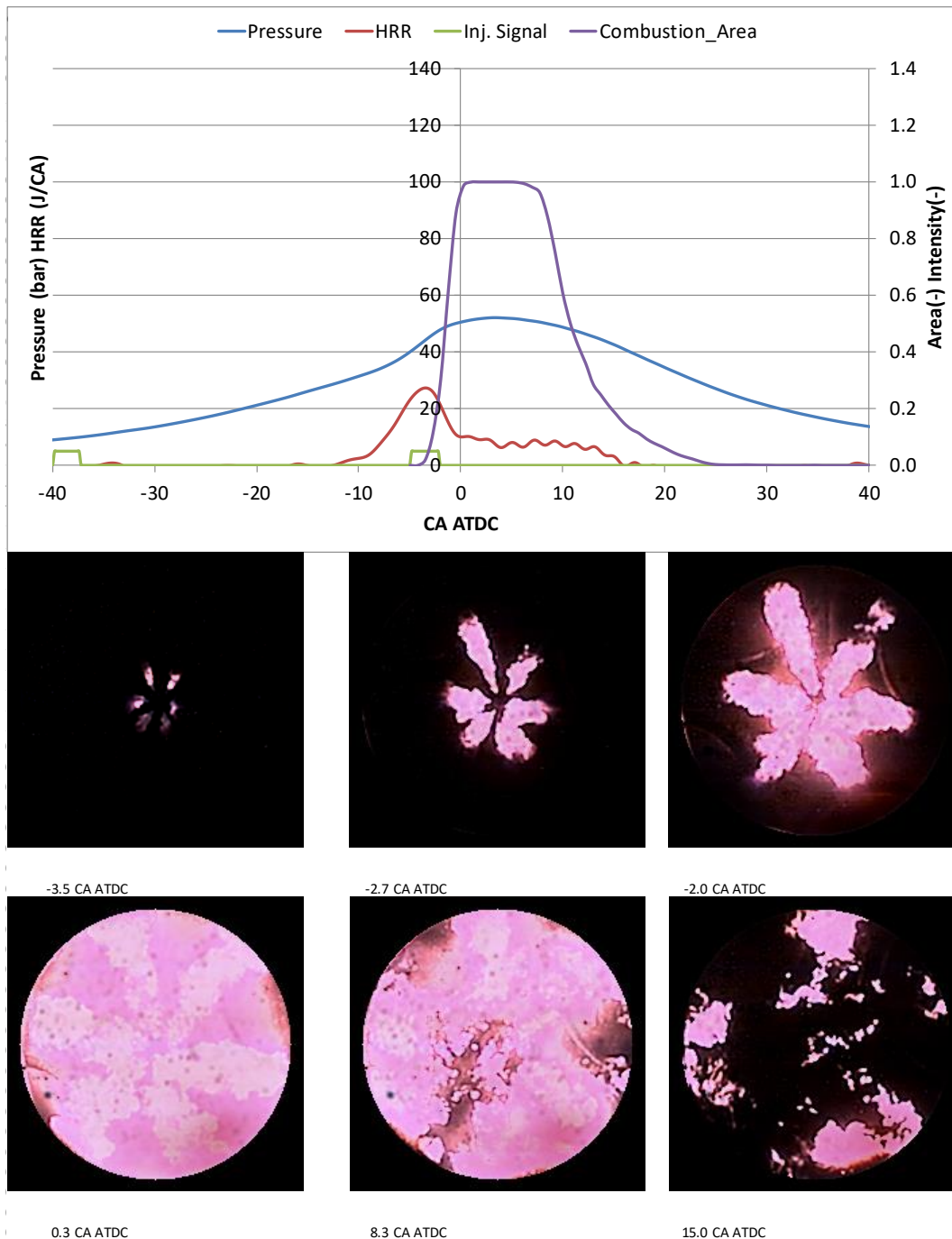
*Figure 7.15 Direct combustion Image with intensifier when substitution ratio is 60%, diesel injection is split injection and SOI is 40-5CA BTDC*

Figure 7.15 shows in-cylinder pressure, HRR, combustion area, intensity of combustion luminosity and the image sequence with image intensifier at split dual fuel combustion when SOI is 40°-5° CA BTDC, substitution ratio is 60%. second injection timing is the same as Figure 7.12. At the first frame -1.8° CA ATDC, combustion luminosity begins at the upper side of the injection nozzle. In the following frame, the luminance spreads, with stronger luminosity occurring around

the injector nozzle close to the exhaust valves, and fuel spray jet is visualized thanks to the strong luminosity. At the third frame, the area with strong luminosity expands. This strong luminosity is due to diffusion combustion of diesel fuel mixture due to the shorter ignition delay time caused by higher in-cylinder temperature of the combustion of first injection. At 4th frame the combustion can be seen in the entire combustion chamber, where the area of the strong luminosity peaked and then decreased through fourth to sixth frame. In the graph, the intensity, pressure and combustion area peak at around the same point, but the HRR peaks at two different stages, one of which earlier than intensity, due to the initial diesel injection, and again at TDC, just before the intensity peak, caused by the second diesel injection, with the start of this second increase in HRR, matching the start of intensity and combustion area increasing just before the first frames CA. Strong luminosity from diffusion combustion indicates more soot formation, illuminating strongly during combustion. In the diffusion combustion flame, NO may not be generated so much due to lack of oxygen. This diffusion combustion can enhance the temperature around the centre of combustion chamber and reduce the temperature around the wall with shorter spray penetration length at combustion beginning before end of injection, which may reduce heat loss.

Figure 7.16 shows the images from the same condition when no image intensifier is used for collecting the high-speed video, thus, only the luminosity from the diesel combustion is recorded. Compared to Figure 7.15, it shows a much smaller value for the total combustion area, with the same pressure curve and similar, but not identical HRR curve, which could be caused by a slight difference in testing conditions between the two operations.

In the frames included in this figure, the path of the diesel injection is well illustrated and it is easy to see how the combustion starts with the start of the second diesel injection, and following the path of the injection spray as it develops, until the fourth frame at  $0.3^\circ$  CA ATDC, where the entire combustion chamber is illuminated, but the luminosity of the diesel spray still dominating the most of the image. The fifth frame shows the combustion area, and the intensity beginning to fade away, and at a very minimum by the last frame included in the figure at  $15^\circ$  CA ATDC.



*Figure 7.16 Direct combustion Image without intensifier when substitution ratio is 60%, diesel injection is split injection and SOI is 40-5CA BTDC*

Figure 7.17 illustrates in-cylinder pressure, HRR, combustion area, intensity of combustion luminosity and the image sequence with image intensifier at single dual fuel combustion when diesel SOI is 40° CA BTDC, gasoline substitution ratio is 75%. At first frame, combustion starts at the upper sides where the exhaust valves are located, and then at the next frame shows the advancement of the combustion still at the top and close to the exhaust valves.

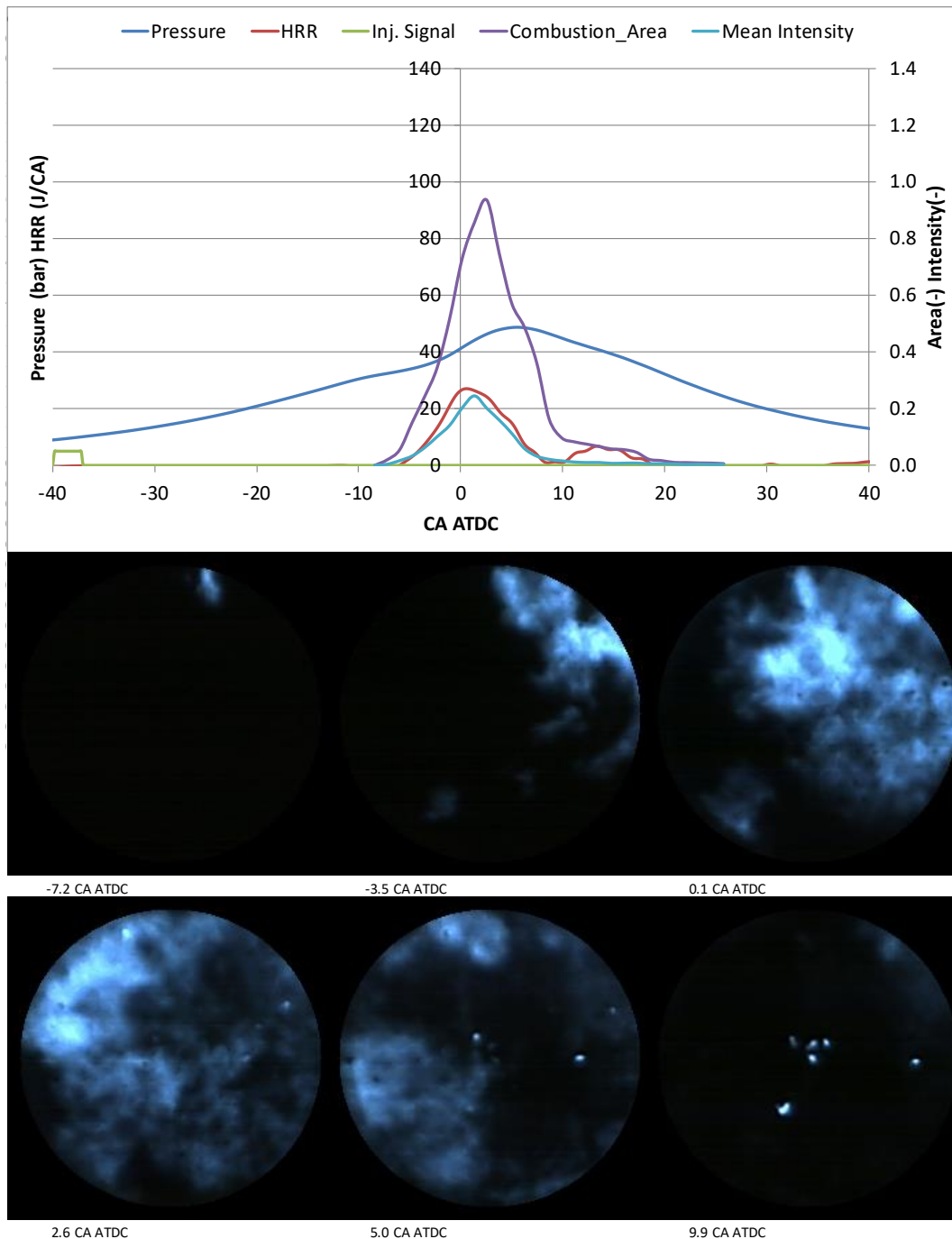


**Figure 7.17 Direct combustion Image with intensifier when substitution ratio is 75%, diesel SOI is 40CA BTDC**

Through the second frame to the fourth frame, which is  $-3.5^{\circ}$  CA ATDC to  $2.6^{\circ}$  CA ATDC, combustion area spreads and mean intensity of combustion luminosity increases and peaks in the graph. Although combustion area, intensity and HRR reach the peak by this point, combustion luminosity is still very faint in some area around lower right side of the combustion chamber. At the fifth and sixth frames, some bright spots are seen that seems to be luminous flame of soot caused by injector dribbling.

## 7.5 Summary

In this chapter, the results obtained from the optical analysis of the dual fuel operations, namely diesel-ethanol and diesel-gasoline, are presented and analysed. The main findings are summarised as follows.

- In the case of single diesel injection during the dual fuel operations with either premixed ethanol or gasoline, combustion starts around the wall of combustion chamber downstream of diesel fuel sprays, and then spread towards the centre. Late injection timing results in stronger luminosity than that of early injection timing because of the greater diffusion combustion of diesel. Combustion luminosity is dominated by areas near the diesel spray region when injection occurs near TDC whereas combustion is observed throughout the combustion chamber with the earlier injection.
- With split diesel injections, early split injection produces weaker luminosity than that of single early injection because split injection makes more homogeneous and leaner mixture. Late split injection operation has much stronger luminosity than that of single late injection because of the immediate combustion of diesel from the second injection. This is because the higher in-cylinder temperature at second injection timing reduces the ignition delay and makes the combustion of second injection more diffusion-like combustion.
- As the premixed fuel substitution ratio is increased, later injection timing is used to get similar combustion timing. Therefore the combustion of the higher substitution ratio operation is characterised with stronger luminosity of the diffusion combustion of the less mixed diesel fuel.
- For both diesel and dual fuel combustion processes with a single diesel injection, the areas near the centre or the region between adjacent fuel sprays remain dark indicating lack of combustion.
- Under similar conditions, such as injection strategy (early or late diesel injection), intake conditions and substitution ratio, the diesel-gasoline operation combustion appears to have higher intensity and as a result higher luminosity compared to the diesel-ethanol operation combustion. This was somewhat realised by the fact that the high speed camera utilized for the

entirety of this study, was able to record the combustion process for most cases of diesel-gasoline operation, even without the use of the high speed image intensifier, nor the copper vapor laser as means of combustion chamber illumination.

- The combustion from the diesel-gasoline operation also had larger flame area when compared to that of the diesel-ethanol operation, under similar testing conditions, which is believed to be due to the gasoline fuels higher volatility.

# Chapter 8.

## Conclusions

### 8.1 Summary

In this study, the in-cylinder fuel injection, fuel mixing and combustion of dual fuel operations using a VCO solenoid injector for delivering diesel direct injection, along with a port fuel injector for delivery of ethanol/gasoline, in an optical single cylinder diesel engine, with diesel-ethanol and diesel-gasoline fuel combinations were examined. The thermodynamic properties and emission production for each operation were studied, with the means of utilizing in-cylinder pressure measurements, exhaust gas emission analyser, as well as in-cylinder high-speed imaging of all the stages of the in-cylinder processes, from injection spray, ignition delay, to combustion intensity and duration.

For the purpose of this study, a variety of intake conditions, as well as diesel injection timings were examined and recorded for each fuel mixture operation, and then the results were compared and the most optimal conditions from each of the two dual fuel operations were selected in order to be compared to one another and the diesel baseline operation, for efficiency and emission output.

### 8.2 Evaluation

Each chapter of this study included a certain engine operation under various conditions and strategies, by utilizing few different techniques for engine performance evaluation i.e. in-cylinder pressure data collection, exhaust gas smoke measurement and emission analysis, as well as high-speed optical evaluation of the combustion process. Here are the summary of what has been concluded from each of these investigations, and a view of the study as a whole.

### 8.2.1 Dual Fuel Operation

The following conclusions were drawn from the examination of thermodynamic analysis and emission sampling of dual fuel operations at different intake conditions and injection strategies:

- In conventional dual fuel combustion that uses a single late diesel injection, EGR is effective in reducing NO<sub>x</sub> produced, because of the lower oxygen concentration and higher heat capacity, and increased thermal efficiency due to less heat loss and less THC. Lower intake temperature has a good effect on NO<sub>x</sub> and thermal efficiency. That suggests that external cooled EGR can have a benefit for emission and thermal efficiency.
- In premixed dual fuel combustion that includes an early diesel injection and a later diesel injection, EGR is effective to reduce THC, and increase thermal efficiency caused by higher equivalent ratio. Increased intake temperature has the advantage of improving THC, and NO<sub>x</sub> levels, and efficiency as well, because of higher in-cylinder temperature and more homogeneous combustion. That suggests that external hot EGR or using internal EGR can have a benefit for emission and efficiency.
- Second injection timing of split injection and injection timing of single injection have similar effects on combustion characteristic, such as ignition delay, CA<sub>50</sub>, PHRR etc. That means that combustion is primarily controlled by latter (second) injection timing, but they are slightly different due to the effect of heat release or distribution of diesel fuel mixture of the 1st injection.
- When second injection timing and single injection timing are the same, NO<sub>x</sub>, THC and CO trend of both injection strategies are similar but NO<sub>x</sub> of split injection is slightly lower.
- Thermal efficiency of split injection is higher when second injection timing and single injection timing are the same. Late second injection timing improves thermal efficiency compared to late single injection, but has worsened soot. This is because late split injection, makes more diffusion-like combustion with shorter ignition delay of second injection since combustion of 1st injection starts before or during the second injection, and this

combustion makes milder heat release rate with lower heat loss and more soot emission.

- Combustion of single diesel injection is more intense than that of dual fuel, with higher PHRR and shorter combustion duration, due to higher chemical reactivity of diesel fuel.
- THC and CO of dual fuel combustion is higher and hence, lower combustion efficiency. This is because ethanol/gasoline homogeneous mixture in piston crevice and around cylinder liner, where are gas with low temperature hardly combusts or is quenched by lower temperature zone.

### **8.2.2 Comparing the Thermodynamic Properties and Emission Testing of Different Fuel Mixtures**

The thermodynamics properties of each dual fuel operation was calculated using the pressure data collected from in-cylinder study of each fuelling concept at different conditions and injection strategies, along with the emission output for all tested cases by analysing the exhaust gases and measuring the soot from exhaust smoke, and the best results from each condition for both fuel mixtures was compared to one another, and then to that of diesel baseline, and below is the conclusion from this comparison:

- When comparing the two dual fuel operations, diesel-ethanol operation and diesel-gasoline operation, with the same substitution ratio to diesel, 60% for this study, the thermal efficiency of the engine operation is higher for operations with lower intake temperature, 100°C being the lower intake temperature for this study, which is possibly due to the lower heat loss for this conditions. of the two dual fuel operations, the diesel-ethanol operation produces the higher thermal efficiency output, with late diesel injection timings close to TDC. Relatively the same results can be achieved from the diesel-gasoline operation under the same conditions, with early diesel injection timings, creating a more HCCI (Homogeneous Charge Compression Ignition) like combustion, also known as RCCI (Reactivity Controlled Compression Ignition) combustion for dual fuel operations.
- At lower intake temperatures, the diesel-gasoline operation allows for a wider range of diesel injection timing, without incurring any misfire or knocking,

compared to the operation range of diesel-ethanol dual fuel operation, which has a smaller diesel injection timing range, thus not allowing for the diesel injection to be advanced much.

- At the same substitution ratio, increasing the intake temperature to higher levels, 150°C being the higher intake temperature for this study, slightly increases the diesel injection timing range before incurring any misfire, allowing for more advanced diesel injection timing, which produces roughly the same thermal efficiency as the lower intake temperature with late diesel injection timing.
- Increasing the intake temperature reduces the diesel injection timing range for the diesel-gasoline operation by increasing the chance of incurring knock, all without improving the thermal efficiency compared to the diesel-ethanol operation with the same intake conditions, nor the diesel-gasoline operation with lower intake temperature.
- However, the same cannot be said about combustion efficiency, as increasing the intake temperature leads to a higher combustion efficiency, with diesel-ethanol operation at 150°C of intake temperature with diesel injection timing having the best combustion efficiency at diesel injection timing of 30° CA BTDC.
- Regardless of intake conditions, the operations with diesel injection timings earlier than 35° CA BTDC produce very little, close to zero, levels of NO<sub>x</sub> emissions. This is mainly due to the longer ignition delay with early diesel SOI, creating a more premixed and leaner, more homogeneous mixture of diesel fuel.
- Knowing that higher intake temperature increases NO<sub>x</sub> at the same diesel SOI timing, the highest level of NO<sub>x</sub> emissions is observed in the diesel-ethanol operation with 150°C of intake temperature and diesel injection timing of 25° CA BTDC. This is also true for the diesel-gasoline operation with diesel injection timing of 5° CA BTDC, where the operation with 150°C of intake temperature has a slightly higher level of NO<sub>x</sub> emission compared to that of the operation with 100°C of intake temperature.

- Where the NOx emission level is available for all, or most, operation conditions at the same diesel injection timing, lower intake temperature results in lower NOx with the diesel-ethanol operation having the lowest level with early diesel injection timing, and diesel-gasoline operation having the lowest NOx emission level for late diesel injection timing, suggesting that early diesel injection at lower intake temperature with diesel-ethanol operation, allows for a leaner diesel fuel mixture, resulting in a more RCCI like combustion with lower NOx emission levels.
- When diesel SOI is near TDC, NOx emissions are similar in all conditions, including diesel condition. This is due to the combustion of the diesel fuel mixture being dominant source of NOx formation, as there is not enough time, short ,ignition delay, to create a well-mixed fuel.
- Soot emission is very low in all conditions of the diesel-ethanol dual fuel operation. It is assumed that soot levels peak at around 25° CA BTDC diesel injection timing with 100°C of intake temperature, is caused by the diesel fuel not being injected into the combustion bowl properly.
- Increasing intake temperature decreases soot when not using EGR. This is true for most conditions, and specially at early diesel injection timings, and where the soot levels is available for all conditions at the same diesel SOI, the diesel-ethanol operation with higher intake temperature has the lowest level of soot emission level.

### **8.2.3 High-Speed Optical Analysis**

This section summarizes the results and outcomes from the optical analysis of the combustion from each of the two duel fuel operations, namely diesel-ethanol and diesel-gasoline, using the high speed images collected from the combustion during engine operation:

- In general, the dual fuel combustion starts around the wall of combustion chamber downstream of diesel fuel sprays, and then spread towards the centre
- Late injection timing results in stronger luminosity than that of early injection timing. That means that later injection makes local richer mixture and higher

temperature zone before and during combustion, that can make more NO<sub>x</sub> and soot emission.

- Later combustion seems to have un-combusted area without luminosity near the centre of combustion chamber or the regions between fuel sprays, whereas combustion is observed throughout the combustion chamber with the earlier injection.

This means that some areas without enough diesel fuel mixture distributed do not have enough temperature for chemical process of combustion of premixed ethanol mixture causing high THC.

- Early split injection has weaker luminosity than that of single early injection because split injection makes more homogeneous and leaner mixture. Faint luminosity with split injection means lower temperature of combustion that results in lower NO<sub>x</sub> but higher THC due to incomplete combustion of the premixed ethanol mixture.
- Late split injection has much stronger luminosity than that of single late injection due to the heat release of first injection. The higher in-cylinder temperature at second injection timing reduces the ignition delay and makes the combustion of second injection more diffusion-like combustion. That may be helpful to reduce heat loss because higher temperature zone is concentrated more around the centre of combustion chamber but can increase soot emission.
- As the ethanol substitution ratio is increased, later injection timing is used to get similar combustion timing. Therefore the combustion of the higher substitution ratio operation is characterised with stronger luminosity of the diffusion combustion of the less mixed diesel fuel.
- In single diesel combustion, blue flame, that is premixed combustion, and yellow flame, that is diffusion combustion, are seen simultaneously due to ununiformed mixture whereas single dual fuel combustion does not seem to have diffusion-like combustion due to the presence of more premixed leaner ethanol/gasoline mixture.

- for both diesel and dual fuel combustion processes with a single diesel injection, the areas near the centre or the region between adjacent fuel sprays remain dark indicating lack of combustion. In the case of the dual fuel operation, the presence of such regions would contribute to the higher THC<sub>s</sub> from the premixed ethanol/gasoline mixture.

At the end, it can be said that according to the results of this study, dual fuel combustion has a big advantage in reducing soot emission because of leaner diesel fuel mixture, especially with diesel-ethanol operations under certain conditions, while THC and CO of dual fuel combustion is higher and hence, lower combustion efficiency when compared to that of diesel baseline operation. Therefore, other than environmental and economic advantages of using fuels that are not fossil fuels and are from renewable sources such as ethanol, these fuels also offer reduced pollution output, in some cases very significant reduction, as well as efficiency that under certain operation conditions could be matching that of an engine burning only diesel as the main fuel source.

However, there are other factors that manufacturers need to look into when deciding which fuel is best suited for their systems, such as local economy and environmental issues, local legislations and limitations, as well as availability and accessibility. There is no point in having an engine that runs on ethanol if the ethanol production is dependent on using and burning of fossil fuels, just as much as there are no environment benefits to using an electric vehicle (EV) where fossil fuels are used to produce the electricity that runs the vehicle.

### 8.3 Future Work

The sensitivity of the optical engine when in optical mode i.e. when using the glass piston head, does not allow for continuous operation of the engine, which in terms separates the resulting outcome of thermodynamics testing, and to some extent emission testing, from the real world scenarios and operation conditions. this however is not an obstacle that could not be resolved entirely at research level, other than by

the means of applying suitable techniques for collecting the data, which is what was done for the purpose of this study.

Here are some recommendations as to what could possibly be done in the future work on this subject that has a potential to compliment and/or complete this study:

- Completing diesel-gasoline dual fuel operation testing using diesel split injection for further comparison with other injection strategies as well as with diesel-ethanol split injection operations.
- Further testing of diesel-gasoline operation by introducing different levels of EGR to the system during operation.
- Replacing pure ethanol (E100) with variety of wet ethanol, with different percentages of water in the fuel, in diesel-ethanol dual fuel operation testing, and comparing findings with the former.
- To better understand the benefits of dual fuel operation, further testing of diesel baseline under similar conditions as the dual fuel operation testing, including optical analysis, would be beneficial.
- Further and more in depth analysis and comparison of the optical testing results, using all three different fuel operations, given the diesel baseline optical testing is more comprehensive.
- Modifying the engine to operate using diesel and natural gas as a dual fuel alternative, and conducting all the similar and relative testing in order to enable comparison with other dual fuel operations, specifically diesel-ethanol operation, by means of thermodynamics, emissions, and optical testing and analysis while utilising similar conditions and techniques for all fuel mixtures.
- To measure the other chemical substance or radical such as CO, CH<sub>2</sub>O, by employing optical filter, in order to better understand the behaviour of dual fuel combustion for all fuel mixtures.
- To evaluate the effect of other basic parameters such as compression ratio, rail pressure, and engine speed on the results of each fuel mixture.
- Measuring and comparing the combustion illumination level for different fuel mixtures and testing conditions.



## References

- [1] Busch-Sulzer Bros.-Diesel Engine Company, The diesel engine, St. Louis: Busch-Sulzer Bros.-Diesel Engine Company, St. Louis, 1913.
- [2] Heywood, John B., Internal Combustion Engine Fundamentals, Singapore: McGraw-Hill Education, 1988.
- [3] MAN Diesel & Turbo, “MAN B&W Low Speed Small Bore Engines,” MAN Diesel & Turbo, Denmark, 2014.
- [4] Office of Energy Efficiency and Renewable Energy, “freedom CAR & vehicle technologies program,” U.S. Department of Energy, 2003.
- [5] Eur-Lex, Access to European Law, “Eu Law,” Eur-Lex, [Online]. Available: <http://eur-lex.europa.eu/homepage.html>. [Accessed 01 June 2017].
- [6] Association of International Motor Vehicle Manufacturers, “European exhaust gas emission standards,” 31 February 2017. [Online]. Available: <http://www.vdik.de/departement/environment/european-exhaust-gas-emission-standards.html>. [Accessed 01 June 2017].
- [7] Karim, Ghazi A., Dual-Fuel Diesel Engines, CRC Press, 2015.
- [8] RFA, Renewable Fuels Association, “World Fuel Ethanol Production,” RFA, Renewable Fuels Association, Washington, 2017.
- [9] U.S. Department of Energy, “Alternative Fuels Data Center,” U.S. Department of Energy's Vehicle Technologies Office, 27 February 2017. [Online]. Available: [https://www.afdc.energy.gov/fuels/ethanol\\_benefits.html](https://www.afdc.energy.gov/fuels/ethanol_benefits.html). [Accessed 01 July 2017].
- [10] Majewski, W. Addy, “What Are Diesel Emissions,” DieselNet Technology Guide, 2012.
- [11] W. Addy Majewski, Magdi K. Khair, Diesel Emissions and Their Control, SAE International, 2006.

- [12] Klaus Mollenhauer, Helmut Tschöke, *Handbook of Diesel Engines*, Berlin, Germany: Springer, 2010.
- [13] Pischinger, S., *Verbrennungsmotoren. Vorlesungsumdruck-druck*, Aachen, Germany: RWTH Aachen University, 2001.
- [14] Steinparzen, F., “Dieselmotoren für PKW: Gestern – Heute – Morgen,” in *18th AVL Conference “Engine and Environment”*, Graz, Austria, 2006.
- [15] B. Cooper, et al., “Advanced Diesel Technology to Achieve Tier 2 Bin 5 Emissions Compliance in US Light-Duty Diesel Applications,” in *SAE 2006 World Congress & Exhibition*, Detroit, 2006.
- [16] Hammer, J., “Evolution of the Common Rail Technology,” in *ATA International Symposium “Diesel Engine: The NOx and PM Emissions Challenge”*, Monopoli (Bari), Italy, 2004.
- [17] Commission Regulation (EU) No 133/2014., “The European Parliament and the Council of the European Union,” *Official Journal of the European Union* 2014;47., 2014.
- [18] Zeldovich, Y.B., “Zhur. Tekhn. Fiz.,” *NACA Tech Memo*, vol. 19, p. 1199, 1950.
- [19] European Environment Agency, “Directive 70/220/EEC (Measures to be taken against air pollution by emissions from motor vehicles),” European Environment Agency, Copenhagen, Denmark, 2002.
- [20] Hohenberg, G., “Partikelmessverfahren. Abschlussbericht zum Forschungsvorhaben,” BMWi/AiF 11335, 2000.
- [21] Hagelüken, C., “Autoabgaskatalysatoren.,” *Reihe Kontakt & Studium*, 2005.
- [22] Robert Bosch GmbH, *Dieselmotor-Management*, Wiesbaden, Germany: Springer Vieweg Berlin, 2004.
- [23] Gary L. Borman, Kenneth W. Ragland, *Combustion Engineering*, Michigan: McGraw-Hill, 1998.
- [24] Zelenka P, Aufinger H, Reczek W, Catellieri W., “Cooled EGR - A Key Technology for Future Efficient HD Diesels,” in *International Congress &*

*Exposition*, Detroit, 1998.

- [25] Kreso AM, Johnson JH, Gratz LD, Bagley ST, Leddy DG., “A Study of the Effects of Exhaust Gas Recirculation on Heavy-Duty Diesel Engine Emissions,” in *International Fuels & Lubricants Meeting & Exposition*, Detroit, 1998.
- [26] Ming Zheng, Graham T. Reader, J. Gary Hawley, “Diesel engine exhaust gas recirculation—a review on advanced and novel concepts,” *Energy Conversion and Management*, vol. 45, no. 1, p. 883–900, 2004.
- [27] Pulkrabek, Willard W., *Engineering Fundamentals of the Internal Combustion Engine*, New Jersey: Prentice Hall, 2003.
- [28] Mehdi Jangia, Tommaso Lucchinib, Gianluca D’Erricob, Xue-SongBai, “Effects of EGR on the structure and emissions of diesel combustion,” *Proceedings of the Combustion Institute*, vol. 34, no. 2, pp. 3091-3098, 2013.
- [29] A. Maiboom, X. Tazua and J. Hétet., “Experimental study of various effects of exhaust gas recirculation (EGR) on combustion and emissions of an automotive direct injection diesel engine.,” *Energy*, vol. 33, pp. 22-34, 2008.
- [30] Y. Wakisaka, Y. Hotta, M. Inayoshi, K. Nakakita, I. Sakata and T. Takano, “Emissions Reduction Potential of Extremely High Boost and High EGR Rate for an HSDI Diesel Engine and the Reduction Mechanisms of Exhaust Emissions,” in *SAE Paper 2008-01-1189*, 2008.
- [31] D. Six, T. Van Herzele, L. Vervaeke, M. Bastiaen, J. Galle, R. Sierens and S. Verhelst, “Development and Testing of an EGR System for Medium Speed Diesel Engines.,” in *SAE Paper 2012-01-0680*, 2012.
- [32] J. Lee, S. Choi, J. Lee, S. Shin, S. Lee, H. H. Song, K. Min and H. Choi, “Emission Reduction using a Close Post Injection Strategy with a Modified Nozzle and Piston Bowl Geometry for a Heavy EGR Rate.,” in *SAE Paper 2012-01-0681*, 2012.
- [33] T. Li, H. Ogawa, R. Moriwaki and T. Suzuki, “Effects of EGR and Pilot Injection on Characteristics of Combustion and Emissions of Diesel Engines

- with Low Ignitability Fuel.,” in *SAE Paper 2012-01-0853*, 2012.
- [34] lu, P., “investigation of gasoline partially premixed combustion in a single cylinder optical diesel engine. PhD Thesis.,” Brunel University, London, 2014.
- [35] Chatterjee S, Naseri M, Li J., “Heavy Duty Diesel Engine Emission Control to Meet BS VI Regulations.,” in *SAE Technical Paper.*, 2017.
- [36] Vinícius Bernardes Pedrozo, “An experimental study of ethanol-diesel dual-fuel combustion for high efficiency and clean heavy-duty engines. PhD Thesis.,” Brunel University, London, 2017.
- [37] Kamm S, Schraml S, MAN Truck & Bus AG., “Future Requirements & Challenges on Aftertreatment of Heavy Duty Diesel Engines Future Requirements & Challenges.,” in *Presentation at SAE 2016 Heavy-Duty Diesel Emissions Control Symposium*, Gothenburg, 2016.
- [38] Johnson T V., “Diesel Emissions in Review,” *SAE International Journal of Engines* , no. 4, 2011.
- [39] Johnson T, Joshi A, “Review of Vehicle Engine Efficiency and Emissions,” *SAE Technical Paper*, no. 1, 2017.
- [40] Hannes Kannisto, Volvo Penta, “Exhaust aftertreatment system – a cleaning process for exhausts,” 8 September 2016. [Online]. Available: <http://nordicblog.volvopenta.com/exhaust-aftertreatment-system-cleaning-process-exhausts/>. [Accessed 30 July 2017].
- [41] López - De Jesús YM, Chigada PI, Watling TC, Arulraj K, Thorén A, Greenham N, et al., “NO<sub>x</sub> and PM Reduction from Diesel Exhaust Using Vanadia SCRF®,” *International Journal of Engines*, vol. 9, no. 2, pp. 1247-1257, 2016.
- [42] Walker A, Johnson Matthey, “Catalyst-Based Emission Control Solutions for the Global HDD Market – What Does the Future Hold?,” in *Presentation at SAE 2016 Heavy-Duty Diesel Emissions Control Symposium*, Gothenburg, 2016.
- [43] Posada F, Chambliss S, Blumberg K., “Costs of emission reduction

- technologies for heavy-duty diesel vehicles.,” The ICCT White Paper, 2016.
- [44] Pedrozo VB, Zhao H., “Improvement in high load ethanol-diesel dual-fuel combustion by Miller cycle and charge air cooling.,” *Applied Energy*, vol. 210, pp. 138-151, 2018.
- [45] Dallmann T, Menon A., “Technology Pathways for Diesel Engines Used in Non-Road Vehicles and Equipment.,” The ICCT White Paper, 2016.
- [46] Hanson R, Ickes A, Wallner T., “Comparison of RCCI Operation with and without EGR over the Full Operating Map of a Heavy-Duty Diesel Engine.,” *SAE Technical Paper.*, 2016.
- [47] Environmental Protection Agency (EPA) - National Highway Traffic Safety Administration (NHTSA)- Department of Transportation (DOT)., “Greenhouse Gas Emissions and Fuel Efficiency Standards for Medium- and Heavy-Duty Engines and Vehicles - Phase 2,” Federal Register - Rules and Regulations 2016;81, 2016.
- [48] Zhao H., Advanced direct injection combustion engine technologies and development. Volume 2: Diesel engines., Cambridge: Woodhead Publishing, 2009.
- [49] Dec, J.E., “A Conceptual Model of DI Diesel Combustion Based on Laser-Sheet Imaging,” in *International Congress & Exposition*, Detroit, 1997.
- [50] Dec, John E., “Advanced compression-ignition engines—understanding the in-cylinder processes,” *Proceedings of the Combustion Institute*, vol. 32, no. 2, pp. 2727-2742, 2009.
- [51] Gary D. Neely, Shizuo Sasaki, Yiqun Huang, Jeffrey A. Leet and Daniel W. Stewart, “New Diesel Emission Control Strategy to Meet US Tier 2 Emissions Regulations,” *SAE Technical Paper.*, 2005.
- [52] Curran, S., Hanson, R., Barone, T., Storey, J., Wagner, R., “Performance of advanced combustion modes with alternative fuels: Reactivity controlled compression ignition case study,” Energy and Transportation Science Division, Oak Ridge National Laboratory, Oak Ridge, 2012.

- [53] Maria Grahn, Frances Sprei, "Future alternative transportation fuels," Chalmers University of Technology, Department of Energy and Environment, division of Physical, Gothenburg, Sweden, 2015.
- [54] F. Zhao, F., T.W. Asmus, D.N. Assanis, J.E. Dec., J.A. Eng., P.M. Najt, Homogeneous Charge Compression Ignition (HCCI) Engines: Key Research and Development Issues, SAE International, 2003.
- [55] M. Christensen, B. Johansson, B., "Influence of Mixture Quality on Homogeneous Charge Compression Ignition," in *SAE, International Fall Fuels and Lubricants Meeting and Exposition*, San Francisco, CA, 1998.
- [56] M. Christensen, B. Johansson, P. Amne'us, F. Mauss, "Supercharged Homogeneous Charge Compression Ignition," in *International Congress & Exposition*, Anaheim, California, 1998.
- [57] M. Sjo'berg, J.E. Dec, "Influence of Fuel Autoignition Reactivity on the High-Load Limits of HCCI Engines," in *SAE World Congress & Exhibition*, Detroit, 2008.
- [58] M. Christensen, A. Hultqvist, B. Johansson, "Demonstrating the Multi Fuel Capability of a Homogeneous Charge Compression Ignition Engine with Variable Compression Ratio," in *International Fuels & Lubricants Meeting & Exposition*, Dearborn, Michigan, 1999.
- [59] M. Christensen, B. Johansson, "Supercharged Homogeneous Charge Compression Ignition (HCCI) with Exhaust Gas Recirculation and Pilot Fuel," in *CEC/SAE Spring Fuels & Lubricants Meeting & Exposition*, Paris, France, 2000.
- [60] M. Yao, Z. Chen, Z. Zheng, B. zhang, Y. Xing, "Study on the controlling strategies of homogeneous charge compression ignition combustion with fuel of dimethyl ether and methanol," *Fuel*, vol. 85, no. 14-15, pp. 2046-2056, 2006.
- [61] P. Risberg, G. Kalghatgi, H.-E. A ° ngstro"m, F., "Auto-ignition quality of Diesel-like fuels in HCCI engines," in *2005 SAE Brasil Fuels & Lubricants Meeting*, Rio De Janeiro, Brasil, 2005.

- [62] N. Kaneko, H. Ando, H. Ogawa, N. Miyamoto, "Expansion of the Operating Range with In-Cylinder Water Injection in a Premixed Charge Compression Ignition Engine," in *Spring Fuels & Lubricants Meeting & Exhibition*, Detroit, 2002.
- [63] Zhao, H, HCCI and CAI Engines for the Automotive Industry, Cambridge, UK: Woodhead Publishing, 2007.
- [64] S. Onishi, S. H. Jo, K. Shoda, P. D. Jo, S. Kato, "Active Thermo-Atmosphere Combustion (ATAC) - A New Combustion Process for Internal Combustion Engines," in *1979 Automotive Engineering Congress and Exposition*, Detroit, 1979.
- [65] P.M. Najt, D. E. Foster, "Compression-ignited homogeneous charge combustion," in *SAE International Congress and Exposition*, Detroit, 1983.
- [66] Thring, R. H., "Homogeneous-charge compression-ignition (HCCI) engines," in *1989 SAE International Fall Fuels and Lubricants Meeting and Exhibition*, Baltimore, 1989.
- [67] J.O. Olsson, P. Tunest<sup>o</sup>al, B. Johansson, "Closed-loop control of an HCCI engine," in *SAE 2001 World Congress*, Detroit, 2001.
- [68] M. Stockinger, H. Sch<sup>o</sup>apert<sup>o</sup>ns, P. Kuhlmann, "Versuche an einem gemischansaugenden mitSelbsz<sup>u</sup>ndung," *MTZ - Motortechnische Zeitschrift*, vol. 53, 1992.
- [69] J. O. Olsson, O. Erlandsson, B. Johansson, "Experiments and simulation of a six-cylinder homogeneous charge compression ignition (HCCI) engine," in *International Fuels & Lubricants Meeting & Exposition*, Paris, France, 2000.
- [70] Mohammad Izadi Najafabadi, Nuraini Abdul Aziz, "Homogeneous Charge Compression Ignition Combustion: Challenges and Proposed Solutions," *Journal of Combustion*, vol. 2013, no. 1, p. 14, 2013.
- [71] Ryan TW, Callahan TJ., "Homogeneous charge compression ignition of diesel fuel," in *International Fuels & Lubricants Meeting & Exposition*, Kansas City, 1996.

- [72] Gowthaman S, Sathiyagnanam A.P, “A review of Homogeneous charge compression ignition (HCCI) engine,” *International Journal of Scientific & Engineering Research*, vol. 6, no. 1, pp. 779-798, 2015.
- [73] Bendu H, Murugan S., “Homogeneous charge compression ignition (HCCI) combustion: mixture preparation and control strategies in diesel engines.,” *Renewable and Sustainable Energy Reviews*, vol. 38, no. 1, pp. 732-746, 2014.
- [74] Saxena S, Schneider S, Aceves S, Dibble R., “Wet ethanol in HCCI engines with exhaust heat recovery to improve the energy balance of ethanol fuels.,” *Applied Energy*, vol. 98, no. 1, pp. 448-457, 2012.
- [75] Lu XC, Han D, Huang Z., “Fuel design and management for the control of advanced compression-ignition combustion modes.,” *Progress in Energy and Combustion Science*, vol. 37, no. 6, pp. 741-783, 2011.
- [76] Pravin Kumar, A. Rehman, “Homogeneous Charge Compression Ignition (HCCI) Combustion Engine- A Review,” *Journal of Mechanical and Civil Engineering*, vol. 11, no. 6, pp. 47-67, 2014.
- [77] Stanglmaier RH, Roberts CE., “Homogeneous charge compression ignition (HCCI) benefits, compromises and future engine applications.,” in *International Fuels & Lubricants Meeting & Exposition*, Dearborn, Michigan, 1999.
- [78] D. Goldman and A. S. Popel, “A computational study of the effect of capillary network anastomoses and tortuosity on oxygen transport,” *J. Theor. Biol.*, vol. 206, pp. 181-194, 2000.
- [79] M. Odaka, H. Suzuki, N. Koike and H. Ishii, “Search for Optimizing Control Method of Homogeneous Charge Diesel Combustion,” in *SAE Paper 1999-01-0184*, 1999.
- [80] H. Suzuki, N. Koike and M. Odaka, “Combustion Control Method of Homogeneous Charge Diesel Engines,” in *SAE Paper 980509*.
- [81] H. Ishii, N. Koike, H. Suzuki and M. Odaka, “Exhaust Purification of Diesel Engines by Homogeneous Charge with Compression Ignition Part 2: Analysis

- of Combustion Phenomena and NO<sub>x</sub> Formation by Numerical Simulation with Experiment.,” in *SAE Paper 970315*.
- [82] H. Suzuki, N. Koike, H. Ishii and M. Odaka, “Exhaust Purification of Diesel Engines by Homogeneous Charge with Compression Ignition Part 1: Experimental Investigation of Combustion and Exhaust Emission Behavior Under Pre-Mixed Homogeneous Charge Compression Ignition Method.,” in *SAE Paper 970313*.
- [83] Y. Iwabuchi, K. Kawai, T. Shoji, Y. Takeda, “Trial of New Concept Diesel Combustion System - Premixed Compression-Ignited Combustion,” in *International Congress & Exposition, Detroit, 1999*.
- [84] H. Akagawa, T. Miyamoto, A. Harada, S. Sasaki, N. Shimazaki, T. Hashizume, K. Tsujimura, “Approaches to Solve Problems of the Premixed Lean Diesel Combustion,” in *SAE Paper 1999-01-0183, 1999*.
- [85] Y. Takeda, N. Keiichi and N. Keiichi, “Emission Characteristics of Premixed Lean Diesel Combustion with Extremely Early Staged Fuel Injection.,” in *SAE Paper 961163*.
- [86] N. Shimazaki, H. Akagawa and K. Tsujimura, “An Experimental Study of Premixed Lean Diesel Combustion.,” in *SAE Paper 1999-01-0181, 1999*.
- [87] Y. Nishijima, Y. Asaumi and Y. Aoyagi, “Premixed Lean Diesel Combustion (PREDIC) using Impingement Spray System.,” in *SAE Paper 2001-01-1982, 2001*.
- [88] H. Yokota, Y. Kudo, H. Nakajima, T. Kakegawa and T. Suzuki, “A New Concept for Low Emission Diesel Combustion.,” in *SAE Paper 970891*.
- [89] B. Walter and B. Gatellier, “Development of the high power NADI (TM) concept using Dual Mode Diesel Combustion to Achieve Zero NO<sub>x</sub> and Particulate Emissions.,” in *SAE Paper 2002-01-1744, 2002*.
- [90] Y. Mase, J. Kawashima, T. Sato and M. Eguchi, “Nissan's New Multivalve DI Diesel Engine Series.,” in *SAE Paper 981039*.

- [91] S. Kimura, O. Aoki, Y. Kitahara and E. Aiyoshizawa, "Ultra-Clean Combustion Technology Combining a Low-Temperature and Premixed Combustion Concept for Meeting Future Emission Standards.," in *SAE Paper 2001-01-0200*, 2001.
- [92] H. Ogawa, S. Kimura, M. Koike and Y. Enomoto, "A Study of Heat Rejection and Combustion Characteristics of a Low-Temperature and Pre-Mixed Combustion Concept Based on Measurement of Instantaneous Heat Flux in a Direct-Injection Diesel Engine.," in *SAE Paper 2000-01-2792*, 2000.
- [93] Epping, K., Aceves, S.M., Bechtold, R.L., Dec, J.E., "The Potential of HCCI Combustion for High Efficiency and Low Emissions," in *SAE Powertrain & Fluid Systems Conference & Exhibition, Future Car Congress*, 2002.
- [94] Miyamoto, T., Hayashi, A. K., Harada, A., Sasaki, S., Hisashi, A., Tujimura, K., "A Computational Investigation of Premixed Lean Diesel Combustion - Characteristics of Fuel-Air Mixture Formation, Combustion and Emissions," in *International Congress & Exposition, Detroit*, 1999.
- [95] Zhao, H., Peng, Z., Williams, J., Ladommatos, N., "Understanding the Effects of Recycled Burnt Gases on the Controlled Autoignition (Cai) Combustion in Four-Stroke Gasoline Engines," in *SAE 2002 World Congress & Exhibition, SAE International Fall Fuels & Lubricants Meeting & Exhibition*, 2001.
- [96] S. M. Aceves, D. L. Flowers, F. Espinosa-Loza, A. Babajimopoulos, D. N. Assanis, "Analysis of Premixed Charge Compression Ignition Combustion with a Sequential Fluid Mechanics-Multizone Chemical Kinetics Model," in *2005 SAE World Congress, Detroit*, 2004.
- [97] Lechner GA, Jacobs T, Chryssakis C, Assanis DN, Siewert RM., "Evaluation of a narrow spray cone angle, advanced injection timing strategy to achieve partially premixed compression ignition combustion in a diesel engine.," in *SAE 2005 World Congress & Exhibition, Detroit*, 2005.
- [98] Fang T, Lee CF, Coverdill RE, White RA., "Smokeless combustion within a small-bore HSDI diesel engine using a narrow angle injector.," in *SAE World Congress & Exhibition, Detroit*, 2007.

- [99] R. Manimaran, R. Thundil Karuppa Raj, K. Senthil Kumar, “Premixed Charge Compression Ignition in a Direct Injection Diesel Engine using Computational Fluid Dynamics,” *WSEAS TRANSACTIONS on HEAT and MASS TRANSFER*, vol. 8, no. 1, pp. 17-29, 2013.
- [100] Taro Aoyama, Yoshiaki Hattori, Jun'ichi Mizuta, Yasuo Sato, “An Experimental Study on Premixed-Charge Compression Ignition Gasoline Engine,” in *International Congress & Exposition*, Detroit, 1996.
- [101] K. Inagaki, T. Fuyuto, K. Nishikawa, K. Nakakita, I. Sakata, “Dual-Fuel PCI Combustion Controlled by In-Cylinder Stratification of Ignitability,” in *SAE 2006 World Congress & Exhibition*, Detroit, 2006.
- [102] J. E. Dec, M. Sjöberg, “Isolating the Effects of Fuel Chemistry on Combustion Phasing in an HCCI Engine and the Potential of Fuel Stratification for Ignition Control,” in *SAE 2004 World Congress & Exhibition*, Detroit, 2004.
- [103] Ojeda, W. d., “Super Truck-Development and Demonstration of a Fuel-Efficient Class 8 Tractor & Trailer Engine Systems,” National Energy Technology Laboratory Department of Energy, WASHINGTON, D.C., 2013.
- [104] National Instruments Corporation., “Subsystems Required to Control Low Temperature Combustion Engines,” 20 April 2017. [Online]. Available: <http://www.ni.com/white-paper/13516/en/>. [Accessed 01 June 2017].
- [105] A. Gray, T.W. Ryan III, “Homogeneous Charge Compression Ignition (HCCI) of Diesel Fuel,” in *International Spring Fuels & Lubricants Meeting & Exposition*, Detroit, 1997.
- [106] T. Kamimoto, M. Bae, “High Combustion Temperature for the Reduction of Particulate in Diesel Engines,” in *SAE International Congress and Exposition*, Detroit, 1988.
- [107] K. Akihama, Y. Takatori, K. Inagaki, S. Sasaki, A.M. Dean, “Mechanism of the Smokeless Rich Diesel Combustion by Reducing Temperature,” in *SAE 2001 World Congress*, Detroit, 2001.
- [108] S. Kook, C. Bae, P.C. Miles, D. Choi, L.M. Pickett, “The Influence of Charge

- Dilution and Injection Timing on Low-Temperature Diesel Combustion and Emissions,” in *Powertrain & Fluid Systems Conference & Exhibition*, Toronto, 2005.
- [109] Mark P.B. Musculus, Paul C. Miles, Lyle M. Pickett, “Conceptual models for partially premixed low-temperature diesel combustion,” *Progress in Energy and Combustion Science*, vol. 39, no. 2-3, p. 246–283, 2013.
- [110] C. De Boer, J. Chang and S. Shetty, “Transonic Combustion - A Novel Injection-Ignition System for Improved Gasoline Engine Efficiency,” in *SAE 2010 Powertrains Fuels & Lubricants Meeting*, Rio de Janeiro, Brazil, 2010.
- [111] P. Zoldak, C. de Boer and S. Shetty, “Transonic Combustion - Supercritical Gasoline Combustion Operating Range Extension for Low Emissions and High Thermal Efficiency,” in *SAE 2012 World Congress & Exhibition*, Detroit, 2012.
- [112] Luis Padrela, Miguel A.Rodrigues, Sitaram P.Velaga, Henrique A.Matos, Edmundo Gomes de Azevedo, “Formation of indomethacin–saccharin cocrystals using supercritical fluid technology,” *European Journal of Pharmaceutical Sciences*, vol. 38, no. 1, pp. 9-17, 2009.
- [113] Bansal, Chhabile Sharan, “Transonic Engine,” Vellore Institute of Technology (VIT university), Vellore, India, 2015.
- [114] Martz, Jim, “THE BASICS OF CONVERTING DIESELS TO DUAL-FUEL OPERATION, Advanced electronic controls invigorate an established technology,” Diesel & Gas Turbine Publications, U.S.A., 2012.
- [115] Weaver, C., Turner, S., “Dual Fuel Natural Gas/Diesel Engines: Technology, Performance, and Emissions,” in *International Congress & Exposition*, San Diego, 1994.
- [116] Henham A, Makkar MK., “Combustion of simulated biogas in a dual-fuel diesel engine. Energy Conversion and Management,” *Energy Conversion and Management*, vol. 39, no. 16-18, pp. 2001-2009, 1998.
- [117] B.B. Sahoo a, N. Sahoo b, U.K. Saha b,, “Effect of engine parameters and type of gaseous fuel on the performance of dual-fuel gas diesel engines—A critical

- review,” *Renewable and Sustainable Energy Reviews*, vol. 13, no. 6-7, pp. 1151-1184, 2009.
- [118] OMI., Nwafor, “Combustion characteristics of dual-fuel diesel engine using pilot injection ignition.,” *Institution of Engineers (India) Journal*, vol. 84, no. 1, pp. 22-25, 2003.
- [119] R.G Papagiannakis, D.T Hountalas, “Combustion and exhaust emission characteristics of a dual fuel compression ignition engine operated with pilot Diesel fuel and natural gas,” *Energy Conversion and Management*, vol. 45, no. 18-19, pp. 2971-2987, 2004.
- [120] G.H. Abd Alla, H.A. Soliman, O.A. Badr, M.F. Abd Rabbo, “Effect of pilot fuel quantity on the performance of a dual fuel engine.,” *Energy Conversion and Management*, vol. 41, no. 6, pp. 559-572, 2000.
- [121] Shuaiying Ma, Zunqing Zheng, Haifeng Liu, Quanchang Zhang, Mingfa Yao, “Experimental investigation of the effects of diesel injection strategy on gasoline/diesel dual-fuel combustion,” *Applied Energy*, vol. 109, pp. 201-212, 2013.
- [122] Jesús Benajes, Santiago Molina, Antonio García, Eduardo Belarte, Michel Vanvolsem, “An investigation on RCCI combustion in a heavy duty diesel engine using in-cylinder blending of diesel and gasoline fuels,” *Applied Thermal Engineering*, vol. 63, pp. 66-76, 2014.
- [123] J. Li, W.M. Yang, H. An, D.Z. Zhou, W.B. Yu, J.X. Wang, L. Li, “Numerical investigation on the effect of reactivity gradient in an RCCI engine fueled with gasoline and diesel,” *Energy Conversion and Management*, vol. 92, p. 342–352, 2015.
- [124] S. L. Kokjohn, R. M. Hanson, D. A. Splitter and R. D. Reitz, “Experiments and Modeling of Dual-Fuel HCCI and PCCI Combustion using in-Cylinder Fuel Blending.,” in *SAE Paper 2009-01-2647*, 2009.
- [125] R. M. Hanson, S. L. Kokjohn, D. A. Splitter and R. D. Reitz, “An Experimental Investigation of Fuel Reactivity Controlled PCCI Combustion in a Heavy-Duty

- Engine.,” in *SAE Paper 2010-01-0864*, 2010.
- [126] C. S. Lee, K. H. Lee and D. S. Kim, “Experimental and numerical study on the combustion characteristics of partially premixed charge compression ignition engine with dual fuel.,” *Fuel*, vol. 82, pp. 553-560, 2003.
- [127] S. Ma, Z. Zheng, H. Liu, Q. Zhang and M. Yao, “Experimental investigation of the effects of diesel injection strategy on gasoline/diesel dual-fuel combustion.,” *Applied Energy*, vol. 109, pp. 202-212, 2013.
- [128] World Press, “BIO-ENERGY,” World Press, 5 April 2012. [Online]. Available: <https://biowesleyan.wordpress.com/first-generation-biofuels/ethanol/case-study-brazil/sugarcane-vs-corn-based-ethanol/>. [Accessed 15 January 2018].
- [129] Jason Hill, Erik Nelson, David Tilman, Stephen Polasky, Douglas Tiffany, “Environmental, economic, and energetic costs and benefits of biodiesel and ethanol biofuels,” *PNAS, Proceedings of the National Academy of Sciences of the United States of America*, vol. 103, no. 30, pp. 11206-11210, 2006.
- [130] Owen, K., Coley., C.S. Weaver, *Automotive Fuels Reference Book*, Society of Automotive Engineers, 1995.
- [131] Janet Yanowitz, Robert L. McCormick, “Effect of E85 on Tailpipe Emissions from Light-Duty,” *Journal of the Air & Waste Management Association*, vol. 59, no. 2, pp. 172-182, 2009.
- [132] Kelly, K., Bailey, B., Coburn, T., Clark, W. et al., “Federal Test Procedure Emissions Test Results from Ethanol Variable-Fuel Vehicle Chevrolet Lumina,” in *SAE, International Fuels & Lubricants Meeting & Exposition*, Orlando, 1996.
- [133] Brinkman, N., Halsall, R., Jorgensen, S.W., & Kirwan, J.E., “The Development Of Improved Fuel Specifications for Methanol (M85) amd Ethanol (Ed85),” in *SAE, International Congress & Exposition*, Chicago, 1994.
- [134] Saylor.org, “Alcohol fuel,” [Online]. Available: <https://www.saylor.org/site/wp-content/uploads/2011/06/Alcohol-Fuel.pdf>. [Accessed 01 May 2017].

- [135] Erjavec, Jack, *Automotive Technology: A Systems Approach*, Clifton Park, N.Y.: Delmar Cengage Learning, 2009.
- [136] The Sydney Morning Herald., “NSW to mandate ethanol in petrol,” *The Sydney Morning Herald.*, p. 1, 11 May 2007.
- [137] Alan C. Hansen, Qin Zhang, Peter W.L. Lyne, “Ethanol–diesel fuel blends—a review,” *Bioresource Technology*, vol. 96, no. 3, pp. 277-285, 2005.
- [138] “Biofuel Mandates in the EU by Member State in 2017,” USDA Foreign Agricultural Service, Berlin, 2017.
- [139] Isaias C. Macedo, Joaquim E.A. Seabra, Joao E.A.R. Silva, “Green house gases emissions in the production and use of ethanol from sugarcane in Brazil: The 2005/2006 averages and a prediction for 2020,” *Biomass and Bioenergy*, vol. 32, no. 7, pp. 582-595, 2008.
- [140] Suani Teixeira Coelho, José Goldemberg, Oswaldo Lucon, and Patricia Guardabassi, “Brazilian sugarcane ethanol: lessons learned,” *Energy for Sustainable Development*, vol. 10, no. 2, pp. 26-39, 2006.
- [141] Christine L. Crago, Madhu Khanna, Jason Barton, Eduardo Giuliani, Weber Amaral, “Competitiveness of Brazilian sugarcane ethanol compared to US corn ethanol,” *Energy Policy*, vol. 38, no. 11, p. 7404–7415, 2010.
- [142] Zhongyi JIANG, Hong WU , Songwei XU , Shufang HUANG, “ENZYMATIC CONVERSION OF CARBON DIOXIDE TO METHANOL BY DEHYDROGENASES ENCAPSULATED IN SOL-GEL MATRIX,” *Fuel Chemistry Division Preprints*, vol. 1, no. 47, p. 306, 2002.
- [143] Bob Flach, Sabine Lieberz, Antonella Rossetti, “EU Biofuels Annual 2017 Report,” United States Department of Agriculture (USDA), Washington, D.C., 2017.
- [144] EIA, U.S. Energy Information Administration, “Monthly Energy Review,” *Monthly Energy Review March 2017*, p. 155, 21 March 2017.
- [145] Anthony Maciorowski, EPA, Notice Of Decision Granting A Partial Waiver, “Partial Grant of Clean Air Act Waiver Application Submitted by Growth

Energy To Increase the Allowable Ethanol Content of Gasoline to 15 Percent; Decision of the Administrator,” *U.S. Federal Register*, vol. 76, no. 17, pp. 4662-4683, 26 January 2011.

- [146] Knoll, K., B. West, W. Clark, R. Graves, J. Orban, S. Przesmitzki, and T. Theiss, “Effects of Intermediate Ethanol Blends on Legacy Vehicles and Small Non-Road Engines,” National Renewable Energy Laboratory, Golden, Colorado, 2009.
- [147] ASTM International, *Standard Specification for Ethanol Fuel Blends for Flexible-Fuel Automotive Spark-Ignition Engines*, West Conshohocken: ASTM International, 2011.
- [148] General Motors, “2014 Chevrolet Silverado Specifications,” 2016. [Online]. Available:  
<http://media.gm.com/media/us/en/chevrolet/vehicles/silverado/2014.tab1.html>. [Accessed 01 July 2017].
- [149] Thomas, J. F., S. P. Huff, B. H. West, “Fuel Economy and Emissions of a Vehicle Equipped with an Aftermarket Flexible-Fuel Conversion Kit,” OAK RIDGE NATIONAL LABORATORY, Oak Ridge, 2012.
- [150] Thomas, J., B. West, S. Huff, “Effects of High-Octane Ethanol Blends on Four Legacy Flex-Fuel Vehicles, and a Turbocharged GDI Vehicle,” OAK RIDGE NATIONAL LABORATORY, Oak Ridge, Tennessee, 2015.
- [151] U.S. Department of energy. The official U.S. government source for fuel Economy information, EPA, “Ethanol,” U.S. Department of energy. The official U.S. government source for fuel Economy information, EPA, [Online]. Available: [www.fueleconomy.gov/feg/ethanol.shtml](http://www.fueleconomy.gov/feg/ethanol.shtml). [Accessed 01 July 2017].
- [152] U.S. Department of Energy, Energy Efficiency and renewable Energy, United States Environmental Protection Agency, Office of Transportation and Air Quality, “fueleconomy.gov,” 2017. [Online]. Available: <http://www.fueleconomy.gov>. [Accessed 01 May 2017].
- [153] Hannu Jääskeläinen, “Ethanol-Diesel Blends,” DieselNet.com, 2016.

- [154] Nord, A.J., J.T. Hwang, W.F. Northrop, “Emissions from a Diesel Engine Operating in a Dual-Fuel Mode Using Port-Fuel Injection of Heated Hydrous Ethanol,” *Proceedings of the ASME 2015 Internal Combustion Engine Division Fall Technical Conference ICEF2015*, vol. 1, p. 9, 2015.
- [155] J Kashdan, B Thirouard, “Optical Engines as Representative Tools in the Development of New Combustion Engine Concepts,” *Oil & Gas Science and Technology – Rev. IFP Energies nouvelles*, vol. 66, no. 5, pp. 759 - 777, 2011.
- [156] Kashdan J.T., Mendez S., Bruneaux G., “On the Origin of Unburned Hydrocarbon Emissions in a Wall-Guided, Low NO<sub>x</sub> Diesel Combustion System,” in *JSAE/SAE International Fuels & Lubricants Meeting*, Kyoto, Japan, 2007.
- [157] Kashdan J.T., Anselmi P., Walter B., “Advanced Injection Strategies for Controlling Low-Temperature Diesel Combustion & Emissions,” in *SAE, Powertrains, Fuels and Lubricants Meeting*, Florence, Italy, 2009.
- [158] Hwang W., Dec J.E., Sjöberg M., “Spectroscopic and Chemical-Kinetic Analysis of the Phases of HCCI Autoignition and Combustion for Single- and Two-Stage Ignition Fuels,” *Combustion and Flame*, vol. 154, no. 3, pp. 387-409, 2008.
- [159] Nicolas Dronniou, Julian Kashdan, Bertrand Lecointe, Kyle Sauve, Dominique Soleri, “Optical Investigation of Dual-fuel CNG/Diesel Combustion Strategies to Reduce CO<sub>2</sub> Emissions,” *SAE International Journal of Engines*, vol. 1, no. 1313, pp. 873-887, 2014.
- [160] Changzhao Jiang, Xiao Ma, Hongming Xu, Steve Richardson, “An Optical Study of DMF and Ethanol Combustion Under Dual-Injection Strategy,” *SAE International*, vol. 1, no. 1237, 2012.
- [161] Matthew Blessinger, Joshua Stein, Jaal Gandhi, “An Optical Investigation of Fuel Composition Effects in a Reactivity Controlled HSDI Engine,” *SAE International*, vol. 1, no. 691, pp. 516-525, 2012.
- [162] Volker Sick, Michael C. Drake, Todd D. Fansler, “High-speed imaging for

- direct-injection gasoline engine research and development,” *Experiments in Fluids*, vol. 49, no. 4, pp. 937-947, 2010.
- [163] M. R. Herfatmanesh, P. Lu, M. A. Attar, H. Zhao, “Experimental investigation into the effects of two-stage injection on fuel injection quantity, combustion and emissions in a high-speed optical common rail diesel engine,” *Fuel*, vol. 109, no. 1, pp. 137-147, 2013.
- [164] C. Arcoumanis, A. Hadjiapostolou and J. Whitelaw, “Flow and Combustion in a Hydra Direct-Injection Diesel Engine,” in *SAE, International Congress & Exposition*, Detroit, 1991.
- [165] M. Lai, N. A. Henein, X. Xie, T. Chue, Y. Itoh and W. Bryzik, “Diesel Cold-Starting Study using Optically Accessible Engines,” in *1995 SAE International Fall Fuels and Lubricants Meeting and Exhibition*, Toronto, 1995.
- [166] N. Shimazaki, H. Hatanaka, K. Yokota and T. Nakahira, “A Study of Diesel Combustion Process Under the Condition of EGR and High-Pressure Fuel Injection with Gas Sampling Method,” in *International Congress & Exposition*, Detroit, Michigan, 1996.
- [167] I. Yamaguchi, T. Nakahira, M. Komori, S. Kobayashi, “An Image Analysis of High Speed Combustion Photographs for DI Diesel Engine with High Pressure Fuel Injection,” in *SAE, International Off-Highway & Powerplant Congress & Exposition*, Milwaukee, Wisconsin, 1990.
- [168] R. S. G. Baert, D. E. Beckman, A. Veen, “Efficient EGR Technology for Future HD Diesel Engine Emission Targets,” Society of Automotive Engineers, 1999.
- [169] Sison, K., “In-cylinder Studies of Diesel Combustion with Oxygenated Fuels and Multiple Injections. PhD Thesis,” Brunel University, London, 2006.
- [170] LUND UNIVERSITY, “Internal combustion engines,” LUND UNIVERSITY, 06 11 2015. [Online]. Available: <http://www.forbrf.lth.se/english/research/applications-in-combustion-devices/internal-combustion-engines/>. [Accessed 31 March 2017].
- [171] Jeroen Wehmeijer, Bert van Geest, “High-speed imaging: Image

- intensification,” *Nature Photonics*, vol. 4, no. 1, pp. 152-153, 2010.
- [172] Fuji Electric Co. Ltd., “Gas Analyzers Operating principles,” Fuji Electric Co. Ltd., 2017. [Online]. Available: [https://www.fujielectric.com/products/instruments/products/anlz\\_gas/genri.html](https://www.fujielectric.com/products/instruments/products/anlz_gas/genri.html). [Accessed 01 May 2017].
- [173] Harvey, David, “12.4: Gas Chromatography,” 28 July 2017. [Online]. Available: [https://chem.libretexts.org/Textbook\\_Maps/Analytical\\_Chemistry\\_Textbook\\_Maps/Map%3A\\_Analytical\\_Chemistry\\_2.0\\_\(Harvey\)/12\\_Chromatographic\\_and\\_Electrophoretic\\_Methods/12.4%3A\\_Gas\\_Chromatography](https://chem.libretexts.org/Textbook_Maps/Analytical_Chemistry_Textbook_Maps/Map%3A_Analytical_Chemistry_2.0_(Harvey)/12_Chromatographic_and_Electrophoretic_Methods/12.4%3A_Gas_Chromatography). [Accessed 30 July 2017].
- [174] K2BW Environmental Equipment Co., “CHEMILUMINESCENCE NO / NOX GAS ANALYSIS,” 2013. [Online]. Available: [http://www.k2bw.com/5\\_c\\_31.htm](http://www.k2bw.com/5_c_31.htm). [Accessed 30 July 2017].
- [175] Teledyne Hastings Instruments, A Teledyne Technologies Company, “Teledyne Hastings Instruments INSTRUCTION MANUAL 200/202 SERIES FLOWMETERS/CONTROLLERS,” TELEDYNE HASTINGS INSTRUMENTS, HAMPTON, VIRGINIA, 2011.
- [176] Joel, R., *Basic Engineering Thermodynamics*, 5th edition, London: LONGMAN, 1996.
- [177] Withrow, G. M. Rassweiler and L., “Motion Pictures of Engine Flames Correlated with Pressure Cards,” in *Annual Meeting of the Society*, Canada, 1938.
- [178] Zhao, Hua; Ladommatos, N., “Engine combustion instrumentation and diagnostics,” in *Society of Automotive Engineers*, Warrendale, PA, 2001.
- [179] Zhang, H., “Experimental investigation of gasoline-Dimethyl Ether dual fuel CAI combustion with internal EGR. PhD Thesis.,” Brunel University, London, 2011.
- [180] D'Alleva, B. A., “Procedure and Charts for Estimating Exhaust Gas Quantities

- and Compositions.,” Research Laboratories, General Motors Corporation, 1960.
- [181] Eltinge, L., “Fuel-Air Ratio and Distribution from Exhaust Gas Composition,” in *1968 Automotive Engineering Congress and Exposition*, 1968.
- [182] Spindt, R. S., “Air-Fuel Ratios from Exhaust Gas Analysis,” in *SAE Mid-Year Meeting*, 1965.
- [183] Brettschneider, J., “Berechnung des luftverhältnisses lambda von luft-kraftstoffgemischen und des einflusses von messfehlern auf lambda,” *BOSCH TECH BER*, vol. 6, 1979.
- [184] Simons, W., “Berechnungen zur Bestimmung der Luftzahl bei Ottomotoren,” *MTZ Motortechnische Zeitschrift*, vol. 46, pp. 257-259, 1985.
- [185] Fukui, Y. Tamura, S. Omori and S. Saitoh, “Accuracy of A/F Calculation from Exhaust Gas Composition of SI Engines,” in *Passenger Car Meeting & Exposition*, Dearborn, Michigan, 1989.
- [186] Vinícius B. Pedrozo, Ian May, Thompson D.M. LanzaNova, HuaZhao, “Potential of internal EGR and throttled operation for low load extension of ethanol–diesel dual-fuel reactivity controlled compression ignition combustion on a heavy-duty engine,” *Fuel*, vol. 179, p. 391–405, 2016.
- [187] European Biomass Industry Association, “BIOETHANOL IN THE WORLD,” European Biomass Industry Association, 2017. [Online]. Available: [www.eubia.org/cms/wiki-biomass/biofuels-for-transport/bioethanol](http://www.eubia.org/cms/wiki-biomass/biofuels-for-transport/bioethanol). [Accessed 01 September 2017].
- [188] U.S. Environmental Protection Agency, “Gasoline Standards,” EPA, 25 1 2018. [Online]. Available: <https://www.epa.gov/gasoline-standards/gasoline-reid-vapor-pressure>. [Accessed 1 3 2018].
- [190] U.S. Energy Information Administration, “EIA.gov,” 12 April 2017. [Online]. Available: [https://www.eia.gov/dnav/pet/PET\\_PRI\\_GND\\_DCUS\\_NUS\\_W.htm](https://www.eia.gov/dnav/pet/PET_PRI_GND_DCUS_NUS_W.htm). [Accessed 01 May 2017].
- [191] air-quality, “Motor Vehicle Emission Controls: Fuel Types,” [air-quality.org](http://www.air-quality.org), [Online]. Available: <http://www.air-quality.org.uk/26.php>. [Accessed May

2017].

- [192] AVL LIST GmbH, "AVL Smoke Meter," 2017. [Online]. Available: <https://www.avl.com/-/avl-smoke-meter>. [Accessed 30 July 2017].
- [193] Noguchi M, Tanaka Y, Tanaka T, Takeuchi Y, "A Study on Gasoline Engine Combustion by Observation of Intermediate Reactive Products during Combustion," in *1979 SAE International Off-Highway and Powerplant Congress and Exposition*, 1979.
- [194] Dolenc, A., "The injection equipment of future high speed DI diesel engine with respect to power and pollution requirement.," IMechE lecture, London, U.K., 1990.
- [195] Nehmer, D., Reitz, R., "Measurement of the Effect of Injection Rate and Split Injections on Diesel Engine Soot and NOx Emissions," in *International Congress & Exposition*, Detroit, MI, U.S.A., 1994.
- [196] Nehmer, D., Reitz, R., "Measurement of the Effect of Injection Rate and Split Injections on Diesel Engine Soot and NOx Emissions.," in *International Congress & Exposition*, Detroit, 1994.
- [197] Tow, T.C., Pierpont, D.A., Reitz, R.D., "Reducing Particulate and NOx Emissions by Using Multiple Injections in a Heavy Duty D.I. Diesel Engine.," in *International Congress & Exposition*, Detroit, MI, U.S.A., 1994.
- [198] Pierpont, D.A., Montgomery, D.T., Reitz, R.D., "Reducing Particulate and NOx Using Multiple Injections and EGR in a D.I. Diesel," in *International Congress & Exposition*, Detroit, MI, U.S.A., 1995.
- [199] Minami, T., Takeuchi, K., Shimazaki, "Reduction of Diesel Engine NOx Using Pilot Injection.," in *International Congress & Exposition*, Detroit, MI, U.S.A., 1995.
- [200] Farrell, P.V., Chang, C.T., Su, T.F., "High Pressure Multiple Injection Spray Characteristics," in *International Congress & Exposition*, Detroit, MI, U.S.A., 1996.

- [201] Han, Z., Uludogan, A.N., Hampson, G.J., Reitz, R.D., “Mechanism of Soot and NOx Emission Reduction Using Multiple-injection in a Diesel Engine,” in *International Congress & Exposition*, Detroit, MI, U.S.A., 1996.
- [202] Zambare, V.V., Winterbone, D.E., “A Photographic Investigation of Multi-Stage Fuel Injection in a Single Cylinder DI Diesel Engine,” in *International Fuels & Lubricants Meeting & Exposition*, Dearborn, Michigan, 1999.
- [203] Koyanagi, K., Oing, H., Renner, G., Maly, R., “Optimizing Common Rail-Injection by Optical Diagnostics in a Transparent Production Type Diesel Engine.,” in *International Fuels & Lubricants Meeting & Exposition*, Dearborn, Michigan, 1999.
- [204] Mbarawa M, Milton BE, Casey RT, “An investigation of the effects of diesel pilot injection parameters on natural gas combustion under diesel conditions.,” *Journal of the Institute of Energy*, vol. 74, no. 500, pp. 81-90, 2001.
- [205] Zhang, Y., Ito, T., Nishida, K., “Characterization of Mixture Formation in Split-Injection Diesel Sprays via Laser Absorption-Scattering (LAS) Technique,” in *Spring Fuels & Lubricants Meeting & Exhibition, SAE International Fall Fuels & Lubricants Meeting & Exhibition*, Detroit, MI, U.S.A., 2001.
- [206] Montgomery, D.T., Reitz, R.D., “Effects of Multiple Injections and Flexible Control of Boost and EGR on Emissions and Fuel Consumption of a Heavy-Duty Diesel Engine,” in *SAE 2001 World Congress*, Detroit, MI, U.S.A., 2001.
- [207] Makame Mbarawa, Brain Edward Milton, Robert Thomas Casey, “Experiments and modelling of natural gas combustion ignited by a pilot diesel fuel spray.,” *International Journal of Thermal Sciences*, vol. 40, no. 10, pp. 927-936, 2001.
- [208] Mansour C, Bounif A, Aris A, Gaillard F., “Gas–diesel (dual-fuel) modelling in diesel engine environment.,” *International Journal of Thermal Science*, vol. 40, no. 4, pp. 409-424, 2001.
- [209] Erlandsson, O., “Early swedish hot-bulb engines—efficiency and performance compared to contemporary gasoline and diesel engines,” in *SAE 2002 World Congress & Exhibition*, Detroit, 2002.

- [210] Kitamura T, Ito T, Senda J, Fujimoto H., “Mechanism of smokeless diesel combustion with oxygenated fuels based on the dependence of the equivalence ratio and temperature on soot particle formation.,” *International Journal of Engine Research*, vol. 3, no. 4, pp. 223-248, 2002.
- [211] Ricaud, J.C., Lavoisier, F., “Optimizing the Multiple Injection Settings on an HSDI Diesel Engine.,” *Thermo- and Fluid Dynamic Processes in Diesel Engines 2*, vol. 2, no. 1, pp. 199-234, 2002.
- [212] Jun D, Ishii K, Iida N., “Combustion analysis of natural gas in four stroke HCCI engine using experiment and elementary reactions calculation.,” in *SAE 2003 World Congress & Exhibition*, Detroit, 2003.
- [213] Zhang, Y., Nishida, K., “Vapor/Liquid Behaviors in Split-Injection D.I. Diesel Sprays in a 2-D Model Combustion Chamber,” in *2003 JSAE/SAE International Spring Fuels and Lubricants Meeting*, Yokohama, Japan, 2003.
- [214] Bach C, Lammle C, Bill R, Soltic P, Dyntar D, Janner P, et al., “Clean engine vehicle. A natural gas driven EURO 4/SULEV with 30% reduced CO2 emissions,” in *SAE 2004 World Congress & Exhibition*, Detroit, 2004.
- [215] Juneja, H., Ra, Y., Reitz, R.D., “Optimization of Injection Rate Shape Using Active Control of Fuel Injection.,” in *SAE 2004 World Congress & Exhibition*, Detroit, MI, USA, 2004.
- [216] Shayler, P.J., Ng, H.K., “Simulation Studies of the Effect of Fuel Injection Pattern on NO and Soot Formation in Diesel Engines,” in *SAE 2004 World Congress & Exhibition*, Detroit, MI, U.S.A., 2004.
- [217] Tanabe, K., Kohketsu, S., Nakayama, S., “Effect of Fuel Injection Rate Control on Reduction of Emissions and Fuel Consumption in a Heavy Duty DI Diesel Engine.,” in *SAE 2005 World Congress & Exhibition*, Detroit, MI, USA, 2005.
- [218] Liu, Y., Reitz, R.D., “Optimizing HSDI Diesel Combustion and Emissions Using Multiple Injection Strategies,” in *SAE 2005 World Congress & Exhibition*, Detroit, MI, U.S.A., 2005.
- [219] Shayler, P.J., Brooks, T.D., Pugh, G.J., Gambrill, R., “The Influence of Pilot

- and Split-Main Injection Parameters on Diesel Emissions and Fuel Consumption,” in *SAE 2005 World Congress & Exhibition*, Detroit, MI, U.S.A., 2005.
- [220] Haeng Muk Choa, Bang-Quan He, “Spark ignition natural gas engines-A review,” *Energy Conversion and Management*, vol. 48, no. 2, pp. 608-618, 2007.
- [221] Sclar, Deanna, *Auto Repair For Dummies*, John Wiley & Sons, 2008.
- [222] Johnson, Tim, “Diesel Engine Emissions and Their Control,” *Platinum Metals Review*, vol. 53, no. 1, pp. 23-37, 2008.
- [223] Gill, K., Zhao, H., “In-cylinder Studies of Fuel Injection and Combustion from a Narrow Cone Fuel Injector in a High Speed Single Cylinder Optical Engine,” in *2008 SAE International Powertrains, Fuels and Lubricants Congress*, Shanghai, China, 2008.
- [224] Mustafa Balat, Havva Balat, Cahide Öz., “Progress in bioethanol processing,” *Progress in Energy and Combustion Science*, vol. 34, no. 5, pp. 551-573, 2008.
- [225] Lee, S., Choi H., Chung J., “The Effects of Injection Timing and Piston Bowl Shape on PHCCI Combustion with Split injections,” in *SAE 2010 World Congress & Exhibition*, Detroit, MI, U.S.A., 2010.
- [226] T. Korakianitis, A.M. Namasivayam, R.J. Crookes, “Natural-gas fueled spark-ignition (SI) and compression-ignition (CI) engine performance and emissions,” *Progress in Energy and Combustion Science*, vol. 37, no. 1, pp. 89-112, 2011.
- [227] Chris Ebbs, Martin Saarinen, “Auto Express UK,” 25 Aug 2017. [Online]. Available: <http://www.autoexpress.co.uk/car-news/consumer-news/90816/euro-6-emissions-standards-what-do-they-mean-for-you>. [Accessed 30 Aug 2017].
- [228] Chatterjee S, Naseri M, Li J, “Heavy Duty Diesel Engine Emission Control to Meet BS VI Regulations,” *SAE Technical Paper*, no. 26, 2017.
- [229] Herfatmanesh, M.R., “Investigation Of Single And Split Injection Strategies In An Optical Diesel Engine. PhD Thesis.,” Brunel University, London, 2010.



## Appendix 1: Software Screenshots

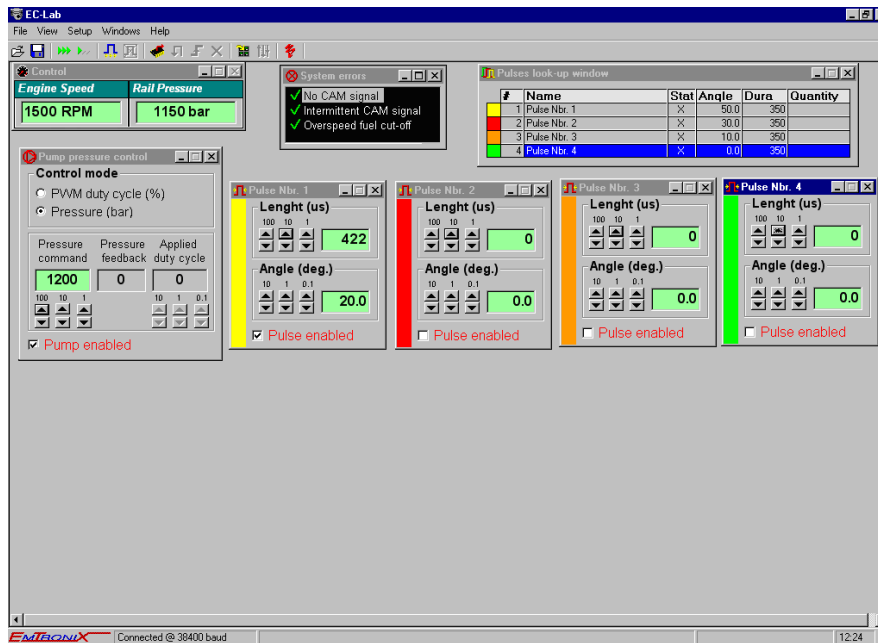


Figure A1.0.1 Screenshot of EC-Lab Software

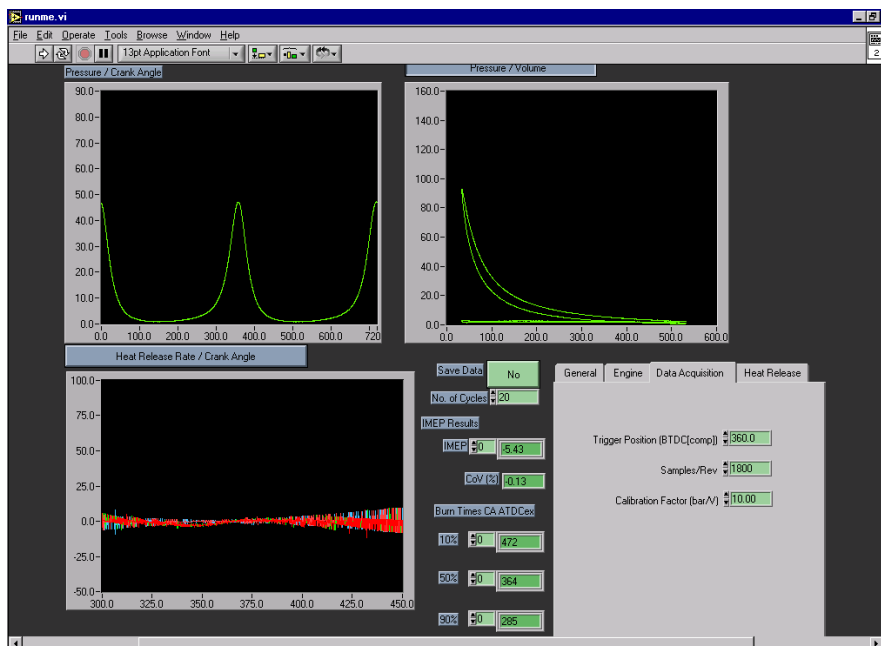
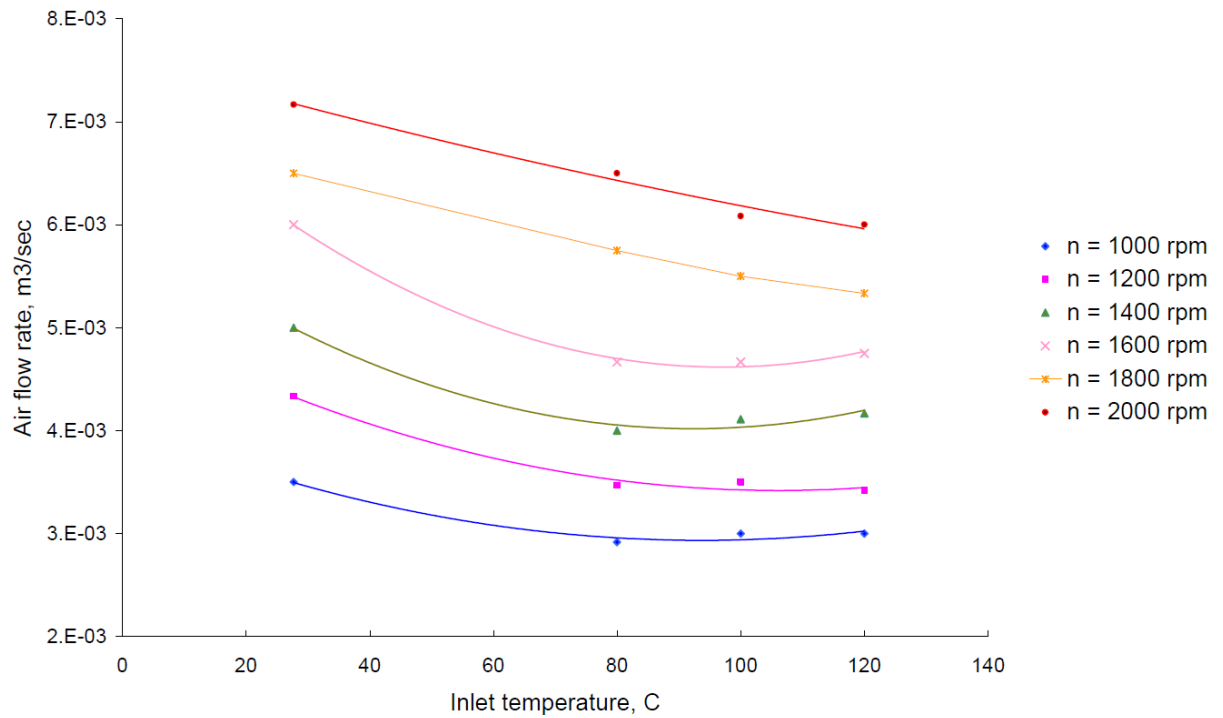


Figure A1.0.2 Screenshot of Data Acquisition Software

Screenshots from the control and data acquisition programs used for this study to control fuel injection and to collect data, respectively, as discussed in Section 3.3.2.

## Appendix 2: Hydra Airflow Rate Graph



*Figure A2.0.1 Hydra Airflow Rate Graph [169]*

The graph of Figure A2.0.1 illustrates the flow rate of the Ricardo Hydra Optical Research Diesel Engine used in this study, as discussed in Section 3.6.

## Appendix 3: Diesel fuel specification

PHILLIPS 66 LIMITED / JET :- UK MARKETING SPECIFICATION



**SULPHUR FREE (MAXIMUM 10 PPM) GAS OIL TO BS 2869:2010-PART 1: CLASS A2**

PROPERTY & UNITS	LIMIT		TEST METHOD Note (1)
	Typical Range	Free from visible water and sediment	
Appearance		Free from visible water and sediment	Visual
Colour		Red	Visual
Odour		Merchantable	
Density @ 15C (kg/m <sup>3</sup> )	Typical Range	820.0 - 875.0	BS EN ISO 3675 / 12185
<b>Cold Filter Plugging Point</b>			BS EN 116
Winter C (Note 2)	Max	-12	
Summer C (Note 2)	Max	-4	
<b>Cloud Point</b>			ASTM D2500 / IP219
Winter C (Note 2)	Max	-2	
Summer C (Note 2)	Max	+3	
Flash Point (PMCC) C	Min	56	BS EN ISO 2719
Cetane Number / DCN or Cetane Index	Min	45.0 (Note 5)	BS EN ISO 5165 / BS 2000-498
	Min	45.0 (Note 5)	BS EN ISO 4264
Kinematic viscosity mm <sup>2</sup> /s @ 40C	Min - max	2.00 - 5.00	BS EN ISO 3104
<b>Sulphur content (mg/kg)</b>			BS EN ISO 20846 / 20884
At point of manufacture	Max	10 (Note 8)	
At point of distribution to end user	Max	20 (Note 8)	
Copper Corrosion (3 Hr @ 50C)	Class	1	BS EN ISO 2160
Carbon Residue (micro) :- Residue wt% on 10% Bottoms	Max	0.30	BS EN ISO 10370
Ash content % (m/m)	Max	0.01	BS EN ISO 6245
Particulate content (mg/kg)	Max	24	IP 415
Water content (mg/kg)	Max	200	BS EN ISO 12937
<b>Distillation C</b>			BS EN ISO 3405
% Vol Rec @ 350C	Min	85	
% Vol Rec @ 250C	Max	65	
50% Vol Recovered (Note 3)	Range	240 - 340	
Strong Acid Number (mgKOH/g)		Zero	BS ISO 6618
Lubricity (wear scar dia, micron)	Max	460	BS 2000 - 450
<b>Oxidation stability</b>			BS 2000-388
0.0% - 7.0% FAME g/m <sup>3</sup> (Note 6)	Max	25	BS EN 15751
2.0% - 7.0% FAME h	Min	20	
FAME content (%w/v) (Note7)	Max	7.0	BS EN 14078
<b>Notes.</b>			
1) Latest Test Methods or technical equivalent used		5) May contain an Ignition improver in which case (i) the carbon residue test is not valid and (ii) the cetane number minimum will apply.	
2) Unless otherwise advised the following seasonal dates apply ex refinery or Import terminal:- Summer : 16 March - 15 October Inc Winter : 16 October - 15 March Inc Winter : 01 November - 15 March Inc for delivery from terminals		6) This test applies to all fuels, additional Rancimat only applies to those fuels containing > 2.00% FAME	
3) 50 % evaporated is an HMRC requirement.		7) FAME must meet BS EN 14214	
4) Product will be marked with HMR&C statutory marker		8) 10/20 ppm sulphur limits applicable from 1 January 2011	
<b>THIS SPECIFICATION IS ACCURATE AT THE DATE OF ISSUE, AND SUPERSEDES ALL PREVIOUS ISSUES.</b>			

PQ Issue 6 : July 2012

Figure A3.0.1 Diesel fuel specification

# Appendix 4: Diesel fuel analysis

**Intertek** Sunbury Technology Centre

ITS Testing Services (UK) Ltd  
 Sunbury Technology Centre  
 Unit 'A' Shears Way  
 Brooklands Close  
 Sunbury-on-Thames  
 Middlesex TW16 7EE  
 Tel : 01932 73 2100  
 Fax : 01932 73 2113

To: John Williams BP Global Fuels Technology Castrol Technology Centre Whitchurch Hill Pangbourne Reading RG8 7QR	Report No. Date:  Phoenix No. Order No. Quote No. Date Sample(s) Received Total Cost for Analysis	RT/FLS/5142 06/10/2014  UK760-0017458 4500083403 Email 08/09/2014 £394.00
---	--	--

## Diesel Analysis Report

Lab Sample No: FST-264556  
 Sample Description: Brunel University Diesel sample

ANALYSIS	RESULTS	UNITS
D5291 (MT/ELE/13) Carbon Content	86.3	% wt/wt
D5291 (MT/ELE/13) Hydrogen Content	13.2	% wt/wt
D5622 (MT/ELE/21) Oxygen Content*	0.16	% wt/wt
IP12 Gross Calorific Value <sup>#</sup>	45.58	MJ/kg

\* Test not UKAS accredited  
<sup>#</sup> Test carried out in another Intertek Laboratory

Analysis has been carried out on samples as received, independent of sampling procedure, using the latest versions of all test methods. Samples will be disposed of after 1 month unless alternative arrangements have been made in agreement with the customer.

Reported By: A. Shadrake  
 Alison Shadrake  
 Fuels Analyst

Checked By: J.A. AMERO  
 James Amero  
 Section Head, Fuels and Lubricants

Contact No.: +44(0)1932 732 157



Figure A4.0.1 Diesel fuel analysis

## Appendix 5: Ethanol fuel specification



### Ethanol 100% BP/EP

This Product has been tested and conforms to the current BP 2017 / EP 9.0 monographs.

Definition	Content: NLT 99.5% V/V @ 20 °C	
Characteristics Appearance Solubility  Boiling Point	Colourless, clear, volatile, flammable liquid, hygroscopic Miscible with water & methylene chloride It burns with a blue, smokeless flame About 78 °C	
Identification	Relative density: 0.790 – 0.793 Infrared Absorption	
Acidity or Alkalinity	The solution is pink (30 ppm, expressed as acetic acid)	
Absorbance (5cm Cell)	240 nm	NMT 0.40
	250-260 nm 270-340 nm	NMT 0.30 NMT 0.10
	Spectrum shows steadily descending curve with no peaks or shoulders	
Volatile impurities (V/V)	Methanol	NMT 200 ppm
	Acetaldehyde and acetal	NMT 10 ppm, expressed as acetaldehyde
	Benzene	NMT 2 ppm
	Total of other impurities Disregard limit	NMT 300 ppm NMT 9 ppm
Residue on evaporation	NMT 25 ppm m/V	

Haymankimia Ethanol 100% BP/EP is tested beyond these criteria as follows:

Strength	NLT 99.9% V/V @ 20 °C
Water Content	NMT 0.1%

Haymankimia is a division of Hayman Group Ltd.

Reference No: 1/3  
Issue Date: 01/07/17

Figure A5.0.1 Ethanol fuel specification